



**Fakultät für Medizin**

**Institut für Mikrobiologie, Immunologie und Hygiene**

# **Development of a truncated EGFR marker as a safeguard for adoptive T cell therapy**

**Paulina Joanna Paszkiewicz (M.Sc.)**

Vollständiger Abdruck der von der Fakultät für Medizin der Technischen Universität München zur Erlangung des akademischen Grades eines

**Doctor of Philosophy (Ph.D.)**

genehmigten Dissertation.

Vorsitzender: Univ.-Prof. Dr. J. Ruland

Betreuer: Univ.-Prof. Dr. D. Busch

Prüfer der Dissertation:

1. Univ.-Prof. Dr. A. Krackhardt

2. Prof. Dr. St. Riddell, University of Washington / USA

Die Dissertation wurde am 16.06.2014 bei der Fakultät der Technischen Universität München eingereicht und durch die Fakultät für Medizin am 27.08.2014 angenommen.

*Meinen Eltern  
und Nico*

## Contents

Summary.....	IV
Abbreviations.....	VI
1 Introduction.....	1
1.1 T cell immunity in infection and cancer .....	1
1.1.1 T cell subsets and function in infection.....	2
1.1.2 Dual role of T cells in cancer.....	5
1.2 Adoptive T cell therapy .....	9
1.2.1 Direct transfer of unmodified T cells.....	10
1.2.2 Genetic engineering.....	13
1.2.2.1 Recombinant T cell receptors .....	14
1.2.2.2 Chimeric antigen receptors .....	16
1.2.3 Clinical experience with gene-modified T cells.....	21
1.2.3.1 Clinical studies with TCR- and CAR-engineered T cells.....	22
1.2.3.2 Risks of current approaches .....	24
1.3 Strategies to increase efficacy and safety of ACT .....	27
1.3.1 Composition of the T cell product.....	27
1.3.2 Clinical tracking of transferred T cells .....	30
1.3.3 Suicide gene systems .....	32
1.3.3.1 Drug-based suicide mechanisms .....	33
1.3.3.2 Antibody-dependent depletion mechanisms.....	34
1.4 Cetuximab .....	37
1.4.1 Mechanism of action.....	37
1.4.2 Application in tumor therapy.....	38
2 Aim of this PhD thesis.....	40
3 Material and Methods .....	41
3.1 Material.....	41
3.1.1 Chemicals and reagents .....	41
3.1.2 Media and buffers .....	43
3.1.3 Gels.....	45
3.1.4 Antibodies.....	45
3.1.5 Enzymes.....	46
3.1.6 Kits.....	47
3.1.7 Cells and cell lines .....	47
3.1.8 Plasmids.....	47
3.1.9 Mice.....	48

---

3.1.10	Equipment .....	48
3.1.11	Software .....	49
3.2	Methods.....	50
3.2.1	Cell culture.....	50
3.2.1.1	General techniques.....	50
3.2.1.2	Rapid expansion protocol .....	50
3.2.2	Transduction .....	51
3.2.2.1	Retroviral transduction .....	51
3.2.2.2	Lentiviral transduction .....	52
3.2.3	Functional analysis <i>in vitro</i> .....	53
3.2.3.1	Killing assay.....	53
3.2.3.2	Chromium release assay .....	53
3.2.4	Adoptive T cell transfer and depletion <i>in vivo</i> .....	54
3.2.4.1	T cell transfer and mAb infusion.....	54
3.2.4.2	Analysis of blood and serum.....	54
3.2.4.3	Isolation and processing of organs.....	55
3.2.5	Magnetic cell separation .....	56
3.2.5.1	Nanobead-based cell selection (MACS).....	56
3.2.5.2	Microbead-based cell selection.....	56
3.2.6	Flow cytometry.....	57
3.2.6.1	Surface staining .....	57
3.2.6.2	Staining cells of the lymphoid and myeloid lineage .....	57
3.2.6.3	<i>Streptamer</i> staining.....	58
3.2.6.4	Cell sorting by FACS.....	58
3.2.6.5	Intracellular cytokine staining .....	58
3.2.6.6	Quantitative flow cytometry .....	59
3.2.7	Molecular biology techniques.....	60
3.2.7.1	Cloning of EGFR Fab fragments.....	60
3.2.7.2	Protein expression and purification .....	61
3.2.7.3	Gel electrophoresis.....	61
3.2.7.4	Western blot .....	62
3.2.7.5	Silver staining .....	62
3.2.8	Statistics .....	62
4	Results .....	63
4.1	Characterizing the EGFRt as a tracking marker.....	63
4.1.1	Co-expression of the EGFRt marker and other transgenes.....	63
4.1.2	Stable expression of the EGFRt <i>in vitro</i> and <i>in vivo</i> .....	68
4.2	Development of a reversible EGFR-specific Fab <i>Streptamer</i> .....	71
4.2.1	Generation and evaluation of the wildtype anti-EGFR Fab.....	72
4.2.2	Reversibility of EGFR Fab fragments with single mutations .....	76
4.2.3	Evaluation of EGFR Fab fragments with double mutations .....	83

---

4.3	Selection of gene-modified T cells by targeting the EGFRt .....	86
4.3.1	Magnetic enrichment of EGFRt <sup>+</sup> T cells using nanobeads.....	87
4.3.2	EGFR Fab-based selections using larger beads.....	94
4.4	Evaluation of the EGFRt-based depletion mechanism in model systems....	103
4.4.1	<i>In vitro</i> analysis of Cetuximab-mediated ADCC.....	103
4.4.2	Depletion of EGFRt <sup>+</sup> T cells in the OT-I mouse model .....	106
4.4.2.1	The effect of irradiation on the endogenous NK cell population.....	106
4.4.1	<i>In vivo</i> depletion of CD19-CAR/EGFRt-transduced OT-I cells.....	108
4.4.2	Inhibition of <i>ex vivo</i> EGFR staining by Cetuximab.....	110
4.4.3	<i>In vivo</i> depletion of sorted GFP/EGFRt <sup>+</sup> OT-I cells.....	112
4.4.4	<i>In vivo</i> depletion of T cells with high or low EGFRt expression.....	121
4.5	<i>In vivo</i> depletion of anti-mouse CD19-CAR/EGFRt <sup>+</sup> T cells.....	125
4.5.1	Analysis of anti-mouse CD19-CAR <sup>+</sup> T cell function <i>in vitro</i> .....	125
4.5.2	<i>In vivo</i> depletion of functional m1928E <sup>+</sup> T cells .....	127
4.6	<i>In vivo</i> depletion of S-CAR/EGFRt <sup>+</sup> T cells in the HBV mouse model.....	131
4.7	Evaluation of the EGFRt marker in the non-human primate .....	136
5	Discussion .....	139
5.1	The EGFRt is a reliable cell-surface tracking marker .....	139
5.2	The quest for a reversible EGFR-specific selection reagent.....	142
5.3	Selection of EGFRt <sup>+</sup> T cells works with small magnetic beads .....	145
5.3.1	Magnetic selections might depend on the number of target molecules .....	146
5.4	The EGFRt can be targeted by Cetuximab .....	148
5.4.1	Cetuximab is a suitable reagent for T cell depletion .....	148
5.4.2	<i>In vitro</i> ADCC of EGFRt <sup>+</sup> T cells.....	149
5.4.3	Depletion studies in the OT-I mouse model .....	150
5.4.4	Opportunities to enhance the EGFRt-based depletion strategy.....	152
5.5	T cell depletion in clinically relevant mouse models .....	155
5.5.1	T cell depletion prevents liver toxicity in HBV-tg mice .....	155
5.5.2	B cell aplasia can be reversed by eliminating mCD19-CAR T cells.....	156
5.6	Cinical scenarios for the application of the EGFRt as a depletion marker ...	159
5.6.1	Long-term toxicities.....	159
5.6.2	Acute toxicities.....	160
5.6.3	Systemic adverse effects of T cell therapies .....	162
5.6.4	Clinical use of the EGFRt.....	163
6	Bibliography.....	165
7	Publication list.....	180
8	Acknowledgements.....	181

## Summary

Adoptive transfer of T cells that are engineered to carry defined antigen-specific receptors, both T cell receptors (TCRs) and chimeric antigen receptors (CARs), has shown to be effective in different clinical settings, especially for the treatment of B cell malignancies. Optimized receptor design and increased persistence of transferred T cells have led to better clinical outcomes, but unfortunately, several incidents of serious on- and off-target toxicities were also reported. Thus, key issues still need to be addressed to improve the quality and safety of gene-modified cell products for therapy. These include: 1) optimized selection protocols to obtain a highly pure cell population that expresses the introduced antigen receptor, and 2) a safety mechanism to facilitate elimination of transferred cells in the event of adverse effects. A promising strategy is to co-express the transgenic receptor with a truncated cell surface marker derived from the human epidermal growth factor receptor (EGFRt).

The aim of this PhD thesis was to evaluate and further develop the EGFRt for cell selection, *in vivo* tracking and cell ablation.

For validating the EGFRt as a tracking marker, we genetically modified T cells with different CAR/EGFRt constructs and confirmed stable expression of the EGFRt *in vitro* and *in vivo* over long time periods. For obtaining highly pure cell products, we developed cell selection protocols based on the *Streptamer* technology. Therefore, we generated a reversible EGFR-specific Fab fragment that could be multimerized on magnetic nanobeads to enrich EGFRt<sup>+</sup> T cells with high purities and good yields. As reversible *Streptamer* selection reagents can be completely removed from the cell surface after the selection procedure, the purified cell product can directly be transferred into the patient in future applications.

For *in vivo* depletion of engineered cells, the EGFRt marker is targeted by the clinically approved anti-EGFR antibody Cetuximab, which mediates antibody-dependent cellular cytotoxicity. To study the feasibility and efficiency of this strategy, we established a mouse model that allowed for efficient transfer of GFP/EGFRt<sup>+</sup> T cells, reliable *in vivo* tracking using GFP as an additional marker and sensitive analysis of the extent of the depletion by using ovalbumin-specific (OT-I) cells that can be expanded *in vivo* by vaccination. We found that T cells with high expression levels of the EGFRt were completely eliminated by Cetuximab.

We also addressed the question whether T cell depletion via the EGFRt safeguard can counteract T cell-mediated toxicities in clinically relevant mouse models. In a syngeneic mouse model, we transferred functional anti-mouse CD19-CAR/EGFRt-transduced T cells that suppressed the growth of endogenous B cells. However, if T cells were eliminated using Cetuximab, the B cell population recovered within few weeks. In HBV-transgenic mice, the function of HBV-specific T cells can be analyzed by monitoring the levels of alanine aminotransferase (ALT) as a measure for T cell killing of HBV<sup>+</sup> hepatocytes. We could show that Cetuximab-mediated depletion of functional HBV-specific, EGFRt<sup>+</sup> T cells prevented liver toxicity as indicated by unchanged ALT levels.

In addition, we evaluated the EGFRt-based depletion strategy in a pilot study in non-human primates. Therefore, we transduced macaque T cells with an EGFRt lentiviral construct and subsequently purified the cells using EGFR Fab *Streptamers*. Importantly, both the transfer of EGFRt<sup>+</sup> T cells and Cetuximab infusions appeared to be safe and we observed a decrease in EGFRt<sup>+</sup> T cells after Cetuximab treatment.

In summary, these data demonstrate that the EGFRt marker is a safe and valuable tool for clinical cell purification, *in vivo* tracking and effective cell depletion. The approach can be readily made available for clinical application and can be transferred to other types of cell-based therapies. The co-expression of EGFRt therefore represents a promising concept to improve the safety of therapies based on gene-engineered cells.

## Abbreviations

aa	Amino acid
ACT	Adoptive cell therapy
ADCC	Antibody-dependent cellular cytotoxicity
ADCP	Antibody-dependent cellular phagocytosis
ALT	Alanine aminotransferase
APC	Antigen Presenting Cell
-APC	-Allophycocyanin
B-LCL	B-lymphoblastoid cell line
BSA	Bovine serum albumin
CAIX	Carbonic anhydrase
CAR	Chimeric antigen receptor
CD	Cluster of differentiation
CDC	Complement-dependent cytotoxicity
cDNA	complementary DNA
CDR	Complementarity Determining Region
CEA	Carcinoembryonic antigen
CML	Chronic myeloid leukemia
CMV	Cytomegalovirus
cpm	counts per minute
CRC	Colorectal carcinoma
CT antigen	Cancer/testis antigen
CTL	Cytotoxic T lymphocyte
CTLA-4	Cytotoxic T-Lymphocyte Antigen 4
CTLL-2	Cytotoxic T Lymphoblast line-2
DC	Dendritic cell
DLI	Donor lymphocyte infusion
DTT	Dithiothreitol
DNA	Deoxyribonucleic acid
dNTP	Deoxynucleoside-triphosphate
EBV	Eppstein-Barr virus
<i>E. coli</i>	<i>Escherichia coli</i>
EDTA	Ethylendiaminetetraacetate
EFG(R)	Epidermal growth factor (receptor)
FACS	Fluorescence activated cell sorting
FAP	Fibroblast activation protein
Fc part	Fragment crystallizable part
FCS	Fetal calf serum
FDA	Federal Drug Administration
FHBG	fluoro-3-hydroxymethylbutyl guanine
FITC	Fluorescein-isothiocyanat
FoxP3	Forkhead box P3
FR- $\alpha$	Folate receptor- $\alpha$
Fz domain	Frizzled domain

---

GCV	Ganciclovir
GFP	Green fluorescent protein
GM-CSF	Granulocyte macrophage-colony stimulating factor
GVHD	Graft versus Host Disease
GVL	Graft versus Leukemia
GVT	Graft versus Tumor
HBsAg	Hepatitis B-derived surface antigen
HBV	Hepatitis B virus
HIV	Human immunodeficiency virus
HLA	Human leukocyte antigen
HNSCC	Head and neck squamous cell carcinoma
HSCT	Hematopoietic stem cell transplantation
HSV1-TK	Herpes Simplex virus 1 thymidine kinase
GMP	Good manufacturing practice
GPI anchor	Glycophosphatidylinositol anchor
iCasp9	inducible caspase 9
IFN	Interferon
Ig	Immunoglobulin
IL	Interleukin
IRES	intraribosomal entry site
i.p.	intraperitoneal
i.v.	intravenous
IVIG	Intravenous immunoglobulins
LCMV	Lymphocytic choriomeningitis virus
LTR	Long-term repeats
LV	Lentiviral
mAb	monoclonal antibody
MACS	Magnetically activated cell sorting
MART-1	Melanoma antigen recognized by T cells-1
mHAg	minor Histocompatibility antigen
MHC class I/II	Major histocompatibility complex class I/II
MFI	Mean fluorescence intensity
MOI	Multiplicity of infection
MRI	Magnetic resonance imaging
mRNA	Messenger RNA
MSCV	Murine stem cell virus
MVA	Modified vaccinia virus Ankara
NGFR	Nerve growth factor receptor
NHP	Non-human primate
NK cell	Natural killer cell
OVA	Ovalbumin
PBMC	Peripheral blood mononuclear cell
PBS	Phosphate buffered saline
PCR	Polymerase chain reaction
PD-1/PD-L1	Programmed death-1/Programmed death-ligand1
PE	Phycoerythrin

---

PECy7	Phycoerythrin-Cy7
PET	Positron emission tomography
PGK	Phosphoglycerate kinase
PI	Propidium iodide
pMHC	peptide MHC
REP	Rapid expansion protocol
RNA	Ribonucleic acid
ROR1	Receptor tyrosine kinase-like orphan receptor
RT	Room temperature
SA	Streptavidin
SCID	Severe Combined Immune Deficiency
scFv	single chain variable fragment
SD	Standard deviation
SPR	Surface plasmon resonance
ST	<i>Strep</i> -Tactin
SV40	Simian virus 40
TAA	tumor-associated antigen
Tcm	central memory T cell
TCR	T cell receptor
Teff	effector T cell
Tem	effector memory T cell
TGF	Transforming-growth factor
Th cells	helper T cells
TIL	Tumor infiltrating lymphocyte
TKI	Tyrosine kinase inhibitors
Tn	naive T cell
TNF	Tumor-necrosis factor
Treg	regulatory T cell
Tscm	stem cell-like memory T cell
VEGFR	Vascular endothelial growth factor receptor
wt	wild type
WT-1	Wilms' tumor-1

# 1 Introduction

## 1.1 T cell immunity in infection and cancer

The innate and adaptive immune systems have evolved in vertebrates to protect the host against intruding infectious pathogens. The hallmarks of T cell-mediated adaptive immunity are high specificity of recognition and long-term protection, which has been extensively studied in infectious diseases. Evidence accumulates that T cells also contribute significantly to controlling malignant cells, but the role of T cells in cancer patients is less well understood. Protective as well as counter-regulatory T cell responses have been described in experimental tumor models as well as tumor patients. Identification and exploration of the protective arm of anti-tumor immunity is regarded as a promising area for the development of more effective and disease-specific therapies. In this context, adoptive transfer of suitable T cells is gaining increasing recognition. The adoptive transfer of antigen-specific T cells has shown to be effective for some virus infections and increasing knowledge has been acquired about cell-intrinsic and environmental factors that are important for functionality and survival of transferred T cells. T cells specific for tumor-associated antigens are often less effective because these antigens are usually self-antigens underlying central and peripheral tolerance mechanisms. To overcome tolerance of adoptively transferred tumor-specific T cells, current investigations explore methods of genetic engineering to equip the cell products with high-avidity antigen-specific receptors and optimal qualities for *in vivo* function and maintenance. And indeed, first clinical studies demonstrate the therapeutic potential of genetically modified T cells in cancer patients. However, introducing new genes into cells also gives rise to safety concerns that need to be carefully investigated. The safety and efficacy of T cell-based immunotherapies can be further improved by extending our knowledge about T cell function and immune regulatory mechanisms in infectious diseases and cancer, as well as by the development of strategies allowing specific depletion of transferred T cells in the case of unacceptable toxicity or long-term side effects.

### 1.1.1 T cell subsets and function in infection

T lymphocytes that express the  $\alpha/\beta$  T cell receptor (TCR) develop from lymphoid precursors that originate in the bone marrow and mature in the thymus. During T cell development, the antigen specificity of T cells is determined by the rearrangement of genes encoding for the complementarity-determining region 3 (CDR3) regions of  $\alpha$  and  $\beta$  chains of the TCR. In addition to genetic recombination, pairing of  $\alpha$  and  $\beta$  chains contributes to the high diversity of TCRs. The effective TCR repertoire in healthy individuals comprises around  $2.5 \times 10^6$  unique TCR $\beta$  CDR3 sequences in the naïve T cell population [1]. Although this number is smaller than the estimated number of distinct TCRs calculated from all possible recombinations, this range of specificities still allows T cells to detect a large variety of host and foreign structures. More specifically, the TCR recognizes peptide fragments from proteins that are presented on major histocompatibility complex (MHC) molecules, expressed on the surface of antigen presenting cells (APCs) [2]. During the T cell development in the thymus, immature T cells are selected for their ability to bind self MHC molecules in a process termed positive selection. TCR binding to MHC molecules is stabilized by the mutually exclusive co-receptors CD4 and CD8 that are expressed on the T cell surface. CD4<sup>+</sup> T cells are restricted to bind MHC class II molecules, whereas CD8<sup>+</sup> T cells usually recognize MHC class I molecules, which will guide the functional properties of these two T cell subsets. T cells binding self-peptides with too high affinity are eliminated by apoptosis, a process termed negative selection [3]. Therefore, the naïve T cell population leaving the thymus is selected to be tolerant to self-antigens and is able to recognize a broad range of foreign peptides presented on self MHC molecules.

After being educated in the thymus, naïve CD4<sup>+</sup> and CD8<sup>+</sup> T cells (T<sub>n</sub>) are released into the periphery to survey secondary lymphoid organs including lymph nodes, the spleen and bone marrow, which is facilitated by the expression of the homing receptor CD62L (L-selectin) and the chemokine receptor CCR7 [4]. In steady state, resting APCs, e.g. dendritic cells (DCs), present self-antigens to the T cells during transient contacts – so-called immunological kinapses – that are not sufficient to promote T cell activation [5]. In some cases, insufficient T cell activation causes T cell anergy that is characterized by a non-responsive status of the T cell [6]. This mechanism serves to induce peripheral tolerance and to prevent the development of autoimmune diseases [7]. During infection, DCs phagocytose the microbes or the infected apoptotic cells and

present processed foreign antigens on MHC class I and II molecules in addition to self-antigens. In response to pathogen-associated stress or danger signals, DCs are activated and consequently enhance antigen processing, upregulate expression of MHC and costimulatory receptors, and produce cytokines and chemokines [8]. CD4<sup>+</sup> T cells specifically recognize peptides loaded on MHC class II molecules and induce expression of costimulatory molecules on the surface of the same DC. This so-called licensing of DCs supports efficient induction of T cell responses [9]. When a CD4<sup>+</sup> or CD8<sup>+</sup> T cell encounters its cognate pMHC expressed on an activated DC, so-called immunological synapses are formed to maintain a long-lasting interaction of T cell and DC, further stabilized by recruiting adhesion molecules to the interface [5]. TCR engagement (signal 1) leads to phosphorylation of the CD3 coreceptor, ZAP70 and downstream Src kinases and induces a signaling cascade that results in T cell proliferation and differentiation [10]. The CD28 costimulatory molecule of the Immunoglobulin (Ig) receptor family is expressed on the T cell surface and binds to its ligand CD80/86 on mature DCs (signal 2). Further intracellular kinases and adaptor proteins are recruited to the triggered TCR, thereby amplifying the TCR signals [11]. T cell survival and effector functions can be further augmented by engaging other costimulatory molecules of the tumor-necrosis factor (TNF) receptor family, such as OX40 (CD134) and 4-1BB (CD137) [12]. Inflammatory cytokines, e.g. interleukin (IL)-12 and type I interferons (IFNs) are also involved in supporting T cell expansion and function, therefore considered to be 'signal 3' in T cell activation [13]. Thus, in response to cognate antigen, T cells clonally expand and adopt different functional profiles. They also down-regulate the expression of CD62L and CCR7, which enables both CD8<sup>+</sup> and CD4<sup>+</sup> T cells to exit lymphatic organs.

Activated T cells circulate through the periphery and are able to extravasate into inflamed tissue to exert effector function at sites of infection [4]. Cytotoxic CD8<sup>+</sup> T cells are able to kill pathogen-infected cells by cell-cell contact dependent pathways through release of toxic granules or engagement of the TNF receptor family member Fas (CD95). Preformed cytolytic molecules are delivered to the contact area between T cell and target cell by directed exocytosis. Pore-forming proteins, such as perforin, cause membrane lesions and the serine proteases granzyme A and B induce caspase-linked apoptosis. Programmed cell death is also triggered by the binding of Fas ligand (FasL) on activated CD8<sup>+</sup> T cells to its receptor Fas on the target cell. Further non-cytolytic functions of CD8<sup>+</sup> T cells contribute to the inflammatory response. Secretion of pro-

inflammatory cytokines IFN- $\gamma$  and TNF- $\alpha$  plays a critical role in recruiting and activating innate immune cells and supporting antigen recognition [14].

A main function of CD4<sup>+</sup> T cells, also called helper T cells (Th) is to support and regulate the immune response against a wide variety of pathogens. Th cells were initially subdivided into two major subpopulations with distinct cytokine expression profiles [15]. Cytokines present at the time of T cell priming are important for driving the CD4<sup>+</sup> T cell differentiation to type I (Th1) or type II (Th2) helper T cells [16]. In the presence of IL-12 and IFN- $\gamma$  Th1 cells are induced to produce IL-2, IFN- $\gamma$  and TNF- $\alpha$  and are directly promoting the local CD8<sup>+</sup> T cell response against intracellular pathogens. In contrast, IL-4 is required for differentiation of CD4<sup>+</sup> T cells into Th2 cells that secrete IL-4, IL-5, IL-10 and IL-13 to support antibody production by B cells that is important for eliminating extracellular pathogens [17]. In addition to Th1 and Th2 cells, primed CD4<sup>+</sup> T cells can also give rise to a third effector population when IL-6, transforming-growth factor (TGF)- $\beta$  and IL-23 are available. These differentiated cells were designated Th17 cells as they were characterized to produce IL-17 and IL-22, and they were shown to regulate tissue inflammation [18]. The fourth cell population derived from naïve CD4<sup>+</sup> T cells, the regulatory T cell (Treg) subset, plays an important role in constraining the immune response against self-antigens, thereby limiting autoimmunity. Tregs are usually characterized by a CD4<sup>+</sup>CD25<sup>+</sup>Foxp3<sup>+</sup> phenotype. Immunosuppressive Treg functions encompass cytolytic activity, expression of inhibitory receptors and secretion of suppressive cytokines IL-10 and TGF- $\beta$  [19]. Similar mechanisms are at play to modulate the extent of the immune response against pathogens. For example, the inhibitory programmed death-1 (PD-1) ligand on the Treg cell surface can engage with its receptor PD-1 expressed on activated T cells and attenuate TCR signaling and function by different molecular mechanisms [20].

During the typical course of an immune response to acute infections, antigen-specific T cells are activated in the lymph nodes and migrate to infected tissue, clonally expand and specifically lyse infected cells within a week. After clearance of the infection most of the T cells undergo apoptosis during the contraction phase, as shown in detailed studies of lymphocytic choriomeningitis virus (LCMV) infection in mouse models [21, 22]. These investigations also revealed that 5-10% of the initial size of an immune response is spared and enables the development of immunological memory. Memory cells are long-lived antigen-experienced cells that provide protection against secondary infection. They can be maintained for a long time in the absence of antigenic

stimulation due to their ability to respond to homeostatic cytokines IL-7 and IL-15. Memory T cells can be subdivided into two subsets with distinct phenotypic and functional profiles [23, 24]. Effector memory T cells (Tem) are maintained in peripheral tissues due to the absence of lymph node homing receptors CD62L and CCR7 and can confer immediate effector functions upon repeated encounter of the pathogen. In contrast, central memory T cells (Tcm) constitutively express CCR7 and CD62L and localize to secondary lymphoid organs. They exhibit a strong proliferative capacity, depend less on costimulation than Tem and differentiate rapidly to effector T cells (Teff). The differentiation path from naïve T cells to effector and memory T cells is still under debate. Tracking the fate of individual T cells in mice exposed to bacterial infection revealed that T cell differentiation can follow a progressive differentiation model with increasing proliferation rates and decreasing differentiation potential along the hierarchy Tn → Tcm → Tem → Teff [25, 26].

During chronic infections, the immune system faces repeated antigenic stimulation that leads to T cell exhaustion [27]. The exhausted state is characterized by decreased effector functions, such as cytokine production, and increased expression of inhibitory receptors, e.g. PD-1 and cytotoxic T-lymphocyte antigen-4 (CTLA-4). Blocking the PD-1 pathway can reverse the phenotype of exhausted T cells and represents an interesting approach to re-activate non-functional T cells in settings of chronic inflammation due to chronic infections or cancer [28].

### 1.1.2 Dual role of T cells in cancer

Persistent antigen presentation and chronic inflammation are characteristics that are shared by chronic infections and the tumor environment. The current understanding of the role of T cells in cancer is largely deduced from studies of T cell function in response to chronic viral infections that were subject to intense research. Tumors often arise and grow in the presence of immune control over long periods of time. Therefore, it is important to shed light on the complex and contradictory effects of the immune system on the tumor and vice versa. Tumorigenesis is based on the ability of mutated cells to alter and exploit the normal physiological pathways, controlling tissue homeostasis, proliferation and cell death [29]. As such, tumors are able to manipulate their environment, including infiltrating innate and adaptive leukocytes. In turn, T cells

were implicated in the control of emerging malignant cells in mouse models [30] and human studies [31].

Only recently, it has been appreciated that mouse models have to account for the co-evolution of tumors and the immune system. Transplanted tumors usually grow very fast at unphysiological sites and are often rejected in an immune-competent host [32]. In contrast, sporadic tumor models reflect the slow tumor progression and induction of immune tolerance more closely. As single transformed cells are eliminated by the immune system, the tumor has to reduce its immunogenicity and/or suppress the immune system in order to expand. This process coined immunoediting that involves elimination, equilibrium and escape can take years to decades in humans and results in the presence of a progressing tumor in an immunocompetent individual [33].

During the elimination phase, the immune system is capable of tumor prevention in three ways [34]. First, it eliminates viruses that might cause virus-induced malignancies, such as Epstein-Barr virus (EBV)-related lymphomas. Second, the efficient protection against pathogens restricts the duration of an inflammatory condition. A correlation between unresolved inflammation and tumor promotion, angiogenesis and metastasis has been shown for several human cancers [35]. Finally, immune cells can recognize tumor-specific alterations, e.g. tumor-associated antigens (TAAs) presented on MHC class I, and eliminate mutated cells before a tumor is established. Evidence for cancer immunosurveillance has been acquired in many studies of spontaneous tumor development in mice lacking specific cell populations (T cells, natural killer cells), critical cytokines (IFN- $\gamma$ ) or receptors (TCR, IFN- $\gamma$  receptor) [34]. In immunodeficient mice, carcinogen-induced sarcomas, for example, occur more frequently and within shorter time frames as compared to wildtype mice [36]. Similarly, a higher prevalence of virus-associated and non-virus-associated cancers, e.g. lung cancer, was observed in immunocompromised AIDS patients [37, 38]. Even more convincingly, spontaneous immune responses to cancer are occasionally observed in melanoma patients, which lead to regression of the tumor as a consequence [39].

If the immune system fails to eliminate tumor cells, it can still contribute to maintaining the tumor in a dormant or slowly growing state, where there is a relative equilibrium between tumor growth and immune control [40]. During that time the tumor acquires mutations that reduce its immunogenicity and mediate immune suppressive functions. Supporting this idea, tumors that have developed in immunodeficient mice were found to be more immunogenic as compared to tumors that have grown in wildtype mice [41].

The concept of 'survival of the fittest' in tumorigenesis is based on the selection of the mutated cell with best immune evasive capabilities under immunological pressure [34]. Tumors acquire a more aggressive phenotype and higher metastatic potential. This immune-guided process called immune editing inevitably plays a role in optimizing the tumor for surviving in the host [33, 42].

Malignant immune escape variants are able to avoid recognition and evade killing in multiple ways [43]. On one hand, the tumor cell itself can undergo changes that interfere with antigen processing and presentation or proper MHC class I expression. An immune-adapted tumor can also lack specific tumor-associated antigens, which renders the tumor invisible to antigen-specific T cells, or it can upregulate inhibitory molecules, such as PD-L1, to directly counteract T cell attack. On the other hand, the tumor acts on the immune system to induce functional tolerance [44]. The tumor recruits and activates myeloid suppressor cells and Tregs that suppress tumor-specific immune cells by expression of inhibitory receptors and secretion of the inhibitory cytokines TGF- $\beta$  and IL-10. In addition, tumor or stromal cells directly secrete other soluble factors, for example metabolic factors, that limit T cell function [45]. The immunosuppressive microenvironment, together with poor costimulation provided by the tumor cells, leads to T cell anergy or adaptive tolerance. Anergic antigen-specific T cells are hyporesponsive, long-lived and produce low levels of IL-2. In addition to anergy, T cells can be driven into exhaustion when they are constantly stimulated by the tumor [46].

Multiple strategies are developed to reverse the inhibition of the immune system and improve tumor-directed immunity. These efforts are supported by the observation that cytotoxic T cells at the tumor site are correlated with a good prognosis in a number of different tumor types, including melanoma [47], ovarian cancer [48] and colon carcinoma [31]. To boost the existing anti-tumor response, vaccination protocols were investigated that ranged from using inactivated whole tumor cells as a vaccine to the adoptive transfer of TAA-pulsed DCs. These approaches did not yield an improved clinical prognosis in most cases because vaccination failed to overcome the highly immunosuppressive tumor environment [49]. Consequently, manipulating the tumor environment has received great attention. Most promising therapeutic interventions include antibody blockade of the inhibitory molecules PD-1 and CTLA-4 [50, 51]. For example, treatment with the anti-CTLA-4 mAb ipilimumab was associated with increased survival of melanoma patients in a clinical phase III study [51]. In addition,

---

cellular immunotherapies were developed that are usually based on expanding and activating tumor-specific T cells outside of the unfavorable environment. *Ex vivo* manipulations offer many ways to permanently rescue the anti-tumor activity of tolerized endogenous T cells. These range from genetically modifying T cells to make them resistant against tumor-associated inhibitory factors, e.g. TGF- $\beta$  [52], to redirecting T cell specificity by introducing transgenic tumor-specific receptors [53].

## 1.2 Adoptive T cell therapy

Over the past decades the most widely used form of adoptive immunotherapy, namely allogeneic hematopoietic stem cell transplantation (HSCT), has proven to be successful for treating hematological malignancies. The initial purpose of the transplant was to rescue the patient's hematopoiesis that was destroyed by intensive chemoradiotherapy that significantly eradicated the tumor. In addition, it was observed that also donor lymphocytes mediate a beneficial graft versus leukemia (GVL) effect. Unfortunately, donor lymphocyte infusions (DLI) also correlated with the development of graft versus host disease (GVHD), an often very severe and life-threatening tissue pathology, predominantly affecting the gut, liver, lung, skin and bone marrow [54]. T cells were identified as the main mediators of both GVHD and the GVL effect, as the administration of T cell-depleted transplants reduced GVHD and was associated with a higher risk of tumor relapse [55]. Despite their high risk to induce GVHD, DLIs are routinely used to provide the GVL effect, especially in case of relapse after HSCT. In patients with relapses of acute or chronic leukemia, DLI achieved durable clinical responses, leading to complete remissions in 73% of chronic myeloid leukemia (CML) patients [56]. In most cases, the GVL effect of DLI is associated with GVHD that is mediated by allo-reactive lymphocytes responding to recipient human leukocyte antigen (HLA)-peptide complexes, termed minor histocompatibility antigens (mHAg) derived from polymorphic genes that differ between donor and recipient [57]. Identifying tissue-specific mHAg, such as HA-1 and HA-2 that are only expressed on hematopoietic cells, might allow separating the GVL effect from GVHD in the case of hematological malignancies. As proof of concept, patients with relapsed leukemia have been treated with mHAg-specific CD8<sup>+</sup> T cell clones that indeed led to transient complete remission in several patients; however, unexpected pulmonary toxicities were observed in some cases [58].

The transfer of more defined antigen-specific T cells was an important step towards a tailored tumor therapy that circumvents alloreactivity. The principles of antigen-specific adoptive cell transfer (ACT) in humans were first established in the clinical setting of viral infections in immunocompromised patients due to easier access to virus-specific cell populations. T cells were infused into immunosuppressed patients after HSCT for immediate protection against latent reactivating viruses, e.g. cytomegalovirus (CMV) or EBV [59, 60]. For these viruses, specific epitopes for T cell recognition are known,

which facilitated isolation of defined antigen-specific T cells for transfer. Further characteristics of T cells for optimal clinical outcome were identified: they should efficiently migrate to the target tissues, exert cytotoxic function upon activation and persist long-term *in vivo*. These acquired insights laid the foundation for the development of ACTs for treating tumor diseases. However, to overcome the tolerance-inducing mechanisms in the tumor environment, it seems advantageous to enhance the cellular products by genetic engineering to ensure optimal efficacy and safety.

### 1.2.1 Direct transfer of unmodified T cells

Latent viruses such as CMV and EBV reactivate in patients after allogeneic HSCT because of deficient T cell immunity. While healthy individuals can control those chronic viruses, CMV and EBV infection can be life-threatening in immunosuppressed patients. As the prevalence of CMV, for example, ranges from 40 to 100% depending on the geographical region [61], healthy donors can serve as a source for virus-specific T cells that can be used for adoptive cell transfer. Donor-derived PBMCs are cocultivated with antigen-presenting cells pulsed with known viral peptides, and CMV-reactive T cells are expanded to oligoclonal T cell lines or monoclonal T cell clones in prolonged cultures [59]. Shorter protocols to generate CMV-specific T cell populations are based on the T cells' ability to secrete cytokines upon stimulation in IFN- $\gamma$  capture assays [62]. Alternatively, virus-specific T cells can be isolated from peripheral blood by magnetic selection of T cells that bind peptide-loaded MHC-multimers [63]. The isolated cells are either directly transferred into the patient or expanded *in vitro* if higher cell numbers are required. Several clinical studies have shown that transferred CMV-specific T cells persisted in transplant patients and restored protective immunity against CMV infection, even if only low T cell numbers were infused [60, 64, 65].

CMV and EBV reactivations are not the only serious infectious complications after HSCT for which adoptive T cell therapy might be beneficial. Especially in a prophylactic setting, extension of specificities of adoptively transferred T cells to additional viruses, e.g. adenovirus and polyoma BK virus, might be of clinical value. One approach for the rapid production of multivirus-specific T cell lines is to stimulate PBMCs with clinical peptide libraries in the presence of IL-4 and IL-7 [66]. Alternatively, approaches to adoptively transfer low numbers of donor-derived T cells from defined memory subsets

(especially central memory T cells), where multi pathogen-specific T cells are enriched and GVHD-mediating T cells are rare, are currently being explored.

In contrast to restoring T cell immunity to viruses after allogeneic HCT using donor-derived virus-specific T cells, it is much more difficult to identify, isolate, and propagate autologous T cells specific for tumor antigens for treating cancer patients. As most tumor-associated antigens are self-antigens, high affinity tumor-specific T cells are often eliminated during thymic development [67]. Potentially better targets are neoantigens, i.e. novel peptides that are derived from mutated proteins in a tumor cell. Recently, tumor-specific phosphopeptides resulting from activation of kinase pathways in cancer cells and presented on HLA class I were described as a new class of tumor-specific antigens [68]. However, the tumor environment also induces peripheral tolerance of tumor-specific T cells by inhibiting effector functions and restricting T cell proliferation due to decreased IL-2 production and cell cycle arrest of the T cells [46]. Consequently, the number of tumor-specific T cells in the tumor tissue or in peripheral blood is very low or the existing T cells are of weak functionality, potentially limiting the access to effective T cells for adoptive tumor immunotherapy. Nevertheless, tumor-specific T cell populations were successfully isolated from resected melanoma tissue that harbored tumor-infiltrating lymphocytes (TILs). After *in vitro* expansion, TILs were selected for tumor reactivity. In a first clinical trial of such a TIL therapy in melanoma patients, only minor responses were observed, and cells became undetectable within two weeks [69]. However, subsequent studies with melanoma-specific TILs or T cell clones demonstrated transient clinical responses at least in few patients [70, 71]. In a five-year series of TIL therapy, it was feasible in only 27% cases (107 out of 402 patients) to use TILs from resected melanoma tissue for therapy [72], which reflects the limited applicability of this approach.

Yet, the early TIL therapy studies revealed an important correlation between clinical benefit and persistence of transferred cells [73]. Retrospective analysis helped to understand how *in vivo* cell survival was affected by culture conditions and composition of the T cell product. Long *in vitro* cell culturing in presence of IL-2 drives cell differentiation to late stage effector cells that do not survive long-term *in vivo* as opposed to memory cells [74]. To overcome this problem, expansion protocols were shortened and alternative cytokines were tested. For example, the use of IL-21 in cell cultures preserved a less differentiated phenotype and was associated with enhanced tumor regression in mouse models [75, 76]. *In vivo* persistence of infused cells could

be improved by additional treatment of the patient, e.g. with low-dose IL-2 administration [71]. Lymphodepletion by non-myeloablative radiation or chemotherapy also showed advantages for engraftment and survival of the transferred cells [77, 78]. In a lymphodepleted individual, less endogenous cells compete for homeostatic cytokines, such as IL-7 and IL-15. Furthermore, a lower tumor burden and reduced numbers of endogenous regulatory T cells favors persistence of donor T cells [79]. As an example, improved clinical outcomes were obtained, when melanoma patients were pre-treated with non-myeloablative chemotherapy, before infusing melanoma-specific T cells. Cancer regression in 6 out of 13 patients was correlated with an improved T cell persistence [77, 78]. The beneficial effect of lymphodepletion on the outcome of TIL therapy was confirmed in larger melanoma patient cohorts [80].

In addition to resected tumor tissue, the peripheral blood represents a source for tumor-specific T cells. Peripheral lymphocytes can be stimulated with autologous melanoma cells or APCs pulsed with tumor-specific peptides, such as MART-1 (melanoma antigen recognized by T cells-1) and tyrosinase for melanoma or Wilms' tumor-1 (WT-1) for acute myeloid leukemia [81]. Based on this approach, WT-1-specific CD8<sup>+</sup> T cell clones were generated, transferred into leukemia patients and conferred anti-tumor activity in 5 out of 11 patients, extending the successful application of ACTs to other tumors than melanoma [82].

Major limitations were encountered during early development of adoptive T cell therapy to treat malignancies: (i) Tumor-specific T cells are rare populations. Attempts to isolate them from TILs or PBMCs were rather disappointing as they were only successful in about 30-40% of the cases [83]. (ii) Naturally occurring T cells react very weakly to tumor cells due to low TCR affinity, as they have already been subjected to systemic and local tolerance mechanisms. (iii) Extensive expansion was required before transfer, as it was generally accepted that high T cell numbers ( $10^{10}$ - $10^{11}$ ) were required to show a substantial anti-tumor effect [73, 84]. The accumulating knowledge about 'ideal' tumor targets and the availability of technologies to genetically modify cells fueled the idea to redirect a cell population of choice to specifically target the tumor instead of relying on pre-existing tumor-specific T cells.

### 1.2.2 Genetic engineering

Introducing a transgenic receptor into autologous T cells partly solves the problem of isolating tumor-reactive T cells directly from the autologous T cell repertoire of the patient. The tumor specificity can be imposed either by transgenic TCRs or chimeric antigen receptors (CARs) (Fig. 1-1). While genes for transgenic TCR  $\alpha$  and  $\beta$  chains are derived from tumor-reactive T cells, a CAR is a synthetic receptor that usually comprises a single chain variable fragment (scFv) of a TAA-specific antibody and signaling molecules from the TCR. Receptor genes can be transferred to any cell by genetic engineering, thereby representing an off-the-shelf reagent to equip T cells with the required specificity. This approach does not depend on isolation and transfer of tolerized TILs, but in fact offers the advantage of using any cell population with defined phenotype and functional qualities for ACT. The functionality of the transgenic receptor itself can also be optimized by tuning the affinity or modulating expression and signaling of the receptor.

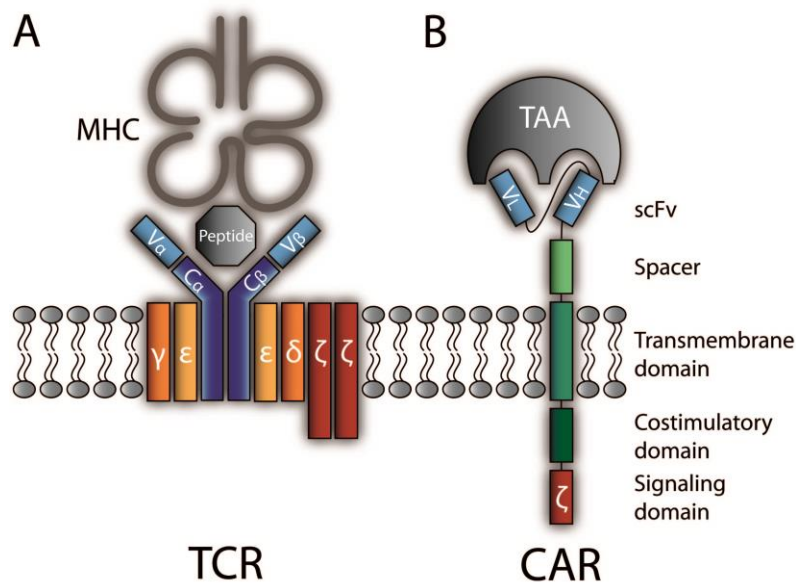


Fig. 1-1: Structure of TCRs and CARs. A. The  $\alpha$  and  $\beta$  chain of the TCR consist of constant (C) and variable (V) regions that mediate binding to the cognate peptide-MHC complex. The TCR is associated with the  $\gamma$ ,  $\delta$ ,  $\epsilon$  and  $\zeta$  chains of the CD3 complex. B. The ectodomain of a CAR is derived from a single chain variable fragment (scFv) that determines specificity to the tumor associated antigen (TAA). The scFv is linked to a spacer, a transmembrane domain and an endodomain that most commonly contains a signaling domain, derived from the  $\zeta$  chain of the TCR complex, and costimulatory domains, such as CD28 or 4-1BB.

### 1.2.2.1 Recombinant T cell receptors

The efficient transfer of TCR  $\alpha$  and  $\beta$  genes into T cells was pioneered by Dembic *et al.* [85] and this approach was later applied to melanoma-specific TCRs [86]. There, the cDNA sequences for TCR  $\alpha$  and  $\beta$  chains were obtained from tumor-reactive T cells isolated from TILs. Long co-cultures with APC, loaded with relevant tumor-derived peptides, are usually used to expand tumor-reactive T cell clones that can be further characterized by MHC multimer binding or functional assays to determine those with the highest functional avidity. In the meantime, MHC multimer-based single cell sorting and advanced PCR methods allow for isolation of TCR gene sequences from single cells without the need for prior *in vitro* expansion [87]. TCR genes are then cloned into a viral vector for subsequent transduction of T cells [81]. So far only a limited number of cancer antigens have been targeted with clinical TCR-engineered T cells, including the melanoma-related antigens MART-1, MAGE-A3, NY-ESO-1 and gp100 and the colorectal cancer antigen CEA [88]. Identifying suitable tumor targets lays the foundation for improved T cell therapies. A list of so-called “optimal cancer antigens” was published by the National Cancer Institute providing valuable direction for the field, however it is likely that more suitable tumor antigens for effective immunotherapy remain to be discovered [89].

To effectively redirect T cells by gene transfer, the main requirements are to achieve high expression of the introduced TCR genes and to ensure correct assembly and pairing of the synthetic TCR chains on the T cell surface [90]. A high level of transgene expression can be achieved by using strong promoters including those derived from viruses, e.g. murine stem cell virus (MSCV) and simian virus 40 (SV40), or promoters of cellular origin, such as  $\beta$ -actin and phosphoglycerate kinase (PGK) [91, 92]. Transgene expression can be further increased by ensuring high RNA stability [93] and codon optimization of the TCR gene sequences [94]. The latter approach aims at optimizing genes such that they exclusively contain codon triplets that are frequently used in the host. For simultaneous expression, the transgenic TCR  $\alpha$  and  $\beta$  chains were encoded in one vector, separated by a viral intraribosomal entry site (IRES). As the expression of genes upstream and downstream of IRES varied, this linker was substituted by the ‘self-cleaving 2A sequence’ from picornavirus or other viruses [92]. 2A-linked genes are transcribed to one mRNA strand, then separate peptides are generated by a ribosome-skipping mechanism which facilitates equimolar expression [95].

The  $\alpha$  and  $\beta$  chains of the transgenic TCR can potentially pair with the corresponding chains of the endogenous TCR in any  $\alpha/\beta$  combination. This event of 'mispairing' diminishes expression of the correctly paired new TCR and can result in toxicity due to the creation of novel, unpredictable and potentially self-reactive TCR specificities [96]. Accordingly, mixed TCR dimers were detected in TCR gene-modified T cells, which caused lethal GVHD in mouse models [96].

Overcoming the problem of TCR mispairing has been the subject of intensive research and several strategies have been developed. First, the constant regions of the introduced human TCR chains were changed to murine sequences, termed murinization. This led to preferential pairing of the transgenic  $\alpha$  and  $\beta$  chains and enhanced expression levels of the introduced TCR at the cell surface [97]. Unfortunately, the murine gene sequences elicited an antibody response in a subset of patients which might limit the persistence of donor T cells [98]. Thus, only nine amino acids that are involved in enhanced binding of the constant regions were exchanged to generate minimally murinized TCRs. These TCR constructs mediated preferential pairing, while the risk of immunogenicity was reduced [99]. Second, an additional cysteine was introduced into both transgenic TCR chains, which allowed formation of an additional disulfide bond that enhanced pairing of the two introduced chains [100, 101]. The third approach to ensure correct pairing is based on silencing of the endogenous TCR by introducing siRNA sequences that are specific to conserved regions of the TCR [102]. The transgenic TCR is rendered unresponsive to the introduced siRNA by altering the genetic sequences for the targeted regions. An even more elegant and truly 'permanent' strategy is based on using zinc-finger-nucleases to introduce double-strand breaks at specific sites of the DNA in the endogenous TCR gene locus, which due to error-prone repair leads to complete disruption of the TCR gene [103]. Applying this technique, T cells were completely retargeted to a leukemia-specific antigen in a multi-step process by eliminating endogenous TCR sequences before introducing the transgenic TCR genes [104].

It has been shown that TCR avidity correlates with T cell functionality against viruses [105] and tumors [106]. Tumor-specific T cells predominantly bind self-antigens that are overexpressed on the tumor cell surface with low avidity. This poses a major obstacle to isolating TCRs that can mediate high functionality upon transfer into T cells. TCR avidity is dependent on the affinity of each TCR as well as the number of receptors and coreceptors (CD8) on the cell surface. To improve the TCR affinity, yeast or phage

display has been used to screen for mutations in the TCR sequence that lead to higher binding capacity [107]. Affinity-enhanced TCRs can reach an affinity in the nanomolar range [108], whereas naturally circulating T cells display TCRs of much lower affinity ( $10^{-4}$  to  $10^{-6}$  M) [67]. Increased affinities are directly correlated with accelerated T cell responses, as shown for T cells within the natural TCR affinity range [109]. In contrast, supraphysiological TCR affinities beyond  $10\mu\text{M}$  did not further improve the *in vitro* and *in vivo* function of T cells in another study [110]. One explanation is that long off-rates prevent the TCR from serially engaging multiple pMHC molecules on the target cell. Prolonged contact duration negatively affects T cell activation, particularly if antigens are present at low levels [109]. A major concern is that affinity-enhanced TCRs partially lose their specificity, which could result in potentially toxic antigen promiscuity. In line with this hypothesis, T cell clones that were selected for strong binding to the model antigen 2C additionally recognized endogenous self pMHCs [111].

In summary, the challenges of using TCRs to engineer therapeutic T cells are isolating suitable TCR genes from scarce tumor-specific T cell populations, overcoming the low avidity of naturally occurring TCRs for self-antigens and designing a genetic construct that ensures high expression and correct pairing of the TCR. Furthermore, the engineered TCRs can only be used to redirect T cells to peptides that are presented in context of the HLA I molecule on the tumor cell. Such tumor targets therefore need to be accessible to the antigen processing and presenting machinery that is often manipulated by immune evasion mechanisms of the tumor.

### 1.2.2.2 Chimeric antigen receptors

Chimeric antigen receptors (CARs) are synthetic molecules that usually contain an scFv of a monoclonal antibody (mAb) as an ectodomain that is covalently bound to a transmembrane domain and an endodomain with signaling capacity derived from CD3 $\zeta$  (first generation CARs). The first study to show that chimeric receptors with this structural pattern can mediate antigen-specific stimulation, IL-2 production and target cell lysis was published in 1993 [112]. The modular structure of CARs offers multiple ways to design receptors with optimized function.

As an absolute pre-requisite, a functional CAR needs to specifically recognize a target antigen, which is mediated by the scFv, i.e. the antigen-binding domains of an antibody's heavy and light chain, usually linked in a linear fashion [113]. Utilizing the wide range of available antibody specificities, this allows for redirection of T cells to

surface-expressed targets in an MHC-independent manner. Suitable tumor targets include proteins, carbohydrates and glycolipids that are either exclusively present on tumor cells, e.g. the splice variant of EGFR (EGFRvIII), or overexpressed by the tumor, e.g. HER2, GD2 and CAIX and more [114]. In addition, CARs are also developed to target lineage-specific markers, e.g. CD19 or CD20, for treating hematological malignancies.

As stated before, the affinity of a receptor is a major determinant of its function, providing the rationale for developing affinity-enhanced TCRs. The analysis of a range of HER2-specific CARs with different affinities confirmed that increasing the CAR affinity correlates with better T cell activation [115]. Similar observations were made with two CARs against the same epitope of the receptor tyrosine kinase-like orphan receptor ROR1 that is expressed on many human tumors [116]. The high affinity CAR mediated superior function, reflected in higher amounts of secreted cytokines and greater proliferation of stimulated T cells. However, increasing the affinity beyond the putative threshold of  $10^{-8}$  M did not induce a more potent target cell lysis [115]. In fact, low-affinity T cells displayed better selectivity as they were only activated by tumor cells overexpressing the target antigen and not by healthy cells. Still, the question whether there is an affinity threshold for optimal CAR signaling requires further investigation.

More recent investigations addressed the role of the spacer that resides between the scFv and the transmembrane domain. It is commonly derived from the constant domain of a human immunoglobulin (Ig), provides flexibility and regulates the distance between the CAR-T cell and its target cell. To study the effect of spacer length, Hudecek *et al.* introduced a long, intermediate and very short spacer, derived from IgG4, into CAR constructs that are specific for an epitope at the interface of the Ig and Frizzled (Fz) domains of ROR1 [116]. Both *in vitro* and *in vivo* function were superior when T cells were transduced with the short spacer CAR. Interestingly, if the CAR does not recognize a membrane-distal, but a membrane-proximal epitope, e.g. within the Kringle domain of ROR1, the opposite result was found, as only the long spacer-CAR led to full T cell activation [117]. This suggests that the optimal CAR design needs to be determined for each epitope individually. These findings allude to the opposing characteristics of spacers: 1) a short spacer reduces the distance that needs to be overcome by cytolytic molecules, and 2) a long spacer provides flexibility which is important for binding epitopes that are not easily accessible, e.g. due to a membrane-proximal position. Earlier work supports the hypothesis that antigen position can be

important for proper T cell activation. Using CARs specific for two different epitopes of the carcinoembryonic antigen (CEA), it was shown that targeting a membrane-proximal epitope led to more efficient activation [118].

A lot of work focused on the role of the intracellular part of the CAR that is essential to induce T cell activation via the CD3 $\zeta$  domain. On the basis of the physiological TCR signaling network, one or more costimulatory domains were integrated into the design of second and third generation CARs, respectively. The most frequently used costimulatory molecules include CD28 that engages the PI3 kinase signaling pathway, and OX40 as well as 4-1BB, that recruit the TNF receptor adaptor proteins [114]. Including CD28 in the CAR construct did not alter the antigen threshold for activation or the affinity of the receptor, but it allowed for IL-2 production independent of endogenous costimulation. Thereby, the proliferation and long-term function of CAR-T cells was improved [119, 120]. Even more, CARs with the 4-1BB costimulatory domain endowed T cells with superior cytotoxicity [121].

Equipping the CAR construct with own signaling and costimulatory domains allows for CAR-mediated signaling that is completely independent of the endogenous TCR, as conclusively demonstrated in T cells by knocking out the TCR $\alpha\beta$  expression [122]. Nevertheless, CARs that are designed with a CD3 $\zeta$  transmembrane domain can associate with the endogenous TCR complex, yielding better antigen sensitivity [123]. On the other hand, CARs containing a CD3 $\zeta$  transmembrane domain were shown to be less stable on the cell surface than CARs with CD28-derived domains, which are therefore widely used as transmembrane domains [124]. The mechanism of CAR signaling is not completely understood. Upon ligand binding, CARs most likely dimerize and thereby enable phosphorylation of the intracellular ITAMs of the CD3 $\zeta$  domains and recruitment of endogenous components of the TCR downstream signaling network [114]. CAR-engineered T cells are still able to signal through their natural TCR, which has permitted the comparison of the qualities of CAR- and TCR-mediated signaling in the same cell. The level of activation through the CAR and the TCR in bispecific T cells were comparable with regard to early downstream signaling (e.g. phosphorylation of CD3 $\zeta$ , ZAP70 and ERK) and induced proliferation [125]. This is a surprising finding as TCRs and CARs largely differ in receptor affinity; on the one hand, low-affinity TCRs require serial engagement of multiple pMHCs and integration of signals for full activation. On the other hand, CARs are based on antibodies with high affinity of  $10^{-9}$  to  $10^{-12}$  M yielding very different binding kinetics [67]. Presumably, one binding event

could lead to activation of the CAR, which in turn would not require the full formation of a complex immunological synapse as described for TCR-mediated signaling. Thus, CAR signaling is possible in T cells with impaired endogenous mechanisms of TCR signaling, such as synapse formation and costimulation. This kind of hyporesponsive state is characteristic of T cell exhaustion and in fact, it has been shown that the functionality of exhausted T cells can be rescued by introducing CARs [126].

In contrast to TCRs, CARs recognize any surface-expressed molecule that does not need to be presented on MHC class I. Thereby, T cells engineered with CARs may be effective for tumors that have downregulated MHC expression or impaired antigen processing. CAR-T cells may also be applied to a wide range of different tumors for which peptide antigens presented by MHC have not been identified. However, intracellular tumor-specific proteins, such as bcr-abl, cancer/testes antigens and others, can only be detected by TCR-engineered T cells, as these targets remain invisible to typical CAR-engineered T cells [88]. Recently, it has been described how to produce antibodies against HLA-restricted peptides, which might facilitate the generation of CARs targeting pMHCs [127].

Identifying targets that are unique for tumor cells is still a major hurdle for developing highly specific cellular therapies. Many potential target molecules for CARs and TCRs are also expressed on some normal cells in addition to tumor cells. Several approaches aim at improving selective recognition of tumor cells, taking advantage of the modular structure of CARs. Combining two specificities in a single CAR has been demonstrated in a proof-of-concept study [128]. These so-called TanCARs are generated by linking two different variable antibody fragments and allow for dual targeting with synergistic effects on activation. This strategy could serve different purposes, e.g. improving the distinction between tumor and healthy tissue or targeting both the tumor and its microenvironment. Appropriate antigen candidates need to be selected and scFv affinities need to be fine-tuned to optimally utilize a multiplexed CAR. Another strategy is based on introducing an inhibitory CAR (iCAR) in addition to a usual tumor-specific CAR into a T cell [129]. Sadelain and colleagues could demonstrate that the PD-1 or CTLA-4-based iCARs inhibit T cell proliferation and effector functions that are induced by activating CARs or an endogenous TCRs. If the iCAR is directed against a universal antigen that is expressed on healthy cells, this approach would provide a tool to prevent unwanted toxicities.

In an attempt to uncouple designed receptors from a defined specificity, ‘universal receptors’ were developed. They comprise a streptavidin or a FITC binding moiety that allows for binding of biotinylated or FITC-conjugated antibodies or small molecules, respectively [130, 131]. Selecting and mixing reagents with different specificities offers the possibility to switch and multiply antigen specificity of an otherwise inert chimeric receptor on demand. While such new developments hold promise to facilitate CAR modulation after transfer into the patient, further investigation is required to show *in vivo* applicability. The knowledge about individual CAR components is accumulating and CAR designs evolve beyond the initial structure, but it is yet unclear whether observations made *in vitro* and in mouse models will translate into valid concepts for clinical application.

### 1.2.3 Clinical experience with gene-modified T cells

An increasing number of clinical trials demonstrated that autologous T cells can be engineered to express a tumor-reactive TCR or CAR, propagated *in vitro* and adoptively transferred back to the patient (Fig. 1-2). Until today, TCR-engineered T cells are mainly being tested in melanoma and sarcoma patients, while most clinical trials with CAR-modified T cells are performed in patients with B cell malignancies. The clinical benefit of initial studies with TCR-engineered T cells was only transient and limited to few patients, as the persistence and efficacy of transferred T cells was low. Thus, the primary aim of research in the last three decades was to develop functional transgenic receptors and efficient T cell products. Changes in the receptor design indeed improved the survival and function of T cells, but also revealed safety issues of transferring long-lived and highly potent T cells into patients. As unexpected toxicities have been encountered, it is now becoming evident that much has to be learned about managing the risks of immunotherapies.

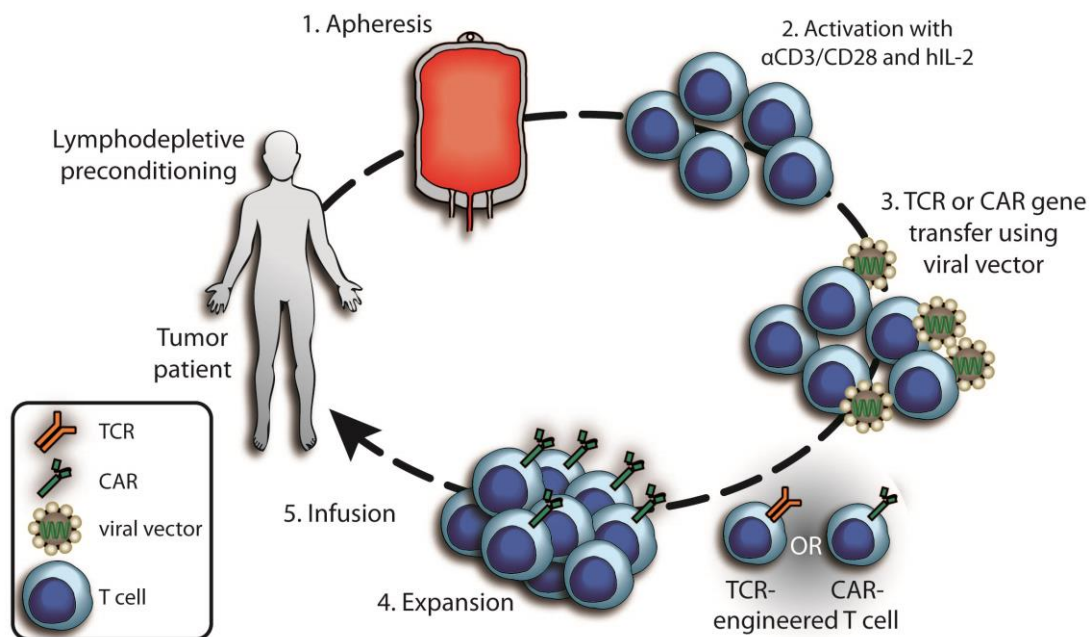


Fig. 1-2: Scheme of adoptive cell therapy using gene-engineered T cells. Autologous T cells are obtained by apheresis, activated with anti-CD3/CD28 in presence of hIL-2 and genetically modified by viral vectors to express a tumor-specific TCR or CAR. After *in vitro* expansion of gene-engineered T cells, they are infused into the tumor patient that has been lymphodepleted prior to cell transfer. hIL-2: human interleukin-2, TCR: T cell receptor, CAR: chimeric antigen receptor.

### 1.2.3.1 Clinical studies with TCR- and CAR-engineered T cells

Morgan *et al.* performed the first study that examined the feasibility and safety of using TCR-engineered lymphocytes to treat a tumor [132]. In this study, 2 out of 13 melanoma patients had a complete response, when transfused with T cells that were engrafted with a MART-1-specific TCR by retroviral transduction. In the responding patients, T cells could be tracked up to 20 months after transfer by quantitative polymerase chain reaction (qPCR), staining for the V $\beta$ 12 chain of the transgenic TCR or binding of MART-1 tetramers. The different measurements yielded discordant numbers of persisting cells, which indicated the need for suitable tracking markers to reliably quantify gene-marked cells. As MART-1 is also expressed in melanocytes, tumor regression was commonly associated with skin toxicities [77, 133]. Therefore, succeeding studies examined alternative target antigens that were not expressed in normal melanocytes. The cancer/testis (CT) antigen NY-ESO-1 is a promising candidate because it is expressed in a variety of cancers, but not in healthy tissue except in testis [134]. In a small study, 17 melanoma patients and 6 patients with synovial cell sarcoma were treated with T cells that were engrafted with a NY-ESO-1-specific TCR. Clinical responses were observed in five and four patients, respectively [134]. For the first time, this trial demonstrated the efficacy of TCR-transduced T cells targeting tumors other than melanoma. Infusions were generally well-tolerated, but only minimal expansion and persistence *in vivo* was reported, when utilizing physiological self-antigen-specific TCRs with rather low tumor-reactivity.

Similar disappointing observations were made in initial studies using T cells engineered with first generation CARs to treat patients with advanced ovarian cancer or neuroblastoma. After transfer, CAR-T cells were barely detectable in the blood and did not induce a clinical response [135, 136]. Second generation CARs were developed by including a costimulatory domain in the signaling module; they improved antitumor activity in animal models [137] and led to major breakthroughs in the clinic. For direct comparison, six lymphoma patients simultaneously received T cells that were transduced either with a first generation CD19-specific CAR with CD3 $\zeta$  (CD19-CD3 $\zeta$ -CAR) or with the same CAR that additionally contained the CD28 signaling domain [124]. This second generation CAR indeed mediated better expansion and persistence of CAR-T cells *in vivo*. Durable anti-tumor responses were demonstrated in other studies with CD19-CD28/CD3 $\zeta$ -CARs in advanced, progressive B cell malignancies [138], follicular lymphoma [139] and acute lymphoblastic leukemia [140, 141]. Impressive clinical results were also obtained with a CD19 CAR implementing 4-1BB

as the costimulatory domain in a trial performed by June and colleagues. Two out of three patients with chronic lymphocytic leukemia had complete remissions, sustainable for 10 months. Here, persistence of engineered cells was demonstrated in blood and bone marrow at high levels for at least six months, resulting in elimination of leukemic cells and normal CD19<sup>+</sup> B cells due to expected on-target toxicity [142, 143]. Treatment with next generation CARs was commonly accompanied with a cytokine release syndrome due to significant T cell expansion *in vivo*. Elevated levels of cytokines can usually be curtailed by treatment with steroids or antibodies that specifically inhibit IL-6 (tocilizumab) or TNF- $\alpha$  (infliximab) [138, 140]. In some cases, the cytokine storm posed a severe risk to the patient's health, so clinical protocols need to be established to ameliorate these symptoms [144].

Beside hematological malignancies, researchers explore the use of CAR therapies to treat solid tumors, which is associated with additional challenges [113]. First, CAR-T cells need to migrate to the site of a solid tumor tissue as opposed to hematological malignancies, where tumor cells and T cells circulate in the same compartment. Second, T cells need to overcome the mechanisms of immune suppression in the tumor environment. Third, identifying tumor-specific antigens is still a major issue, which has been bypassed in B cell malignancies, for example, by targeting the lineage-specific antigen CD19. These hurdles became apparent during the evaluation of first-generation CARs specific for carbonic anhydrase (CAIX), folate receptor  $\alpha$  (FR- $\alpha$ ) and disialoganglioside GD-2 in patients with different solid tumors. The main limiting factors were lack of persistence [145, 146], no evidence of anti-tumor activity and failure of homing to tumor tissue [135]. Clinical experience with next-generation CARs in solid tumors is limited to few trials. While second generation HER2-CARs were not efficient in osteosarcoma patients [114], third generation HER2-CARs resulted in lethal toxicity [147]. Better safety profiles might be achieved with CAR-T cells directed against antigens that are more specifically expressed in the tumor, such as EGFRvIII in glioma. Third-generation CARs were evaluated on *ex vivo* EGFRvIII<sup>+</sup> tumor cells and are currently tested in the clinic [114, 148]. To overcome the low efficacy of CAR-T cells against solid tumors, alternative targets have been proposed, including the stroma-associated Fibroblast activation protein (FAP) [149] or vascular endothelial growth factor receptor 2 (VEGFR-2) on tumor vasculature, which are explored in ongoing clinical trials [114, 150].

Beyond selection of appropriate targets and receptor design, other strategies are investigated to enhance *in vivo* expansion and efficacy of CAR-T cells. Clinical protocols of ACT commonly include pretreatment with lymphodepleting drugs as well as addition of immunostimulatory cytokines, e.g. IL-2 and IL-15 [114]. Transferred T cells can also be specifically expanded through their native TCR, as shown for CAR-modified EBV-specific T cells upon transfer into EBV-seropositive tumor patients [151]. Finally, immune suppressive signals can be averted to prevent exhaustion and boost functionality of infused T cells, e.g. via a PD-1 blocking antibody [152].

### 1.2.3.2 Risks of current approaches

The on-going development of improved transgenic receptors includes affinity-enhanced TCRs and next-generation CARs that mediate better and more sustainable anti-tumor responses. Yet, more potent ACTs often harbor the risk of severe and sometimes unpredicted on- and off-target toxicities due to the non-physiological nature of gene-modified T cells. In two clinical trials, T cells were engrafted with a high avidity MART-1 or CEA-specific TCR, that were both generated in HLA-A2 transgenic mice, and led to on-target toxicities due to low expression of the targeted antigens in healthy tissues [153, 154]. Unpredicted on-target toxicities were encountered when targeting CAIX with CAR-redirectioned T cells due to previously unknown expression of CAIX in the liver [146]. Albeit these adverse effects were severe, the destruction of healthy tissue could be halted by administration of steroids and cessation of the T cell therapy.

In order to further improve ACT efficacy, TCRs were artificially optimized by affinity maturation, which unfortunately led to lethal toxicities in two clinical trials. In one case, an affinity-enhanced MAGE-A3/A12-specific TCR was introduced into T cells of nine patients that predominantly suffered from melanoma and mediated on-going tumor regression in two patients [155]. Neurological toxicities were reported in two individuals and could be attributed to the previously unknown expression of MAGE-A12 in a rare subpopulation of neurons in the brain. Hence, this optimized TCR is able to recognize multiple peptides from the MAGE-A family (MAGE-A2, -A6, -A12), which gives reason for caution in choosing such a multi-reactive TCR for therapy [156]. In the other trial, T cells carried a different MAGE-A3-specific affinity-enhanced TCR and led to cardiac toxicity and two deaths within few days after T cell transfer into patients with stage III/IV melanoma [157]. In a follow-up study, a heteroclitic epitope was found in the unrelated protein titin that is expressed in beating cardiac and skeletal muscles [158]. Importantly, the wildtype MAGE-A3 TCR did not show cross-reactivity to titin in a

beating cardiomyocyte culture. This report reveals the risk of affinity-enhanced TCRs to acquire additional reactivities against unrelated peptides, which needs to be curbed by detailed pre-clinical evaluation of the TCR specificity and by exploring strategies to rapidly eliminate toxic T cells.

For CAR-T cell therapy, similar correlations between improved receptors and higher incidence of toxicities should apply as for the use of TCR-engineered T cells. In fact, the transfer of T cells that were engineered with a third generation HER2-specific CAR led to the death of a colon cancer patient, which was caused by destruction of lung epithelial cells that expressed low levels of HER2 [147]. Apart from this case, all other published clinical trials involved CAR-T cells that target the lineage-specific antigens CD19 and CD20. Effective treatment of B cell malignancies with CD19- or CD20-specific T cells will inevitably result in B cell depletion as the main on-target toxicity [88]. The resulting hypogammaglobulinemia can be treated by intravenous infusions of immunoglobulins (IVIG). Even if IVIG therapy is usually well-tolerated, it might be beneficial to eliminate CAR-T cells after they completely eradicated the tumor to allow for complete recovery of B cell functions.

Additional risks by transferring genetically modified T cells are inherent to the transgene itself. Both TCRs of murine origin and CARs that comprise a murine scFv might elicit an immune response upon transfer into a human patient. The immunological rejection of the T cell graft obviously restricts the duration of the T cell-mediated therapeutic effects, as shown in several cases [98, 159, 160]. Other components of the artificial receptors or their fusion sites can also be immunogenic. For example, the immunogenicity of the virus-derived 2A peptide was under much debate, as it remains partly on the upstream protein and is therefore part of the ectodomain of TCRs or CARs. However, no cytotoxic T cell response was elicited by 2A peptide mixtures in *ex vivo* cultures derived from 16 donors [161]. Although unfavorable for treatment outcome, the risk of immunogenicity of the transgenic receptors should not pose a severe threat to the patient's health.

More importantly, the risk of insertional mutagenesis needs to be examined by long-term follow up of patients infused with genetically modified cell products. T cells are commonly transduced with retroviral vectors that preferentially integrate in the vicinity of active promoters, posing a risk of altering gene transcription [162]. This was observed in CD34<sup>+</sup> bone marrow cells that were retrovirally transduced with the common  $\gamma$  chain from the IL-2 receptor to treat X-linked severe combined

immunodeficiency (SCID-X1) [163]. Success of the gene therapy was overshadowed by the occurrence of lymphoproliferative disease, which was most likely caused by the transgene integration into the promoter of the LMO2 proto-oncogene resulting in enhanced expression of LMO2. More recently, the safety of retrovirally transduced T cells was addressed in a long-term follow-up study of HIV patients [164]. After engineering T cells with a CD4 $\zeta$  CAR to mediate recognition of the gp120 envelope protein on HIV-infected cells, CAR-T cells were transferred into HIV patients and persisted for more than 10 years. The transgene expression was shown to be stable over time and no expansion of dominant T cell clones was detected by integration site analysis. In line with this finding, Recchia *et al.* demonstrated safety of retrovirally transduced donor lymphocytes, despite integration around active promoters [165]. Evidence is accumulating that the risk of insertional mutagenesis is not inherent in retroviral vectors, but rather dependent on the cell type. Using HIV-based lentiviral (LV) vectors for genetic modification appears to be safer, because they do not have a preferential site of integration [166]. LV vectors have already become the system of choice for many clinical applications and no safety issues have been reported up-to-date [81].

Employing a non-viral based transduction system seems appealing to overcome technical issues for clinical grade integration of recombinant TCR- or CAR constructs. One approach is based on the Sleeping Beauty transposon/transposase system, which is usually combined with introduction of transgenes by electroporation. To assess the insertion sites in this system requires investigations in a clinical setting, such as the initiated clinical trial with CD19 CAR-T cells [167].

Altogether, major safety issues of adoptive immunotherapy with engineered T cells are associated with the acquired T cell reactivity against healthy cells, rather than the introduction of transgenes itself. The Recombinant DNA Advisory Committee of the NIH highlighted the need of careful dose-escalation protocols and discussed the potential to limit late toxicities by including suicide genes into the T cells [168].

### 1.3 Strategies to increase efficacy and safety of ACT

Improving the efficacy and safety of adoptive therapy with TCR and CAR-modified T cells requires efficient methods for purifying transduced cells of defined composition to allow analysis of a potential dose/response relationship. Further, monitoring of *in vivo* efficacy will rely on methods to track cell migration and persistence, as well as strategies regulating the survival of cells to reverse toxicities whenever necessary. So far, clinical studies were performed with gene-modified cell products that were highly heterogenous in their composition, i.e. differentiation status and phenotype of modified cells, which makes more conclusive analyses of individual parameters and their effect on clinical outcome impossible. Therefore, methods for improved cell processing are currently developed to facilitate generation of pure, well-characterized and highly functional cell products. To assess the therapeutic effect of transferred cells, it is important to monitor cell persistence and trafficking to tumor sites. Gene-modified T cells can be equipped with tracking markers that can be used to detect the cells in patient samples. Current methods are usually restricted to peripheral blood or tumor biopsies, but it would be favorable to assess the distribution of infused cells in the whole organism. Thus, non-invasive *in vivo* imaging modalities are in the process of development for the use in ACT. Better monitoring tools might, for example, reveal T cell expansion at off-tumor sites and unpredicted T cell-mediated attack of healthy tissue, urging clinicians to abrogate potentially harmful responses. This should best be achieved by selective elimination of the adoptively transferred gene-modified cells. Therefore, several research groups are currently focusing on the implementation of suicide genes that can mediate specific and efficient T cell depletion.

#### 1.3.1 Composition of the T cell product

Several important properties relevant for optimal adoptive T cell therapy have been identified: the cells need to migrate to tumor sites, proliferate upon specific stimulation, exert cytotoxic function and persist sufficiently long to eradicate all tumor cells. Different qualities have been attributed to distinct T cell subsets, and it has been subject to detailed analysis whether the functional profiles of different T cell subpopulations affect their capacity to confer durable tumor responses upon adoptive transfer. So far, research groups mainly focused on CD8<sup>+</sup> T cells subdivided into naïve,

memory and effector subsets. Effector T cells, being the cell type with the highest cytolytic capacity, did not yield best therapeutic effects, which at first glance seems contradictory [169]. In fact, T cell clonotypes that differentiated into end-stage effectors *in vivo* more slowly than others also showed better persistence, which was correlated with a sustained tumor regression [169]. Several ACT trials confirmed the correlation between long-term survival of infused T cells and clinical benefit [88].

Long-term persistence is mainly ascribed to the memory T cell compartment due to its ability to proliferate in response to homeostatic cytokines. Two major memory subsets are known, Tem with immediate effector functions, and Tcm with both a high proliferative capacity and the ability to generate new effector cells. To determine the *in vivo* behavior of Tem and Tcm upon transfer, Berger *et al.* generated effector T cell clones from isolated CMV-specific Tem or Tcm and transferred the clones into macaques [170]. While Tem-derived T cell clones survived in the peripheral blood for less than a week, Tcm-derived clones could be detected long-term in blood, lymph nodes and bone marrow. Prolonged monitoring of the animals revealed that Tcm-derived clones persisted for more than four years [117]. In culture, T cell clones from both subsets consisted mostly of cells with an effector phenotype and had equal cytolytic functions. *In vivo*, however, the different T cell clones behaved distinctly, as only Tcm-derived T cell clones reacquired phenotypic markers of central memory T cells, migrated to memory cell niches in lymph nodes and bone marrow and were capable of proliferating upon antigen challenge [170]. These results were confirmed with human Tcm- and Tem-derived effector cells transferred into Nod/Scid/ $\gamma$  chain null mice [171]. Consequently, Tcm were suggested as a promising candidate for long-lasting therapeutic effects.

Naïve T cells are an interesting subset for ACT due to their capacity to repopulate the entire spectrum of memory and effector T cell subsets. It was demonstrated that a single antigen-specific naïve T cell can be sufficient to derive effector and long-lasting memory T cells in normal recipient mice upon immunization [172]. This enormous proliferative and differentiating potential has also been documented in tumor mouse models [173]. Here, naïve T cells mediated superior anti-tumor immunity, proliferated to a greater extent and produced higher levels of cytokines after transfer when compared to Tcm [75].

An additional subset named 'stem cell-like memory T cells' (Tscm) has been described and allocated to reside between Tn and Tcm subsets due to its unique surface marker profile (CD45RA<sup>+</sup>, CD62L<sup>+</sup>, CD28<sup>+</sup>, CD95<sup>+</sup>) [174]. It has been hypothesized that Tscm account for maintenance of the memory pool by homeostatic proliferation. T cells with a Tscm phenotype were first identified *in vivo* in a mouse model by Zhang *et al.* [175]. In humans, a subset in the memory compartment with self-renewal capacities was identified according to the Tscm phenotype and could also be generated *in vitro* from naïve T cells [174]. Upon transfer into humanized mice, these cells had better proliferative capacity and induced more potent anti-tumor responses as compared to Tcm. Whether this subset is a truly distinct cell type still awaits further verification. However, repetitive transfer of single Tcm cells over generations of mice revealed unequivocally that Tcm fulfill all criteria of tissue stem cells [176]. These results challenge the idea that Tscm represent a distinct subset that is necessary to maintain long-term memory.

If a defined cell population, e.g. Tcm, should be used for the generation of a cell product, it first needs to be purified. Most commonly, blood is used as the primary source for isolation. As CD8<sup>+</sup> Tcm frequencies in the blood are highly variable and often below 5% [177], suitable cell selection methods need to be robust, specific and efficient. This is even more challenging since cell subsets can only be distinguished from others by a set of phenotypic markers. For example, human CD8<sup>+</sup> Tcm are characterized by the simultaneous expression of CD8, CD62L and CD45RO. Clinical cell selection of defined populations is in most cases done with magnetically labeled antibodies. Here, positively labeled cells can be retrieved within a magnetic field and thereby separated from unlabeled cells. It is difficult to perform positive selection for different markers with available technologies, therefore an indirect approach of magnetic Tcm selection based on a negative selection step to remove CD4<sup>+</sup> helper T cells, CD14<sup>+</sup> monocytes and CD45RA<sup>+</sup> naïve T cells, followed by a positive selection of CD62L<sup>+</sup> cells that segregates central memory from effector memory T cells has been established [125]. However, besides relatively high costs (especially for GMP conditions), highly variable purities and yields limit the applicability of this strategy. A novel technology based on *Streptamers* allows for removal of the selection reagent and facilitates serial positive enrichments [178]. Fab *Streptamers* are composed of low-affinity Fab fragments that are multimerized on a *Strep*-Tactin backbone for stable binding. By linking *Streptamers* to magnetic beads, they can be used for magnetic enrichment of a cell population. To remove the *Streptamer* reagent from the cell

surface, the multimer is disrupted by adding D-biotin, which is a high-affinity competitive ligand for the *Strep*-Tactin binding sites. Residual Fab monomers spontaneously dissociate from the cell, which is subsequently completely label-free. With such reversible selection reagents it is for the first time possible to enrich Tcm by three sequential positive selections of CD8<sup>+</sup>, CD62L<sup>+</sup> and CD45RO<sup>+</sup> T cells [178]. As the *Streptamer*-based technology facilitates cell selections with higher purities and yields compared to former protocols, it is currently integrated into an on-going clinical trial with CAR-engineered Tcm. This cell selection method can also be applied to other T cell subsets, for example CD4<sup>+</sup> T cells that might be utilized to support infused cytotoxic T cells based on a recent study on the beneficial effect of CD4<sup>+</sup> CAR-T cells upon transfer into tumor-bearing mice [117].

A uniform and highly effective cell product should not only be based on a defined cell subset as the source for genetic modification, it should also contain cells with similar transgene expression. In currently generated cell products, however, the frequency and expression level of CAR-modified T cells is highly variable due to unstable transduction efficiencies. Therefore, strategies are explored to specifically enrich for successfully engineered T cells. This can for example be done by the use of a transduction marker that indicates the CAR expression level of individual cells.

### 1.3.2 Clinical tracking of transferred T cells

The clinical effect can be evaluated by monitoring the *in vivo* persistence, migration to tumor sites and bioactivity of infused T cells. For cell tracking, it is essential to be able to distinguish transferred and endogenous cells by using genetic or surface markers. The initial concept of gene marking was to track regeneration of the hematopoietic system after HSCT [179]. In early studies, the antibiotic resistance gene *neo* was extensively used to selectively grow gene-marked cells by adding the antibiotic G418 during cell culture, and to detect gene-marked cells by PCR using specific primers [180]. For tracking of TCR- or CAR-engineered T cells, PCR primers can be designed to specifically target the unique genetic sequences of the transgene. PCR-based methods can be employed to monitor the presence of genetically modified cells in patient samples, but they do not provide information on phenotypic and/or functional attributes at the same time. The use of surface markers for cell tracking allows to integrate a range of additional information regarding cell phenotype, activation status

and homing preferences based on polychromatic flow cytometry [181]. As cell surface markers have been widely used for cell tracking, the properties of an 'ideal' surface marker for a clinical cell product can be outlined as follows: (i) stable cell surface expression, (ii) no immunogenicity, (iii) being functionally inert (iv) clear distinction between gene-modified and endogenous cells, either alone or in combination with other markers, (v) in parallel suitability for cell selection.

One example for such a marker already in clinical use is the truncated nerve growth factor receptor  $\Delta$ NGFR [182]. It was derived from the human NGFR, truncated intracellularly to prevent any NGFR-mediated signaling and did not affect T cell function [183]. As the endogenous NGFR is not expressed on hematopoietic cells, the marker  $\Delta$ NGFR mediates specific detection of gene-engineered cells in blood samples.  $\Delta$ NGFR-expressing cells can also be enriched *in vitro* by using commercially available NGFR-specific antibodies. For these reasons, the  $\Delta$ NGFR was frequently used as a tracking and selection marker in several clinical studies that confirmed safety of this marker in humans [184].

Other truncated surface molecules, such as tCD19 or tCD34, were also used as tracking markers [180]. They met the basic criteria of being stably expressed, functionally inert and non-immunogenic. The tCD19 or tCD34-modified cells can be specifically detected in the blood if additional markers are stained to discriminate engineered cells from endogenous CD19<sup>+</sup> B cells or CD34<sup>+</sup> HSCs, respectively. Both tCD19 and tCD34 are also suitable targets for immunoselection methods. As techniques for magnetic cell purification have been adapted to GMP-compliance, an increasing number of clinical processing protocols now integrate a selection step. This procedure is believed to make the transfer of gene-modified T cells more predictable, since the number and quality of transferred cells can be better controlled. Furthermore, with prior enrichment of cells that stably express the selection marker, all transferred cells can be tracked *in vivo* and correlated with therapeutic or adverse effects. This is difficult to achieve if a fraction of the cell product expresses no or only low levels of the transgene.

The fate of infused cells is most commonly monitored in blood samples. Blood analyses might be sufficient to assess the effect of the T cell therapy in patients with hematological diseases. However, it would be desirable if T cell trafficking could additionally be studied in peripheral tissues, for example to document efficient infiltration into a solid tumor, and also when toxicities in tumor-free healthy organs

occur. *In vivo* imaging in principle enables fast and non-invasive localization of infused cells at any site in the body. In preclinical research, optical imaging of bioluminescent or fluorescent reporter proteins is heavily used in small animals. In humans, optical tracking is restricted to surface tissues due to the low penetration depth of light. More suitable imaging modalities to monitor patients include positron emission tomography (PET) and magnetic resonance imaging (MRI). Cells can be directly labeled *ex vivo* with magnetic nanoparticles for MRI or radionuclides for PET imaging [181]. For long-term monitoring, cells need to be engineered to express a reporter gene that is able to bind, take up or metabolize a probe that can be injected anytime into the patient. *In vivo* T cell imaging by PET was first demonstrated by Yaghoubi *et al.*, where the Herpes Simplex virus 1 thymidine kinase (HSV1-TK) served as the reporter gene that mediated accumulation of the radio-labeled probe [<sup>18</sup>F]FHBG inside T cells [185]. After infusing tumor-specific, HSV1-TK<sup>+</sup> T cells into a glioma patient, [<sup>18</sup>F]FHBG was applied and radioactivity indicated T cell trafficking to the tumor site. Although feasible, *in vivo* imaging of infused T cells still requires further development to overcome technical difficulties regarding selectivity of the probe, resolution of the imaging and correct localization of labeled cells.

### 1.3.3 Suicide gene systems

Gene markers can also be designed to mediate specific elimination of gene-modified cells, which would enable clinicians to reverse toxicities. For example, as a long-term side effect, persistent B cell aplasia has been observed during CD19 CAR-T cell therapy when transferring cells that are capable of surviving in the patients for many years. If complete and sustained tumor regression has been achieved, it might be justified to deplete CD19 CAR-T cells via an effective suicide mechanism to let the normal B cell compartment recover. Recent reports on acute toxicities after ACT highlight the risk of unexpected T cell attack against healthy tissue. In such situations it would be of particular relevance to be able to deplete the harmful cells via suicide genes. If toxicities are severe, T cells need to be eliminated early during the course of therapeutic intervention, which also averts any therapeutic activity of the cells. As toxicities mainly depend on expression of the introduced receptor, an alternative safety strategy would be the integration of an on/off switch that regulates transgene expression without irreversibly destroying the cells [117]. One possibility to achieve this is to introduce an RNA-based regulatory system that controls gene expression in

response to drug input [186]. This and other strategies hold promise that *in vivo* T cell activity could be regulated on demand, but require further validation to be used in humans. As TCR- and CAR-engineered T cells are moving into clinical application fast, many research groups work on solutions that can readily be used in clinical settings.

### 1.3.3.1 Drug-based suicide mechanisms

The first and most widely studied suicide marker is based on the use of the Herpes Simplex virus thymidine kinase (HSV-TK) (Fig. 1-3). The virus-derived enzyme converts the pro-drug ganciclovir into its active form, acting as a nucleotide analog that aborts DNA chain elongation in proliferating cells [183]. Ganciclovir is not recognized by the human thymidine kinase, which makes this drug highly specific for engineered cells. This safety strategy was successfully used for controlling GVHD after allo-HSCT under highly immunosuppressive circumstances [187]. The main limitation of this approach is the immunogenicity of HSV-TK that was shown to lead to rejection of infused cells in immunocompetent individuals [188]. The use of HSV-TK also excludes ganciclovir as a therapeutic option to treat reactivating CMV in immunosuppressed patients.

More recently, a caspase suicide construct (iCasp9) was evaluated in patients that received virus-specific T cells for protection against viral infection after HSCT [189]. The synthetic drug AP1903 causes dimerization of iCasp9 that initiates the intracellular caspase cascade, ultimately leading to cell apoptosis. Upon administration into T cell graft recipients, the dimerizing drug eliminated over 90% of transferred cells within 30 minutes. Symptoms of T cell-induced GVHD were abolished without reoccurrence, while few residual virus-specific T cells mediated long-term viral control. As compared to HSV-TK, the iCasp9 suicide gene was entirely based on human sequences and was therefore non-immunogenic. It also mediated faster clearance of the cells. However, the limited availability of the dimerizer constrains the broader application of the iCasp9 suicide gene in clinical studies. In addition, it is difficult to utilize intracellular suicide constructs for cell selection and *in vivo* tracking. Thus, additional surface markers were integrated into transduction constructs, for example  $\Delta$ NGFR in combination with the HSV-TK construct and tCD19 in the iCasp9 approach. Including multiple markers for different purposes will eventually exceed the limited capacity of viral vectors and increases the chances for subpopulations that lack expression of individual components; hence it would be advantageous to develop a multifunctional marker.

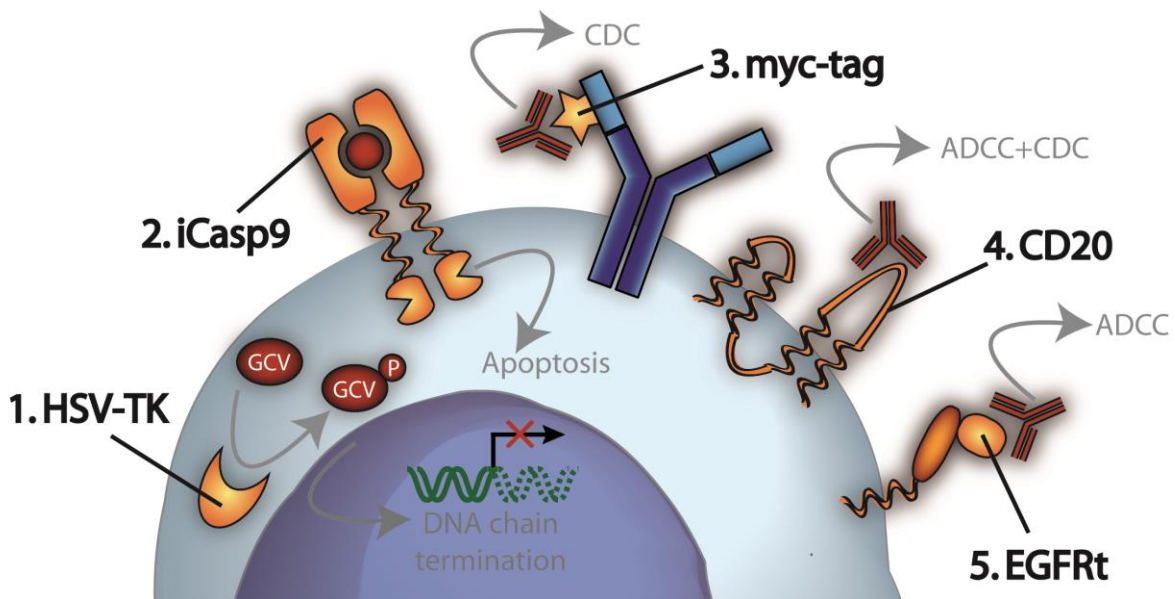


Fig. 1-3: Safety mechanisms in genetically engineered T cells. 1. Herpes Simplex virus thymidine kinase (HSV-TK) monophosphorylates (P) the pro-drug ganciclovir (GCV) that causes termination of DNA chain elongation. 2. The inducible Caspase 9 (iCasp9) is dimerized and activated by AP1903 (red circle) to induce apoptosis. 3. The myc-tag (yellow star) at the TCR is targeted by an anti-myc mAb for complement-dependent cytotoxicity (CDC). 4. The CD20 is bound by the anti-CD20 mAb Rituximab for antibody-dependent cellular cytotoxicity (ADCC) and CDC. 5. The truncated epidermal growth factor receptor (EGFRt) is detected by the anti-EGFR mAb Cetuximab that mediates ADCC.

### 1.3.3.2 Antibody-dependent depletion mechanisms

A cell surface marker can fulfill multiple functions because it can be accessed by selection reagents as well as by depleting antibodies for target cell lysis. One example for an antibody-mediated depletion mechanism is based on the use of the human CD20 molecule as a surface marker [190]. Here, cell depletion requires application of a CD20-specific antibody, e.g. Rituximab that is clinically approved for treating B cell lymphoma. Tumor cell lysis is mediated by binding of Rituximab that recruits either cytotoxic cells, e.g. natural killer cells, or the complement system, thereby initiating antibody-dependent cellular cytotoxicity (ADCC) or complement-dependent cytotoxicity (CDC), respectively. These cytolytic mechanisms were redirected to T cells that were engineered with the CD20 gene [191]. *In vitro* studies demonstrated that CD20<sup>+</sup> T cells could be selected and depleted via Rituximab, and the mechanism of depletion was shown to include CDC and ADCC [192]. Efficiencies of cell selection and killing were poor, most likely because CD20 expression was low and unstable. These issues were significantly improved by codon-optimization of the CD20 gene that facilitated efficient *in vivo* depletion of transplanted T cells in Rag-1<sup>-/-</sup> mice [193]. As an adverse effect,

Rituximab treatment inevitably leads to transient depletion of endogenous CD20<sup>+</sup> B cells.

All approaches described so far depend on the introduction of a safety marker in addition to the transgenic receptor. Considering the limited capacity of viral vectors, Kieback *et al.* developed a receptor-intrinsic safety mechanism [194]. Here, a myc-tag, derived from the human transcription factor c-myc, is covalently linked to the variable region of the TCR  $\alpha$  chain. As part of the receptor molecule, the myc-tag seems a reliable marker for elimination of TCRmyc-expressing T cells by using a myc-specific antibody. This was confirmed in an autoimmune diabetes mouse model, where the transfer of self-reactive, myc-tagged T cells induced autoimmune insulinitis. Symptoms of autoimmunity could be reversed by depleting transferred cells with the anti-myc antibody. This safety approach should be specific to myc-tagged T cells, as the endogenous c-myc protein is localized in the nucleus. The human origin of the myc tag argues for low immunogenicity. The major downside of this strategy is the lack of a clinically approved anti-myc antibody, which prevents the direct translation of this elegant strategy to the clinic.

As an alternative safety switch, the human EGFR was rendered functionally inert by removing the extracellular domain I and II – harboring the binding site for endogenous ligands – and the cytoplasmic region to exclude signaling domains [195]. This small truncated EGFR (EGFRt) still contained domain III and IV, including the binding site of the clinically approved anti-EGFR chimeric mAb Cetuximab that can mediate target cell depletion. Coordinated expression of both the safety marker and a CD19 CAR was demonstrated in human T cells. Multiple possible applications could be demonstrated for EGFRt marker expression, including immunomagnetic purification with biotinylated Cetuximab, tracking by flow cytometry and immune histochemistry, as well as *in vivo* elimination of EGFRt<sup>+</sup> murine CTLL-2 (Cytotoxic T Lymphoblast line-2) cells by infusing Cetuximab [195]. While these findings are very promising, some issues still need to be clarified: (i) Magnetic cell selection with conventional antibodies leaves bound reagent, so cells could not be immediately infused into patients. (ii) Cell tracking was performed in immunodeficient mice that lack endogenous T cells. Thus, it has not formally been shown that the EGFRt marker can be used to distinguish between transferred and endogenous cells. (iii) *In vivo* cell ablation was not tested with primary T cells and the time required for elimination was not studied. Importantly, (iv) mice were not tracked after ceasing antibody infusions to exclude outgrowth of few remaining cells, and

elimination was not performed in a setting, where cells were stimulated by antigen. These questions were addressed during the presented PhD thesis to further elucidate whether the truncated EGFR is a versatile tool for controlling engineered T cells.

## 1.4 Cetuximab

A good safety mechanism for engineered T cells requires both a well-designed marker and a suitable drug that mediates cell depletion. One major advantage of using Cetuximab for this purpose is that it has been approved for clinical application based on thorough studies in mouse models and clinical trials. The mechanisms of cell lysis are well-characterized for targeting EGFR-overexpressing tumor cells with Cetuximab and they are in principle compatible with using Cetuximab for T cell depletion. Importantly, only minor side effects were linked to the administration of Cetuximab, hence Cetuximab infusions appear to be a feasible and safe strategy to deplete EGFRt-marked T cells in humans.

### 1.4.1 Mechanism of action

The mechanism by which Cetuximab eliminates EGFR<sup>+</sup> tumor cells is dependent on the nature of its target molecule. EGFR is a 170 kDa transmembrane glycoprotein that belongs to the ErbB family of receptor tyrosine kinases. It can be activated by endogenous ligands, such as EGF and TGF- $\alpha$  that induce conformational changes of the receptor, which was revealed by crystallization of both the monomeric and dimeric form of EGFR [196]. In detail, the ligand binds to the extracellular domain I and III and stabilizes an extended (untethered) conformation which facilitates dimerization through multiple contacts of the dimerizing arm of domain II [197]. As a consequence, the intracellular tyrosine kinases are trans-autophosphorylated and initiate several signaling cascades that are involved in important cellular responses, e.g. cell proliferation, survival, invasion and DNA repair [198]. In the truncated EGFR-derivative, however, ligand binding and signaling are precluded by removing the domains that are involved in EGFR function [195]. The EGFRt can therefore not be targeted by small molecule tyrosine kinase inhibitors (TKIs) that represent a highly effective class of EGFR-specific drugs for inhibiting EGFR signaling. The other therapeutic approach involves monoclonal antibodies, such as Cetuximab that binds within the extracellular domain III of the EGFR. As this domain is preserved in the EGFRt construct, the range of Fab- and Fc-related effects of Cetuximab can potentially be directed against EGFRt-expressing T cells [190].

The Fab domain determines the binding site of an antibody and therefore decides on the antibody's capability to inhibit binding of the ligand to the receptor. Cetuximab binds to EGFR with high affinity ( $K_D = 0.39$  nmol/L) and interferes directly with the interaction of ligand and receptor [199]. It also inhibits the EGF receptor from adopting the activated (tethered) conformation necessary for dimerization [200]. Finally, binding of the mAb to the EGFR can initiate receptor internalization and degradation [201]. All of these Fab-related effects aim at inhibiting EGFR function to attenuate tumor cell growth, rather than to lyse the target cell. Thus, such mechanisms of Cetuximab will not contribute to the depletion of EGFRt-marked T cells.

The Fc part of an antibody can be detected by Fc receptors on immune effector cells, such as natural killer (NK) cells, macrophages and monocytes. Therefore, antibody-coated tumor cells might be eliminated by antibody-dependent cellular cytotoxicity or phagocytosis (ADCC or ADCP). Fc parts can also form a binding site for C1q, which initiates the complement cascade that results in complement-dependent cell lysis (CDC) [190]. In general, these Fc-mediated cytolytic effects are well applicable to T cell elimination strategies. There is a large body of evidence based on *in vitro* studies with human tumor cell lines [202] that ADCC, but not CDC, plays a dominant role in Cetuximab-mediated effects. *In vivo*, anti-tumor function of Cetuximab was decreased in mice lacking NK cells or in FcγR-deficient mice [203, 204]. Further, studies in humans revealed a correlation between FcγR polymorphism and clinical benefit of Cetuximab therapy, confirming that ADCC is the main mechanism of Cetuximab [205]. ADCC can be re-directed to EGFRt-modified T cells, which has already been shown *in vitro* [195].

#### 1.4.2 Application in tumor therapy

Cetuximab is the most widely used EGFR-specific mAb and has therefore been investigated with regard to its application in many different tumors that are associated with abnormal expression of EGFR. As deregulation of EGFR promotes tumorigenesis, angiogenesis and metastasis formation, EGFR is frequently overexpressed in many epithelial tumors, e.g. in 80-100% of head and neck cancers as well as 22-75% of colon cancers [206].

Cetuximab was approved for EGFR-positive metastatic colorectal carcinoma (CRC) in 2004 by the US Federal Drug Administration (FDA). This decision was based on

clinical phase II and III studies that reported response rates of 9-12% for the Cetuximab monotherapy and 17-25% response rates for the combination therapy, comprised of Cetuximab and irinotecan, in CRC patients [207]. The half-life of Cetuximab was reported to be approximately seven days [208], hence it is recommended to start the therapy with an initial dose of 400mg/m<sup>2</sup>, followed by weekly infusions of 250mg/m<sup>2</sup> [209]. Beneficial effects of Cetuximab alone or in combination with radiotherapy were shown in patients with head and neck squamous cell carcinoma (HNSCC) and guided the approval of Cetuximab for HNSCC in 2006 [210]. Cetuximab is currently tested in a number of clinical phase II and III trials for efficacy in other solid tumors of epithelial origin, such as gastric and pancreatic cancer [207].

The main adverse effects that have been linked to Cetuximab treatment were skin-related toxicities that were usually limited to grade 1 or 2 skin rash and occurred in 86% of treated patients [209]. Severe side effects (grade 3 or 4) were observed in 10-15% of patients and no life-threatening side effects were reported. Other dermatologic adverse effects also occurred, e.g. erythema and acne. These side effects might be associated with endogenous EGFR expression in keratinocytes and skin fibroblast and can be treated symptomatically [211]. Occasionally, additional adverse effects were observed, including severe infusion reaction, IgE against oligosaccharides and hypomagnesaemia, which are easily manageable [212].

Altogether, the safety profile of Cetuximab therapy with only mild side effects offers an opportunity to use this antibody for mediating elimination of cells engineered with a truncated EGFR. In immunosuppressed cell graft recipients, there is no reason to believe that potential side effects should occur at any higher extent as in immunocompetent tumor patients. Clearly, Cetuximab is capable of eliminating EGFR-overexpressing tumor cells. However, when Cetuximab is used to target a truncated version of the EGFR on T cells, the kinetics and efficacy of cell depletion might be different, and therefore these issues need to be carefully studied in mouse models.

## 2 Aim of this PhD thesis

Recent clinical trials demonstrated the therapeutic potency of immunotherapies based on adoptive transfer of genetically engineered T cells. Persistence and functionality of T cells were identified as the key determinants of the clinical benefit. Advanced technologies of clinical cell purification and genetic engineering laid the foundation for developing more effective T cell products by defining the cell composition and designing optimal transgenic receptors. However, T cell therapy is still not reproducibly effective and can mediate severe on- and off-target toxicities. Thus, challenges remain to increase efficacy and safety of this therapeutic approach. There is a growing need in cell engineering for a tool that facilitates cell purification, *in vivo* monitoring and that can be used as a target for ablating cells in case of adverse effects. Co-expression of the truncated human EGFR (EGFRt) in engineered T cells, a strategy originally developed by Jensen and colleagues [195], might represent such a universal tool.

The aim of this PhD thesis was to further characterize the EGFRt with regard to its utility for cell tracking, selection and depletion via the clinically approved Cetuximab.

First, we analyzed *in vitro* and *in vivo* whether the EGFRt is stably expressed on T cells and whether it can be reliably detected with EGFR-specific staining reagents. The next major objective was to adopt the *Streptamer* technology to improve selections of EGFRt<sup>+</sup> cells. For this purpose, we generated a reversible EGFR-specific selection reagent that was then evaluated in optimized protocols of cell selections using magnetic beads. Finally, we wanted to examine the efficiency and kinetics of T cell ablation based on targeting the EGFRt with the depleting antibody Cetuximab. Therefore, we had to establish a mouse model that allowed for monitoring T cell depletion in a reliable and sensitive manner. As a crucial part of the project, we wanted to address the question whether the EGFRt-based depletion strategy can prevent or reverse T cell-mediated toxicities. We had to develop clinically relevant mouse models that demonstrated CAR-mediated T cell function (e.g. killing of HBV<sup>+</sup> hepatocytes) and/or reflected T cell-mediated toxicities (e.g. B cell aplasia). These models allowed us to investigate whether integrating the EGFRt into functional T cells can be beneficial for maintaining safety of T cell therapies.

### 3 Material and Methods

#### 3.1 Material

##### 3.1.1 Chemicals and reagents

Reagent	Supplier
Acrylamide/Bis 30%	Biorad, München
Agarose	PAA Laboratories, Pasching, Austria
Ammoniumchloride (NH <sub>4</sub> Cl)	Sigma, Taufkirchen, Germany
Ampicillin	Sigma, Taufkirchen, Germany
Anhydrotetracycline (AHT)	IBA, Göttingen, Germany
Biocoll Ficoll solution	Biochrom, Berlin, Germany
Bovine serum albumin (BSA)	Sigma, Taufkirchen, Germany
D-Biotin	Sigma, Taufkirchen, Germany
Desthiobiotin	Sigma, Taufkirchen, Germany
Dimethyl sulfoxid (DMSO)	Sigma, Taufkirchen, Germany
Dithiothreitol (DTT)	Agilent, Waldbronn, Germany
DMEM	PAA Laboratories, Pasching, Austria
Dynabeads® Human T-Activator CD3/CD28	GibcoBRL, Karlsruhe, Germany
dNTP	Roche, Mannheim, Germany
Ethylene diamine tetraacetic acid (EDTA)	Sigma, Taufkirchen, Germany
Ethanol	Klinikum rechts der Isar, Munich, Germany
Ethidium-monoazide-bromide (EMA)	Molecular Probes, Leiden, The Netherlands
Fetal calf serum (FCS)	Biochrom, Berlin, Germany
Formaldehyde (HCOH), 37%	Merck KgaA, Darmstadt, Germany
Gentamycin	GibcoBRL, Karlsruhe, Germany
Golgi-Plug	BD Biosciences, Heidelberg, Germany
Hanks' Balanced Salt Solution	Invitrogen, Carlsbad, CA, USA
Heparin-Natrium-25000	Ratiopharm, Ulm, Germany
Human serum	in-house production with Institute of Virology and Krackhardt group
Hydrochloride (HCl)	Roth, Karlsruhe, Germany
HEPES	GibcoBRL, Karlsruhe, Germany
Interleukin-2, human (Proleukin® S)	Novartis, Basel, Switzerland
Interleukin-15, human	PeptoTech, Hamburg, Germany
Ionomycin	Sigma, Taufkirchen, Germany
Isopropanol	Roth, Karlsruhe, Germany
L-Glutamine	GibcoBRL, Karlsruhe, Germany

Reagent (continued)	Supplier
Magnesiumsulfate (MgSO <sub>4</sub> )	Sigma, Taufkirchen, Germany
Magnesiumchloride (MgCl <sub>2</sub> )	Sigma, Taufkirchen, Germany
Methanol	Roth, Karlsruhe, Germany
PageRuler Protein Ladder	Fermentas, St. Leon-Rot, Germany
Penicillin	Roth, Karlsruhe, Germany
Phorbol-myristate-acetate (PMA)	Sigma, Taufkirchen, Germany
Phosphate buffered saline (PBS)	Biochrom, Berlin, Germany
Poly-L-Lysine	Sigma, Taufkirchen, Germany
Polybrene (Hexadimethrine bromide)	Sigma, Taufkirchen, Germany
Potassium phosphate (K <sub>2</sub> PO <sub>4</sub> )	Sigma, Taufkirchen, Germany
Propidium iodide (PI)	Invitrogen, Carlsbad, CA, USA
Protamine sulfate	Sigma, Taufkirchen, Germany
Retronectin	Takara Bio Euroe S.A.S., Saint-Germain-en-Laye, France
Rotisafe GelStain	Roth, Karlsruhe, Germany
RPMI 1640	PAA Laboratories, Pasching, Austria
Silver nitrate (AgNO <sub>3</sub> )	Merck KGaA, Darmstadt, Germany
Sodium acetate (C <sub>2</sub> H <sub>3</sub> NaO <sub>2</sub> )	Merck KGaA, Darmstadt, Germany
Sodium azide (NaN <sub>3</sub> )	Sigma, Taufkirchen, Germany
Sodium carbonate (Na <sub>2</sub> CO <sub>3</sub> )	Merck KGaA, Darmstadt, Germany
Sodium chloride (NaCl)	Roth, Karlsruhe, Germany
Sodium EDTA (Na <sub>2</sub> -EDTA)	Sigma, Taufkirchen, Germany
Sodium hydroxide (NaOH)	Roth, Karlsruhe, Germany
Sodium thiosulfate (Na <sub>2</sub> S <sub>2</sub> O <sub>3</sub> ·xH <sub>2</sub> O)	Roth, Karlsruhe, Germany
<i>Strep</i> -Tactin-APC	IBA, Göttingen, Germany
<i>Strep</i> -Tactin-magnetic microbeads	IBA, Göttingen, Germany
<i>Strep</i> -Tactin-magnetic nanobeads	IBA, Göttingen, Germany
<i>Strep</i> -Tactin-PE	IBA, Göttingen, Germany
Streptavidin eFluor450	eBioscience, Frankfurt, Germany
Streptavidin PE	BD Pharmingen, San Diego, USA
Streptavidin PECy7	BD Pharmingen, San Diego, USA
Sucrose	Sigma, Taufkirchen, Germany
Tris-hydrochloride (Tris-HCl)	Roth, Karlsruhe, Germany
Triton X-100	Biorad, Munich, Germany
Trypan Blue	Sigma, Taufkirchen, Germany
Western Lightning Plus ECL color reagent	Perkin-Elmer, Heidelberg, Germany
β-Mercaptoethanol	Sigma, Taufkirchen, Germany

### 3.1.2 Media and buffers

Media	Composition
RP10 <sup>+</sup> cell culture medium	1x RPMI 1640 10% (w/v) FCS 0.025% (w/v) L-Glutamine 0.1% (w/v) HEPES 0.001% (w/v) Gentamycin 0.002% (w/v) Streptomycin
Human T cell culture medium	1x RPMI 1640 10% (w/v) human serum 0.025% (w/v) L-Glutamine 0.1% (w/v) HEPES 0.001% (w/v) Gentamycin 0.002% (w/v) Streptomycin 0.002% (w/v) Penicillin
cDMEM cell culture medium	1x DMEM 10% (w/v) FCS 0.025% (w/v) L-Glutamine 0.1% (w/v) HEPES 0.001% (w/v) Gentamycin 0.002% (w/v) Streptomycin
Complete freezing medium (CFM)	90% FCS 10% DMSO
Buffers	Composition
Ammonium chloride-Tris (ACT)	0.17 M NH <sub>4</sub> Cl 0.17 M Tris-HCl, pH 7.5 mix NH <sub>4</sub> Cl & Tris-HCl at a ratio 9:1
HBSS/EDTA (lung processing)	1.3mM EDTA (379.86ug/1L)
Digesting buffer (lung processing)	95mL RPMI 1640 20.33mg MgCl <sub>2</sub> 14.7mg CaCl <sub>2</sub> 5mL FCS 0.001g collagenase VIII / 3mL
D-biotin 100mM stock solution	2.4431g D-biotin

---

Buffers (continued)	Composition
FACS buffer	1x PBS 0.5% (w/v) BSA pH 7.45
Periplasmic lysis buffer (P)	100 mM Tris/HCl, pH 8.0 500 mM sucrose 1 mM EDTA
Protein purification washing (W)	100 mM Tris/HCl, pH 8.0 150 mM NaCl 1 mM EDTA
Protein purification elution buffer (E)	100 mM Tris/HCl 150 mM NaCl 1 mM EDTA 2.5 mM desthiobiotin, pH 8.0
Cell lysis buffer	150mM NaCl 0.5% NP-40 Ad 100mL H <sub>2</sub> O
Sample buffer (Laemmli)	10% (w/v) SDS 10mM DTT 20% (v/v) glycerol 0.2M Tris-HCl, pH 6.8 0.05% (w/v) Bromophenolblue
50x TAE buffer	2M Tris 2M acetic acid 50mM EDTA, pH 8.0
PBS-T (western blot)	0.5% Tween
Blocking buffer (western blot)	0.5% milk powder PBS-T
PBS-BSA-Azide (Qifikit)	0.01 mol/L PBS 0.1% BSA 15 mmol/L NaN <sub>3</sub> , pH 7.4

### 3.1.3 Gels

Gel	Composition
1.2% Agarose gel	0.6g Agarose 50mL TAE buffer, boil 2.5uL Rotisafe
10% SDS PAGE Running gel	3.3mL Acrylamid 2.5mL 1.5M Tris-HCl, pH 8.8 100uL 10% (w/v) SDS 4mL H <sub>2</sub> O 10uL TEMED 100uL 10% APS
10% SDS PAGE Stacking gel	0.66mL Acrylamid 0.3mL 2M Tris-HCl, pH 6.8 200uL 10% (w/v) SDS 3.9mL H <sub>2</sub> O 5uL TEMED 25uL 10% APS

### 3.1.4 Antibodies

Reagent	Clone	Supplier
Human CD14 PE-Cy7	61D3	eBioscience, San Diego, USA
Human CD19 ECD	J3-119	Beckman Coulter, Brea, USA
Human CD3 APC	UCHT1	Beckman Coulter, Brea, USA
Human CD3 eF450	OKT3	eBioscience, San Diego, USA
Human CD3 Orthoclone	OKT3	Janssen-Cilag, Neuss, Germany
Human CD3 Pacific Blue	UCHT1	BD Pharmingen, San Diego, USA
Human CD3 PE	UCHT1	Beckman Coulter, Brea, USA
Human CD3 PE-Cy7	UCHT1	eBioscience, San Diego, USA
Human CD4 eF450	OKT4	eBioscience, San Diego, USA
Human CD4 FITC	X35	Beckman Coulter, Brea, USA
Human CD4 Pac. Orange	S3.5	Life technologies, Carlsbad, USA
Human CD8 eF450	OKT8	eBioscience, San Diego, USA
Human CD8 Pacific Blue	B9.11	Beckman Coulter, Brea, USA
Human CD8 PE	RPA-T8	BD Pharmingen, San Diego, USA
Human CD16 FITC		BD Pharmingen, San Diego, USA
Human CD20 PE		BD Pharmingen, San Diego, USA
Human CD56 PE		BD Pharmingen, San Diego, USA
Human IgG A649		Abcam, Cambridge, UK
Human Fc biotin		Jackson ImmunoResearch, West Grove, DA, USA

Human EGFR purified	528	Santa Cruz Biotechnology, Heidelberg, Germany
Cetuximab (Erbix)		Bristol-Myers Squibb, Princeton, NK, USA
Rituximab (Rituxan)		Genentech, South San Francisco, CA, SA
Anti- <i>Streptag</i> purified Cetuximab biotin		IBA, Göttingen, Germany kindly provided by the Riddell group [195]
Mouse CD3 PECy7	145-2C11	eBioscience, San Diego, USA
Mouse CD4 Pac. Orange	RM4-5	Invitrogen, Carlsbad, CA, USA
Mouse CD8 eFluor450	Ly-2	eBioscience, San Diego, USA
Mouse CD11b FITC		Life Technologies, Carlsbad, USA
Mouse CD11c PECy7		BD Pharmingen, San Diego, USA
Mouse CD19 PECF594	1D3	BD Pharmingen, San Diego, USA
Mouse CD45.1 APC	A20	eBioscience, San Diego, USA
Mouse F4/80 APC		eBioscience, San Diego, USA
Mouse IFN- $\gamma$ PECy7	XMG1.2	eBioscience, San Diego, USA
Mouse IL-2 APC	SES6-5714	eBioscience, San Diego, USA
Mouse Ly6C PerCP		BD Pharmingen, San Diego, USA
Mouse Ly6C/G PE		BD Pharmingen, San Diego, USA
Mouse MHCII		eBioscience, San Diego, USA
Mouse NK1.1 PerCPCy5.5	PK136	eBioscience, San Diego, USA
Mouse Thy1.1 APC	HIS51	eBioscience, San Diego, USA
Mouse IgG HRP		Santa Cruz Biotechnology, Heidelberg, Germany
Fc block		Invitrogen, Carlsbad, CA, USA
Mouse CD3 purified	145-2c11	BD Pharmingen, San Diego, USA
Mouse CD28 purified	37.51	BD Pharmingen, San Diego, USA
Mouse NK1.1 purified	PK136	eBioscience, San Diego, USA

### 3.1.5 Enzymes

Benzonase	Sigma, Taufkirchen, Germany
Collagenase	Serva, Heidelberg, Germany
DpnI	Promega, Madison, USA
Herculase II	Stratagene, London, UK
Trypsin	SAFE Biosciences, Hampshire, UK
T4 DNA ligase	Fermentas, St. Leon-Rot, Germany

### 3.1.6 Kits

Cytofix/Cytoperm	BD Biosciences, Heidelberg, Germany
DNeasy Blood & Tissue Kit	Qiagen, Hilden, Germany
Effectene Transfection Reagent	Qiagen, Hilden, Germany
NK cell isolation kit, human	Miltenyi, Bergisch Gladbach, Germany
PureYield Plasmid MiniPrep System	Promega, Mannheim, Germany
PureYield Plasmid MidiPrep System	Promega, Mannheim, Germany
StarGate cloning system	IBA, Göttingen, Germany
Qifikit	Dako via Biozol, Eching, Germany

### 3.1.7 Cells and cell lines

PBMCs from human blood were obtained from volunteer healthy donors upon written informed consent. Usage of the blood samples was approved according to the national law by the local Institutional Review Board (Ethikkommission der Medizinischen Fakultät der Technischen Universität München).

B-LCLs were kindly provided by Angela Krackhardt, Institute of Hematology, Klinikum Rechts der Isar, Munich.

The Platinum E cell line was kindly provided by Karin Wisskirchen, Protzer group, Institute of Virology, Munich.

The following cell lines were kindly provided by Michael Hudecek, Medizinische Klinik und Poliklinik II, Universitätsklinikum Würzburg and Stanley Riddell, FHCRC, Seattle: K562, EGFR<sup>t</sup> LCL, BT-20, H9 (native and EGFR<sup>t</sup>), Jurkat (native and EGFR<sup>t</sup>), CD4 and CD8 primary T cell lines (untransduced and GFP/EGFR<sup>t</sup>).

The *E. coli* strain XL-10 Gold was purchased from Agilent, Santa Clara, USA. The *E. coli* strain JM83 was obtained from IBA, Göttingen, Germany.

### 3.1.8 Plasmids

Plasmid	vector	kindly provided by
hCD19-CAR_T2A_EGFR <sup>t</sup> _epHIV	lentiviral	Jensen lab/Riddell lab
hROR1-CAR_T2A_EGFR <sup>t</sup> _epHIV	lentiviral	Riddell lab
pMIGR1_hCD19-CAR_T2A_EGFR <sup>t</sup>	retroviral	Riddell lab
pMIGR1_TurboGFP_T2A_EGFR <sup>t</sup>	retroviral	Steven Liu, Riddell lab
pMP71_mCD19-CAR_P2A_EGFR <sup>t</sup>	retroviral	Daniel Sommermeyer, Riddell lab; Michele Sadelain
pMP71_S-CAR_T2A_EGFR <sup>t</sup>	retroviral	Karin Wisskirchen, Protzer lab

### 3.1.9 Mice

Mouse strain	genetics	provider
C57BL/6	wildtype	Harlan Laboratories
C57BL/6	OT-I, CD45.1 <sup>+/+</sup>	bred in house, Busch lab
C57BL/6	OT-I, Thy1.1 <sup>+/+</sup>	bred in house, Busch lab
C57BL/6	HBVtransgenic (HBV1.3xfs)	bred in house, Protzer lab

### 3.1.10 Equipment

Beta-counter TopCount NXT	Perkin-Elmer, Heidelberg, Germany
Biofuge fresco table top centrifuge	Heraeus, Hanau, Germany
BioPhotometer	Eppendorf, Hamburg, Germany
Cyan ADP Lx flow cytometer	Dako Cytomation, Fort Collins, USA
Electroporator pulse controller	Biorad, Munich, Germany
FACSAria cell sorter	BD bioscience, Heidelberg, Germany
HE33 agarose gel casting system	Hofer, San Francisco, USA
Heating block Thermomixer compact	Eppendorf, Hamburg, Germany
Gamma radiation source	Buchler, Braunschweig, Germany
Gel Imaging System Eagle Eye	BioRad, Munich, Germany
Incubator Cytoperm 2	Heraeus, Hanau, Germany
Laminar flow hood HERA safe	Heraeus, Hanau, Germany
Microscopes Axiovert S100	Carl Zeiss, Jena, Germany
MoFloII cell sorter	Dako Cytomation, Fort Collins, USA
MidiMACS cell isolation system	Miltenyi, Bergisch Gladbach, Germany
MightySmall SE245 gel casting system	Hofer, San Francisco, USA
NanoDrop spectrophotometer	NanoDrop, Baltimore, USA
Neubauer counting chamber	Schubert, München, Germany
Reflotron Reflovet Plus	Roche, Penzberg, Germany
Shaker Multitron Version 2	INFORS AG, Bottmingen, Germany
Sorvall® RC 6+	Thermo Fisher Scientific, Schwerte, Germany
<i>Strep</i> -Tactin Superflow columns	IBA, Göttingen, Germany
Thermocycler T3	Biometra, Göttingen, Germany
Vacuum filtering system Stericup 0.22 µm	Millipore, Bedford, USA
Variofuge 3.0 RS centrifuge	Heraeus, Hanau, Germany
Waterbath LAUDA ecoline 019	Lauda, Königshofen, Germany
2100 Bioanalyzer System	Agilent Technologies, Waldbronn, Germany

### 3.1.11 Software

Adobe Illustrator

CLC Main Workbench

End Note Program

FlowJo

Graph Pad Prism

Microsoft Office

Summit

Adobe Systems, San Jose, USA

CLC bio A/S, Aarhus, Denmark

Microsoft, Redmond, USA

Treestar, Ashland, USA

Graph Pad Software, La Jolla, USA

Microsoft, Redmond, USA

Dako, Fort Collins, USA

## 3.2 Methods

### 3.2.1 Cell culture

#### 3.2.1.1 General techniques

Cell lines were cultivated in RP10+ (LCL, T cell lines) or cDMEM (PlatE), supplemented as described in the Materials section, at 37°C, 5% CO<sub>2</sub> and 95% humidity. Adherent cell lines were trypsinized and split every 3-4 days, depending on their confluency. Cell lines growing in suspension were controlled for medium usage and cluster formation and split accordingly, at least once a week.

Cells were counted using a Neubauer counting chamber. After diluting cells 1:10 with 0.15% Trypan blue/PBS for live/dead discrimination, the cell number in at least two squares was acquired to calculate the cell concentration according to the following formula:  $\frac{\text{cell no.}}{\text{ml}} = \text{mean cell count/square} * \text{diltution factor} * 10^4$ .

For cryopreservation, cells were centrifuged at 1200rpm for 8 minutes, and cell pellets were resuspended in complete freezing medium (FCS/10% DMSO) at a maximum concentration of  $2 \times 10^7$  per mL. After resting the cells on wet ice for 30 minutes, the cells were kept in a -80°C freezer for 48 hrs and then stored in liquid nitrogen. For thawing, cells were quickly heated up in a 37°C water bath, diluted in 10 mL RP10+ for centrifugation and grown in culture.

#### 3.2.1.2 Rapid expansion protocol

Primary T cells were cultivated in hRP10+, supplemented with human serum. T cells were expanded every 14 days using the Rapid expansion protocol (REP) [213]. To prepare unspecific feeder cells, LCLs were washed twice with RP10+ and  $\gamma$ -irradiated with 50 Gy and similarly, allogeneic PBMCs, kindly provided by the Immune monitoring group of M. Neuenhahn, were thawed, washed twice with RP10+ and  $\gamma$ -irradiated with 35 Gy. On day 0, 50,000 T cells were stimulated with 30ng/mL anti-human CD3 mAb (OKT3),  $5 \times 10^6$   $\gamma$ -irradiated LCLs and  $2 \times 10^6$   $\gamma$ -irradiated PBMCs in a T-25 flask with 20 mL hRP10+. On day 1, 4, 8 and 11, hIL-2 was added at 50U/mL. On day 4, stimulated T cells were subjected to a complete wash by spinning cells down at 1200 rpm for 8 minutes and resuspending the pellet in 20mL of fresh hRP10+. Subsequently, half of the medium volume (= 10mL) was exchanged for fresh hRP10+ every 2-3 days and T cells were split 1:2, depending on the expansion rate, to keep T cell cultures at a

concentration of around  $1 \times 10^6$  cells/mL. Beyond day 14, T cells can be kept in culture with 0.5-1ng/mL of hIL-15.

### 3.2.2 Transduction

#### 3.2.2.1 Retroviral transduction

Retroviral vector plasmids were kindly provided by Michael Hudecek, Steven Liu and Daniel Sommermeyer from the Riddell lab at the FHCRC, Seattle.

One day before transfection, the packaging cell line Platinum-E (PlatE) was plated out at  $2 \times 10^6$  cells/12mL per 10cm cell culture dish that had been coated with Poly-L-Lysine, diluted 1:10 in PBS, at 37°C for one hour and washed twice with PBS. PlatE cells were at a confluency of 40-50%, when they were transfected with 1µg plasmid DNA/plate using 30µL Effectene Transfection reagent according to the manufacturer's protocol (Qiagen). On the next day, the medium was gently exchanged for fresh cDMEM. After 24 and 48 hours, the supernatant containing retroviral particles was collected and filtered through a 0.45µm filter. The filtered retroviral supernatant was either used directly for transductions or stored at -80°C for later use. For optimal retrovirus titers, PlatE cells were in some cases stably transduced with the plasmid DNA in collaboration with Karin Wisskirchen from the Protzer lab (Institute of Virology, Munich).

Mouse splenocytes were isolated from spleens of wildtype or OT-I transgenic C57BL/6 mice. The spleen was transferred to a sterile 70µm cell strainer that had been placed in a 3cm petri dish with 5mL RP10+. After squeezing the spleen through the cell strainer with the plunger of a syringe, the splenocytes were filtered through another 70µm cell strainer to bring them into single-cell-suspension. Collected splenocytes were centrifuged at 1400rpm for 6 minutes. The pellet was resuspended with 3mL ACT buffer and incubated at room temperature for 3 minutes for lysis of the erythrocytes. Lysis was stopped by adding cDMEM ad 15mL and centrifuging again. Splenocytes were then transferred into a T-25 flask with 10mL cDMEM, supplemented with 100U/mL of IL-2, and stimulated over night with anti-mouse CD3 (clone 145-2c11) and anti-mouse CD28 (clone 37.51) at a dilution of 1:500.

One day before transductions, non-tissue-culture-treated 24-well plates were coated with retronectin, diluted in PBS ( $c_{\text{final}} = 12.5\mu\text{g/mL}$ ), at 250µL/well. Retronectin is removed the next day and was stored at -20°C for one more use. Unspecific binding sites on the plates were blocked with 2% BSA in PBS at 37°C for 30 minutes and

plates were washed twice with 2mL PBS. Plates can be stored over night with 2.5% Hepes in PBS at 4°C.

Filtered retroviral supernatant was transferred to the retronectin-coated 24-well plates at 1.5mL/well. Plates were spun at 2000g at 32°C for 90 minutes and 500µL supernatant was removed. Mouse splenocytes were added at  $1 \times 10^6$  cells in 500µL RP10+ per well. After adding IL-2 ( $c_{\text{final}} = 100\text{U/mL}$ ) and protamine sulfate ( $c_{\text{final}} = 4\mu\text{g/mL}$ ), cells were spinoculated onto the retrovirus at 1000g at 32°C for 10 minutes. This procedure was repeated with the retroviral supernatant collected at 48 hours after transfection. Retronectin-coated and blocked plates were spinoculated with the retroviral supernatant. After carefully removing 500µL supernatant from the plates of the 'first transduction', splenocytes were transferred to the plates with fresh retrovirus, supplemented with IL-2 and protamine sulfate, and centrifuged as before.

Alternatively, splenocytes can be spinoculated simultaneously with the retroviral supernatant, supplemented with 100U/mL IL-2 and 5µg/mL polybrene, at 1000g at 32°C for 90 minutes. Two rounds of transduction are recommended for both protocols.

### 3.2.2.2 Lentiviral transduction

Human T cells were genetically engineered by lentiviral transduction in collaboration with Michael Hudecek at the FHCRC, Seattle, as previously described [195]. Briefly, PBMCs were obtained from healthy donors, isolated by density gradient centrifugation over Ficoll solution and washed twice in PBS/1mM EDTA. PBMCs were either used directly or enriched for specific T cell subsets. Cells were stimulated with CD3/CD28 Dynabeads® (cell:bead = 1:3) and 25U/mL IL-2. Two days later, bead-activated cells were transduced with the lentivirus at a multiplicity of infection (MOI) of 1-3 in the presence of 5µg/mL polybrene and 50U/mL IL-2. After spinoculation at 2100rpm at 32°C for 30 minutes and incubation at 37°C for 4 hours, double volume of warm medium was added. Half medium changes were performed and IL-2 was added every 3-4 days. The CD3/CD28 beads were removed with a permanent magnet on day 9 or 10. Transgene expression was analyzed on day 10-14. Subsequently, cells can be magnetically enriched or sort-purified and expanded by the standard REP.

### 3.2.3 Functional analysis *in vitro*

#### 3.2.3.1 Killing assay

Anti-mouse CD19-CAR or mock-transduced Thy1.1<sup>+</sup> mouse splenocytes were coincubated at a ratio of 1:1 with Thy1.1<sup>-</sup> mouse splenocytes that contained a fraction of CD19<sup>+</sup> cells. The final concentration was 400,000 cells in 200 $\mu$ L RP10+ per well of a flat-bottom 96-well plate. After incubating cell mixtures at 37°C over night (around 16 hours), live cells were counted. Cell composition was analyzed by flow cytometry and target cells were discriminated from effectors by staining for Thy1.1 and CD19. The number of CD19<sup>+</sup> target cells was calculated from the frequency and the total cell number. Samples were performed in triplicates.

#### 3.2.3.2 Chromium release assay

Antibody-dependent cellular cytotoxicity via the EGFR-specific mAb Cetuximab was determined in a chromium release assay. The K562 cell line, the EGFR-overexpressing breast cancer cell line BT-20, EGFRt-transduced LCLs and EGFRt-transduced T cells were used as target cell that were labeled with radioactive chromium (<sup>51</sup>Cr) at 37°C for 90 minutes. Excess chromium was removed by washing radiolabeled cells twice.

Effector cells had been generated before by isolating NK cells from PBMCs with the NK isolation kit and expanding them with  $\gamma$ -irradiated PBMCs at a ratio of 1:10 and 200U/mL IL-2. NK effector cells were added to the radiolabeled target cells at different effector-to-target ratios, while keeping the number of target cells constant at 1000 cells/well on a round-bottom 96-well plate. Cetuximab, CD20-specific Rituximab ( $C_{\text{final}} = 10\mu\text{g/mL}$ ) or no mAb were added to the cell mixture with a final volume of 200 $\mu$ L/well. After centrifugation at 800rpm for 3 minutes, cells were coincubated at 37°C for 4 hours. Spontaneous and maximum release was determined by adding medium or a detergent (2% Triton-X) to the target cells instead of effectors. All samples were run in triplicates.

After co-incubation of target and effector cells, 30 $\mu$ L of the supernatant were transferred to solid scintillator-coated lumaplates that were then dried over night. Chromium release was measured as counts per minute (cpm) by analyzing samples with the TopCount scintillation counter. The specific lysis was calculated by using the following formula: % specific lysis = (mean sample release - mean spontaneous release)  $\div$  (mean maximum release - mean spontaneous release) x 100.

### 3.2.4 Adoptive T cell transfer and depletion *in vivo*

#### 3.2.4.1 T cell transfer and mAb infusion

Mouse splenocytes were retrovirally transduced with constructs that encoded the GFP/EGFRt or a CAR/EGFRt as described in 3.2.2.1. The phenotype and transduction efficiency was determined by flow cytometry. Transduced splenocytes were expanded for 2-3 days and enriched for EGFRt-expressing cells by fluorescence-activated cell sorting (FACS) as indicated for individual *in vivo* studies in the result section.

One day before cell transfer, wildtype C57BL/6 mice were sublethally  $\gamma$ -irradiated with 6 Gy. EGFRt- or mock-transduced cells were pooled, washed twice with PBS and subsequently transferred into mice by intravenous (i.v.) injection at 200 $\mu$ L/mouse. Cetuximab or Rituximab as a control mAb was infused intraperitoneally (i.p.) at 1mg/mouse at specified time points. Mice were challenged by i.v. application of modified vaccinia virus Ankara expressing ovalbumin (MVA-OVA) at  $1 \times 10^8$  pfu/mouse. MVA-OVA was kindly provided by Andreas Muschaweckh and Ingo Drexler.

Depletion studies in the HBV model slightly deviated from this protocol, as HBV-transgenic mice were not irradiated and S-CAR-transduced CD8<sup>+</sup> mouse cells were transferred by i.p. injection.

#### 3.2.4.2 Analysis of blood and serum

At different time points during the course of *in vivo* studies, approximately 100 $\mu$ L blood was obtained from the tail vein. On the final days of experiments, mice were sacrificed and 200-400 $\mu$ L blood was collected by heart puncture. Heparinized blood was incubated in 10mL ACT buffer at room temperature for 10 minutes for erythrocyte lysis. After centrifugation at 1500rpm for 6 minutes, residual erythrocytes were lysed again with 5mL ACT buffer for 5 minutes. Lysis was stopped by adding 10mL FACS buffer. After another centrifugation step, cells were transferred to a V-bottom 96-well plate for flow cytometry stainings.

During experiments in the HBV mouse model, an additional blood sample was obtained and incubated at room temperature for at least 30 minutes. To retrieve serum, the blood samples were centrifuged at 5000g for 10 minutes. For measuring the level of the Alanine aminotransferase (ALT), 32 $\mu$ L of serum diluted 1:3 in PBS were used for analysis with the Reflotron system.

### 3.2.4.3 Isolation and processing of organs

At the end of each experiment, mice were sacrificed by cervical dislocation and spleens, lymph nodes, lungs and livers were obtained in addition to blood. Isolation of spleens was described in 3.2.2.1.

Cervical, axillary, brachial, mesenteric and inguinal lymph nodes were collected and squeezed through a 100µm cell strainer to obtain a single-cell suspension.

Lungs were perfused with 10 mL cold PBS/Heparin through the right ventricle of the heart to remove circulating lymphocytes. Isolated lungs were minced into small pieces in a small petri dish on wet ice, transferred to a small beaker glass with HBSS/EDTA and incubated at room temperature for 30 minutes while stirring. Minced pieces were then carefully dissociated through a 100µm cell strainer by using a plunger from a 3mL syringe. The cell strainer was additionally flushed with 5mL FACS buffer to retrieve residual lung cells. Cells were spun down at 1500rpm for 6 minutes and incubated in 3 mL digesting buffer with collagenase VIII in a 37°C water bath for 30 minutes. Cells were washed once with RP10+ and filtered again through a 100µm cell strainer.

Livers were perfused with cold PBS through the portal vein and harvested. Approximately one third of the liver was used to isolate liver-associated lymphocytes. Livers were digested with 4500U collagenase at 37°C for 20 minutes. and squeezed through a 100µm cell strainer. Collected cells were brought into single-cell suspension by pulling them through a 20-gauge needle. Leukocytes were enriched over a 80%/40% Percoll gradient at 1400g for 20 minutes.

Lymph nodes, lungs and livers were processed in a similar manner as described for the spleens (3.2.2.1), including the erythrocyte lysis. The total cell number was acquired and frequencies of transferred and endogenous cell subsets were assessed by flow cytometry staining. Absolute cell numbers could be subsequently calculated for individual cell subsets based on frequency and total cell number.

### 3.2.5 Magnetic cell separation

#### 3.2.5.1 Nanobead-based cell selection (MACS)

For magnetic cell separation, up to  $3 \times 10^7$  cells were incubated with EGFR Fab monomers in 100 $\mu$ L FACS buffer at 4°C for 20-30 minutes. Cells were washed once with 6mL FACS buffer, centrifuged at 1200rpm for 8 minutes and resuspended in FACS buffer. *Strep*-Tactin-nanobeads were added to a final volume of 300 $\mu$ L and incubated with the cells at 4°C for 20-30 minutes. After washing cells with 6mL FACS buffer, they were applied with 500 $\mu$ L FACS buffer onto a pre-equilibrated LS-column that had been placed in the magnetic field of a MACS Separator. Magnetic separation was performed according to the manufacturer's recommendations (Miltenyi). In brief, unlabeled cells were washed off the column by adding 3mL FACS buffer three times. This 'wash fraction' was collected for further analysis.

For collecting the 'positive fraction', the column was removed from the magnetic field and magnetically labeled cells were flushed out with 5mL FACS buffer using the plunger. Magnetic beads and Fab fragments were removed from the cells in the 'positive fraction' by adding 1mM D-biotin and incubating cells at room temperature for 15 minutes. Nanobeads were separated from the cells by spinning down at 1200rpm for 8 minutes. Subsequently, cells were washed three times with 10mL FACS buffer at room temperature and subjected to further analysis by flow cytometry.

#### 3.2.5.2 Microbead-based cell selection

*Strep*-Tactin functionalized microbeads were coated with EGFR Fab monomers at indicated ratios in a final volume of 1mL FACS buffer by incubation at 4°C for 45 minutes under constant agitation. Coated beads were washed once on the magnet to remove excess Fab monomers.

Up to  $4 \times 10^7$  cells were incubated with the Fab-bead complexes and FACS buffer in a final volume of 2mL at 4°C for 30 minutes under constant agitation. Magnetically labeled cells were separated by retention on a permanent magnet and removing the supernatant that contained the unlabeled cells. Cells were washed with 5mL FACS buffer another four times. Unlabeled cells from all washes were collected and pooled as the 'wash fraction' for further analysis.

Magnetically labeled cells were resuspended in 5mL FACS buffer. Beads and Fab monomers were released by incubating cells with 1mM D-biotin at room temperature for 10 minutes. Bead-free cells were separated from the beads on the magnet. Beads

were incubated with 1mM D-biotin in 5mL FACS buffer again to retrieve any cells that were still bound to the beads. Obtained cells from the two release steps were pooled as the 'positive fraction' and washed three times with 10mL FACS buffer at room temperature, including a 10 minute incubation time to allow for dissociation of Fab monomers from the cell surface. Label-free cells in the 'positive fraction' were analyzed by flow cytometry.

### **3.2.6 Flow cytometry**

#### **3.2.6.1 Surface staining**

For antibody staining,  $5 \times 10^6$  or less cells were transferred into 96-well plates and spun down at 1500rpm for 3 minutes. If a biotinylated antibody (anti-EGFR or anti-Fc) was used, cells were first incubated in a 1:50 dilution of the respective antibody in the dark at 4°C for 20 minutes. For staining murine cells, Fc-block (1:400) was added at this incubation step to block Fc receptors. Cells were washed once with 200µL FACS buffer, centrifuged and resuspended in an antibody mix that contained fluorophore-conjugated streptavidin and antibodies at recommended dilutions. Cells were incubated at 4°C in the dark for 30 minutes. For live/dead discrimination, propidium iodide (PI) was added during the last three minutes of the incubation. Cells were then washed with 200µL FACS buffer twice, resuspended in 300µL FACS buffer and analyzed on a CyAn ADP Lx flow cytometer. Data analysis was performed with the FlowJo software.

#### **3.2.6.2 Staining cells of the lymphoid and myeloid lineage**

The staining panel for lymphoid cells contained antibodies against CD45.1 CD3, CD4, CD8, CD19 (B cells), and NK1.1 (NK cells). The staining of myeloid cells was performed using antibodies against CD11b, CD11c, F4/80 and Ly6C, Ly6G and MHCII. The CD11c<sup>+</sup>/MHCII<sup>+</sup> cell population represented dendritic cells (DCs). To distinguish further cell subsets, cells were pre-gated on the CD11b<sup>+</sup> population, and neutrophils were identified as Ly6G<sup>+</sup>. Subsequently, cells were pre-gated on the Ly6G negative population and expression of F4/80, Ly6C and MHCII was used to discriminate between resident macrophages (F4/80<sup>+</sup>), inflammatory monocytes (F4/80 low / Ly6C<sup>+</sup> / MHCII negative) and inflammatory macrophages (F4/80 low / Ly6C<sup>+</sup> / MHCII<sup>+</sup>).

### 3.2.6.3 Streptamer staining

For *Streptamer* staining, EGFR Fab monomers were usually pre-incubated with 3 $\mu$ L *Strep*-Tactin, labeled with phycoerythrin (PE) or allophycocyanin (APC), at 4°C for 45 minutes. The multimers were used for staining up to 5x10<sup>6</sup> cells in a similar manner as antibodies. To test the reversibility of EGFR Fab fragments, cells were incubated in 1mM D-biotin for 15 minutes, centrifuged and washed three times with 10mL FACS buffer. After releasing the *Streptamers*, a cell aliquot was restained with fresh *Strep*-Tactin backbone to test for residual Fab monomers on the cell surface. Another cell aliquot was restained with new Fab *Streptamers* to test for residual D-biotin that would prevent binding of the new *Strep*-Tactin backbone to remaining cell-bound Fab fragments. Additional aliquots were taken directly after *Streptamer* staining and after release with D-biotin to analyze them together with the two restained cell aliquots by flow cytometry.

### 3.2.6.4 Cell sorting by FACS

In some *in vivo* experiments, EGFRt-transduced mouse splenocytes were sorted by FACS before adoptive transfer. Cells were stained with 0.2 $\mu$ g EGFR Fab monomers per 5x10<sup>6</sup> cells and incubated at a concentration of 5x10<sup>6</sup> cells/50 $\mu$ L FACS buffer at 4°C for 30 minutes. Subsequently, 3 $\mu$ L *Strep*-Tactin-PE/5x10<sup>6</sup> cells and further antibodies were directly added to the cell suspension and incubated at 4°C for another 20 minutes, including PI during the last 3 minutes. Cells were washed with 6mL FACS buffer and any cell aggregates were removed by passing stained cells through a sterile 30 $\mu$ m filter. The whole procedure was performed on ice and under sterile conditions. Cells were sorted on a MoFloII cell sorter to obtain living, CD19<sup>-</sup>, EGFRt<sup>+</sup> (and sometimes GFP<sup>+</sup>) cells. Sorted cells were collected into tubes with 1mL FCS and 1mM D-biotin for release of the EGFR Fab *Streptamer* as described in 3.2.6.3.

### 3.2.6.5 Intracellular cytokine staining

To assess cytokine production, CD19-CAR/EGFRt-transduced cells were specifically activated by coinubation with CD19<sup>+</sup> target cells at 37°C for 5 hours. After two hours, secretion of cytokines was prevented by adding GolgiPlug (= Brefeldin A) at 1 $\mu$ g/mL. Background levels of cytokine production were assessed by adding medium instead of target cells. Maximum levels of cytokines were obtained by unspecific stimulation with 25ng/mL phorbol-myristate-acetate (PMA) and 1 $\mu$ g/mL Ionomycin that stimulate cytokine production of T cells independent of the TCR or CAR.

For intracellular staining, cells were washed once and incubated with ethidium monoazide bromide (EMA, diluted 1:1000) for live/dead discrimination and Fc-block (1:400) to saturate Fc receptors under light exposure for 20 minutes. Subsequently, cells were washed once and incubated with antibodies against surface antigens in the dark for 20 minutes. After 3 washes, cells were fixed and permeabilized at 4°C in the dark for 20 minutes as recommended by the manufacturer (BD Biosciences). After two washes with PermWash, intracellular staining for IFN- $\gamma$  and IL-2 was performed in the dark for 30 minutes. Cells were washed with PermWash twice and with FACS buffer once before analysis on a flow cytometer. All incubations and washes were performed at 4°C.

### 3.2.6.6 Quantitative flow cytometry

EGFR expression was quantified using the Qifikit® (Dako). It is recommended for quantitative analysis of surface antigen expression by labeling cells with a purified mouse monoclonal antibody and a secondary anti-mouse antibody, labeled with fluorescein (FITC). Same secondary antibody is used to stain the provided beads that are coated with different, well-defined numbers of mouse antibody molecules (anti-human CD5, isotype IgG2a). By obtaining mean fluorescence intensities (MFIs) of stained Calibration beads, a calibration curve can be set up to correlate MFI and antibody binding capacity (ABC). If all staining antibodies are used at saturating conditions, the ABC corresponds to the number of target molecules on the cell surface.

EGFR-overexpressing breast cancer cell line cells (BT-20) and EGFR<sup>+</sup> T cells were stained with the unconjugated anti-human EGFR mouse mAb (clone 528), isotype IgG2a) at a saturating concentration at 4°C for 30 minutes, following the manufacturer's manual (Dako). As a negative control, anti-human NK1.1 mAb (IgG2a) was used as an irrelevant antibody under the same conditions. Cells were washed with 3mL PBS-BSA-Azide twice. During the incubation, vials containing the beads were thoroughly vortexed to homogenize the solutions and 100 $\mu$ L of Setup and Calibration Beads were transferred to tubes and washed with 3mL PBS-BSA. Both labeled cells and beads were simultaneously incubated with 100 $\mu$ L of a 1:50 dilution of the provided FITC Conjugate at 4°C in the dark for 45 minutes. Cells and beads were washed with 3mL PBS-BSA-Azide twice and analyzed on a flow cytometer. According to the manufacturer's instructions, data was acquired, a calibration curve was set up and ABC per cell was calculated.

### 3.2.7 Molecular biology techniques

#### 3.2.7.1 Cloning of EGFR Fab fragments

The wildtype EGFR Fab fragment was generated by gene synthesis (GeneArt) based on published sequences of the heavy and light variable regions ( $V_H$  and  $V_L$ ) of the anti-EGFR mAb clone A13 [214]. Variable sequences were linked to the constant Fab regions and the heavy chain was fused to a OneSTrEPTag affinity tag (IBA). Further, regulatory elements for the bicistronic expression of both chains were integrated into the gene construct. In a final cloning step, the Fab-*Streptag* fusion gene sequences were introduced into the Acceptor vector pASG-IBAw2, adapted for periplasmatic expression of the Fab protein. Combinatorial cloning was performed using the StarGate cloning system, following the manufacturer's recommendations (IBA). After each cloning step, sequences were verified by Sanger sequencing at the commercial provider GATC using own primers.

To generate EGFR Fab mutants, single amino acids were substituted with alanine (or a functionally similar amino acid) by mutagenesis PCR. The PCR reaction was performed with the following reagent mix and PCR program:

5x Herculase buffer	10 $\mu$ L	98°C	5'	} 20x
Template	1 $\mu$ L	98°C	90''	
Forward / reverse primer (10 $\mu$ M)	1.25 $\mu$ L	48°C	45''	
dNTPs (25mM each)	0.5 $\mu$ L	72°C	7'	
DMSO	0.5 $\mu$ L	72°C	7'	
Herculase polymerase	1 $\mu$ L	4°C	$\infty$	
dd H <sub>2</sub> O	ad 50 $\mu$ L			

The PCR products were digested with DpnI at 37°C for one hour, purified by sodium acetate precipitation and amplified in *E. coli* (XL-10 Gold) as previously described [215]. After confirming the sequence by Sanger sequencing, correct plasmids were used to express the Fab mutant.

Following a similar approach, a ROR1ecd-*Streptag* fusion protein was generated. The human ROR1 extracellular domain (ecd, aa 25-403) was generated by gene synthesis based on the publicly available ROR1 gene sequence (GenBank acc.no. NM\_00501). Subsequently, the ROR1ecd was fused to the *Streptag* and cloned into the Acceptor vector pASG-wt2 as described for the EGFR Fab.

### 3.2.7.2 Protein expression and purification

For Fab protein expression, the *E.coli* strain JM83 was transformed with the final plasmid DNA by electroporation. After growing bacteria to an optical density at 600nm (OD<sub>600</sub>) of 0.5-0.6 in 1L cultures, periplasmatic expression of the Fab-*Streptag* fusion protein was induced by adding anhydrotetracycline (AHT, 1:10,000) that activated the *tet*-promoter in the final expression vector. After three hours of protein expression, bacteria were harvested by centrifuging at 5000g at 4°C for 12 minutes. Pelleted bacteria can be stored at -80°C.

For extracting the Fab protein from the periplasma, bacteria were resuspended in buffer P and incubated at 4°C for 30 minutes. Extracted proteins were separated from solid components of the bacteria by centrifugation at 15,000rpm at 4°C for 15 minutes. To digest the DNA, the supernatant was incubated with Benzonase (1:2000-1:6000) in the presence of 100µL/10-30mL supernatant of 1M MgCl<sub>2</sub> at 4°C for 30 minutes. The digested Fab protein solution was filtered through a sterile 0.2µm filter.

For affinity purification, filtered Fab fragments were applied onto a *Strep*-Tactin superflow column (IBA) that had been equilibrated with 2.5mL buffer W twice. After washing the Fab proteins on the column with 1mL buffer W 5 times, the Fab fragments were eluted from the column by adding 0.8mL, 1.5mL and 1mL buffer E. Using the middle elution fraction, the buffer E is exchanged for PBS (pH 7.5) by dialysis. The protein concentration was measured at 280nm using a NanoDrop spectrometer. Additionally, the size, quantity and purity of Fab fragments were examined by using the Agilent 2100 Bioanalyzer system.

### 3.2.7.3 Gel electrophoresis

To confirm periplasmatic expression of the Fab protein, a 1mL aliquot was obtained from the bacteria culture before and after adding AHT that induced protein expression. Pelleted bacteria were lysed with buffer P at 4°C for 20 minutes and centrifuged at 13,000rpm for 10 minutes. The supernatant was supplemented with 5x Laemmli loading buffer, incubated at 95°C for 5 minutes and shortly spun down.

To assess the quality of the Fab fragments after affinity-purification, an aliquot of the final Fab-*Streptag* fusion protein was processed in a similar manner by adding Laemmli buffer and denaturing the sample by heating.

Samples were subsequently transferred onto a 10% SDS-PAGE gel and separated by electrophoresis at 130V for at least one hour.

#### 3.2.7.4 Western blot

Proteins were transferred from the SDS-PAGE gel to a nitrocellulose membrane by blotting at 1.2 mA/cm<sup>2</sup> for around 80 minutes.

To detect Fab-*Streptag* fusion proteins, the membrane was blocked with 0.5% milk in PBS-T at room temperature for one hour and staining was performed with anti-*Streptag* mAb, diluted 1:2000 in blocking buffer, at 4°C over night. After three washes with PBS-T at room temperature for 10 minutes, the secondary anti-mouse mAb, conjugated with horseradish peroxidase (HRP), was added at dilution of 1:5000 in blocking buffer at room temperature for one hour. After washing three times with PBS-T and once with PBS, membrane was incubated in ECL color reagent at room temperature under light exposure for one minute. Specific signals were captured on a film that was developed in a dark room.

#### 3.2.7.5 Silver staining

Purity of the Fab fragments was assessed by silver staining of the SDS PAGE gel. The following incubation steps were performed under agitation at room temperature. First, the gel was incubated in fixing solution (50% methanol, 5% acetic acid, 45% H<sub>2</sub>O) for 30 minutes and in 50% methanol/ H<sub>2</sub>O for another 15 minutes. Subsequently, gel was washed in H<sub>2</sub>O 5 times with a 5 minute-incubation per wash. Gel was sensitized in 0.02% sodium thiosulfate (0.2g Na<sub>2</sub>S<sub>2</sub>O<sub>3</sub>·5H<sub>2</sub>O, 1L H<sub>2</sub>O) for one minute and washed with H<sub>2</sub>O for one minute twice. Staining of gel is performed by incubation in cold 0.2% silver nitrate solution (0.2g AgNO<sub>3</sub>, 100mL H<sub>2</sub>O) for 25 minutes. After two washes in H<sub>2</sub>O for one minute, gel was developed in 3% sodium carbonate solution (3g Na<sub>2</sub>CO<sub>3</sub>, 100mL H<sub>2</sub>O), supplemented with 25µL of 37% formaldehyde (HCOH). When the staining is sufficient, the color reaction was stopped by incubating gel in H<sub>2</sub>O/EDTA (14g Na<sub>2</sub>-EDTA, 1L H<sub>2</sub>O) for 10 minutes and washing with H<sub>2</sub>O for one minute twice. Finally, gel was incubated in fixing solution (5% glycerol, 10% ethanol, 85% H<sub>2</sub>O) for 15-30 minutes before drying the gel between two foils over night for long-term storage.

#### 3.2.8 Statistics

Statistical analysis was performed with Graph Pad Prism. Level of significance was calculated with the unpaired Mann-Whitney test. For p-values > 0.5, differences between groups are considered non-significant (ns). p-values ≤ 0.5 indicate significant and p-values ≤ 0.005 indicate highly significant differences that are represented by one (\*) or two asterisks (\*\*) in the graphs.

## 4 Results

### 4.1 Characterizing the EGFRt as a tracking marker

The human-derived truncated EGF receptor (EGFRt) was developed by Mike Jensen and colleagues in such a way that it can serve multiple purposes [195]. The human EGFRt was designed to be a suitable marker for tracking, selecting and depleting engineered T cells. The EGFRt is derived from the human full-length EGFR as illustrated in Fig. 4-1A. It was truncated extracellularly by removing domain I and II, which abrogates binding to any endogenous ligands, such as EGF or transforming growth factor (TGF)- $\alpha$ . In addition, its intracellular tyrosine kinase domain was deleted to prevent receptor signaling. The residual EGFRt sequence contains the amino acids (aa) 310-644 of the mature wildtype EGFR and was fused to the GM-CSF receptor leader peptide (22 aa) for surface expression of the EGFRt.

#### 4.1.1 Co-expression of the EGFRt marker and other transgenes

Due to its relatively small size of 358 aa, the EGFRt can be implemented into any gene expression vector (Fig. 4-1B). Genes encoding for the transgenic receptor, e.g. a chimeric antigen receptor (CAR), and the EGFRt are linked by the T2A-ribosomal skip sequence for simultaneous and equimolar expression of both gene products. Every CAR-engineered T cell should then also express the EGFRt marker to a similar extent. Therefore, targeting the marker for different purposes, including staining and selection, should be equivalent to targeting the CAR itself.

We wanted to examine whether the co-expression of a transgene and EGFRt can be shown in a costaining based on flow cytometry. First, mouse splenocytes were genetically engineered by retroviral transduction to express the GFP/EGFRt gene construct, because GFP expression can be directly visualized by detecting the GFP fluorescence (Fig. 4-2A). The EGFRt was detected by staining with a biotinylated anti-EGFR mAb and streptavidin and we observed that expression levels of GFP and the EGFRt were tightly correlated. To test whether this is also true for CAR/EGFRt-engineered cells, human primary T cells were transduced with a lentiviral construct for

the ROR1-CAR and EGFRt (Fig. 4-2). The ROR1-CAR contains an extracellular spacer - derived from human IgG4 - that allows for specific detection with an anti-human IgG antibody. Costaining of the transduced cells with the anti-IgG and anti-EGFR antibodies again showed correlated expression of both transgenes.

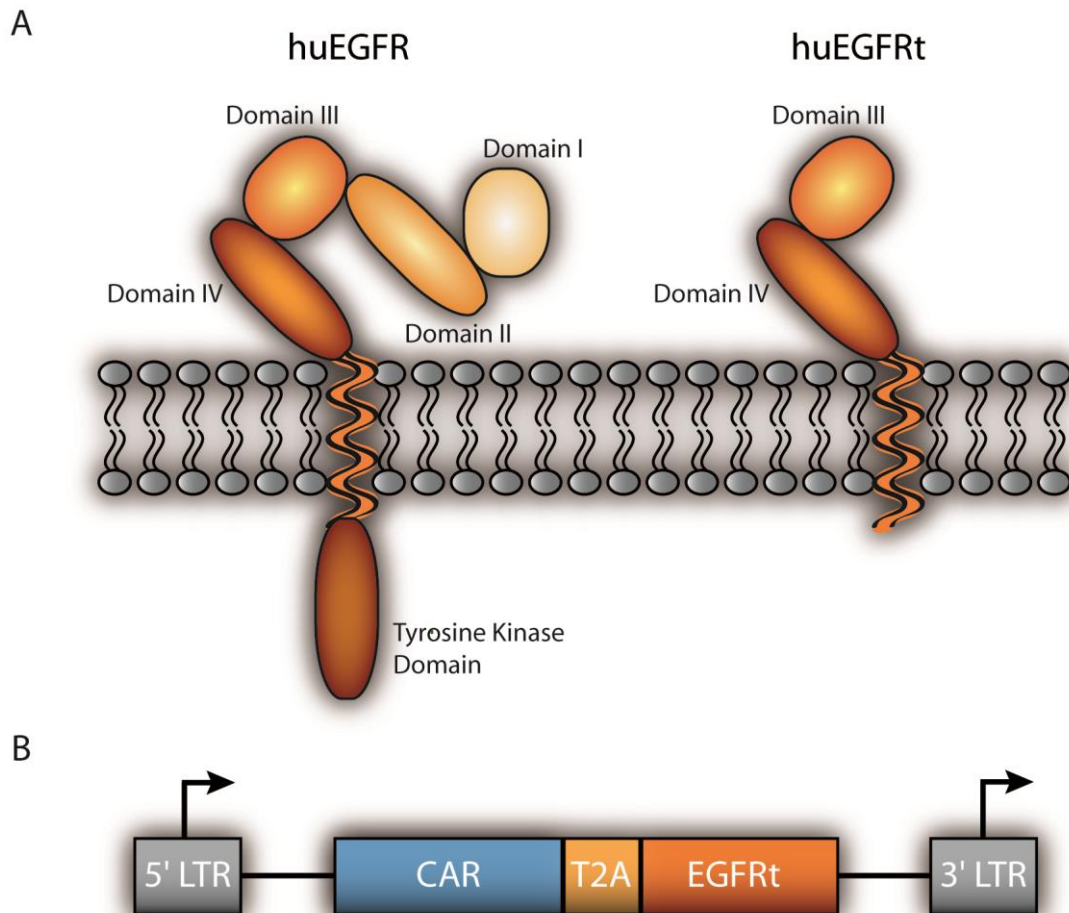


Fig. 4-1: Putative structure of the truncated EGFR and implementation into a gene expression vector. A. Schematic representation of the human EGFR (huEGFR) illustrates the putative structure of the wildtype EGFR, including four extracellular domains and an intracellular tyrosine kinase domain. The truncated form of the EGFR (huEGFRt) lacks domain I and II and most of the cytoplasmic region of the full-length EGFR. B. The EGFRt can be included in any gene expression vector, e.g. encoding for a CAR and including a T2A linker for co-expression. LTR – long-term repeats, CAR – chimeric antigen receptor.

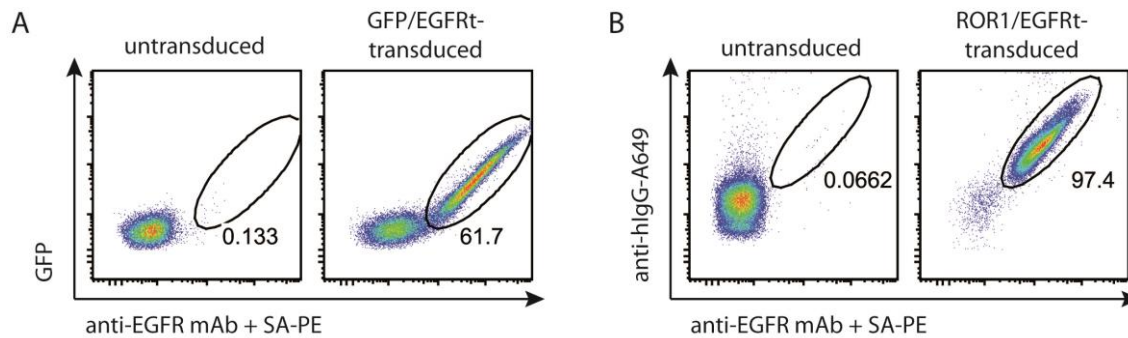


Fig. 4-2: Fluorescent proteins or receptors can be co-expressed with the EGFRt. A. Mouse splenocytes were transduced with a GFP/EGFRt gene construct and stained with an anti-EGFR mAb. B. Human T cells were transduced with a ROR1-CAR/EGFRt construct and stained with anti-human IgG and anti-EGFR antibodies. Similarly stained untransduced cells served as a negative control.

After demonstrating that the EGFRt can be in principle co-expressed with various transgenes, including CARs, it was important to show that the same subpopulation is detected by using a CAR-specific staining reagent and an anti-EGFR mAb. Further, we wanted to test whether the EGFRt can be used as a reliable tracking marker for both human and mouse engineered cells, which would allow for preclinical evaluation of the EGFRt in human T cell *in vitro* as well as in mouse models. First, the specificity of the EGFR staining was confirmed, as only the GFP/EGFRt-transduced human T cells were specifically detected with the anti-EGFR mAb, whereas untransduced human T cells were negative in the EGFR staining (Fig. 4-3A, upper panel). GFP<sup>+</sup> cells or the cell subset that was specifically stained with the EGFR mAb were gated in the histograms to demonstrate that the frequencies of cells identified by one of the two markers were quite similar. This equimolar expression of the transgene (represented by the GFP here) and the marker (= EGFRt here) is an important prerequisite for a tracking marker. The EGFR staining intensity is most likely higher than the GFP fluorescence intensity, because staining intensity is amplified by using a biotinylated anti-EGFR mAb and streptavidin. The middle panel shows the double staining of untransduced and ROR1-CAR/EGFRt-transduced T cells (Fig. 4-3A). The ROR1-CAR was detected with a multimer that was composed of the extracellular domain of ROR1, recombinantly fused to a *Streptag*, and a *Strep-Tactin-APC* backbone. Different staining intensities were commonly observed for the use of different fluorophores that were linked to the staining reagents (mAb, multimer, etc.). In the lower panel, T cells that were transduced with an anti-human CD19 (h19)-CAR/EGFRt construct were only stained with the EGFR mAb (Fig. 4-3A). CAR-specific reagents were not available, as the spacer-specific anti-

human IgG antibody led to an unspecific staining of untransduced human T cells (data not shown). This is an example for the advantage of implementing the EGFRt as an additional marker to overcome limited availability of CAR-specific staining reagents. Fig. 4-3B shows complementary stainings of mouse T cells that were transduced with a GFP/EGFRt (upper panel), a Hepatitis B viral antigen-specific S-CAR/EGFRt (middle panel) or an anti-mouse CD19 (m19)-CAR/EGFRt construct (lower panel). Co-expression of the EGFRt and GFP or the S-CAR was demonstrated by detecting the green fluorescence or by using the anti-human IgG antibody, respectively. Due to the lack of m19-CAR-specific staining reagents, the transduced mouse T cells could only be detected by EGFR staining in the lower panel. These examples show that the EGFRt can be co-expressed with various transgenes to serve as a reliable marker for identifying genetically engineered T cells of mouse and human origin.

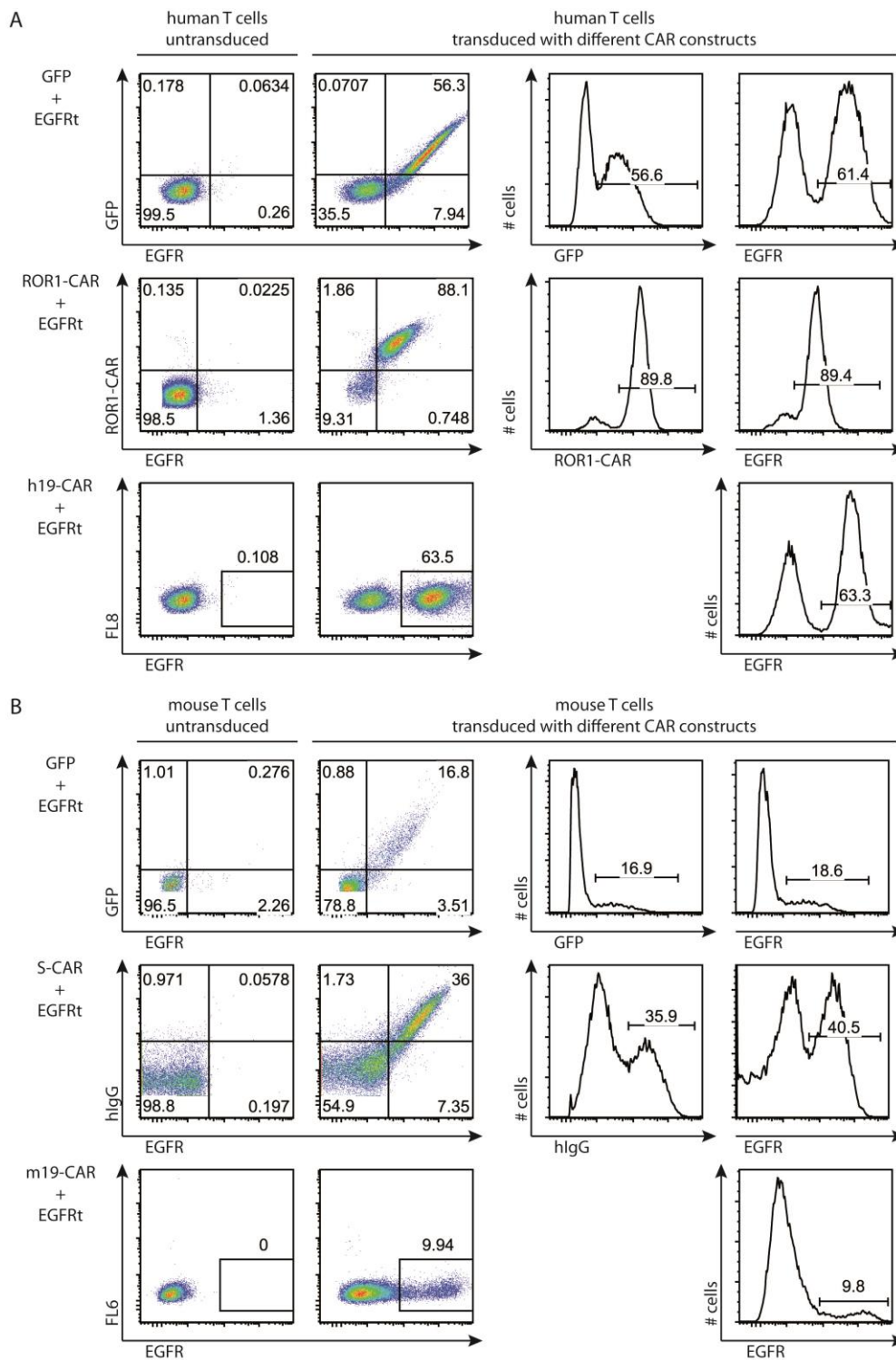


Fig. 4-3: The EGFRt allows for detection of mouse or human cells that were transduced with various constructs. A. Human T cells were transduced with a GFP/EGFRt, a ROR1-CAR/EGFRt or an anti-human CD19 (h19)-CAR/EGFRt gene construct and stained with the anti-EGFR mAb. Co-expression was demonstrated by GFP fluorescence or costaining with a ROR1-*Streptamer*. Positive fractions are gated in the histograms of the single stainings. Stained untransduced T cells served as negative controls. B. Mouse T cells were transduced with a GFP/EGFRt, an S-CAR/EGFRt or an anti-mouse CD19 (m19)-CAR/EGFRt gene construct and stained with the EGFR mAb and a CAR-specific reagent, if available.

#### 4.1.2 Stable expression of the EGFRt *in vitro* and *in vivo*

A reliable tracking marker needs to be detectable independently of the activation status of the cell. To address this question *in vitro*, mouse T cells were transduced with a hCD19- or mCD19-CAR/EGFRt with different transduction efficiencies (70.7% for hCD19, 10.6% for mCD19; Fig. 4-4A). T cells were activated specifically in a 5 hour-coincubation with target cells, i.e. human LCLs (CD19<sup>+</sup>) or wildtype mouse splenocytes (containing a large fraction of CD19<sup>+</sup> B cells), respectively. Transduced T cells were either incubated in medium with DMSO as a negative control or activated by PMA/Ionomycin as a positive control. Representative flow cytometry plots show the staining for EGFR vs. CD45.1 that allowed for distinction of CD45.1<sup>+</sup> transduced T cells and CD45.1<sup>-</sup> LCLs or wildtype splenocytes added as target cells. The geometric mean fluorescence intensity (MFI) of the EGFR staining as a measure for the EGFR expression level did not change in response to activation for both hCD19- and mCD19-CAR/EGFRt-transduced T cells (Fig. 4-4B). Activation of T cells was effective as IFN $\gamma$  secretion was induced in the EGFRt<sup>+</sup> T cell population, when T cells were coincubated with target cells or stimulated with PMA/Ionomycin (Fig. 4-4C). We could not examine whether activation affected the CAR expression due to the lack of staining reagents for both the hCD19 and mCD19-CAR. In summary, *in vitro* activation did not affect EGFR expression levels on transduced mouse T cells.

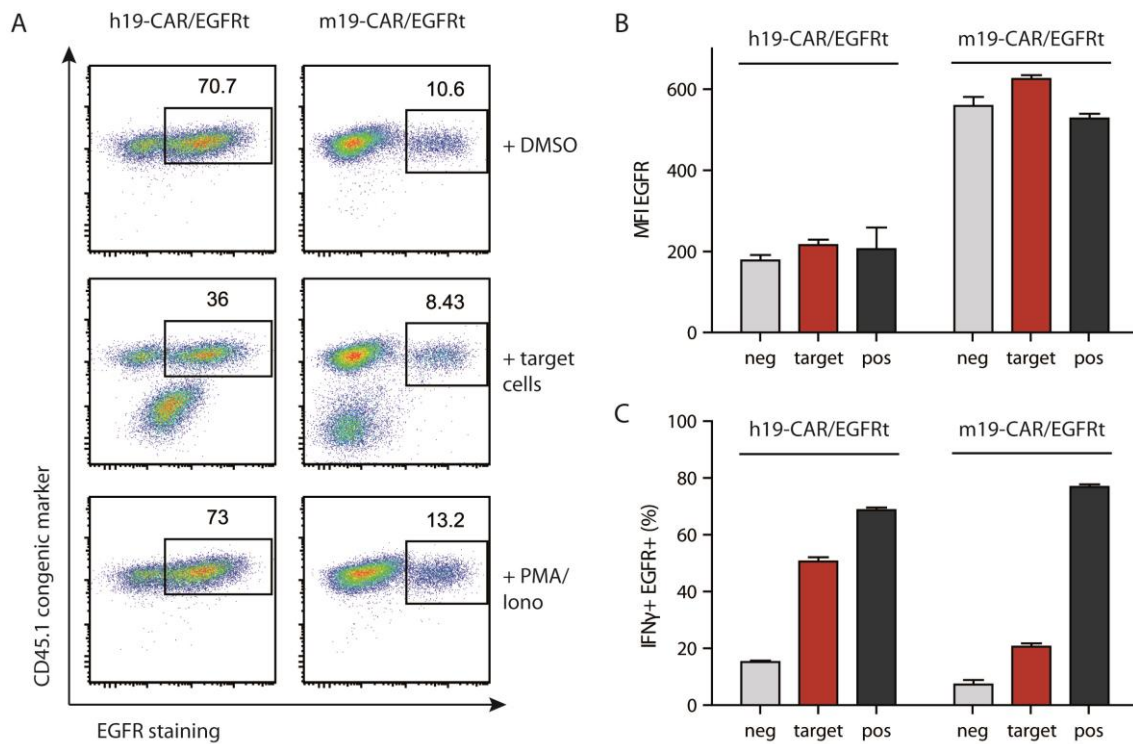


Fig. 4-4: The expression level of the EGFRt appears to be independent of the activation status of the cells *in vitro*. Anti-human CD19 (h19) or anti-mouse CD19 (m19)-CAR/EGFRt-transduced mouse CD45.1 T cells were coincubated for 5 hours with human LCLs or wildtype CD45.2 mouse splenocytes, respectively, as target cells. T cells incubated in medium with DMSO served as a negative control (neg), T cells stimulated with PMA/Ionomycin as a positive control (pos). A. Representative plots show staining of EGFR<sup>+</sup> CD45.1<sup>+</sup> T cells under different activation conditions. B. EGFR expression levels were assessed by the geometric mean fluorescence intensity (MFI) of the EGFR staining. C. IFN $\gamma$  secretion was analyzed by intracellular cytokine staining after adding GolgiPlug for the last 3 hours of coincubation.

The suitability of using the EGFRt as a tracking marker was further analyzed *in vivo* by assessing the stability of EGFR expression over long periods of time. GFP/EGFRt<sup>+</sup> Thy1.1<sup>+</sup> mouse splenocytes were transferred into mice that were sublethally irradiated one day before. The persistence of transferred T cells was monitored in the blood by staining for the congenic marker Thy1.1 and the EGFRt. Both the intracellular GFP and the surface-expressed EGFRt marker were co-expressed, as shown for an aliquot of sorted GFP/EGFRt<sup>+</sup> cells before transfer into mice as well as in a blood sample from day 150 after T cell infusion, pre-gated on the Thy1.1<sup>+</sup> cell population (Fig. 4-5A). The stability of marker expression was measured by the geometric mean of fluorescence intensity (MFI) of the GFP or the EGFR staining (Fig. 4-5B). The MFI for both markers was stable over a time period of 150 days.

Overall, the EGFRt can be used in combination with many different transgenes, including other markers, e.g. GFP, and various CARs. Genetically engineered T cells can be reliably detected with EGFR-specific staining antibodies. The level of EGFRt expression seems to be independent of the activation status of the transduced cells *in vitro*; EGFRt is also stably expressed on transduced cells that had been transferred into mice and were tracked in the blood over long periods of time.

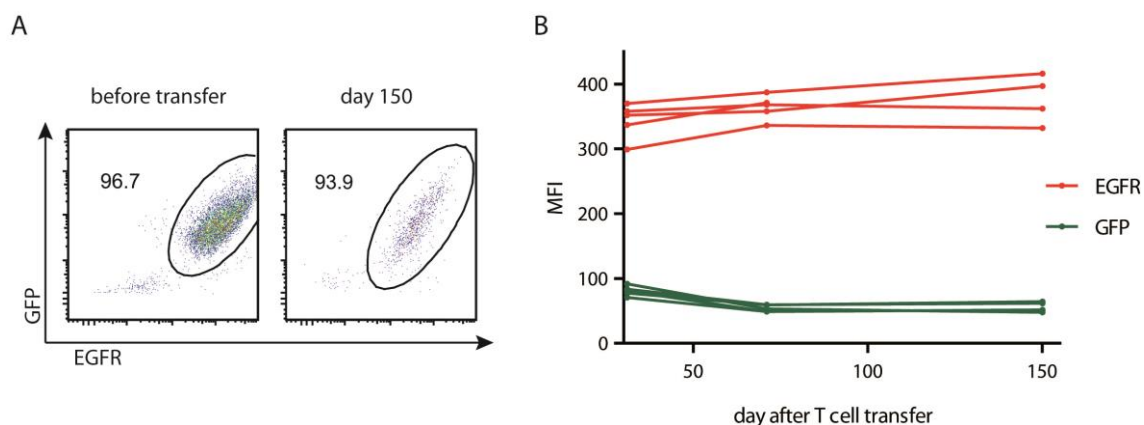


Fig. 4-5: The EGFRt expression is stable for long periods of time *in vivo*. GFP/EGFRt-transduced mouse splenocytes were sort-purified, transferred into sublethally irradiated mice and tracked in the blood. A. Co-expression of GFP and EGFRt could be shown for a sample of the sorted cells before transfer and in a blood sample from day 150 post infusion. Cells were pre-gated on the Thy1.1<sup>+</sup> cell subset. B. The mean fluorescence intensity (MFI) of the GFP and the EGFR staining was stable for 150 days.

## 4.2 Development of a reversible EGFR-specific Fab *Streptamer*

The EGFRt can be used as a selection marker to enrich for successfully engineered T cells before transfer into patients. Magnetic enrichment of EGFRt<sup>+</sup> T cells was previously shown based on the use of a biotinylated anti-EGFR mAb and Streptavidin-nanobeads [195]. Selection reagents are usually stably bound to the cell, which precludes including a selection step directly before infusing the cells into a patient because cell products require specific approval to contain cell-bound antibodies and magnetic particles. Thus, it would be desirable to develop an EGFR-specific selection reagent that is reversible. To meet this aim, a reversible anti-EGFR Fab was developed in collaboration with Christian Stemberger and Stefan Dreher in order to employ the *Streptamer* technology, which has been shown to be applicable to almost any surface marker [178]. As illustrated in Fig. 4-6, EGFRt<sup>+</sup> T cells can be stably bound by anti-EGFR Fab fragments that contain a *Streptag* and have been multimerized on a *Strep-Tactin* backbone. A fluorescent label is covalently linked to the *Strep-Tactin* to enable tracking of the *Streptamer* binding by microscopy or flow cytometry. The EGFR Fab *Streptamer* is disrupted by adding D-biotin that has a much higher affinity to the *Streptag* binding pocket of *Strep-Tactin* as compared to the *Streptag*. The *Strep-Tactin* is saturated with bound D-biotin and is released from the cell. If the residual EGFR Fab monomers are of sufficiently low affinity, they will dissociate spontaneously from the cell surface. The cell is now label-free, as neither Fab *Streptamers* nor individual components thereof are bound to the cell.

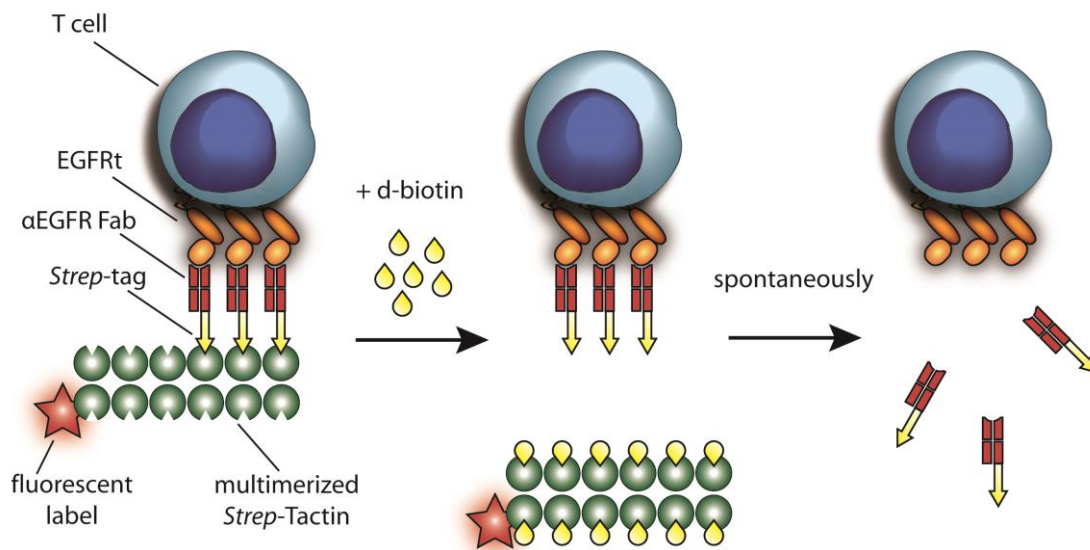


Fig. 4-6: The principle of the *Streptamer* technology. Binding of the anti-EGFR Fab *Streptamer* can be visualized by detecting the fluorescent label. Disruption of the multimer by adding a competitive ligand (d-biotin) results in spontaneous dissociation of the low-affinity Fab monomers.

#### 4.2.1 Generation and evaluation of the wildtype anti-EGFR Fab

The EGFR-specific Fab was based on the published anti-EGFR mAb clone A13 sequence [214]. As the sequence of the parental antibody was known, both the heavy and light variable regions ( $V_H$  and  $V_L$ ) of the Fab were generated using gene synthesis. Several serial cloning steps allowed the fusion of the constructs with the respective constant regions of the heavy and the light chain, the affinity tag as well as the integration of regulatory elements for the bicistronic expression of both chains. In a final cloning step the so generated cistron was cloned into the final Acceptor vector pASG-IBAwt2 using the Stargate cloning system. The pASG-IBAwt2 bacterial expression vector contains a tetracycline (*tet*)-promotor as well as the *ompA* signal sequences for periplasmic expression. The Fab-*Streptag* fusion protein can be expressed in *E.coli* by inducing the *tet*-promoter with anhydrotetracycline (AHT) and is then secreted into the periplasma of the bacteria. After periplasmic extraction and affinity purification of the Fab on a *Strep*-Tactin column, the specificity and purity of the EGFR A13 Fab was evaluated (Fig. 4-7). An aliquot of the *E.coli* culture was taken before (-) and after (+) induction of protein expression by AHT. Protein lysates were obtained from both samples and subjected to western blot to detect the Fab with an anti-*Streptag* mAb and a HRP-conjugated anti-mouse secondary antibody (Fig. 4-7A). In the sample that

contained the expressed protein (+), a band was detected at 26-28 kDa that is the expected size of the  $V_H$  of the EGFR Fab, which was fused to the *Streptag*. To assess the purity, the EGFR A13 Fab that has been eluted from the *Strep*-Tactin column was subjected to SDS-PAGE and the silver staining of the gel showed a high purity of the target protein (Fig. 4-7B). The high purity of the EGFR Fab was further confirmed by analyzing the Fab on a Bioanalyzer (Fig. 4-7C-E). The gel-like image displayed very faint bands at 26 and 30 kDa and corresponding low peaks could be identified in the electropherogram. The additional peaks were derived from the lower and upper markers. The calculated size of the  $V_H$  and  $V_L$  chain of the Fab matched the expected size of the Fab. The relative concentration of the total Fab was relatively low (15.7 ng/ $\mu$ L), whereat the  $V_H$  chain was overrepresented by the factor 2 compared to the  $V_L$  chain. This is commonly observed if Fab purification solely depends on the binding of the *Streptag* on the  $V_H$  chain to the *Strep*-Tactin column. Further affinity tags, such as the His-tag, can be added to the  $V_L$  chain of the Fab to increase purities by a second affinity purification step.

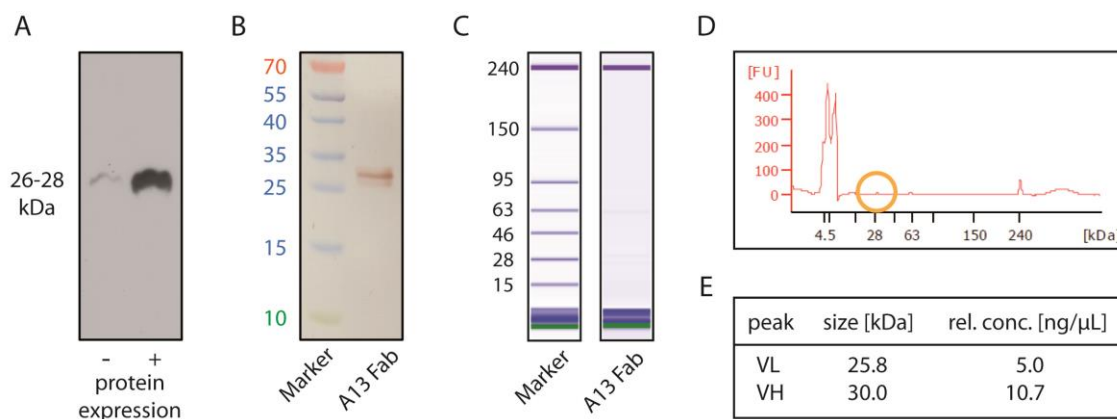


Fig. 4-7: The EGFR-specific Fab can be expressed with high purity by using a bacterial periplasmic expression system. A. In a western blot, the wildtype EGFR Fab-*Streptag* fusion protein that was obtained from an *E.coli* culture after induction of protein expression was detected by the anti-*Streptag* mAb and HRP-conjugated secondary mAb. B. Purity of the Fab-*Streptag* fusion protein, expressed in *E.coli* and purified on a *Strep*-Tactin column, was assessed by silver staining C-E. Purity of the wt EGFR Fab was analyzed on a Bioanalyzer. Gel-like images (C) and the electropherogram (D) are shown for the protein marker and the A13 Fab, highlighted by an orange circle in (D). The size and relative concentration of the individual Fab chains was calculated by the software (E).

Next, we used the purified wildtype (wt) EGFR Fab in stainings to test whether it specifically recognized the EGFRt that was expressed on the genetically modified lymphoma T cell line H9 (Fig. 4-8). To detect the staining by flow cytometry, the EGFR Fab was multimerized on *Strep*-Tactin-APC. The EGFR Fab *Streptamer* specifically

detected EGFRt<sup>+</sup> H9 cells, while the staining of untransduced H9 cells was negative. As the binding site of the paternal mAb A13 was mapped to the extracellular domain III of the wildtype EGFR [214], we expected that the EGFR Fab *Streptamer* could also bind to the truncated EGFR. Nevertheless, the three-dimensional structure of the EGFRt might have been affected by the truncations, but fortunately, there was no evidence for the A13 epitope being less accessible in the EGFRt as compared to the wt EGFR. To potentially improve the staining, the EGFR Fab wt was titrated from 0.01 to 1 $\mu$ g, while the amount of *Strep*-Tactin was kept at the same level. The staining intensity of the EGFR staining increased for up to 0.2 $\mu$ g Fab, but did not improve at higher Fab concentrations.

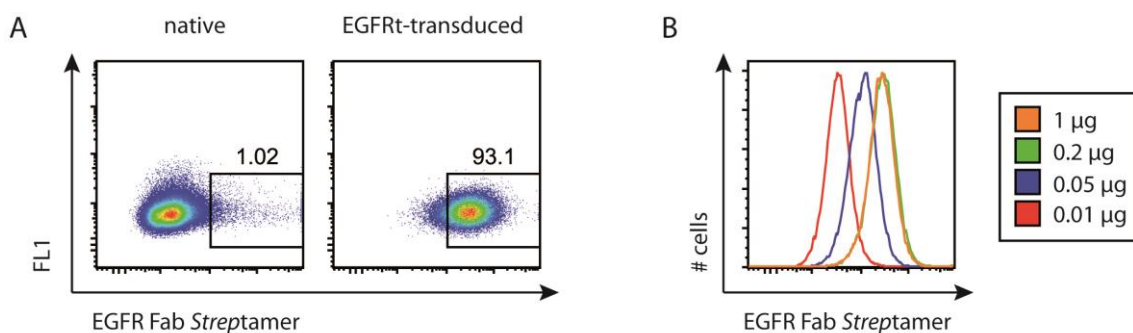


Fig. 4-8: The anti-EGFR Fab-*Streptamer* specifically detects the EGFRt in a concentration-dependent manner. A. The EGFRt-transduced lymphoma T cell line H9 was stained with the EGFR Fab *Streptamer*. Native H9 cells served as a negative control. B. The EGFR Fab concentration was titrated for improving the *Streptamer* staining.

The specificity of staining EGFRt<sup>+</sup> T cells with the EGFR Fab *Streptamer* was confirmed by simultaneous staining with an anti-EGFR mAb (Fig. 4-9). Both the biotinylated EGFR mAb in combination with streptavidin (SA)-PE and the EGFR Fab multimerized on *Strep*-Tactin (ST)-APC detected the EGFRt<sup>+</sup> T cell population in single stainings. As controls, the EGFRt<sup>+</sup> T cells were stained only with SA-PE or ST-APC to exclude unspecific binding. Costaining with both EGFR-specific staining reagents resulted in a PE/APC double-positive T cell population. As expected, the intensity of the staining with the biotinylated EGFR mAb was higher, as the staining is amplified by SA binding to multiple biotins on one mAb. As T cells co-expressed GFP with the EGFRt marker, the specificity of the EGFR staining could be further illustrated by plotting the EGFRt against GFP (Fig. 4-9).

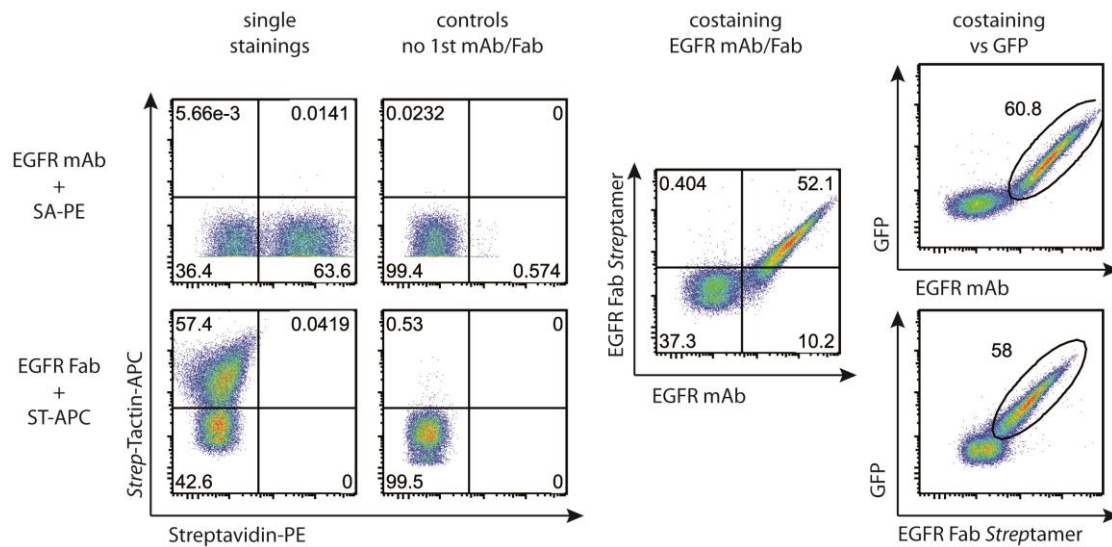


Fig. 4-9: Specificity of the staining with anti-EGFR Fab-*Streptamers* is confirmed by antibody staining. A mix of GFP/EGFR<sup>+</sup> and untransduced T cells was stained either with the EGFR mAb + streptavidin (SA)-PE or with the EGFR Fab + *Strep*-Tactin (ST)-APC in single stainings or costainings. SA-PE and ST-APC only served as controls for unspecific staining. Stained T cells are also shown in EGFR vs. GFP plots.

Finally, the reversibility of the EGFR Fab wt was analyzed in a flow cytometry-based assay. In general, *Streptamer* binding is monitored by detecting the fluorophore that is linked to the *Strep*-Tactin backbone. After disrupting the multimer with D-biotin, the fluorescent signal disappears. To control for residual cell-bound Fab monomers, cells are restained with the *Strep*-Tactin backbone only. Compared to a bivalent parental antibody, the monovalent Fab-fragment should have a lower binding strength to its target, potentially already resulting in spontaneous dissociation from the cell surface without any further modification of the Fab. For testing the reversibility of the wildtype EGFR Fab at 4°C, EGFR<sup>+</sup> H9 cells were stained with the Fab-*Streptamer* (orange, Fig. 4-10). Disruption of the *Streptamer* complex was successful, as the backbone signal vanished (blue). Restaining with the *Strep*-Tactin backbone led to a positive staining of the EGFR<sup>+</sup> cells (green) due to residual EGFR Fab fragments on the cell surface. Stainings are shown as histogram overlays, including a control staining with *Strep*-Tactin only on a separate aliquot of EGFR<sup>+</sup> H9 cells to assess the background due to unspecific staining of the *Strep*-Tactin (Fig. 4-10). The positive *Strep*-Tactin restaining showed that the affinity of the EGFR Fab wt is too high for being spontaneously released from the cell. Hence, the EGFR Fab wt is not reversible in its monomeric form.

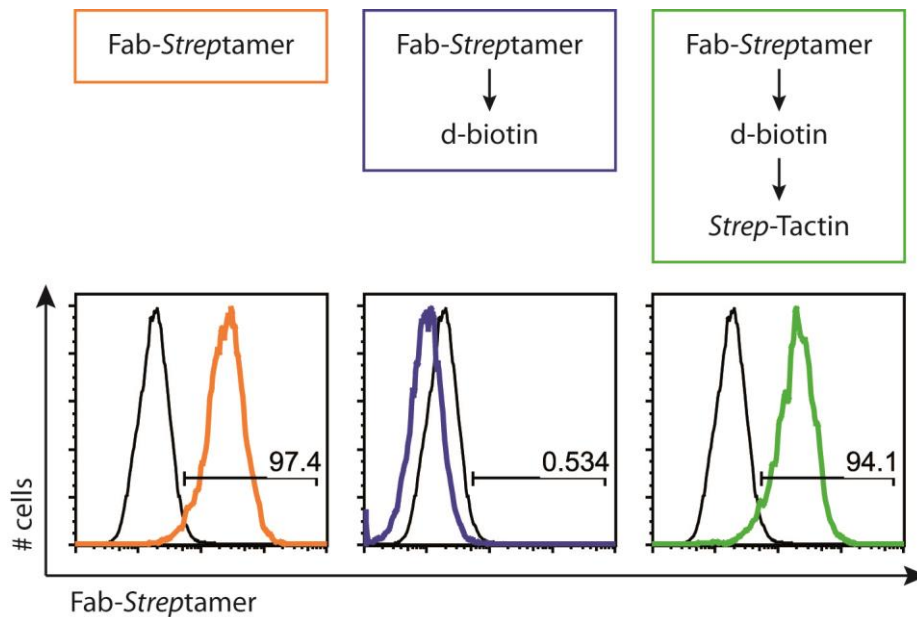


Fig. 4-10: The wildtype anti-EGFR Fab is not reversible at 4°C. EGFRt<sup>+</sup> H9 cells were stained with EGFR Fab *Streptamers* (orange), which was reversed by adding d-biotin (blue). Residual cell-bound Fab fragments were detected by restaining with the *Strep-Tactin* backbone (green). As a control, EGFRt<sup>+</sup> H9 cells were stained with *Strep-Tactin* only (black).

#### 4.2.2 Reversibility of EGFR Fab fragments with single mutations

To develop a reversible anti-EGFR Fab, its affinity had to be decreased by introducing single mutations into the wildtype EGFR Fab sequence. Single amino acids were exchanged for alanine by mutagenesis PCR. Most frequently, amino acids within the framework region in close vicinity to the complementarity determining region (CDR) were mutated, as these positions were found to be important for the binding kinetics of a Fab without completely interfering with the Fab specificity to its target [216]. The EGFR Fab single mutants are summarized in Table 1. The Fab expression levels varied between the different mutants and therefore affected the amount of Fab required for optimal staining. For this purpose, each Fab mutant was titrated and then tested for reversibility at 4°C with comparable staining intensities as a starting point (Fig. 4-11). Depending on the position of the single mutations, they affected the Fab staining and reversibility to different extents. The mutations within the CDR1 mutL1 and mutL2 impaired the overall staining with Fab-*Streptamers* and are therefore not suitable as a reversible Fab reagent. On the other hand, several mutations (e.g. mut76, mut87 and mut93) did not seem to have a major impact on the Fab affinity. In these cases, the EGFRt<sup>+</sup> T cells could be restained with the *Strep-Tactin* backbone with a similar

staining intensity as for the initial *Streptamer* staining, resulting in similar frequencies of gated EGFR<sup>t</sup> T cells. EGFR Fab mut72 was an interesting mutant, as it showed a solid staining when multimerized and a decreased signal intensity upon restaining with *Strep-Tactin*. Compared to the *Streptamer* staining with mut72, the cell population shifted towards the negative control in the *Strep-Tactin* restaining. Thus, the frequency of ST-restained cells was most decreased for the EGFR mut72 (71.1%) as compared to all other staining mutants (81.8 – 98.7%). So far, we were not able to identify an EGFR Fab mutant that was fully reversible at 4°C.

Table 1: Summary of anti-EGFR Fab fragments with single mutations

Mutant	aa pos.	localization	conc. [ug/mL]	staining	reversible (4°C)	reversible (RT)
wt	-	-	66.8	ok	no	no
mutH1	V <sub>H</sub> :119	framework	61.5	ok	no	no
mutL1	V <sub>L</sub> :44	CDR1	415.5	weak	(yes)	(yes)
mutL2	V <sub>L</sub> :47	CDR1	312.8	no	n.d.	no
mutL3	V <sub>L</sub> :48	framework	174.4	ok	no	no
mut67	V <sub>H</sub> :67	framework	61.6	ok	no	no
mut72	V <sub>H</sub> :72	framework	179.6	ok	no	yes
mut76	V <sub>H</sub> :76	framework	n.d.	ok	no	no
mut87	V <sub>H</sub> :87	framework	n.d.	ok	no	no
mut93	V <sub>H</sub> :93	framework	133.5	ok	no	no
mut103	V <sub>L</sub> :103	framework	n.d.	ok	no	no

As binding kinetics highly depend on the temperature, all EGFR Fab mutants were tested for reversibility at room temperature as well (Fig. 4-12). The staining protocol was changed to directly assess the capability of Fab monomers to stably bind to the cells. Instead of staining the EGFR<sup>t</sup> T cells with a pre-formed Fab-*Streptamer*, cells were pre-incubated with 1 µg Fab monomers, before adding *Strep-Tactin* to allow for multimer formation (orange). This strategy generally increased the EGFR staining intensity and also yielded a positive staining with EGFR Fab mutL2 that did not stain as a multimer. Here, only correctly folded and thus functional Fab-fragments bound their antigen and were then integrated into the multimer complex. A separate sample was equally preincubated with Fab monomers, but thoroughly washed with FACS buffer before *Strep-Tactin* was added (green). Fab-fragments of sufficient high affinity stayed bound to the cell, which was observed for most EGFR Fab mutants. As an exception, EGFR Fab mut72 yielded only a very weak staining if Fab monomers were washed off the cells before adding *Strep-Tactin*. The EGFR Fab mut72 was therefore identified as a promising candidate for a reversible EGFR-specific reagent.

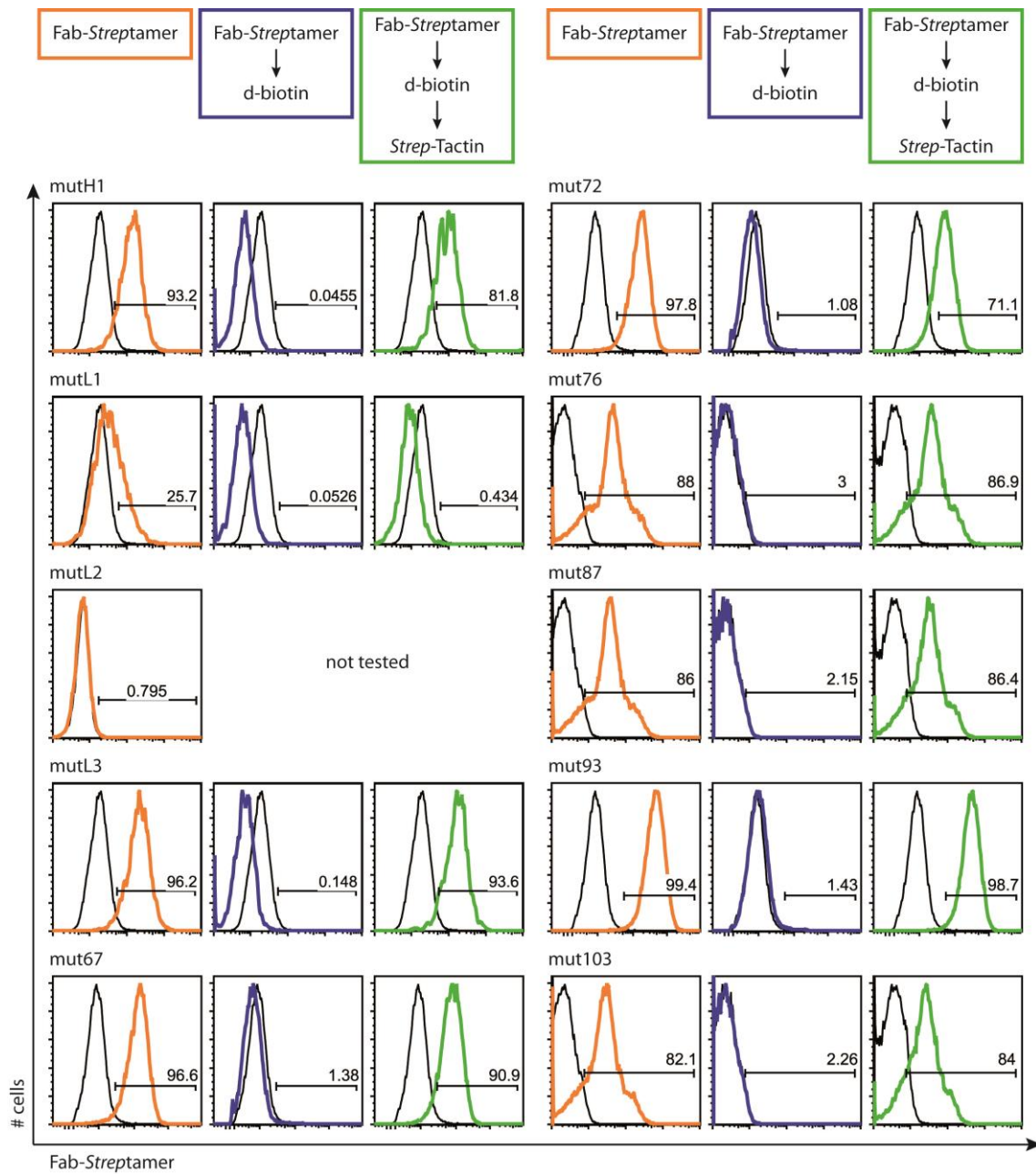


Fig. 4-11: Single mutations affect the Fab affinity to different extents. EGFR<sup>t</sup> T cells were stained with *Streptamers* composed of different EGFR Fab single mutants and *Strep-Tactin* (orange). After disrupting the multimer with d-biotin (blue), T cells were restained with *Strep-Tactin* (green) to test the Fab mutants for reversibility at 4°C.

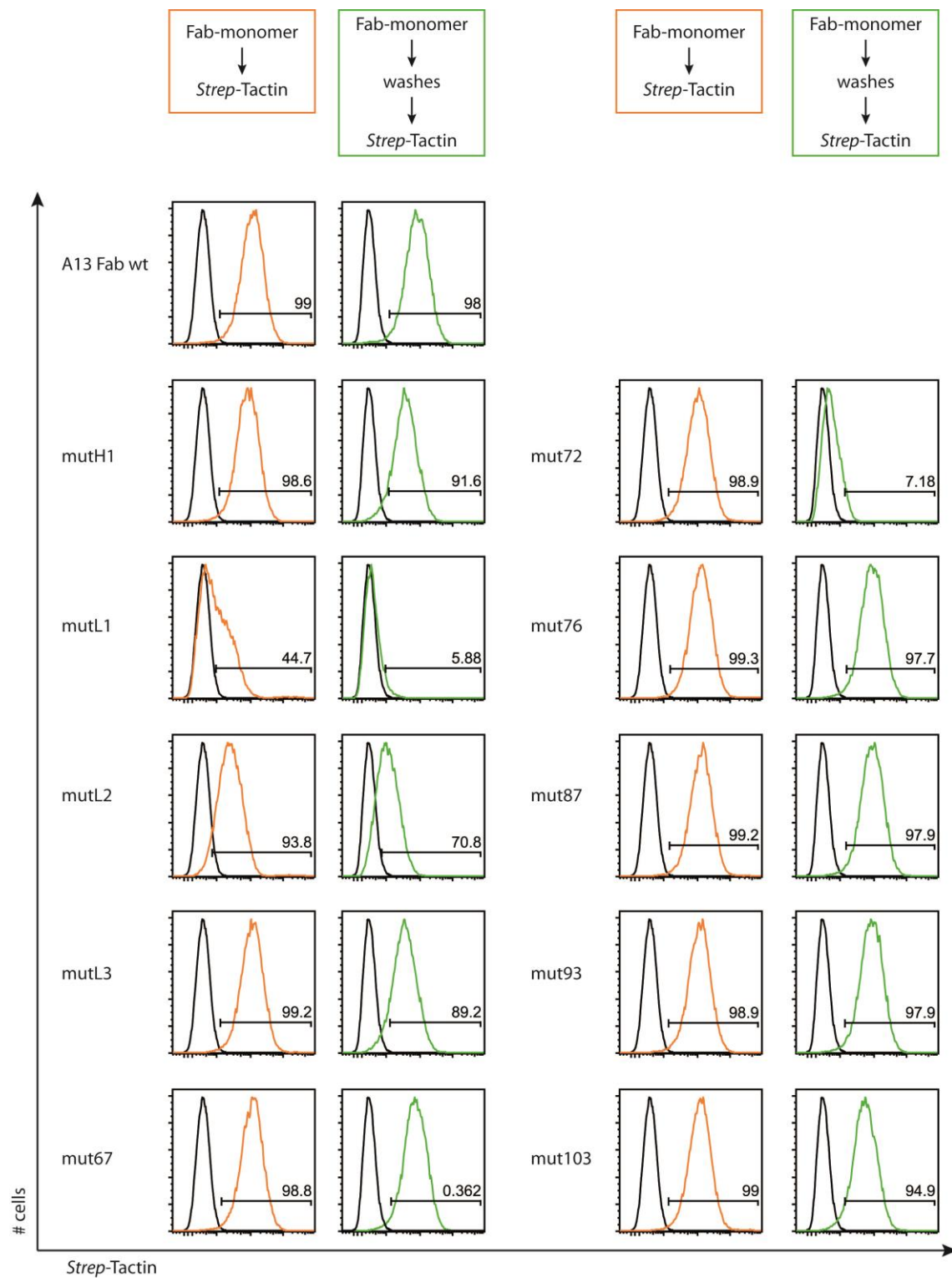


Fig. 4-12: Reversibility at room temperature varies to a great extent between the different EGFR Fab mutants. EGFR<sup>+</sup> T cells were stained by pre-incubating with Fab monomers and then adding *Strep-Tactin* as a reference for positive EGFR staining (orange). To test reversibility, pre-incubated T cells were washed three times with FACS buffer and residual EGFR Fab fragments were then detected by adding *Strep-Tactin* (green).

To further evaluate the EGFR Fab mut72, the *Streptamer* staining was optimized by titrating the Fab concentration from 0.01 to 1  $\mu\text{g}$  on EGFRt-transduced Jurkat cells (T lymphocyte cell line) (Fig. 4-13). The EGFR Fab mut72 specifically stained EGFRt-transduced but not native Jurkat cells. Similarly to the wildtype EGFR Fab, the maximum staining intensity was reached with 0.2  $\mu\text{g}$  Fab mut72.

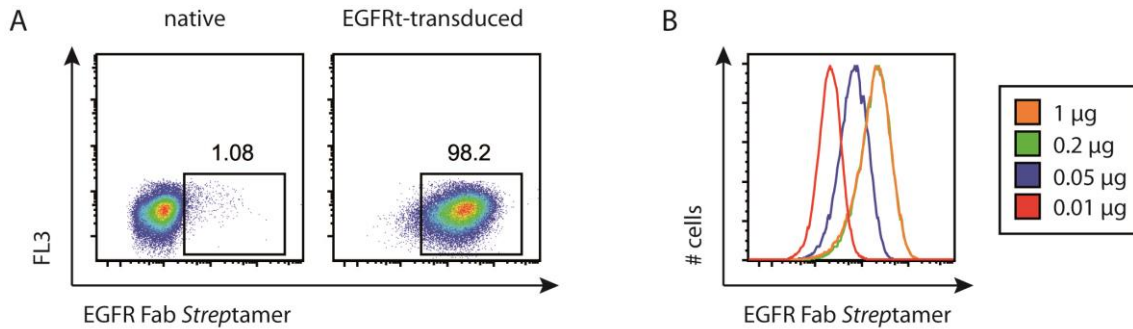


Fig. 4-13: The anti-EGFR Fab mut72 detects the EGFRt in a concentration-dependent manner. A. EGFRt<sup>+</sup> and native Jurkat cells were stained with the *Streptamer*, composed of the EGFR Fab mut72 and *Strep*-Tactin. B. The EGFR Fab mut72 was titrated up to 1  $\mu\text{g}$ .

The evaluation of reversibility of all EGFR Fab mutants at 4°C (Fig. 4-11) and at room temperature (Fig. 4-12) showed a strong correlation between reversibility of the EGFR Fab mut72 and temperature. The effect of temperature was further studied by staining EGFRt<sup>+</sup> Jurkat cells with the EGFR Fab mut72 *Streptamer* under optimal conditions (orange) and monitoring its detachment at 4°C, room temperature and 37°C (Fig. 4-14). Cells were kept at designated temperatures during the time of incubation with D-biotin, during washing and centrifugation steps. Expectedly, the multimer was disrupted at all temperatures as visualized by loss of staining (blue). Positive restaining with the *Strep*-Tactin backbone revealed that the EGFR Fab-fragments did not dissociate from the cell surface at 4°C (green). In contrast, the *Strep*-Tactin restaining intensity was significantly reduced, when cells were kept at room temperature, and further reduced by increasing the incubation temperature to 37°C. In order to test for remaining Fab-fragments, a control restaining with a new Fab *Streptamer* is performed to exclude the presence of residual D-biotin. D-biotin would prevent binding of the *Strep*-Tactin backbone to any residual cell-bound Fab fragments in the restaining control, which would not be a meaningful test for residual Fab monomers then. After release of the EGFR Fab *Streptamers* at different temperatures, a cell aliquot was successfully restained with a new *Streptamer* (red), demonstrating that D-biotin was completely washed off the cells (Fig. 4-14).

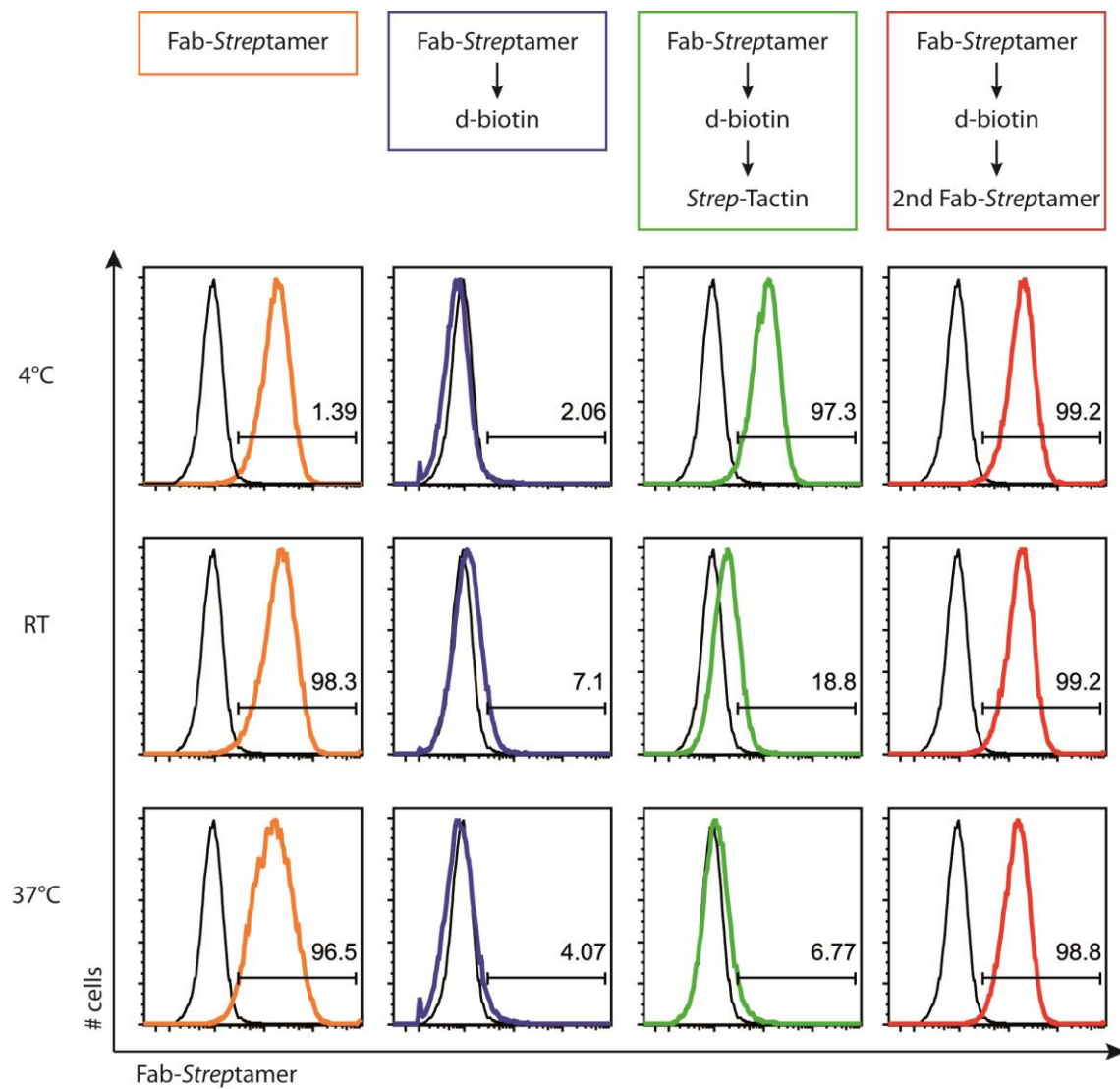


Fig. 4-14: The reversibility of the anti-EGFR Fab mut72 depends on the temperature. EGFR<sup>t+</sup> Jurkat cells were stained with the EGFR Fab mut72 *Streptamer* (orange). The multimer was released from the cells at indicated temperatures (blue). Residual Fab monomers were detected by *Strep-Tactin* remaining (green). Restaining with a new *Streptamer* is a control for presence of d-biotin in the system (red).

The Jurkat cell line is suitable for the evaluation of a big panel of EGFR Fab mutants to screen for potentially reversible mutants in a standardized system. However, the binding kinetics of the Fab could vary between the immortal Jurkat cell line versus primary T cells due to different cell size and membrane composition. To evaluate the potency of the most promising candidate EGFR Fab-fragment, the EGFR Fab mut 72 was then tested on human EGFRt-transduced primary T cells, as this is the cell population that will ultimately be targeted with the EGFR Fab *Streptamer* for clinical tracking or selection (Fig. 4-15). After Fab-*Streptamer* dissociation at 4°C, residual Fab monomers were still detectable by *Strep*-Tactin restaining (green). However, if dissociation of the Fab *Streptamer* was performed at room temperature, no cell-bound EGFR Fab monomers were detectable by restaining with *Strep*-Tactin. The second restaining with a new *Streptamer* confirmed the absence of D-biotin in the system (red).

In summary, the EGFR Fab mut72 was demonstrated to be fully reversible at room temperature. Further increasing the temperature to 37°C is therefore not necessary for complete removal of the EGFR Fab *Streptamer* from primary T cells.

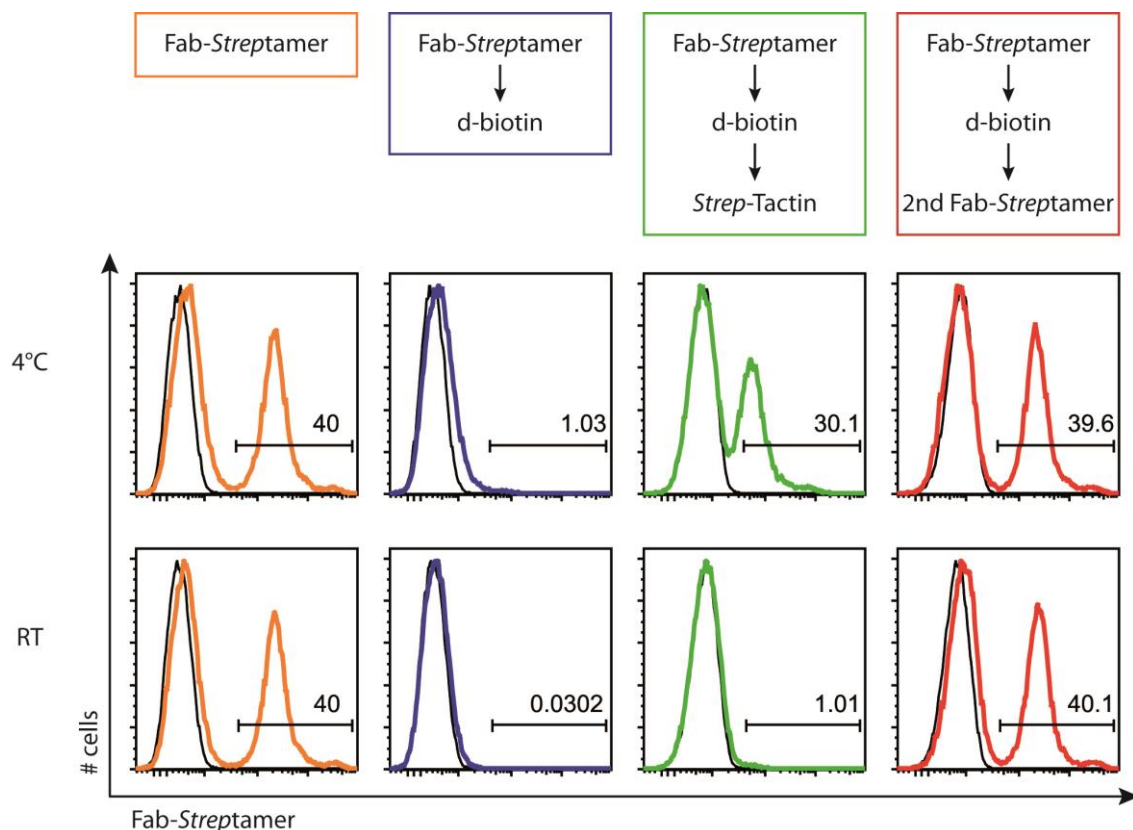


Fig. 4-15: The anti-EGFR Fab mut72 is fully reversible on room temperature. A mix of human EGFRt<sup>+</sup> and untransduced primary T cells were stained with the EGFR Fab mut72 *Streptamer* (orange). Release of the *Streptamer* at 4°C vs. room temperature was monitored (blue) and restainings with *Strep*-Tactin (green) and a new *Streptamer* were performed (red).

### 4.2.3 Evaluation of EGFR Fab fragments with double mutations

It is evident that the affinity of the EGFR Fab was significantly reduced by introducing a single mutation. We asked the question whether it is possible to further decrease the affinity of the EGFR Fab mut72 to reach reversibility at 4°C. Thus, we further modified the single mutant 72 by introducing a second mutation into the genetic sequence. The affinity should only be slightly decreased, so the exchange of the amino acid tryptophan at position 119 to alanine (= mutH1) was chosen as the second mutation, because this single mutation only slightly affected the *Streptamer* staining (Fig. 4-11). The EGFR Fab double mutant H1/72 did not yield a positive staining, when used as a Fab *Streptamer* for staining EGFR<sup>+</sup> T cells (data not shown). Presumably, changing the amino acids to alanine at those two positions reduced the Fab affinity to such an extent that the Fab could not stably bind as a multimer. Alternatively, these two mutations led to such profound changes in the Fab structure that its specificity was abolished. Following this logic, the tryptophan was substituted with a structurally similar amino acid that should have a smaller effect on the binding capacity or structure of the Fab-fragment. Thus, the tryptophan 119 was exchanged for a methionine (mutH1M/72) or a phenylalanine (mutH1F/72), which are both similar in size and contain a carboxyl group as does the tryptophan in the wildtype Fab. Interestingly, the staining was abolished for the EGFR Fab mutH1M/72, but an effective *Streptamer* staining could be achieved with the EGFR Fab mut H1F/72 (Fig. 4-16). The reversibility of the double mutant at room temperature appeared to be even better in a side-by-side comparison with the EGFR Fab single mutant 72. However, the enhanced reversibility of mutH1F/72 was correlated with a reduced intensity of the Fab *Streptamer* staining, which argues for EGFR Fab mut72 to be the better choice for cell tracking and selection.

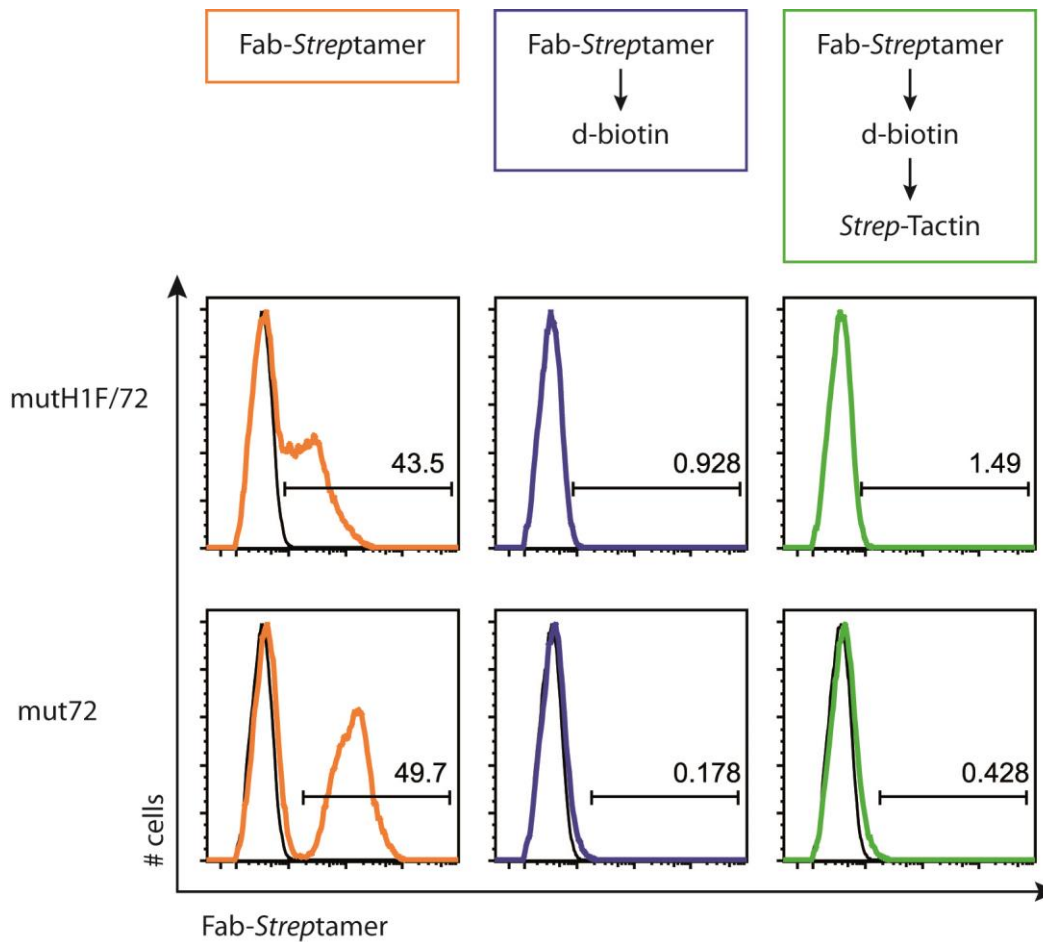


Fig. 4-16: Additional mutations can enhance Fab reversibility at the cost of staining intensity. EGFR<sup>t</sup> T cells were stained with EGFR Fab *Streptamers* containing two mutations (*mutH1F/72*) or one mutation (*mut72*) (orange). Reversibility was tested by adding d-biotin (blue) and restaining with *Strep-Tactin* (green).

We were interested whether the approach of ‘conservative amino acid substitution’ would also work for other double alanine mutants that cannot stably bind to EGFR<sup>t</sup> T cells. The effects of various mutations and their combination on the staining capacity and reversibility of the EGFR Fab is summarized in Table 2. As a second example, the EGFR Fab *mutH1/L1* was modified similarly to the *mutH1/72*, i.e. the tryptophan 119 was exchanged for methionine (*mutH1M/L1*) or phenylalanine (*mutH1F/L1*). As both of these double mutants did not permit stable staining, the exchange of the tyrosine 44 to alanine (=mutL1) seems to already inhibit binding on its own, which overrides the subtle effects of conservative substitution of the tryptophan 119. Consequently, the tyrosine 44 was exchanged for the structurally similar amino acid phenylalanine, which indeed led to a stable staining of *mutH1/L3F*, but did not allow for reversibility (Table 2).

In the third example of double mutants that involved conservative substitutions, the EGFR Fab mutH1F/L3 and mutH1/L3F (tyrosine 48 to phenylalanine) were tested in comparison to the 'original' Fab mutant H1/L3 with two alanine exchanges. Here, only the mutH1/L3F yielded a stable binding of the Fab *Streptamer* to EGFR<sup>+</sup> T cells, which was almost reversible at room temperature (data not shown).

These examples show that the effect of substituting an amino acid with alanine or a structurally similar amino acid has to be tested for each position and for combinations of mutations separately. There seems to be a trade-off between *Streptamer* staining intensity and reversibility. Unfortunately, introducing further mutations into the EGFR Fab mut72 did not result in a Fab of similar staining capacity and enhanced reversibility. Thus, the original EGFR Fab mut72 was taken forward to applications of cell tracking and cell selection.

Table 2: Summary of anti-EGFR Fab fragments with double mutations

Mutant	1 <sup>st</sup> mutation	2 <sup>nd</sup> mutation	conc [ug/mL]	staining	reversible
mutH1/72	V <sub>H</sub> :119 W→A	V <sub>H</sub> :72 R→A	20	no	n.d.
mutH1M/72	V <sub>H</sub> :119 W→M	V <sub>H</sub> :72 R→A	60	no	n.d.
mutH1F/72	V <sub>H</sub> :119 W→F	V <sub>H</sub> :72 R→A	50	<b>yes</b>	<b>yes, at RT</b>
mutH1/L1	V <sub>H</sub> :119 W→A	V <sub>L</sub> :44 Y→A	370	no	n.d.
mutH1M/L1	V <sub>H</sub> :119 W→M	V <sub>L</sub> :44 Y→A	100	no	n.d.
mutH1F/L1	V <sub>H</sub> :119 W→F	V <sub>L</sub> :44 Y→A	80	no	n.d.
mutH1/L1F	V <sub>H</sub> :119 W→A	V <sub>L</sub> :44 Y→F	120	<b>yes</b>	no
mutH1/L3	V <sub>H</sub> :119 W→A	V <sub>L</sub> :48 Y→A	260	no	n.d.
mutH1F/L3	V <sub>H</sub> :119 W→F	V <sub>L</sub> :48 Y→A	90	no	n.d.
mutH1/L3F	V <sub>H</sub> :119 W→A	V <sub>L</sub> :48 Y→F	120	<b>yes</b>	<b>yes, at RT</b>



this, mouse splenocytes were transduced with a CAR/EGFRt with a transduction rate of 27% and sorted by FACS, based on the EGFR Fab *Streptamer* staining (Fig. 4-18). The sort purity was 99%, as shown by restaining the sorted cells with the EGFR mAb. The EGFR Fab *Streptamer* staining itself could not be used to evaluate the sort purity, because the multimer had been released from the cell surface to conduct further experiments with the EGFRt-enriched cells. Sorting of EGFRt<sup>+</sup> cells by FACS was successfully repeated multiple times, both with genetically engineered mouse and human cells.

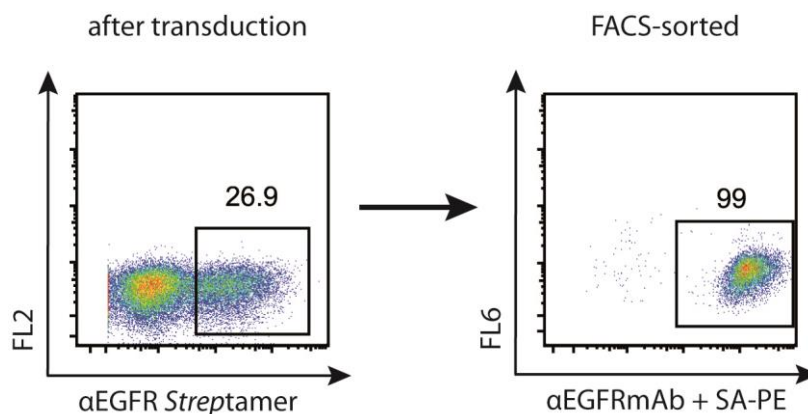


Fig. 4-18: EGFRt-transduced T cells can be enriched by flow cytometry-activated cell sorting (FACS). EGFRt<sup>+</sup> mouse T cells were sorted by FACS based on the staining with the EGFR Fab *Streptamer*. FACS-sorted EGFRt<sup>+</sup> cells were stained with the anti-EGFR mAb and streptavidin (SA)-PE to assess the sort purity.

### 4.3.1 Magnetic enrichment of EGFRt<sup>+</sup> T cells using nanobeads

Sorting cells by FACS is still challenging to get approved for clinical applications. As the EGFRt had to be evaluated for applicability in cell selections for clinical use, magnetic cell selection methods that are more commonly used for clinical applications were the focus of this part of the project. Clinical cell purification is most broadly performed with the Miltenyi platform that is based on labeling the target cell population with 'irreversible' antibodies and superparamagnetic nanobeads (approximately 50 nm in diameter). Such cell separations are performed on MACS columns, which guarantee that labeled target cells are held back in a magnetic field during washing steps. Afterwards, the positive fraction can be eluted from the column. Conventional magnetic nanobeads can be coated with streptavidin for the use with biotinylated antibodies. Similarly, nanobeads can also be covered with *Strep*-Tactin to enable binding to Fab-*Streptag* fusion proteins that guide selection of the cell population of choice. Adapting

this technology to the target molecule EGFRt, we used the EGFR Fab mut72 and *Strep*-Tactin nanobeads to test the magnetic enrichment of human GFP/EGFRt-transduced T cells (Fig. 4-19). The EGFRt<sup>+</sup> T cells made up 8% of the starting population before selection and the frequency increased to above 87% in the positive fraction, which demonstrates that using the EGFR Fab *Streptamer* with magnetic nanobeads for cell selection is feasible.

As the frequency of successfully transduced T cells is highly variable, it is important to show that selection purities are independent of the initial size of the EGFRt<sup>+</sup> cell population. Therefore, T cells with an EGFRt<sup>+</sup> fraction of 9-52% were magnetically enriched with the EGFR Fab *Streptamer* and nanobeads (Fig. 4-19B). One to four separate selections were performed for each sample in individual experiments. Purities of the positive fraction after EGFRt selection were around 90% on average and independent of the frequency of EGFRt<sup>+</sup> cells before selection. This indicates that the magnetic selection procedure using nanobeads is robust and consistently results in EGFRt<sup>+</sup> cell populations of high purity.

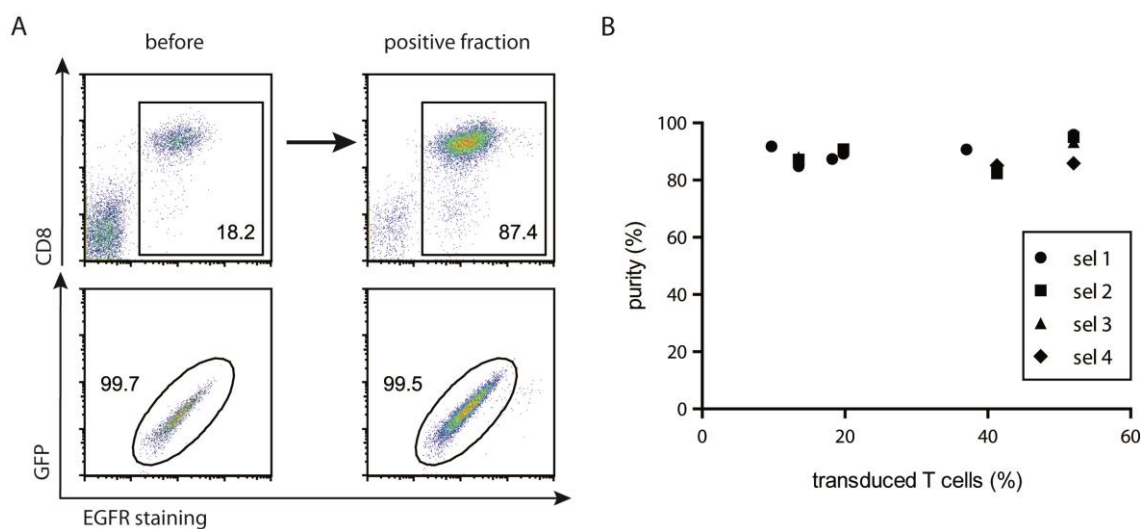


Fig. 4-19: EGFRt-transduced T cells can be enriched from populations with different EGFRt frequencies by using magnetic nanobeads. Human T cells that contained different proportions of EGFRt<sup>+</sup> cells were selected by using the EGFR Fab with *Strep*-Tactin nanobeads. A. Representative example of a magnetic enrichment of GFP/EGFRt<sup>+</sup> T cells, showing an aliquot before and after selection stained with the anti-EGFR mAb. B. Summary of all selections that were performed with 2  $\mu$ g EGFR Fab. Each sample was tested in one to four separate selections.

Purities and yields of the magnetic enrichment can potentially be improved by titration of the Fab. The EGFR Fab mut72 was tested at 2, 4 and 8  $\mu\text{g}$ , while the amount of *Strep*-Tactin nanobeads was kept constant at 25  $\mu\text{L}$ . Human  $\text{CD8}^+$   $\text{EGFR}^+$  T cells were spiked into  $\text{CD4}^+$  untransduced T cells to mimic a cell mix with common transduction efficiencies. Magnetic enrichment of  $\text{EGFR}^+$  T cells yielded a good purity of 86% when using 2  $\mu\text{g}$  Fab (Fig. 4-20A). Increasing Fab amounts to 4 or 8  $\mu\text{g}$  did not improve the purities and also did not have an effect on the yields of the enrichment (Fig. 4-20B, C). Therefore, 2  $\mu\text{g}$  of the EGFR Fab were used for all following selection with nanobeads.

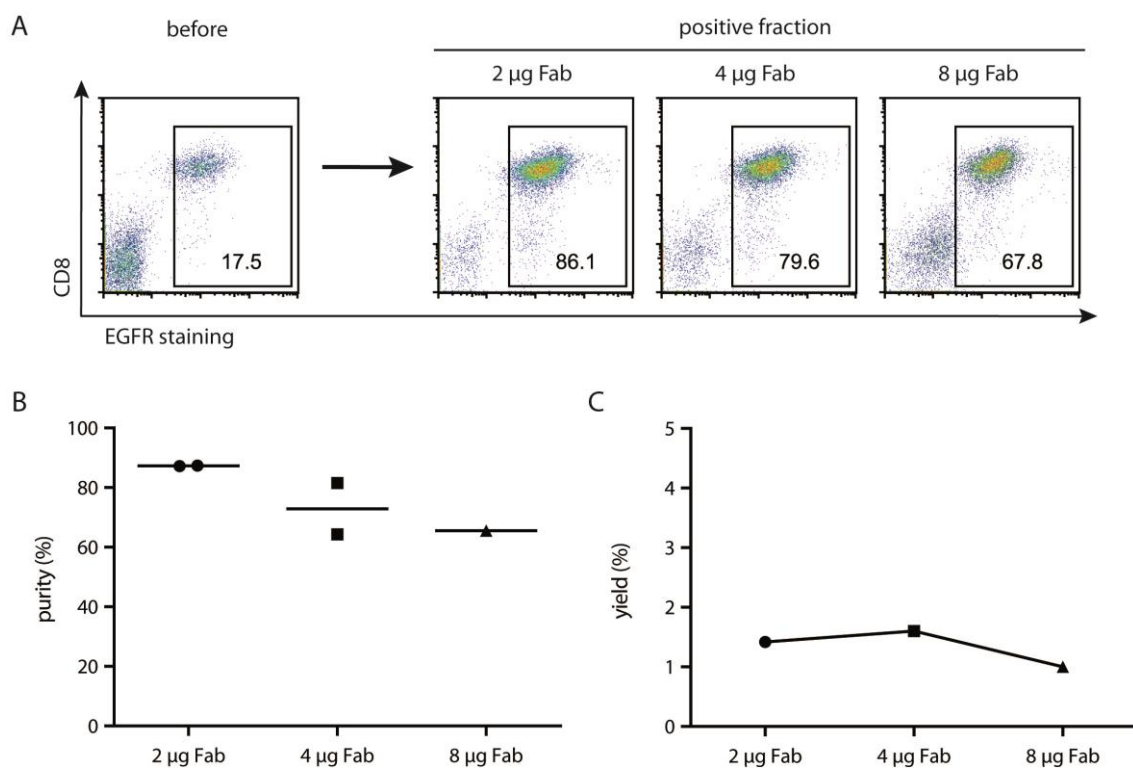


Fig. 4-20: Increasing amounts of Fab reduce the purity of  $\text{EGFR}^+$  T cells that have been enriched with magnetic nanobeads. A. Human  $\text{CD8}^+$   $\text{EGFR}^+$  T cells were enriched by using increasing amounts of the EGFR Fab and 25  $\mu\text{L}$  *Strep*-Tactin nanobeads. B. The frequency of  $\text{EGFR}^+$  cells in the positive fraction equals the purity of selection. C. The yields of the enrichment were calculated from the ratio of the  $\text{EGFR}^+$  cell number in the two aliquots, 'positive fraction' and 'before'.

Another parameter that might influence the outcome of magnetic enrichments is the amount of nanobeads per fixed cell number. In a similar experimental setup as for the Fab titrations, human CD8<sup>+</sup> EGFRt<sup>+</sup> T cells were selected with 2 µg EGFR Fab and increasing amounts of *Strep*-Tactin nanobeads in three separate experiments (Fig. 4-21). Two experiments are shown in Fig. 4-21A and B, where nanobeads were titrated from 12.5 µL to 50 µL and 50 µL to 100 µL per 1x10<sup>7</sup> cells, respectively. The summary graphs of purities and yields include further data from other selections of human T cells (and one selection of macaque T cells), where 2 µg Fab and different amounts of nanobeads were used (Fig. 4-21C, D). Purities were not affected by increasing amounts of nanobeads up to 300 µL per 1x10<sup>7</sup> cells, and ranged from 83 to 96%. On the other hand, yields increased from around 5% to above 30%, when using larger amounts of nanobeads. Experimental conditions were not exactly similar in between individual experiments, indicated by different colors in Fig. 4-21C and D, but the correlation between higher amounts of nanobeads and improved yields was observed in all selections that were pooled in these graphs.

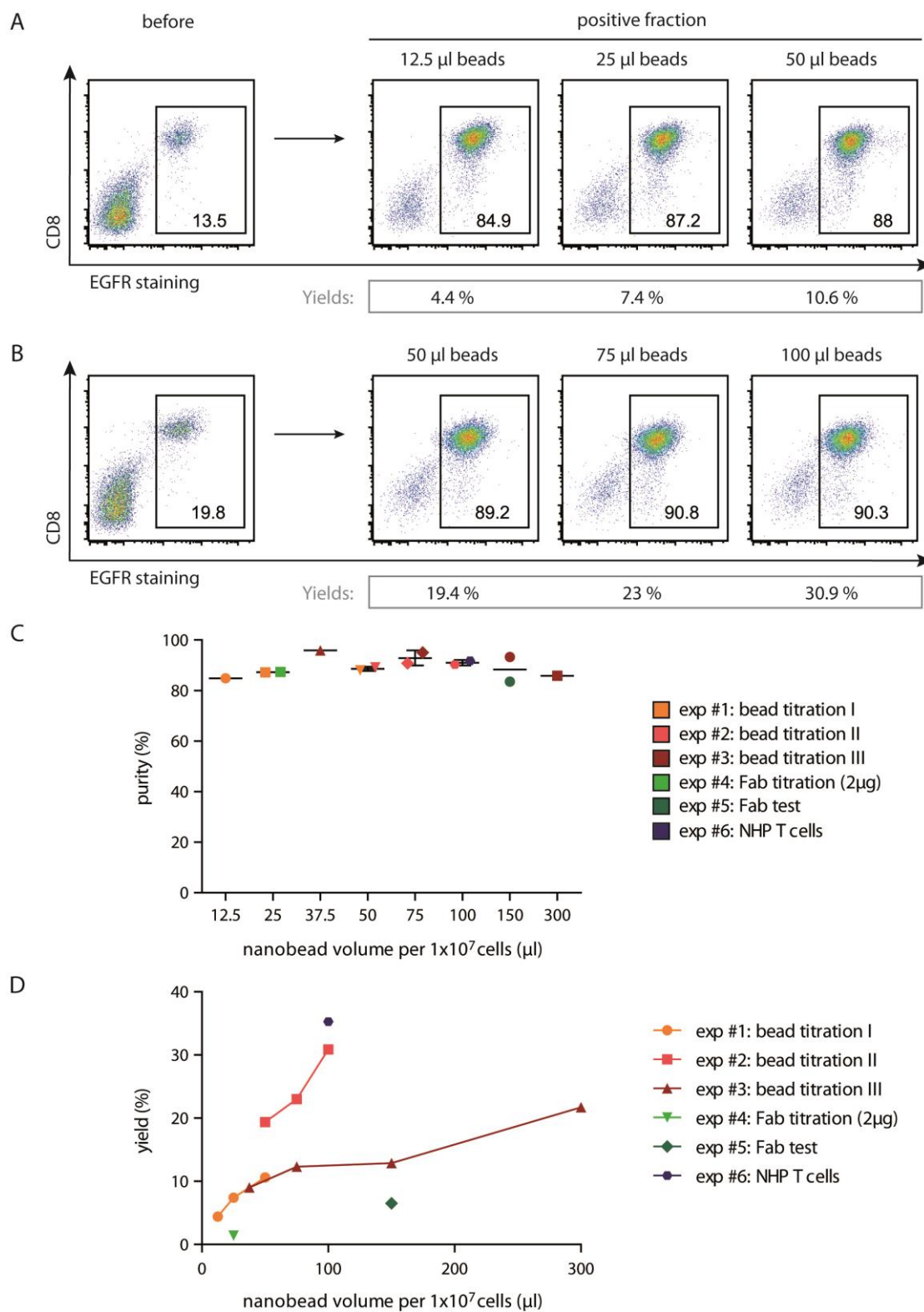


Fig. 4-21: Yields of magnetic selections can be improved by increasing the amount of nanobeads. A and B. Human CD8<sup>+</sup> EGFR<sup>+</sup> T cells were enriched with 2  $\mu$ g EGFR Fab and increasing amounts of *Strep*-Tactin nanobeads. The EGFR staining of the aliquots 'before' and 'positive fraction' are shown. C. Purities of all selections of human and macaque T cells, performed with 2  $\mu$ g EGFR Fab, are shown in correlation to the amount of nanobeads. D. Yields of the same selections as in (C). Data points of the same color belong to individual experiments.

After having optimized the parameters 'amount of Fab' and 'amount of nanobeads', we could show that magnetic enrichment of EGFRt<sup>+</sup> T cells using the EGFR Fab results in high purities and reasonable yields. We then wanted to compare the new reversible Fab-based selection to the 'irreversible' mAb-based selection that had been used to enrich EGFRt<sup>+</sup> T cells so far. The conventional selection method is based on detection of EGFRt<sup>+</sup> cells by the biotinylated anti-EGFR mAb and magnetically labeling these cells with the Streptavidin-coated nanobeads. Fab-based selections require *Strep*-Tactin-coated nanobeads, but are otherwise similar with regard to the experimental procedure. For comparison, human EGFRt<sup>+</sup> T cells were enriched using constant amounts of the EGFR mAb (10 $\mu$ L) or EGFR Fab mut72 (2 $\mu$ g) and a range of nanobead volumes (10-150 $\mu$ L). Purities are similar for both mAb and Fab-based magnetic selections, while yields might be slightly higher, when using the EGFR Fab (Fig. 4-22A, B). Optimal conditions of both selection procedures were chosen for a side-by-side comparison of the enrichment of macaque T cells that had been genetically engineered with an 'EGFRt only' construct with a low transduction efficiency of 9.7% (Fig. 4-22C). In this individual experiment, the purity of the Fab-based approach was higher than the purity of the mAb-based selection (91.8% vs. 84.7%). Importantly, better purities were not associated with a loss in yield, as the Fab-based enrichment also resulted in a 4-fold higher yield as compared to the mAb-based protocol (35.3% vs. 9%).

Several experiments have shown that cell selections with the EGFR Fab and *Strep*-Tactin nanobeads result in at least comparable outcomes regarding purities and yields as the conventional protocols based on the EGFR mAb. In addition, the EGFR Fab selection reagent can be completely released from the cell surface after performing the cell purification step, as confirmed by negative *Strep*-Tactin restaining of the positive fraction in the representative example in Fig. 4-22C.

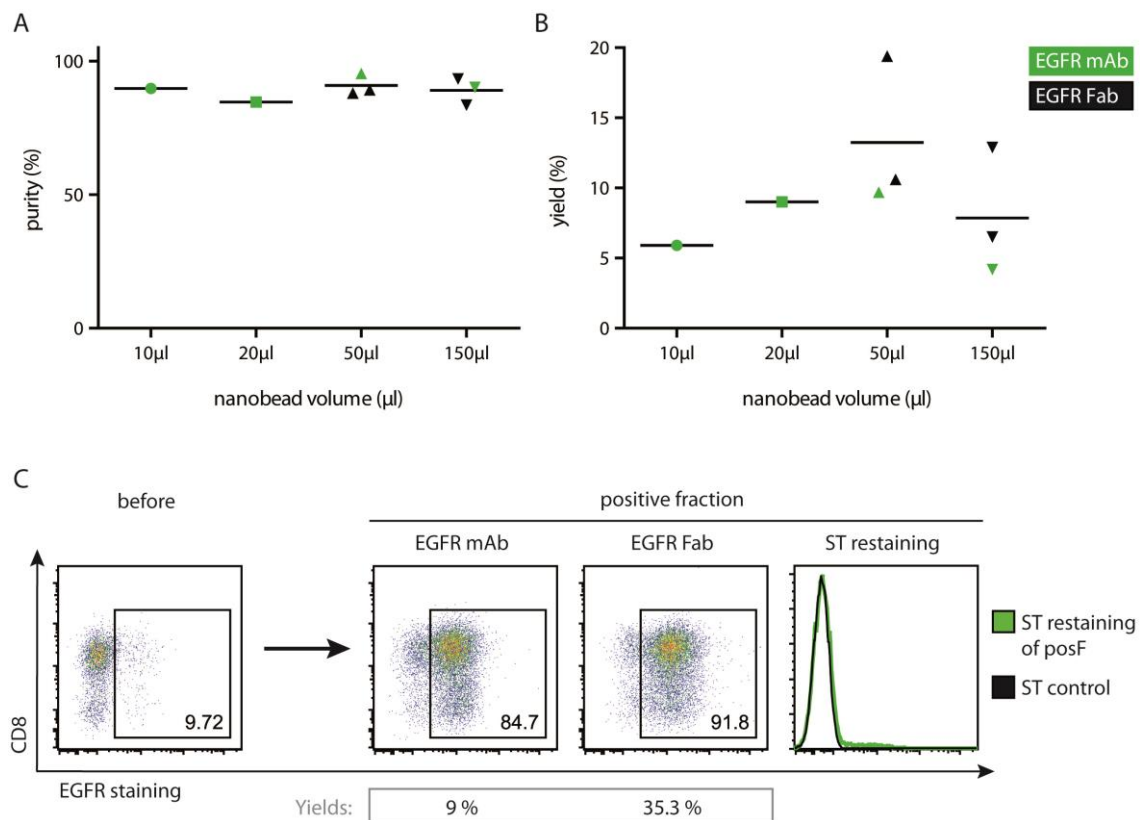


Fig. 4-22: Magnetic selections with EGFR Fab fragments and nanobeads result in similar purities and potentially higher yields compared to EGFR mAb-based selections. A and B. Human EGFR<sup>t</sup> T cells were magnetically enriched with 10μL EGFR mAb or 2μg EGFR Fab reagent and various nanobead volumes in side-by-side comparisons. Purities (A) and yields (B) of selections are shown. C. Macaque T cells were transduced with an 'EGFR<sup>t</sup> only' construct and purified using 10μL EGFR mAb and 20μL streptavidin-nanobeads or 2μg Fab and 100μL *Strep*-Tactin nanobeads. Purities are given in the EGFR<sup>t</sup> gates, yields are calculated from the cell numbers of the aliquot 'before' and 'positive fraction'. The negative *Strep*-Tactin (ST) restaining of the positive fraction after Fab-based selection confirms reversibility of the Fab.

### 4.3.2 EGFR Fab-based selections using larger beads

Alternative technologies of magnetic cell purification have been developed in the Busch laboratory in collaboration with STAGE cell therapeutics GmbH. Very good purities and yields could be achieved, e.g. in selections of memory T cell subpopulations [178]. The target cell subset is magnetically labeled with *Streptag*-Fab fusion proteins that are directed against characteristic cell surface markers and *Strep*-Tactin-coated microbeads (1.5  $\mu\text{m}$  in diameter) or slightly bigger so-called AK12 beads. Cell separation is then performed in a conical tube by applying a permanent magnet on one side of the tube. As this method could substantially accelerate clinical-scale cell purification, it is currently transferred into clinically approved selection processes, so it was interesting to test whether it can be used to enrich EGFR<sup>t</sup> T cells. Thus, human EGFR<sup>t</sup> T cells were selected by using the EGFR Fab and magnetic beads of different size. All performed selections with nano-, micro- and AK12 beads are summarized in Fig. 4-23, including selections with different amounts of EGFR Fab and beads. This overview clearly shows that selections based on the use of larger beads can reach similar purities as nano-bead selections (Fig. 4-23A), but yields are very poor irrespective of the single parameters, such as the amount of Fab or beads, when using larger beads for cell purification (Fig. 4-23).

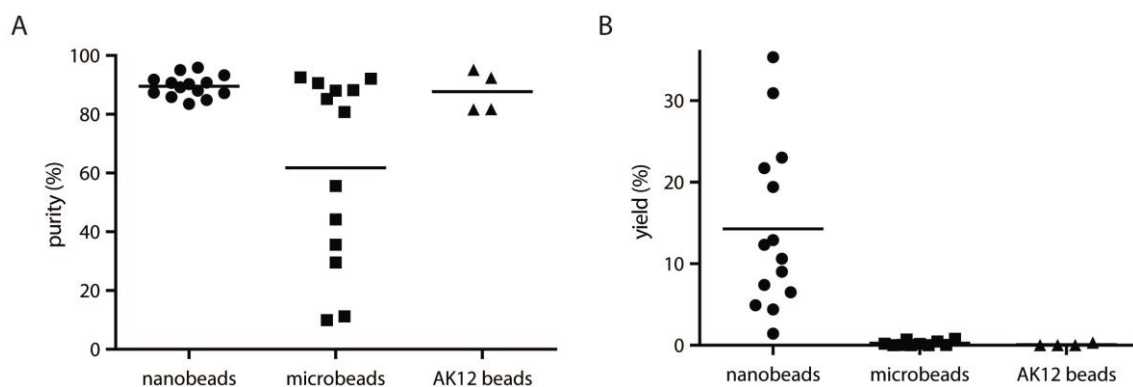


Fig. 4-23: Magnetic enrichments using larger beads than nanobeads result in much lower yields. Purities (A) and yields (B) of all magnetic enrichments of EGFR<sup>t</sup> T cells are summarized, irrespective of the used amount of Fab monomers or beads.

With the aim of improving the outcome of microbead-based selections, we tested different amounts of Fab monomers or Fab-bead reagents. There were no major differences in purities and yields when different amounts of the EGFR Fab were used and the volume of microbeads was kept constant at 30 $\mu$ L per 1x10<sup>7</sup> cells (Fig. 4-24A, B). When keeping the ratio between Fab and microbead constant at 1 $\mu$ g:7.5 $\mu$ L, increasing amounts of Fab-bead reagent led to improved purities in one experiment (Fig. 4-24C). However, this trend could not be confirmed in another experiment using the same maximal amount of Fab-bead (8 $\mu$ g:60 $\mu$ L), and further increase of the Fab-bead amount did not result in a good outcome of the selection (Fig. 4-24D). When other cell surface markers are targeted, best yields are usually achieved with 30 $\mu$ L microbeads, so further experiments were performed using 4  $\mu$ g EGFR Fab and 30 $\mu$ L microbeads. The non-consistent results of these early experiments might partially be explained by varying purities of the Fab fragments, produced in small batches, which potentially contained improperly folded Fab, preventing good binding of the Fab-bead multimer to the cells. Nevertheless, it is striking that the yields of microbead-based selections were extremely low under all tested conditions.

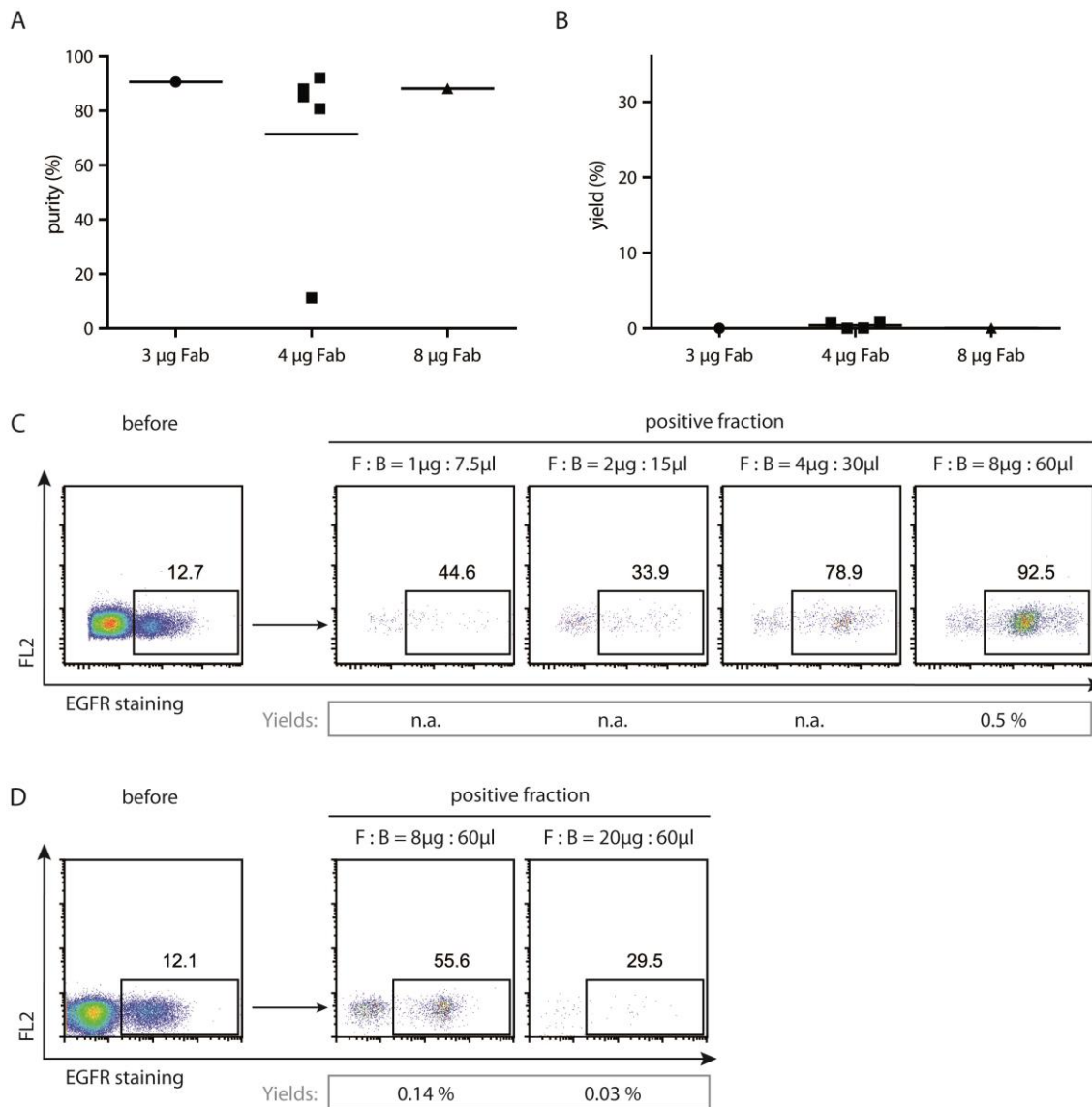


Fig. 4-24: Increasing amounts of Fab-bead complexes can have an effect on purities, but do not improve yields of magnetic selections using microbeads. A and B. Different amounts of the EGFR Fab were tested for magnetic enrichment of human EGFR<sup>+</sup> T cells and obtained purities and yields are shown. C. While keeping the Fab:Bead (F : B) ratio constant, the amount of Fab-bead complexes was increased. Purities of EGFR<sup>+</sup> cells in the positive fraction are given; the yield was only determined for the selection with best outcome. D. In a separate experiment, the highest F : B ratio of (C) was applied and compared to a higher F : B ratio with regard to purities and yields.

To address the question why selecting EGFRt<sup>+</sup> T cells with microbeads is not efficient, we performed selections of EGFRt<sup>+</sup> and CD4<sup>+</sup> T cells in a side-by-side comparison. EGFRt<sup>+</sup> CD4<sup>+</sup> T cell lines were generated to allow for targeting the same cell population with the two selection reagents based on the CD4 and the EGFR Fab in control experiments. Due to the vast experience in the lab group with the CD4 Fab, it was considered to reliably enrich CD4<sup>+</sup> T cells from fresh PBMCs in combination with microbeads. CD4<sup>+</sup> T cell selections have never been performed with cultured cells, so we decided to examine the performance of the CD4 Fab selection reagent in correlation with different cell sources first. The CD4<sup>+</sup> cell population was enriched under optimized conditions from either fresh PBMCs, a mix of CD4<sup>+</sup> GFP<sup>+</sup> cultured cells and fresh PBMCs or a mix of CD4<sup>+</sup> GFP<sup>+</sup> and CD8<sup>+</sup> GFP<sup>-</sup> cultured cells (Fig. 4-25). Purities of selections were above 90% for all three samples. In contrast, variable yields were obtained; while CD4<sup>+</sup> T cells were enriched from fresh PBMCs with a yield of 20% (Fig. 4-25, left), only about 10% of CD4<sup>+</sup> (GFP<sup>+</sup>) T cells were retrieved from the mix of cultured cells by magnetic selection (Fig. 4-25, right). The efficiency of cell selection from fresh vs. cultured cells could additionally be compared in one sample that contained CD4<sup>+</sup> T cells among the fresh PBMCs and CD4<sup>+</sup> GFP<sup>+</sup> cultured cells (Fig. 4-25, middle). The origin of the CD4<sup>+</sup> T cells in the positive fraction could be tracked by the GFP marker. The yield was twice as high for the CD4<sup>+</sup> T cells that were selected from the fresh PBMCs as compared to CD4<sup>+</sup> GFP<sup>+</sup> cultured T cells (28% vs. 14%). This observation was confirmed in independent experiments and it indicates that there are differences between cultured and fresh cells (e.g. vitality, robustness and cell surface properties) that could affect the outcome of magnetic selections. Yet, yields of CD4<sup>+</sup> cell enrichment from cultured cells were constantly above 10%, which is clearly higher than yields of EGFRt<sup>+</sup> cell selections (< 0.5%).

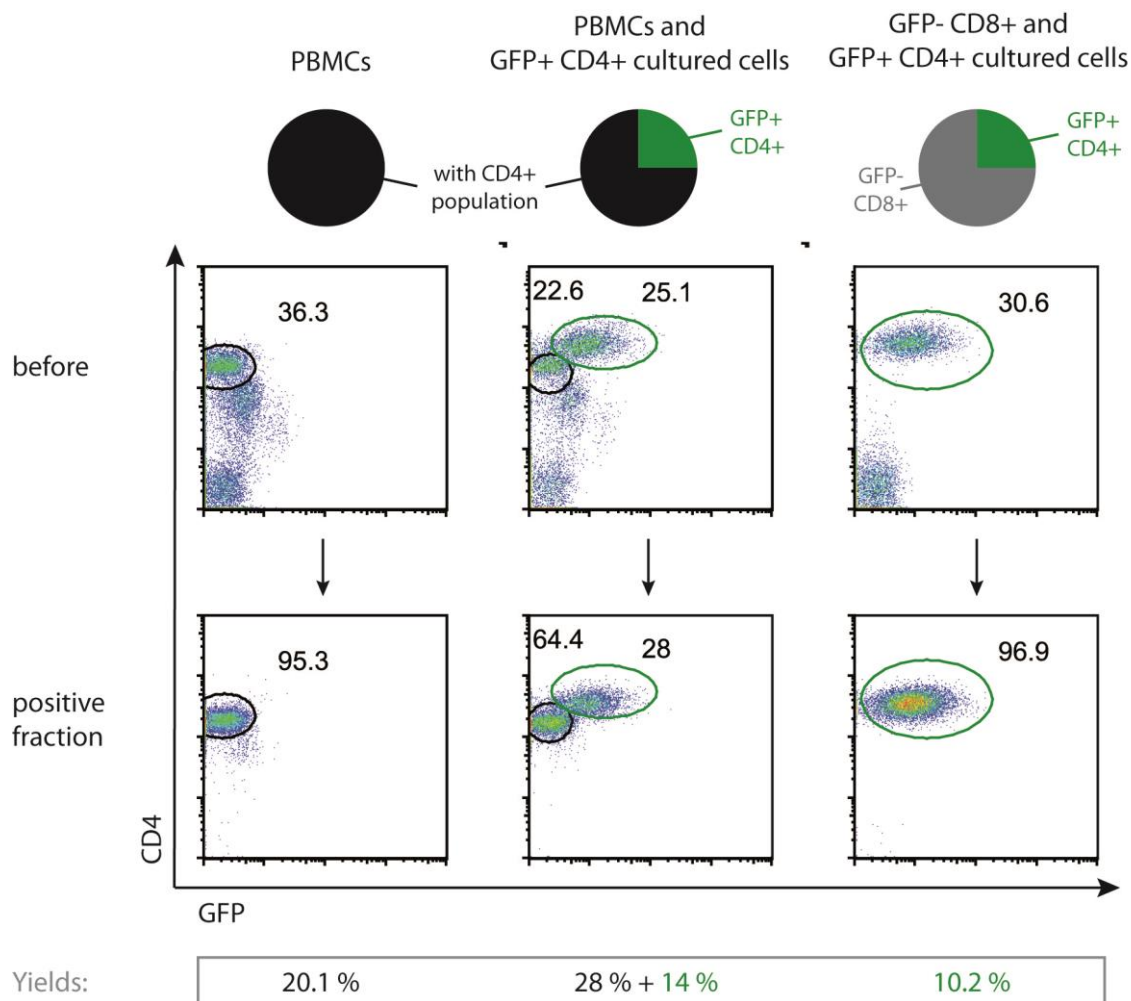


Fig. 4-25: CD4<sup>+</sup> T cells can be enriched from fresh PBMCs with higher yields than from cultured cells using magnetic microbeads. The different samples PBMCs only (left), PBMCs and CD4<sup>+</sup> GFP<sup>+</sup> cultured cells (middle) and a mix of CD4<sup>+</sup> GFP<sup>+</sup> and CD8<sup>+</sup> GFP<sup>-</sup> cultured cells were subjected to the CD4<sup>+</sup> cell selection protocol using 2  $\mu$ g CD4 Fab and 30  $\mu$ L microbeads. Purities are given by gating on CD4<sup>+</sup> GFP<sup>-</sup> cells (derived from fresh PBMCs) or on CD4<sup>+</sup> GFP<sup>+</sup> cells (derived from cultured cells). Based on purities and cell numbers, yields were obtained.

Next, we wanted to show the different outcomes of the enrichment of CD4<sup>+</sup> and EGFRt<sup>+</sup> T cells in a direct comparison under similar conditions. This could be accomplished by performing selections on a mix of CD4<sup>+</sup> T cells that had been transduced with a GFP/EGFRt construct and untransduced CD8<sup>+</sup> T cells. Based on the optimal conditions identified before, selections were performed with 2 μg CD4 Fab and 30 μL microbeads on one aliquot of the cell mix and with 4 μL EGFR Fab and 30 μL microbeads on the other aliquot, hence targeting the same cell population (Fig. 4-26A). Here, the purity of the cell selection with the EGFR Fab was clearly below the purity of CD4<sup>+</sup> cell selection (88% vs. 97%). However, the main difference was observed for the yields that were as low as 0.05% for selecting the target cells with the EGFR Fab and approximately 10% for using the CD4 Fab. The low number of CD4<sup>+</sup> GFP<sup>+</sup> EGFRt<sup>+</sup> target cells in the positive fraction after EGFR Fab-based selection correlated with a ten times higher CD4<sup>+</sup> cell number in the wash fraction (Fig. 4-26A). These cells are lost during the selection procedure, which might be due to ineffective binding of the Fab-bead complex to the cell surface marker EGFRt. Further experiments under the same conditions confirmed that yields are much lower if the EGFRt marker is targeted as compared to aiming for the phenotypic marker CD4.

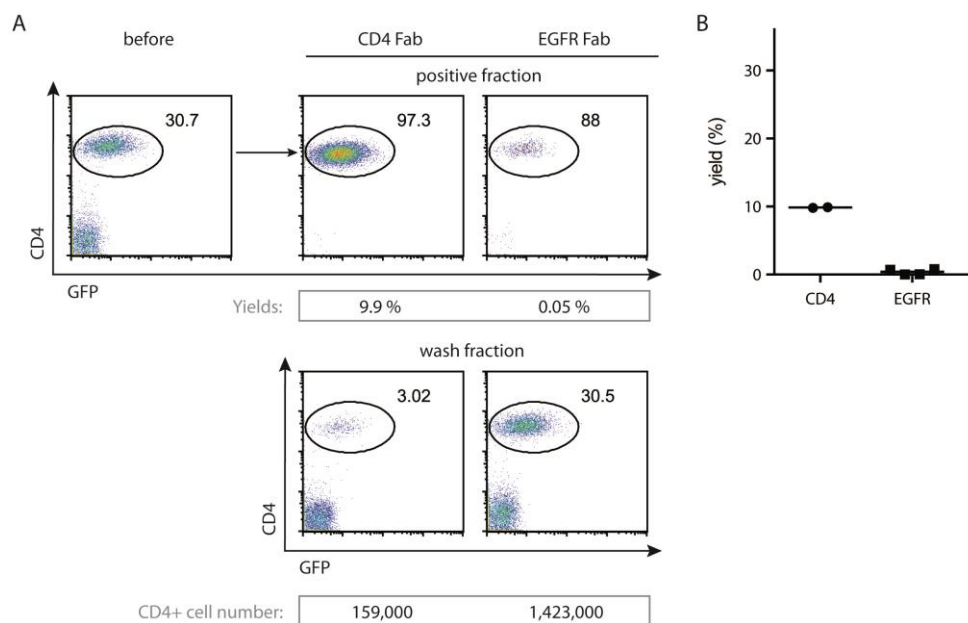


Fig. 4-26: Target cells can be enriched by using the CD4 Fab and microbeads with higher yields as compared to using the EGFR Fab due to lost cells in wash fraction. CD4<sup>+</sup> T cells that also expressed the EGFRt and GFP were enriched either with 2 μg CD4 or 4 μg EGFR Fab and 30 μL microbeads. A. Representative example with purities of the positive fraction and calculated yields. Cells that were collected during washing are shown as the wash fraction, including the number of target cells. B. Yields of all selections performed under the same conditions.

Consequently, we aimed at elucidating why EGFR Fab-bead complexes might not be able to bind as stably to the EGFRt on T cell surfaces as CD4 Fab-bead to CD4. Yields were calculated for T cell subpopulations with high or low EGFRt expression in retrospective analyses of several independent experiments that had been performed with different amounts of Fab monomers and microbeads (Fig. 4-27). Interestingly, cells with high EGFRt expression were selected with an on average ten-fold higher yield than cells with low EGFRt levels. Even for EGFRt-high target cells, selection yields were very low (< 2%). Taken together, the correlation between high EGFRt levels and improved yields indicates that EGFRt-high T cells are more efficiently enriched when using EGFR Fab fragments and microbeads.

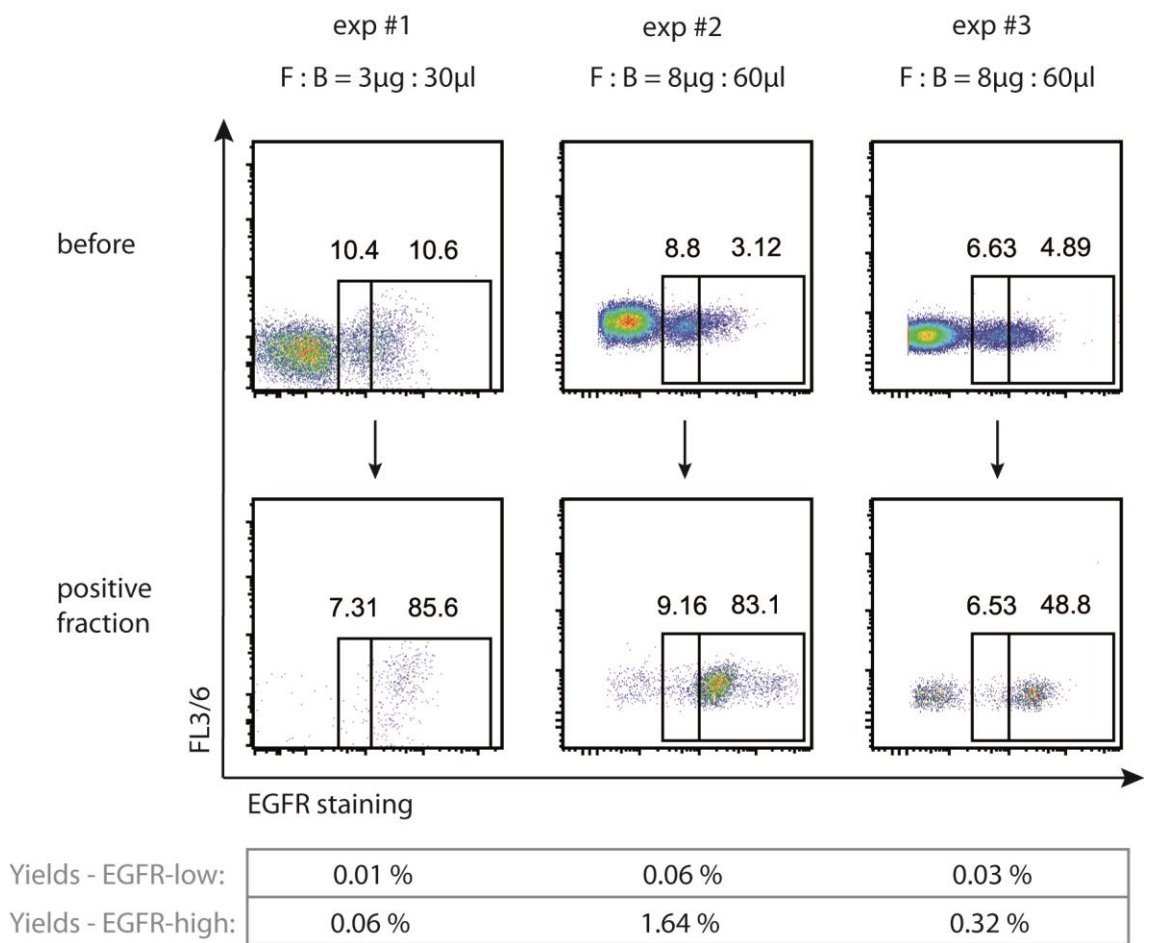


Fig. 4-27: T cells with high expression of EGFRt are preferentially selected when using microbeads. EGFRt<sup>+</sup> T cells were enriched with the indicated amounts of the EGFR Fab and microbeads in three separate experiments. T cells with high and low expression of EGFRt were gated and yields were obtained, based on the frequency of cells within these gates.

To evaluate the level of EGFR<sup>t</sup> expression, a quantification assay based on the Qifikit® (Dako) was set up. There, the antibody binding capacity (ABC) per cell was acquired by staining the EGFR<sup>t</sup> T cells with an unconjugated EGFR mAb and a secondary FITC-conjugated anti-mouse mAb. The same secondary mAb is used to stain the Calibration Beads with a well-defined number of mAb molecules, which is provided with the kit to construct a calibration curve. The ABC only corresponds to the number of antigenic sites on the cell surface if the antibody staining is done under saturating conditions. Therefore, the purified EGFR mAb was titrated on EGFR<sup>t</sup> T cells as shown in Fig. 4-28A. An antibody dilution of 1:500 appeared to result in maximum staining intensity. To make sure that a truly saturating antibody dilution is chosen for further experiments, the mAb titration was repeated and quantification beads were included (Fig. 4-28B). Based on the calibration curve, the ABC/cell was calculated for every sample that was stained with a different antibody dilution. The calculated ABCs did not further increase for an antibody dilution of 1:100 and lower. Thus, the EGFR mAb was used at a 1:100 dilution to determine the number of EGFR molecules on the surface of EGFR<sup>t</sup>-transduced T cells as well as on the breast cancer cell line BT-20, which overexpresses the wildtype full-length EGFR (Fig. 4-28C and D). The ABC/cell, that represents the number of EGFR molecules per cell, was approximately 19,000 for EGFR<sup>t</sup> T cells and approximately 170,000 for the BT-20 cell line. The number of EGFR<sup>t</sup> molecules on transduced T cells appears to be relatively low as compared to the cancer cell line. A better reference would be the number of CD4<sup>+</sup> molecules on T cells. It has been reported to be around 50,000 [218], which is clearly higher than the number of EGFR<sup>t</sup> molecules per cell. This might indicate that a minimum number of target molecules needs to be present on the cell surface to be stably bound by a Fab-microbead complex, which ultimately is the prerequisite for efficient cell selections.

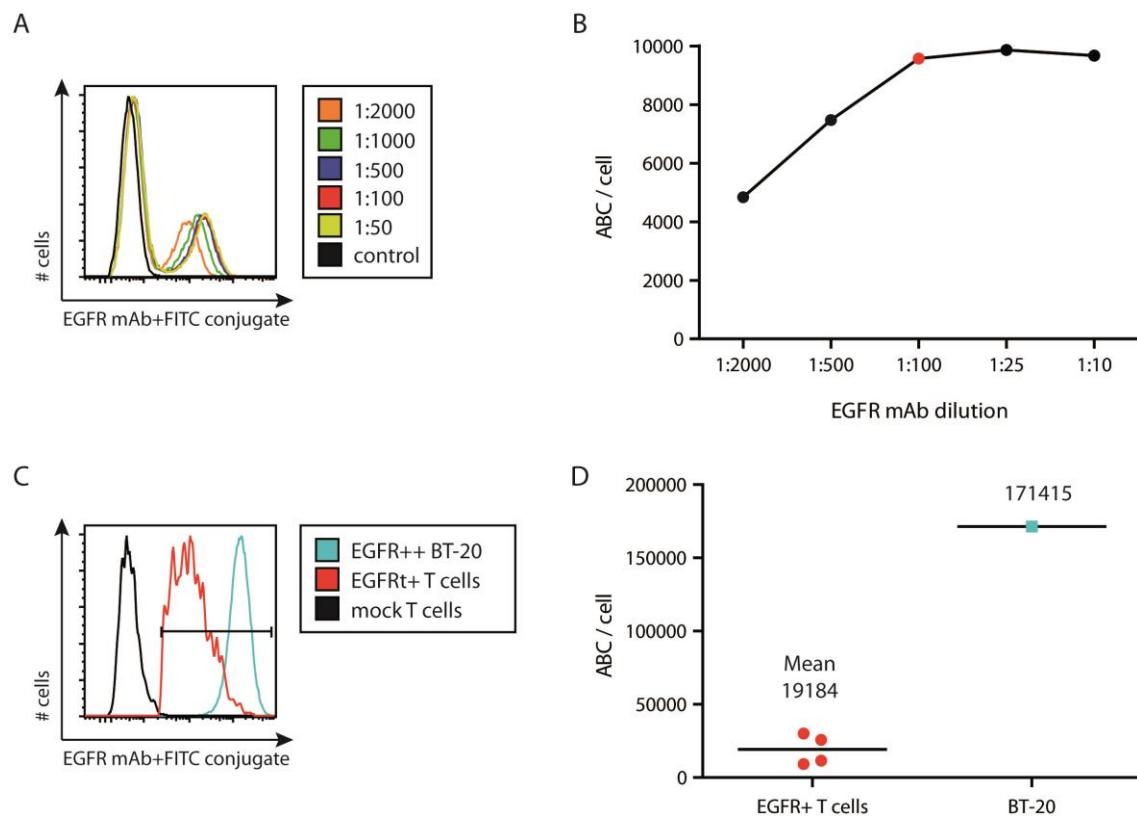


Fig. 4-28: EGFR expression levels are relatively low on EGFR<sup>t</sup>-transduced T cells compared to the BT-20 cell line that overexpresses the wildtype EGFR. A. The purified EGFR mAb was titrated on EGFR<sup>t</sup> mouse T cells and detected by a FITC-conjugated secondary anti-mouse mAb. B. EGFR mAb titration was repeated and the antibody binding capacity (ABC) per cell was acquired for all tested antibody dilutions. C and D. The EGFR<sup>++</sup> BT-20 cell line and several samples of EGFR<sup>t</sup>-transduced mouse T cells were stained with the purified EGFR mAb and the FITC-conjugated anti-mouse secondary mAb to assess the ABC / cell using the Qifikit. C. Histogram overlay of representative samples. D. ABC / cell for each analyzed sample.

In summary, enrichment of EGFR<sup>t</sup> T cells with the EGFR Fab and microbeads did not result in satisfactory outcomes under the tested conditions. Thus, magnetic selections based on the EGFR Fab and nanobeads seem to be the better option to purify EGFR<sup>t</sup>-transduced T cells for clinical applications.

## 4.4 Evaluation of the EGFRt-based depletion mechanism in model systems

The EGFRt marker can be used as a reliable tracking marker and it can be labeled with specific selection reagents to enrich for EGFRt<sup>+</sup> T cells as shown in the first section of the results. As the EGFRt is expressed on the cell surface, it can potentially be targeted with an EGFR-specific antibody that mediates depletion of the EGFRt<sup>+</sup> T cells. Due to the availability of a clinically approved anti-EGFR mAb, i.e. Cetuximab (Erbix<sup>TM</sup>, Merck KGaA) this elimination approach should be safe and easy to be transferred into clinical application. Based on published data that demonstrated that Cetuximab can mediate depletion of EGFRt<sup>+</sup> T cells *in vitro* and elimination of a EGFRt<sup>+</sup> mouse T cell line in a short-term *in vivo* experiment [195], this safety approach was evaluated in more detail in this thesis.

### 4.4.1 *In vitro* analysis of Cetuximab-mediated ADCC

The mechanism of action of the anti-EGFR mAb Cetuximab has been described to include antibody-dependent cellular cytotoxicity (ADCC), inhibition of ligand binding and receptor internalization [207]. To assess whether Cetuximab-mediated ADCC can be directed against human EGFRt<sup>+</sup> primary T cells, a standard chromium release assay was established. First, the experimental conditions were set up by using two control target cell populations: the native breast cancer cell line BT-20, which overexpresses the wildtype EGFR, and a CD20<sup>+</sup> B-lymphoblastoid cell line (B-LCL) that was transduced with the EGFRt (Fig. 4-29A). Effector cells were generated by isolating natural killer (NK) cells from fresh PBMCs that were expanded with  $\gamma$ -irradiated PBMCs and 200U/mL hIL-2. NK cells were stained for CD56 and CD16, which is the Fc $\gamma$  receptor (Fc $\gamma$ R) III and binds to the Fc part of IgGs and thereby induces ADCC of IgG-labeled target cells (Fig. 4-29A). NK cells were incubated with the different target cells at different effector to target ratios for 4 hours, in the absence or presence of the anti-EGFR mAb Cetuximab or the control anti-CD20 mAb Rituximab (Fig. 4-29B-E). NK cells effectively lysed the K562 cell line, which is sensitive to NK cell killing in an antibody-independent manner (Fig. 4-29B). Similarly, the EGFR<sup>++</sup> BT-20 cell line was specifically lysed by the NK cells if Cetuximab was added during the cocubation time (Fig. 4-29C). Adding the control mAb Rituximab or no mAb did not trigger lysis of BT-20

cells. The EGFRt-transduced LCLs expressed the two markers CD20 and EGFRt on their cell surface, so ADCC through each of these markers could be tested in parallel. Indeed, the anti-CD20 mAb Rituximab induced specific killing of the LCLs as compared to samples without addition of any mAb (Fig. 4-29D). Cetuximab also sensitized LCLs to ADCC, but not as efficiently as Rituximab. As we observed that the truncated form of the EGFR can be targeted for Cetuximab-mediated ADCC, it was unexpected that there was no specific lysis of human primary T cells that had been transduced with the same EGFRt as the LCLs (Fig. 4-29E). EGFRt expression on T cells and LCL was verified by EGFR staining in separate experiments, so differences in the expression level could not be deduced from staining intensities. Furthermore, chromium labelling of T cells was as efficient as of LCLs, as similar levels of radioactivity was released from both target cell types after coincubation with a detergent to assess maximum lysis.

This set of experiments showed that in principle the EGFRt marker could be targeted by Cetuximab for triggering ADCC *in vitro*. While EGFRt<sup>+</sup> LCLs were sensitive to Cetuximab-mediated killing, lysis of EGFRt<sup>+</sup> T cells could not be shown under these experimental conditions.

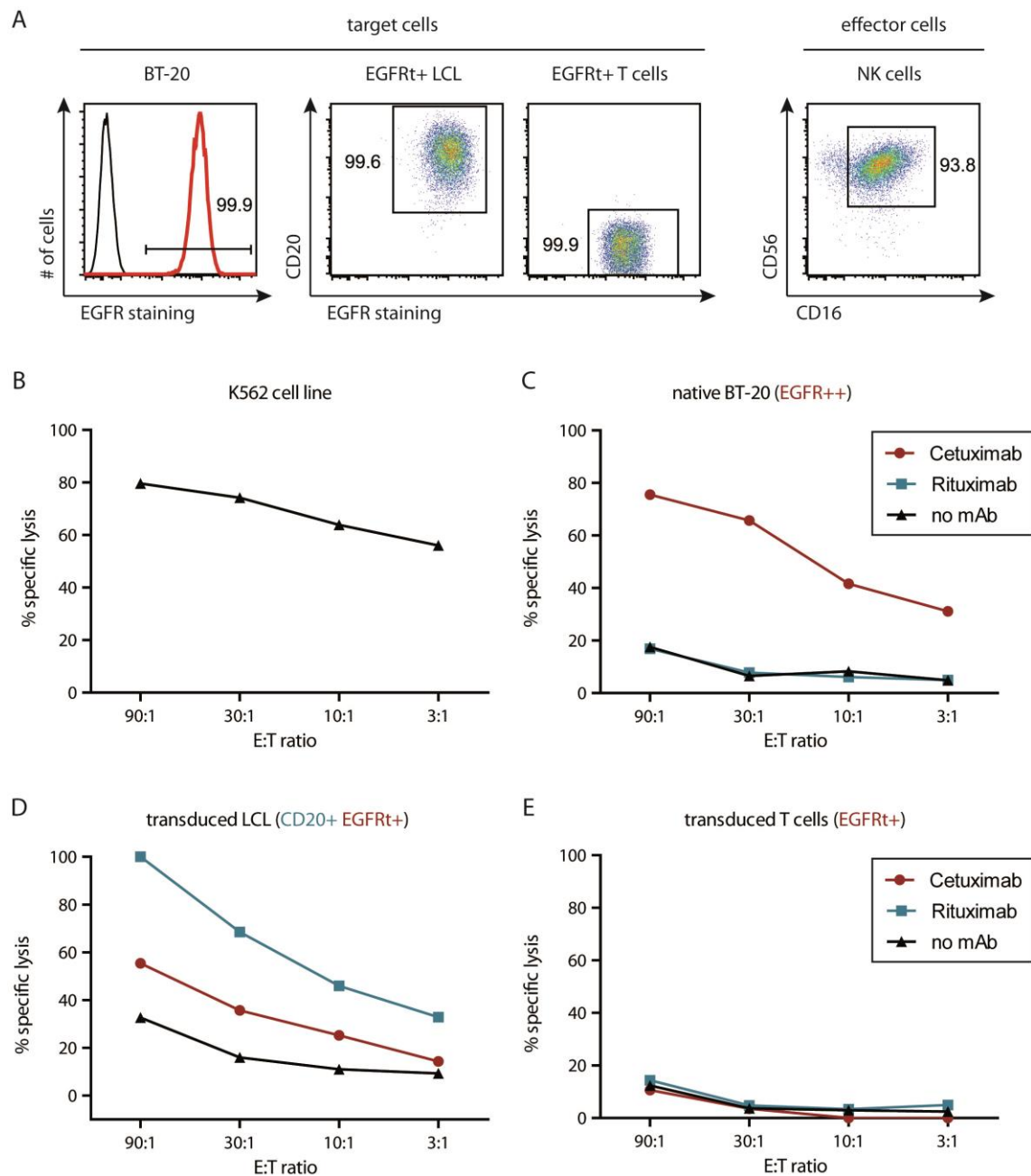


Fig. 4-29: Cetuximab mediates ADCC of EGFRt<sup>+</sup> LCLs, but not EGFRt<sup>+</sup> T cells, *in vitro*. A. Target cells BT-20, EGFRt<sup>+</sup> LCLs and EGFRt<sup>+</sup> T cells were stained for EGFR and CD20. NK cells that were isolated from PBMCs and expanded with  $\gamma$ -irradiated PBMCs and IL-2 were characterized as CD56<sup>+</sup> and CD16<sup>+</sup>. B-E. For a standard chromium release assay, the target cells were radio-labeled and cocultured with NK cells at different effector to target ratios. The anti-EGFR mAb Cetuximab, anti-CD20 mAb Rituximab or no mAb were added as indicated. The target cells were K562 cell line cells (B), native BT-20 cells (C), EGFRt-transduced LCLs (D) and EGFRt-transduced T cells (E).

#### 4.4.2 Depletion of EGFRt<sup>+</sup> T cells in the OT-I mouse model

Despite the fact that *in vitro* ADCC of human EGFRt<sup>+</sup> T cells could not be shown under the used experimental settings, the OT-I mouse model was established in parallel to study depletion of mouse EGFRt<sup>+</sup> T cells *in vivo*. Mouse splenocytes were obtained from OT-I transgenic mice and transduced with an EGFRt construct to generate OT-I transgenic EGFRt<sup>+</sup> T cells. As OT-I cells are specific for a peptide derived from chicken ovalbumin (OVA), even very small numbers of OT-I cells can be expanded *in vivo* by challenging mice with a virus or bacteria that express OVA. Based on the OT-I mouse model, we developed a sensitive method to investigate the efficacy of Cetuximab-mediated T cell depletion.

##### 4.4.2.1 The effect of irradiation on the endogenous NK cell population

Lymphodepletion of mice before cell transfer was considered to allow for easier detection of infused cells since lymphodepletion drastically reduces the numbers of endogenous cell populations in the peripheral blood. In the context of adoptive cell transfer in humans, lymphodepletion is discussed to enhance persistence of transferred cells for example due to better availability of homeostatic cytokines [79]. Lymphodepletion is clinically achieved by non-myeloablative irradiation or treatment with lymphodepleting drugs.

For the use in mouse studies, sublethal irradiation of 600 cGy was evaluated for mediating lymphodepletion. The effect of irradiation on the endogenous NK cell population was monitored, as NK cells are considered to be one of the most important cell types that are able to induce ADCC upon detection of cell-bound Cetuximab [219]. Therefore, endogenous NK cells were tracked in mice that were sublethally irradiated or not on day -1 (Fig. 4-30). NK cells could be detected in the peripheral blood of irradiated mice at similar frequencies as in non-irradiated mice on different time points after irradiation (Fig. 4-30A). These same mice were also infused with  $2 \times 10^6$  (irradiated) or  $8 \times 10^6$  Thy1.1<sup>+</sup> T cells (non-irradiated) on day 0 in order to examine the T cell engraftment. Although lower cell numbers were transferred into the irradiated mice, they had higher frequencies of Thy1.1<sup>+</sup> cells than the non-irradiated mice. This illustrates that it was easier to recover engrafted T cells from peripheral blood in irradiated mice. Tracking the number of NK cells in the peripheral blood over time, we observed that the endogenous NK cell population reconstituted within 8 weeks after irradiation and then reached similar levels as found in non-irradiated mice (Fig. 4-30B).

We concluded from this experiment that sublethal irradiation did not completely eradicate endogenous NK cells, so presumably, NK effector cells are available to mediate T cell depletion at any time point after irradiation.

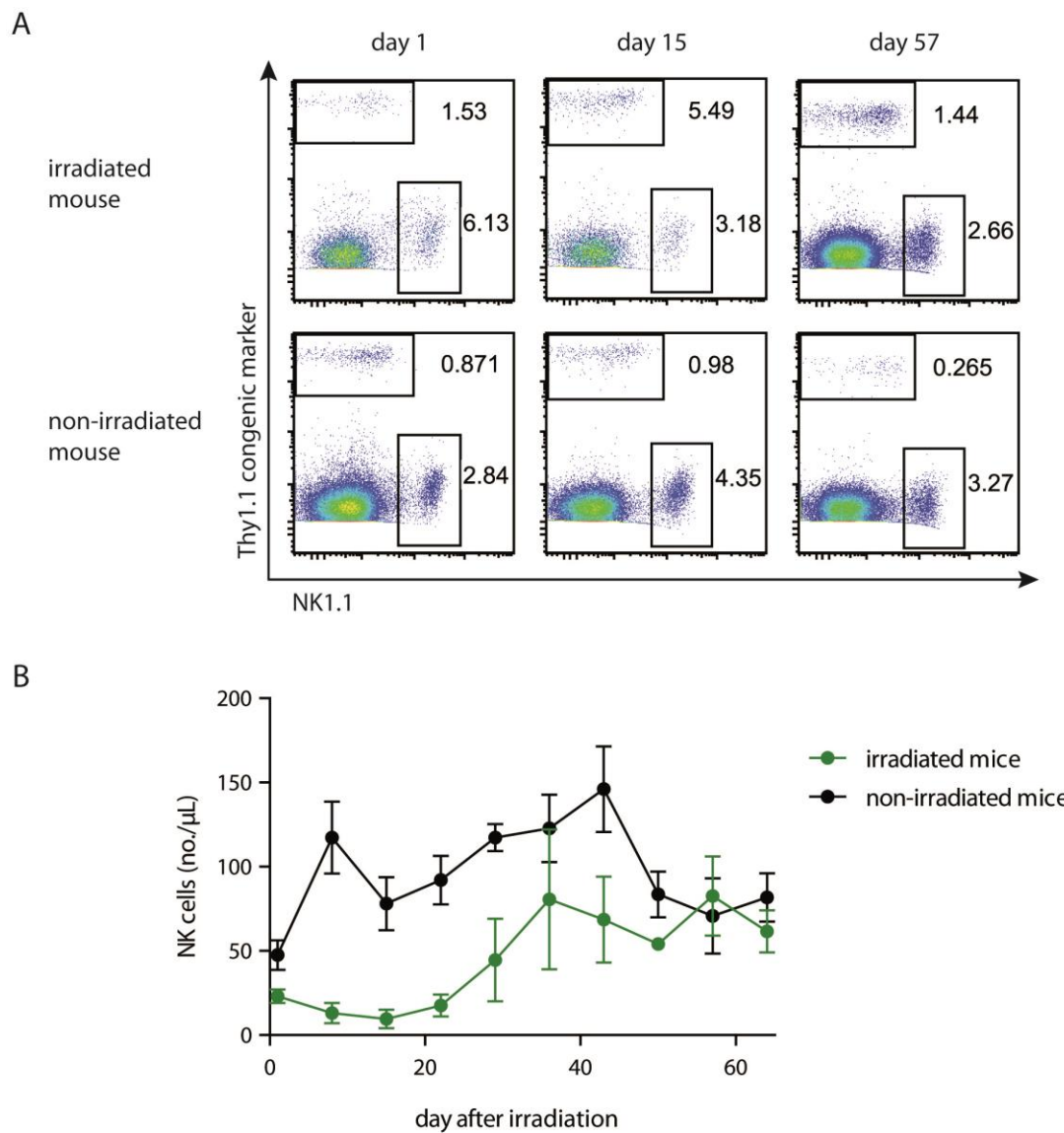


Fig. 4-30: Endogenous NK cells are detectable after irradiation. Mice were sublethally irradiated or not irradiated on day -1 and  $2 \times 10^6$  or  $8 \times 10^6$  T cells were transferred into irradiated or non-irradiated mice, respectively on day 0. A. Representative staining of NK1.1<sup>+</sup> endogenous NK cells and Thy1.1<sup>+</sup> transferred T cells at different time points after cell transfer. B. Numbers of endogenous NK cells per  $\mu\text{L}$  peripheral blood were acquired for irradiated and non-irradiated mice. Means and standard error of the mean (SEM) were plotted over time.  $n=2$  for irradiated mice,  $n=4$  for non-irradiated mice.

#### 4.4.1 *In vivo* depletion of CD19-CAR/EGFRt-transduced OT-I cells

Next, CAR/EGFRt-transduced OT-I cells were transferred into irradiated mice to study the depletion capacity of Cetuximab in this mouse model. Retroviral transductions were performed with a MIGR1 retroviral vector that contained the anti-human CD19-CAR with a CD28 costimulatory domain (h1928), which was linked to the EGFRt transgene by a T2A sequence for simultaneous expression of both the CAR and the EGFRt (Fig. 4-31A). Mouse splenocytes were derived from CD45.1 OT-I transgenic mice, activated with anti-CD3/28 mAbs and transduced with the h1928E construct by spinoculation. After optimizing the protocol, e.g. by generating stably transduced virus packaging cell lines, transduction efficiencies of up to 70% were achieved. Four days after transducing the OT-I cells,  $1.5 \times 10^6$  cells per mouse were injected intravenously (i.v.) into irradiated wildtype C57BL/6 CD45.2 mice and cell engraftment was monitored in the blood (Fig. 4-31B). On day 16 and 20 after T cell transfer, the EGFR-specific mAb Cetuximab or the control mAb Rituximab were injected intraperitoneally (i.p.) at a dose of 1mg mAb/mouse. After mAb-dependent depletion of EGFRt<sup>+</sup> T cells, mice were challenged with modified vaccinia virus Ankara expressing OVA (MVA-OVA) to expand OT-I cells that had not been depleted.

Representative flow cytometry stainings are shown for the mouse groups that either received Cetuximab or Rituximab (Fig. 4-31C). Before mAb application, CD45.1 transferred OT-I cells engrafted well and a frequency of about 40% of EGFRt<sup>+</sup> cells among all transferred cells was maintained. After mAb infusion, there were no detectable EGFRt<sup>+</sup> cells in mice of the Cetuximab group, whereas levels of EGFRt<sup>+</sup> OT-I cells were unaffected in the control Rituximab group. To investigate if there are any EGFRt<sup>+</sup> T cells left after depletion, OT-I cells were expanded by injecting MVA-OVA i.v. at a dose of  $1 \times 10^8$  pfu/mouse. While EGFRt<sup>+</sup> and EGFRt<sup>-</sup> OT-I cells expanded 4-fold in the Rituximab group, only increased levels of EGFRt<sup>-</sup> OT-I cells could be detected in the Cetuximab group. The frequency of EGFRt<sup>+</sup> cells in the Cetuximab and Rituximab group is shown in a time course of the experiment (Fig. 4-31D). Thus, EGFRt<sup>+</sup> cells were not detectable in mice that received Cetuximab, even after expanding both the EGFRt<sup>+</sup> and EGFRt<sup>-</sup> OT-I cells by infusing MVA-OVA.

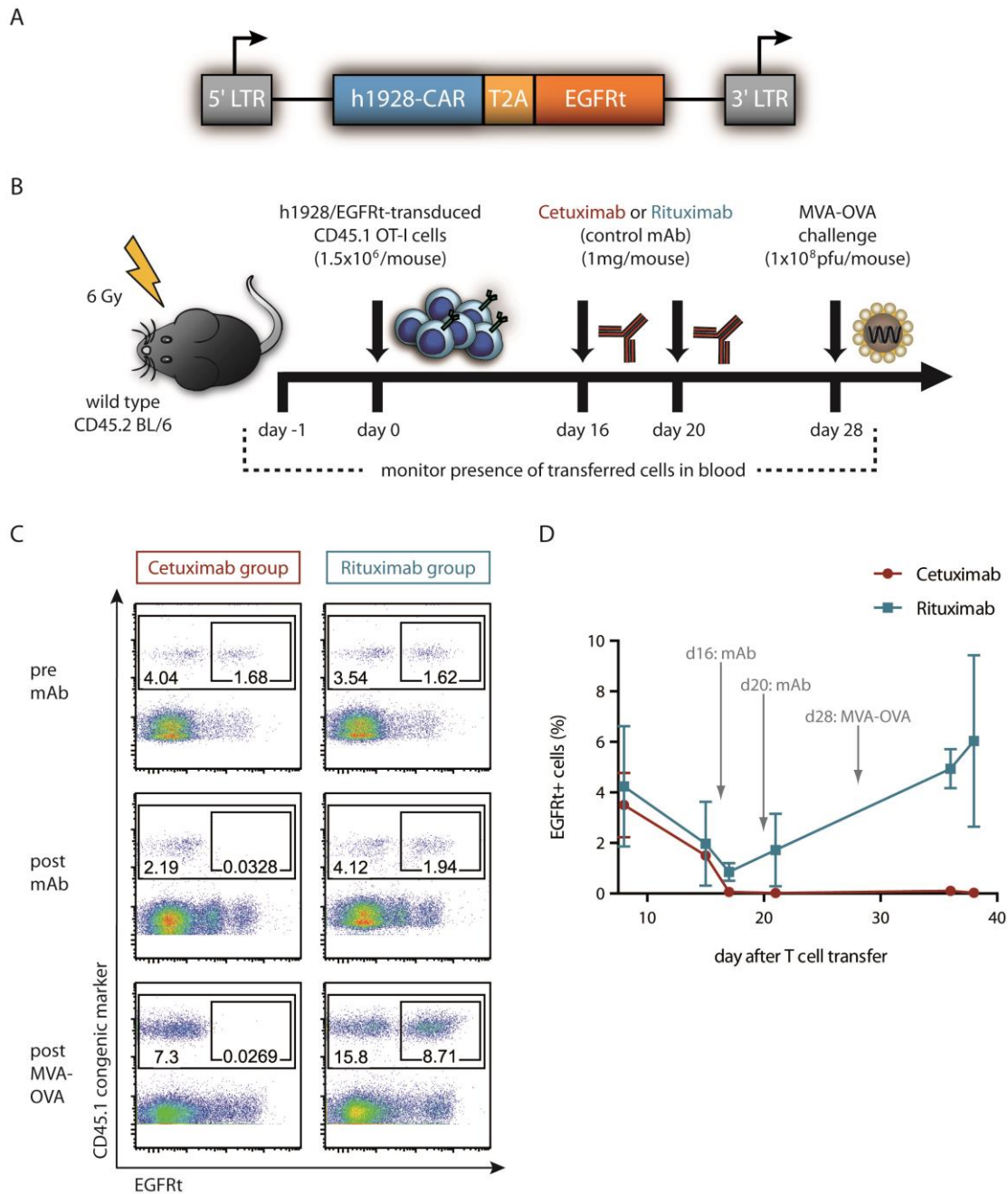


Fig. 4-31: EGFRt<sup>+</sup> T cells are not detectable after Cetuximab infusion into mice. A. Composition of the MIGR1 retroviral vector encoding for an anti-human CD19-CAR, including a CD28 costimulatory domain (h1928-CAR) and the EGFRt, separated by the T2A-linker. LTR – long-term repeats, CAR – chimeric antigen receptor. B. Experimental layout of the depletion study in the OT-I mouse model. C. Frequencies of transferred EGFRt<sup>+</sup> OT-I cells among living lymphocytes before mAb infusion (pre mAb), after mAb infusion (post mAb) and after challenge with MVA-OVA (post MVA-OVA) are shown in representative plots for mice that received either Cetuximab or Rituximab. D. Time course of the frequency of EGFRt<sup>+</sup> cells among living lymphocytes for the Cetuximab and the Rituximab group. Means +/- standard deviations (SD) were plotted. n=3 for each group.

#### 4.4.2 Inhibition of *ex vivo* EGFR staining by Cetuximab

The EGFR<sup>t</sup> marker is stably expressed on the cell surface of transduced T cells and can be used for tracking cells by EGFR staining *in vivo*, as demonstrated for the Rituximab group in Fig. 4-31C. The *ex vivo* staining was performed with biotinylated Cetuximab and streptavidin coupled to a fluorophore, typically phycoerythrin (PE). As the antibody used for staining and depletion is identical, *in vivo* binding of Cetuximab to EGFR<sup>t</sup> cells might interfere with the *ex vivo* EGFR staining.

To address this question, a control staining with an Fc-specific reagent was performed. The anti-Fc reagent should detect cell-bound Cetuximab molecules by binding its Fc part. As this reagent can also be used to detect the spacer of some CARs, the following control experiments were performed with EGFR<sup>t</sup> cells that had not been engineered with a CAR (Fig. 4-32). A depletion study with EGFR<sup>t</sup> OT-I cells was performed as described in Fig. 4-31B and blood cells were obtained from Cetuximab-treated mice (sample 1) or Rituximab-treated mice (sample 2-4). While staining with the EGFR mAb did not detect EGFR<sup>t</sup> cells in sample 1, a distinct EGFR<sup>t</sup> cell population was identified in sample 2 (Fig. 4-32, upper row). In contrast, the Fc staining was positive for sample 1 and negative for sample 2. This observation indicates that only EGFR<sup>t</sup> cells from the Cetuximab group (sample 1) were covered with Cetuximab molecules that were visualized by the Fc-specific staining.

To further provide evidence that soluble Cetuximab is present in the plasma of Cetuximab mice, the plasma was collected for co-incubation with EGFR<sup>t</sup> blood cells from Rituximab mice (Fig. 4-32, sample 3). During the one-hour incubation time at 37°C, putative Cetuximab molecules bind to the EGFR<sup>t</sup> cells, which would lead to inhibition of binding of the biotinylated Cetuximab and hence hamper with the EGFR staining. Indeed, EGFR staining of the plasma-coated blood cells was negative (sample 3, upper row) and Fc staining detected the Cetuximab molecules that had bound the EGFR<sup>t</sup> cells (sample 3, lower row). Stainings of sample 3 were similar to the negative EGFR and positive Fc staining of blood cells that were obtained from Rituximab mice and pre-incubated with 1:2 diluted fresh Cetuximab (sample 4, upper and lower row). This control experiment was performed several times at different time points during a number of independent *in vivo* studies. It strongly suggests that EGFR<sup>t</sup> cells cannot be detected reliably by *ex vivo* EGFR staining if Cetuximab has been

administered to the mice before. For this reason, the data of the first depletion study (Fig. 4-31) cannot be conclusively interpreted.

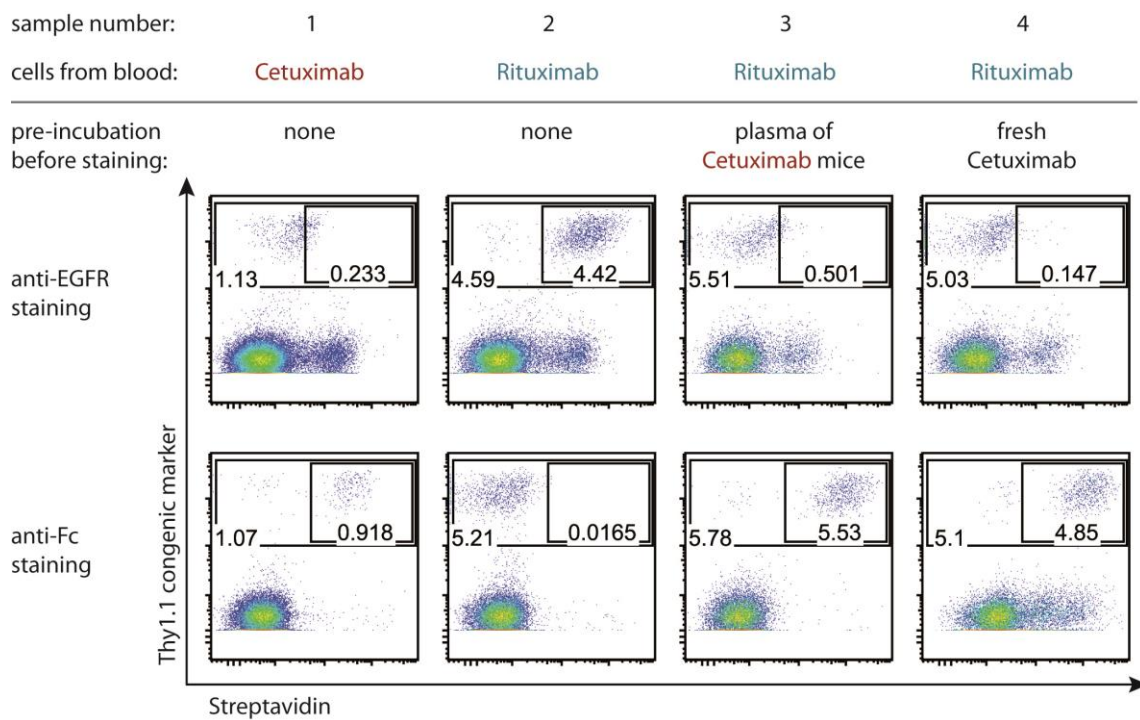


Fig. 4-32: Cell-bound Cetuximab reduces EGFR staining intensity. The *ex vivo* EGFR staining was performed with biotinylated Cetuximab and streptavidin-PE (upper row). The Fc staining was done with a biotinylated Fc-specific Fab reagent and streptavidin-PE (lower row). Blood cells were obtained from Cetuximab- (sample 1) or Rituximab-treated mice (sample 2-4). As controls, EGFR<sup>+</sup> blood cells were pre-incubated with 1:2 diluted plasma from Cetuximab-treated mice (sample 3) or 1:2 diluted fresh Cetuximab (sample 4).

#### 4.4.3 *In vivo* depletion of sorted GFP/EGFRt<sup>+</sup> OT-I cells

The problem of inhibition of the *ex vivo* EGFR staining by cell-bound Cetuximab had to be overcome to reliably detect residual EGFRt<sup>+</sup> cells in mice that were infused with Cetuximab. Therefore, a GFP/EGFRt gene construct was generated by Steven Liu from the Riddell lab at the FHCRC in Seattle. The MIGR1 retroviral vector encodes for the two transgenes, linked by a T2A sequence that allows for co-expression of the intracellular reporter protein GFP and the surface-expressed tracking marker EGFRt (Fig. 4-33A). After transduction, the GFP/EGFRt<sup>+</sup> cell population could be sorted by FACS, based on the GFP fluorescence and on the staining with the reversible EGFR Fab *Streptamer*, with a sort purity of 95% (Fig. 4-33B). The CD45.1 EGFRt<sup>+</sup> OT-I cells were then transferred into CD45.2 wildtype C57BL/6 mice ( $1.1 \times 10^6$  cells/mouse). For T cell depletion, 1 mg Cetuximab or Rituximab per mouse were administered on day 9 and 13 after T cell transfer and MVA-OVA was injected on day 21 at  $1 \times 10^8$  pfu / mouse, following a similar experimental layout as in Fig. 4-31. As shown by EGFR staining of a representative sample of the Cetuximab and the Rituximab group, most transferred CD45.1<sup>+</sup> cells were EGFRt<sup>+</sup> before antibody application (pre mAb, Fig. 4-33C). After infusing Cetuximab, no EGFRt<sup>+</sup> cells could be detected, while Rituximab did not affect persistence of EGFRt<sup>+</sup> cells in the control group (post mAb). The challenge with MVA-OVA resulted in outgrowth of EGFRt<sup>+</sup> OT-I cells in the Rituximab group, but expanded OT-I cells were negative for EGFR in the Cetuximab group (post MVA-OVA). As the EGFR staining is not reliable for tracking EGFRt<sup>+</sup> cells in Cetuximab-treated mice, GFP fluorescence vs. EGFR staining of CD45.1<sup>+</sup> cells is also shown in Fig. 4-33C. In the Cetuximab group, around 50% of transferred cells were GFP<sup>+</sup> in the post mAb and post MVA-OVA sample and GFP fluorescence did not correlate with the EGFR staining intensity. As expected, co-expression of GFP and EGFRt could be visualized for samples of the Rituximab group. As summarized in the time course of this experiment, there is a discrepancy between the persistence of GFP/EGFRt<sup>+</sup> cells that were tracked by EGFR staining or by GFP fluorescence (Fig. 4-33D, E). Both tracking approaches show that many GFP/EGFRt<sup>+</sup> T cells seem to be depleted until day 21 in the Cetuximab group. Only after *in vivo* expansion of OT-I cells by MVA-OVA, the residual GFP/EGFRt<sup>+</sup> cells become detectable by GFP fluorescence (orange circle). This observation could not have been made if tracking was solely based on EGFR staining.

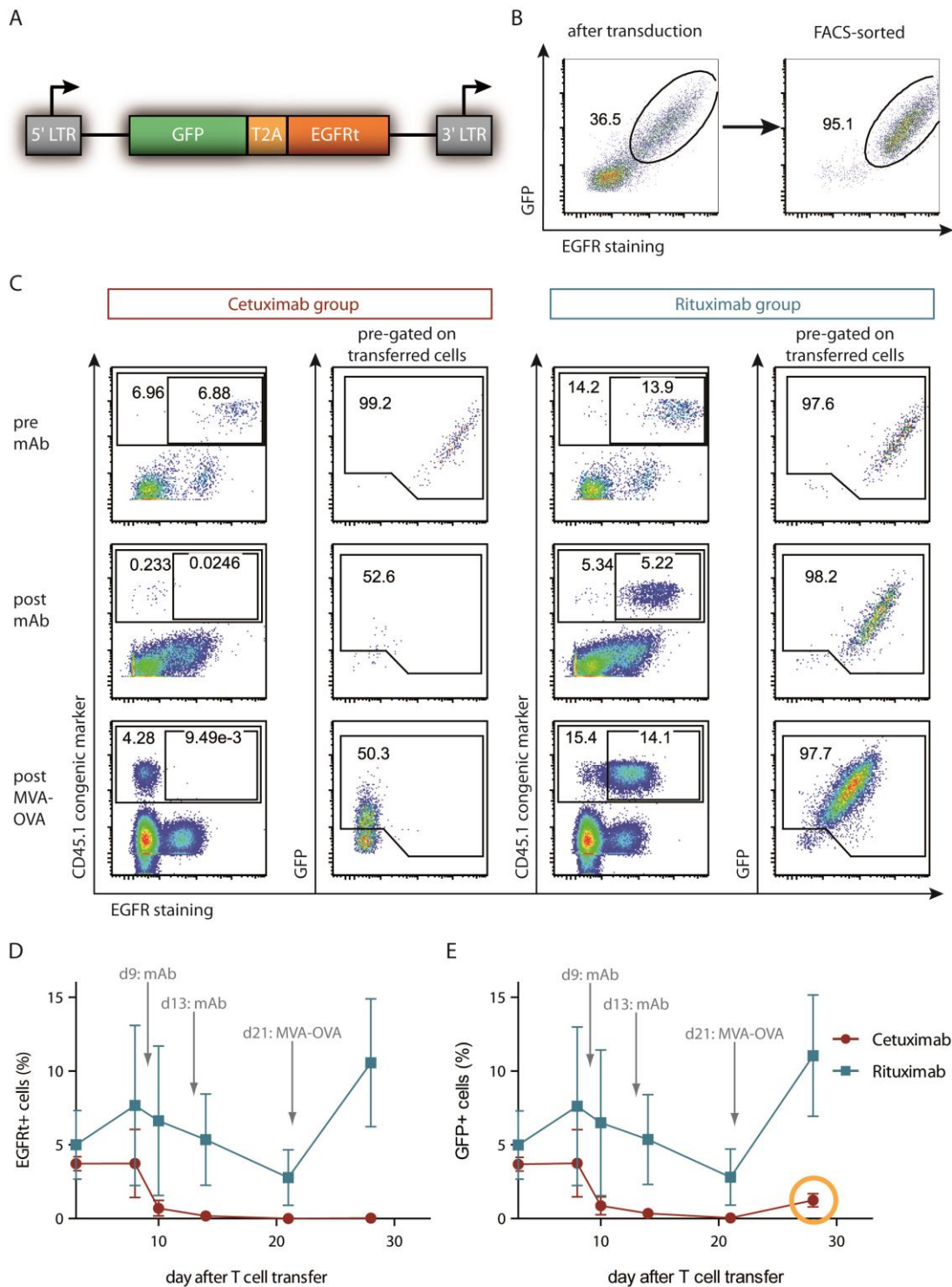


Fig. 4-33: GFP/EGFR<sup>+</sup> T cells can only be detected via the GFP after Cetuximab-mediated depletion. A. Composition of the MIGR1 retroviral vector encoding for GFP and EGFRt. B. GFP/EGFR<sup>+</sup> OT-I cells were sorted by FACS using the EGFR Fab *Streptamer*. C. Representative examples of staining blood cells from Cetuximab or Rituximab-treated mice are shown. GFP vs. EGFR is plotted for CD45.1<sup>+</sup> pre-gated cells. Stainings were performed on indicated timepoints before (pre mAb) and after mAb infusion (post mAb), as well as after MVA-OVA injection (post MVA-OVA). The EGFR staining intensity varied between different time points, because the streptavidin was coupled to different fluorophores. D and E. Frequencies of detected EGFR<sup>+</sup> (D) and GFP<sup>+</sup> cells (E) are shown as means +/- SD over time. The two graphs deviate from each other for day 28, highlight with an orange circle. n=2 per group.

The depletion study with sorted GFP/EGFRt<sup>+</sup> OT-I cells had to be repeated in larger groups of mice. The number of GFP/EGFRt<sup>+</sup>, sorted OT-I cells that could be generated for transfer into mice was limited due to transduction efficiency, massive cell loss during the sort procedure and operability of performing numerous transductions in parallel. Hence, the experimental layout was slightly changed such that transferred cells were expanded *in vivo* by MVA-OVA first, and depleting antibodies were infused afterwards. This protocol allows for transfer of low cell numbers that are increased to detectable levels by *in vivo* expansion with MVA-OVA and has further advantages in addition: 1.) The depletion of large EGFRt<sup>+</sup> cell populations can directly be monitored if OT-I cell populations are expanded first. 2.) Expansion of EGFRt<sup>+</sup> OT-I cells before depletion is unbiased in contrast to expanding OT-I cells after depletion, because the latter order might lead to competitive outgrowth of remaining EGFRt<sup>-</sup> cells in the Cetuximab group, which could complicate the interpretation of completeness of the EGFRt<sup>+</sup> T cell depletion.

After transduction, GFP/EGFRt<sup>+</sup> cells were sorted by FACS to a purity of almost 97% using the EGFR Fab *Streptamer* (Fig. 4-34A). Approximately 250,000 sorted Thy1.1<sup>+</sup> OT-I cells were then transferred into sublethally irradiated wildtype C57BL/6 mice. It was difficult to detect such low numbers of transferred cells before antigen-dependent *in vivo* stimulation (pre MVA-OVA, Fig. 4-34B). On the day of peak expansion during challenge with MVA-OVA at  $1 \times 10^8$  pfu/mouse, Thy1.1<sup>+</sup> cell populations were readily detectable in the Cetuximab- and the Rituximab group and the frequency of GFP/EGFRt<sup>+</sup> cells among all transferred cells was maintained at approximately 97% (post MVA-OVA). As observed in the earlier experiments, EGFRt<sup>+</sup> cells were not detectable after Cetuximab treatment, which is at least partially due to inhibition of the EGFR staining. In line with this interpretation, GFP<sup>+</sup> cells were still detectable together with Thy1.1<sup>+</sup> cells after depletion (post mAb). In the Rituximab group, both the persistence of GFP/EGFRt<sup>+</sup> cells and the EGFR staining were not affected by the administration of the control mAb. Frequencies of Thy1.1<sup>+</sup> transferred cells and GFP<sup>+</sup> cells among living lymphocytes were plotted over time in Fig. 4-34C and D, respectively. Due to the high frequency of GFP<sup>+</sup> cells among the Thy1.1<sup>+</sup> cells after the sort, both graphs are similar. OT-I cell frequencies peak on day 8 after MVA-OVA challenge and decrease during the contraction phase of virus infection. After antibody infusions, Cetuximab clearly depleted a large fraction of GFP/EGFRt<sup>+</sup> cells, while transferred cells were maintained at much higher levels in the Rituximab group (Fig. 4-34C, inlet). In these control mice, the frequency of Thy1.1<sup>+</sup> cells slowly decreased

---

over time with a similar kinetic as observed in mice that received mock-transduced OT-1 cells (data not shown). In Cetuximab-treated mice, the frequency of transferred cells was diminished until day 150. On a very late time point, however, similar levels of Thy1.1<sup>+</sup> cells were detected in both mouse groups.

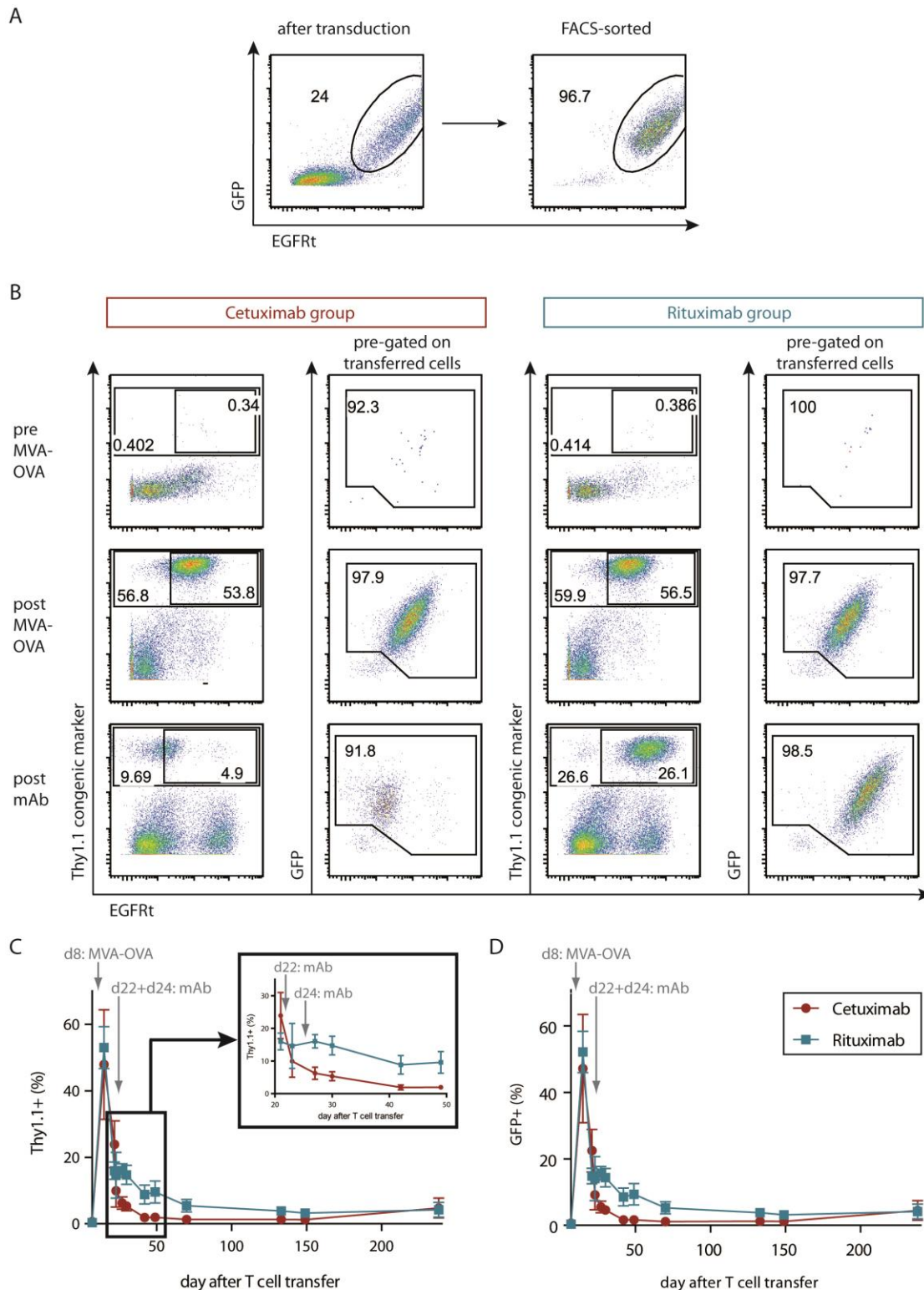


Fig. 4-34: EGFRt<sup>+</sup> T cells are only partially depleted by Cetuximab. A. GFP/EGFRt-transduced T cells were sorted by FACS with the EGFR Fab *Streptamer*. B. Representative examples of the Cetuximab and Rituximab group. Stainings of the Thy1.1 and the EGFRt marker are shown as well as GFP vs. EGFR staining of the Thy1.1<sup>+</sup> pre-gated cells. Stainings were performed before (pre MVA-OVA) and after challenge with MVA-OVA (post MVA-OVA), as well as after mAb infusions (post mAb). C and D. Time course of the Thy1.1<sup>+</sup> (C) – inset shows section from day 21-49 – and GFP<sup>+</sup> cell frequencies (D), means +/- SD are plotted. n=6 per group.

In addition to the monitoring of cell persistence in the blood, it is also important to study T cell migration into other secondary lymphoid organs, such as spleen and lymph nodes, and peripheral organs, e.g. the lung (Fig. 4-35). Overall frequencies of Thy1.1<sup>+</sup> cells were similar on day 238 in blood, spleen and lymph node and slightly higher in lung as shown in representative samples of the Cetuximab and the Rituximab group. Depletion with Cetuximab resulted in decreased numbers of GFP<sup>+</sup> cells among transferred cells compared to the Rituximab group, albeit the differences were not statistically significant (Fig. 4-35B). Greater differences might have been detected at earlier time points, e.g. between day 25 and 50, as shown in the blood monitoring (Fig. 4-34C, inlet). From day 134, the EGFR staining was no longer inhibited in the Cetuximab group, indicating that Cetuximab had been cleared from the blood before that day. The exact time point of clearance cannot be deduced from this experiment, but we could demonstrate that Cetuximab persisted in the blood of mice for at least 50 days (data not shown). Consequently, the analysis of GFP/EGFRt<sup>+</sup> cells in several organs on day 238 was not affected by circulating or cell-bound Cetuximab molecules (Fig. 4-35A). Although frequencies of GFP/EGFRt<sup>+</sup> cells were not significantly decreased in Cetuximab-treated mice, a different staining pattern was noticed in the Cetuximab vs. Rituximab group. While a broad expression range of the GFP and EGFRt marker was detected in the control group, fluorescence intensities of GFP and the EGFRt staining were low in all analyzed organs obtained from Cetuximab-treated mice (Fig. 4-35A). These data indicate that EGFR-high-expressing cells might have been very efficiently depleted by Cetuximab throughout all analyzed organs, whereas low-expressing cells were not completely eliminated.

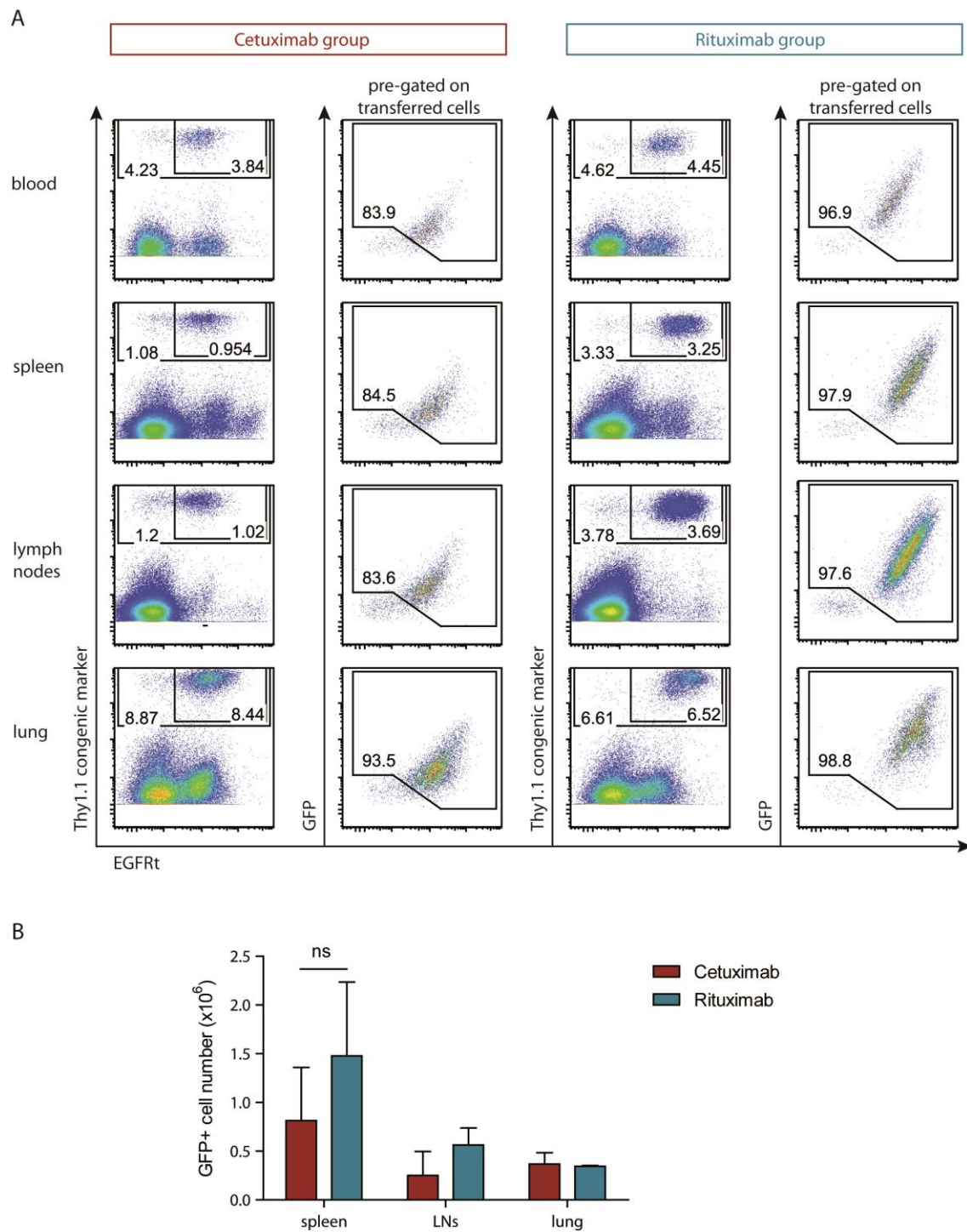


Fig. 4-35: Cetuximab mediates partial depletion of EGFRt<sup>+</sup> T cells in solid organs. On the final day of the experiment (day 238), mice were sacrificed and blood, spleen, lymph nodes and lung were obtained. The stainings were performed in a similar manner as for the blood monitoring. A. Representative stainings of the different organs from one mouse per group are shown. For the GFP vs. EGFRt plots, cells were pre-gated on Thy1.1. B. The number of GFP<sup>+</sup> cells was obtained for spleen, lymph nodes and lung. Means  $\pm$  SD are plotted.  $n=4$  for spleen, significance level was calculated by two-tailed Mann-Whitney test. ns = not significant.  $n=2$  for lymph nodes and lung.

To further elucidate whether depletion of GFP/EGFRt<sup>+</sup> cells is dependent on the expression level of the targeted molecule EGFRt, stainings for GFP/EGFRt<sup>+</sup> cells are shown at day 23 and day 238, which correspond to day 1 and 216 after antibody infusion (Fig. 4-36A). For clarity, a red gate was set on cells with high GFP expression. One day after mAb injection, the frequency of GFP-high cells was already decreased in Cetuximab-treated mice versus control mice (14.6% vs. 37.9% GFP-high cells in the examples given in Fig. 4-36A). In this particular group of mice, the difference further increased to a 60-fold lower frequency of GFP-high cells in Cetuximab vs. Rituximab mice on day 238.

The frequencies of GFP<sup>+</sup> cells in the GFP-high and GFP-low gate of all individual mice are shown for day 15 (pre mAb), day 23 (post mAb) and day 238 (Fig. 4-36B). GFP-high cell frequencies significantly decreased from day 15 to day 23 if Cetuximab was administered to the mice, but stayed unchanged in Rituximab-treated mice. Differences between the two groups are less clear on day 238 due to higher variability in the Cetuximab group. Consistently, significantly higher frequencies of GFP-low cells were observed on day 23 compared to day 15 in the Cetuximab group. Here, the difference between the Cetuximab and the Rituximab group also reached significance. Levels of GFP-low cells were not significantly affected by infusion of Rituximab.

The preferential depletion of GFP/EGFRt-high cells via Cetuximab is also illustrated by plotting the geometric mean fluorescence intensity (MFI) of GFP expression on day 15, 23 and 238 for both groups (Fig. 4-36C). MFIs of GFP were similar on day 15 before mAb infusion, but were significantly lower in the Cetuximab group than in the Rituximab group on day 23 and followed a similar trend on day 238. Decreased MFIs of GFP after Cetuximab infusion are consistent with the hypothesis that GFP/EGFRt-high cells are depleted. However, MFIs of GFP varied in the Rituximab group between the different days (difference between day 23 and 238 was significant), although persistence of GFP/EGFRt<sup>+</sup> T cells should not be affected by Rituximab. Possible explanations for this observation include differences in measured fluorescence intensities due to technical reasons (cell preparation, flow cytometer settings) and biological variations (protein expression, cell activation status). Limited persistence of EGFRt<sup>+</sup> cells due to an immune response against the transgene can also not be excluded.

In summary, the depletion studies with sorted GFP/EGFRt<sup>+</sup> OT-I cells in larger groups of mice indicate that Cetuximab mediates preferential depletion of EGFRt<sup>+</sup> cells depending on the expression level of EGFRt.

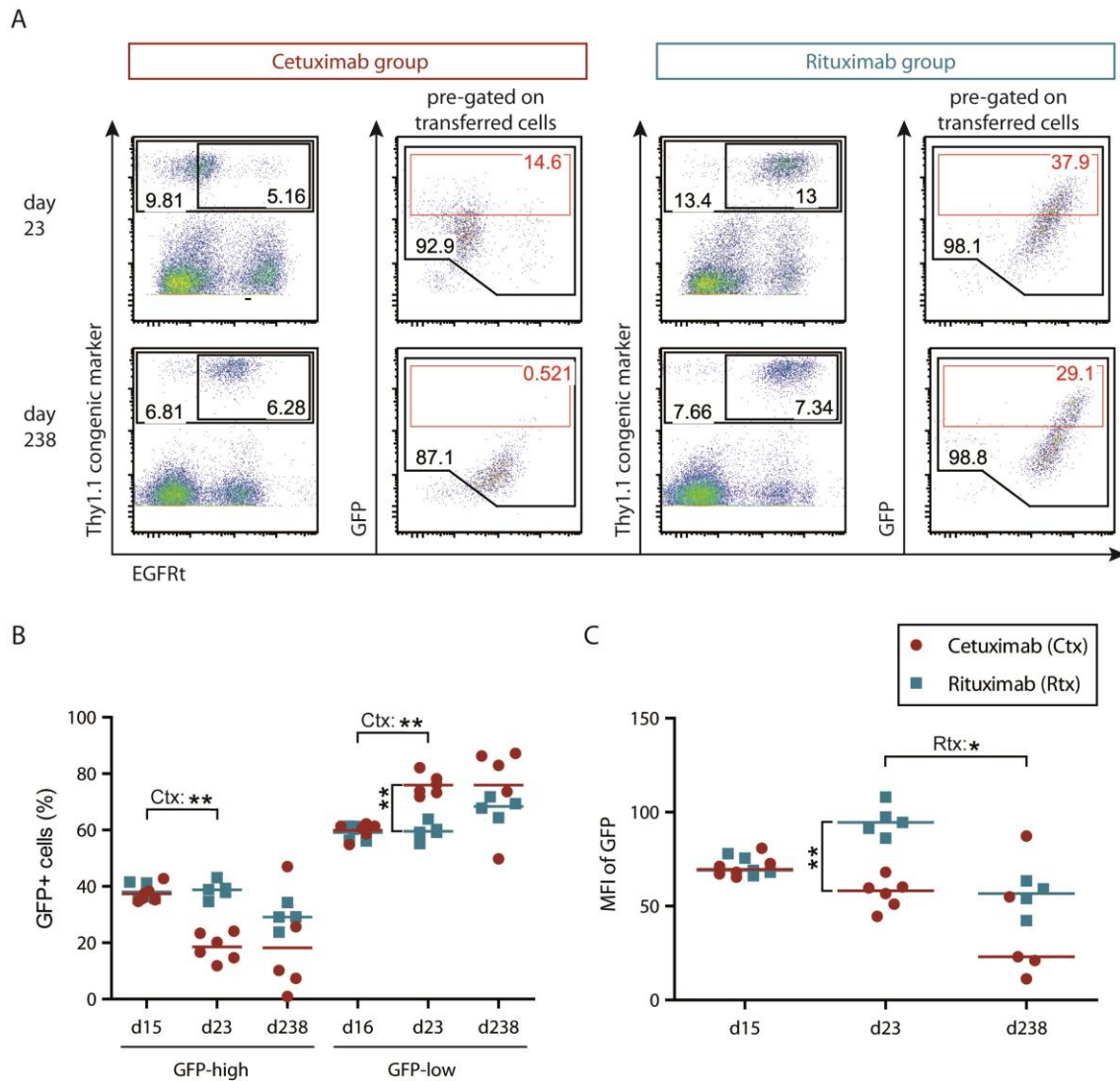


Fig. 4-36: GFP/EGFRt-high T cells are preferentially depleted by Cetuximab. A. Exemplary stainings of Thy1.1 vs. EGFR and GFP vs. EGFR are shown for one Cetuximab- and one Rituximab-treated mouse on day 23 (=day 1 post mAb) and day 238. GFP-high cells are gated in red. B. The frequency of GFP<sup>+</sup> cells in GFP-high or -low gates are shown for all blood samples, acquired on day 15, 23 and day 238 from the Cetuximab and the Rituximab group. C. GFP<sup>+</sup> cells were gated to acquire the geometric mean fluorescence intensity (MFI) of GFP for all blood samples shown in (B). The mean and individual data points are shown in both graphs (B, C). Significance level was calculated by the two-tailed Mann-Whitney test. All significant differences are indicated: (\*) for  $p \leq 0.05$ ; (\*\*) for  $p \leq 0.005$ .

#### 4.4.4 *In vivo* depletion of T cells with high or low EGFRt expression

A correlation between EGFRt expression and depletion efficiency had been found by analysis of the GFP and EGFRt expression level of the transferred GFP/EGFRt<sup>+</sup> OT-I cells after Cetuximab-mediated depletion *in vivo*. T cells with high expression of EGFRt appeared to be preferentially depleted via Cetuximab. To further test this interpretation, OT-I cells were transduced with the GFP/EGFRt construct and then sorted according to their GFP/EGFRt expression level, resulting in EGFRt-high and EGFRt-low cell subsets with a sort purity of above 97% each (Fig. 4-37A). These distinct CD45.1<sup>+</sup> cell populations were transferred at 1x10<sup>6</sup> cells / mouse into C57BL/6 CD45.2 mice that had been sublethally irradiated before.

Following a similar experimental outline as in the previous depletion study, the transferred cells were first expanded *in vivo* by MVA-OVA challenge, which resulted in a well-detectable population of transferred cells that expressed either predominantly high or low levels of GFP and EGFRt (post MVA-OVA, Fig. 4-37B). Both groups of mice were then infused with Cetuximab to investigate the depletion efficiency with respect to EGFRt expression. As indicated by the cell frequency in the GFP<sup>+</sup> gate, OT-I cells with high (GFP/EGFRt) expression were not detectable after Cetuximab infusions, whereas the frequency of OT-I cells with low (GFP/EGFRt) expression were only slightly reduced.

The numbers of CD45.1<sup>+</sup> cells per  $\mu$ L blood were calculated and plotted over time in Fig. 4-37C, showing the expansion peak after MVA-OVA injections and the drop of cell numbers during the contraction phase. The mock group represents mice that received 1x10<sup>6</sup> mock-transduced OT-I cells and Cetuximab infusions, following the same protocol as for the other groups. After the contraction phase, the mock OT-I cells were maintained at more or less same levels. In contrast, the EGFRt-low and EGFRt-high cell numbers were specifically decreased in response to Cetuximab treatment. Interestingly, in this experiment EGFRt-low cells were also depleted quite well, but differences in depletion efficiencies could still be revealed by tracking the number of GFP<sup>+</sup> cells over time. GFP was the most accurate marker for this purpose, as the EGFRt was not accessible for staining due to cell-bound Cetuximab molecules and the CD45.1<sup>+</sup> cell population included the EGFR-negative cell fraction, which varied from mouse to mouse. After two mAb injections, GFP/EGFRt-high cells were completely depleted, while few GFP/EGFRt-low cells were still present (Fig. 4-37D). Better

resolution of the differences between the EGFRt-high and low group could be achieved by plotting the number of GFP<sup>+</sup> cells for the time period of day 17-64 (Fig. 4-37E). In the GFP/EGFRt-high group, GFP<sup>+</sup> cell numbers dropped below detection level - as set by the 'GFP<sup>+</sup>' cell number in the mock group - after the second application of Cetuximab. Conversely, GFP<sup>+</sup> cells could be detected at low levels in the EGFRt-low group after depletion. Interestingly, GFP<sup>+</sup> cell numbers further decreased at later time points, which might indicate that EGFRt-low cells were depleted with a slower kinetic than EGFRt-high cells. The additional drop in cell number coincided with a decreased number of CD45.1<sup>+</sup> cells obtained from the mock group (Fig. 4-37C), so the overall persistence of transferred cells might be generally affected at later time points, independent of depletion effects.

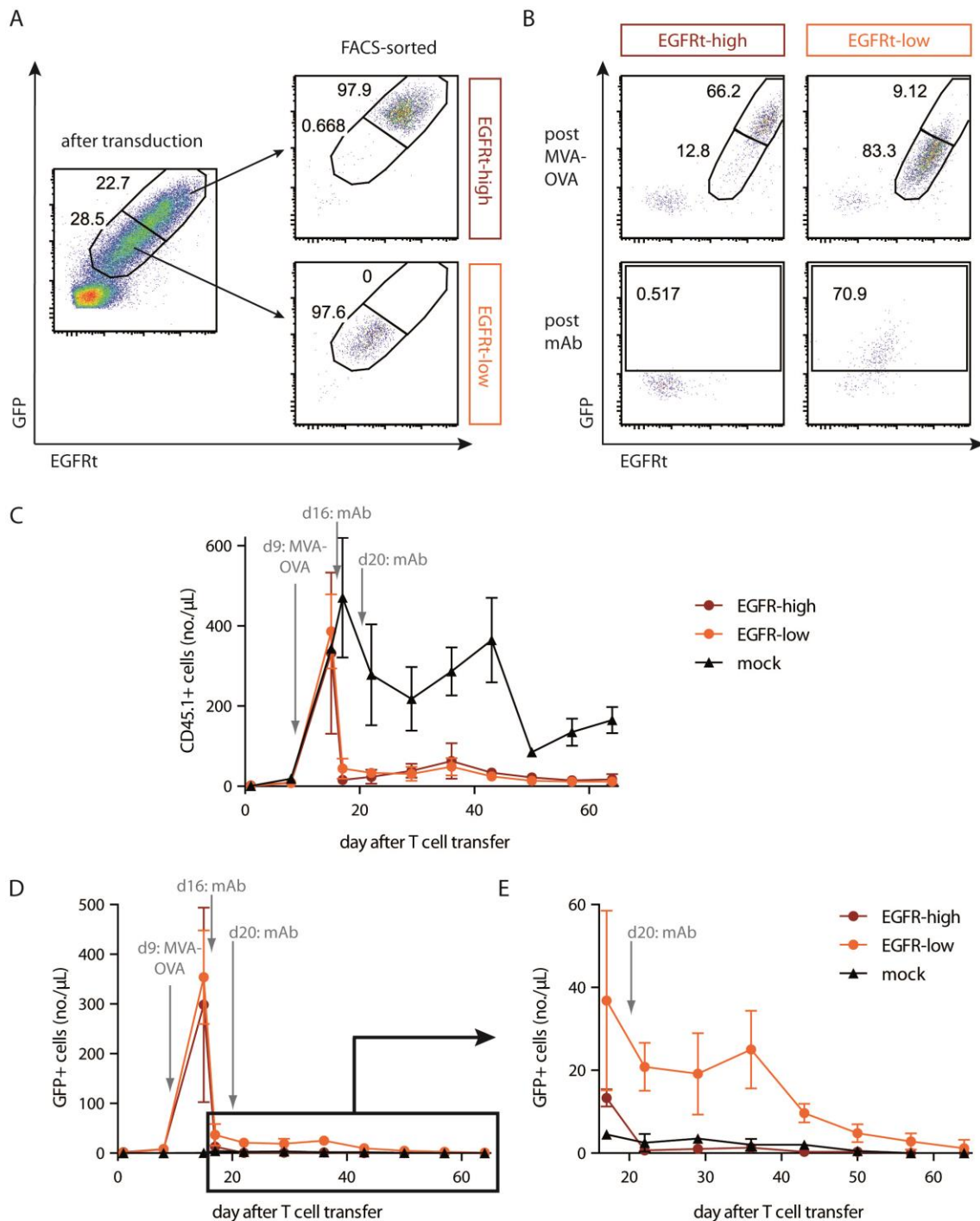


Fig. 4-37: T cells sorted for high EGFRt expression are efficiently depleted by Cetuximab. A. GFP/EGFRt-transduced OT-I cells were sorted into GFP/EGFRt-high and low populations by using the EGFR Fab *Streptamer*. B.  $1 \times 10^6$  sorted OT-I cells were transferred into separate mouse groups, called EGFRt-high or EGFRt-low, and expanded *in vivo* by challenge with MVA-OVA (post MVA-OVA). GFP vs. EGFR staining of CD45.1-prepared cells is shown after Cetuximab infusions (post mAb). C. Number of CD45.1<sup>+</sup> cells per  $\mu\text{L}$  blood is plotted over time for the two mouse groups that received EGFRt-high or low cells and a group that received mock-transduced OT-I cells and was treated in the same way. D. Number of GFP<sup>+</sup> cells per  $\mu\text{L}$  blood was plotted over time. E. A section of the graph in (D) that refers to day 17-64 is shown. Means  $\pm$  SD are plotted in all graphs.  $n=3$  for EGFRt-high,  $n=6$  for EGFRt-low,  $n=2$  for mock.

In summary, the analysis of Cetuximab-mediated T cell depletion in the OT-I mouse model allowed for setting up an experimental layout to monitor depletion of sorted GFP/EGFRt<sup>+</sup> OT-I cells in a reliable and sensitive manner. Data sets from different experimental approaches indicate that depletion efficiency depends on the expression level of the targeted safety marker EGFRt. T cells with high expression of the EGFRt are completely depleted within one day after the second Cetuximab application, while EGFRt-low T cells remain detectable for weeks and seem to follow a much slower Cetuximab-mediated depletion kinetic.

## 4.5 *In vivo* depletion of anti-mouse CD19-CAR/EGFRt<sup>+</sup> T cells

Efficient depletion of T cells with high EGFRt expression had been demonstrated in the OT-I model (Fig. 4-34 - Fig. 4-37). Next, we wanted to address the question whether depletion of EGFRt-high T cells would be sufficient to abrogate T cell-mediated toxicity in a clinically relevant mouse model. As equimolar expression of the EGFRt and a CAR is warranted by the 2A linker, depletion of cells with high levels of the EGFRt should be equivalent to removal of cells with high levels of CAR molecules. A high density of CARs might be associated with high functionality of the T cells, so these cells might be the major players in mediating toxicities.

### 4.5.1 Analysis of anti-mouse CD19-CAR<sup>+</sup> T cell function *in vitro*

A clinically relevant mouse model has been established by others [220], where endogenous B cells are targeted by anti-mouse CD19 (m19)-CAR<sup>+</sup> mouse T cells resulting in long-term B cell aplasia like it is encountered in clinical trials with anti-human CD19 CAR-T cells. We received the m19-CAR construct for our studies as a kind gift from Michele Sadelain. The CAR construct was further modified to include a CD28 costimulatory domain; furthermore, the EGFRt was attached via a P2A linker for simultaneous expression and the gene construct (m1928E) was cloned into the MP71 retroviral vector by Daniel Sommermeyer in the Riddell lab at the FHCRC in Seattle (Fig. 4-38A).

To assess CAR-mediated function, the final m1928E construct was used to transduce Thy1.1<sup>+</sup> mouse splenocytes for an *in vitro* killing assays (Fig. 4-38B). Wildtype Thy1.1<sup>+</sup> splenocytes that contained approximately 40% CD19<sup>+</sup> B cells were used as target cells. Next, 200,000 target cells/well were coincubated with 200,000 mock- or m1928E-transduced effector cells/well. As a control, only target cells were plated out at 200,000 cells/well. All samples were incubated in complete DMEM (cDMEM) without IL-2 in a flat-bottom 96-well plate for approximately 16 hours. Most importantly, the CD19<sup>+</sup> cells among target cells were efficiently killed when coincubated with m1928E-transduced cells (Fig. 4-38B). Overall cell numbers decreased by 50% after over night incubation due to the low viability of mouse splenocytes in the absence of IL-2. When coincubating target cells with mock-transduced cells and taking the viability issue into account, numbers of CD19<sup>+</sup> cells were at similar levels both before incubation

(estimated 80,000 CD19<sup>+</sup> cells/well) and after incubation (mean = 67,000 cells/well). The viability of 'target cells only' was much lower than of the other samples (15% vs. approximately 50% living cells). The number of surviving CD19<sup>+</sup> cells in the 'target cells only' control was even lower than for the control 'target cells + mock T cells'. One reason might be that the mock T cells support overall survival of cells in the same well by secretion of cytokines.

In order to demonstrate an activation-dependent effect on the effector cells, numbers of Thy1.1<sup>+</sup> and EGFRt<sup>+</sup> T cells are shown in Fig. 4-38C. If effector cells were incubated in cDMEM as a negative control (-), numbers decreased from 200,000 to 100,000 Thy1.1<sup>+</sup> cells/well, which was similar to the 50% cell loss in the 'target cells only' control (Fig. 4-38B). Higher cell numbers were detected when effector cells were coincubated with target cells (co), which was most likely correlated with better survival and/or proliferation in response to activation by the target cells. Effector cells were unspecifically stimulated with PMA/Ionomycin as a positive control (+), which led to the highest decrease in Thy1.1<sup>+</sup> cell numbers, possibly due to activation-induced cell death. Numbers of EGFRt<sup>+</sup> cells followed the same pattern as observed for Thy1.1<sup>+</sup> cells and a frequency of 10% EGFRt<sup>+</sup> cells was maintained independent of the stimulus. A CAR-specific effect on expansion of effector T cells could not be observed if mouse splenocytes were used as target cells.

As m1928E-transduced mouse T cells proved functional in the *in vitro* killing assay, they were subsequently tested in an *in vivo* mouse model.

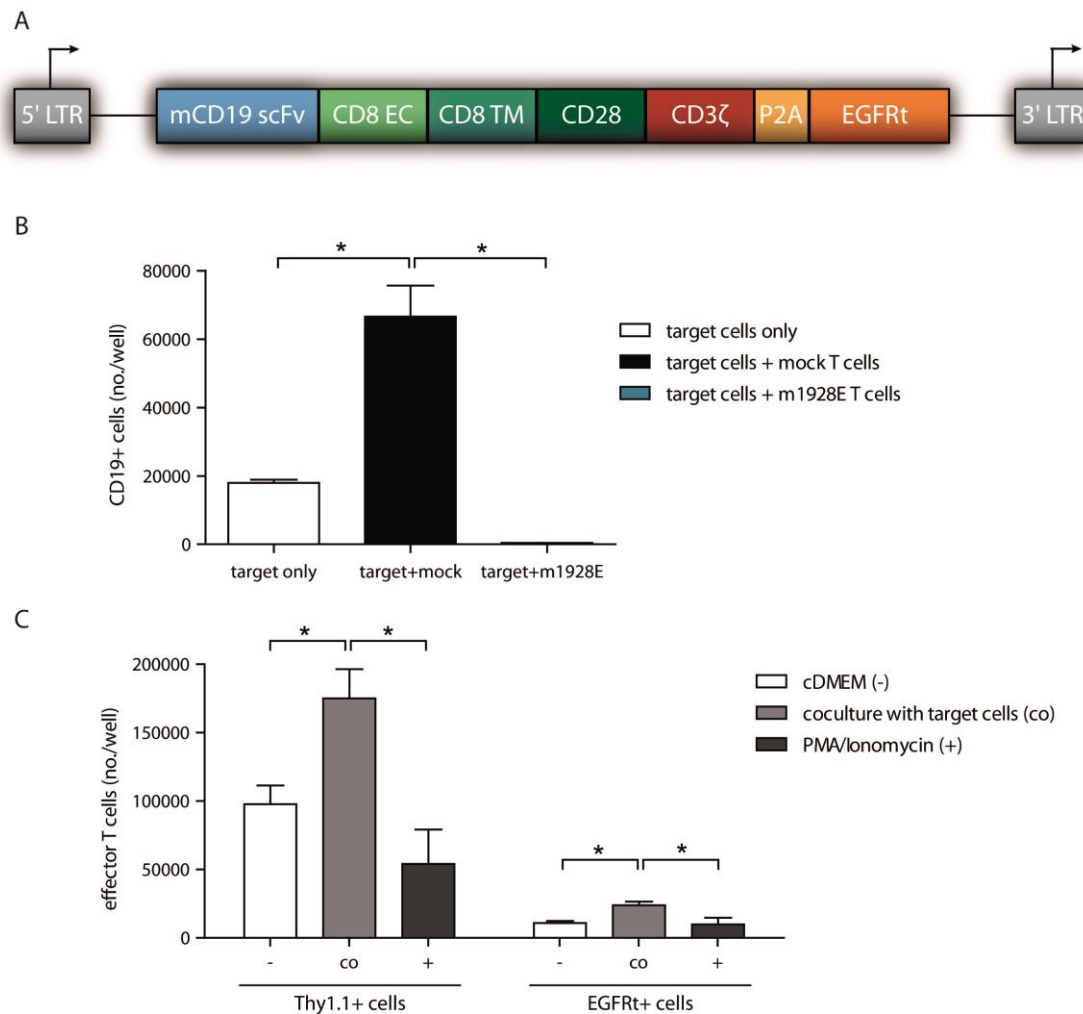


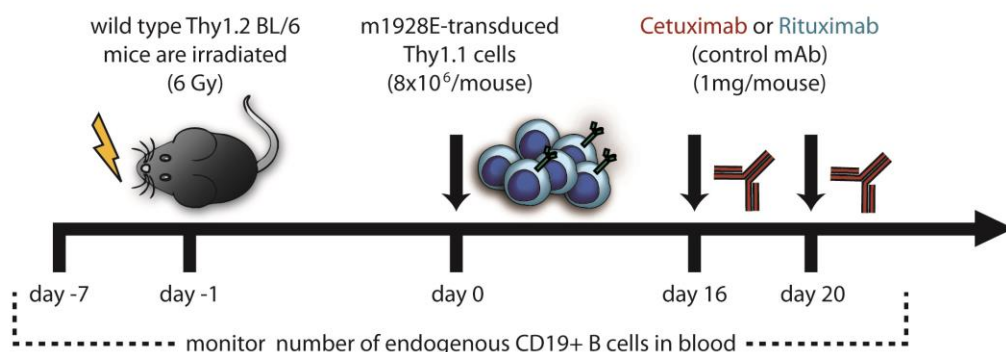
Fig. 4-38: m1928E-transduced T cells mediate killing of CD19<sup>+</sup> B cells *in vitro*. A. Detailed depiction of the composition of the MP71 retroviral vector encoding for the m1928-CAR/EGFRt gene construct. B. m1928E-transduced Thy1.1<sup>+</sup> mouse splenocytes were coincubated with wildtype Thy1.2 mouse splenocytes as target cells for 16 hours to assess CAR-mediated killing of CD19<sup>+</sup> cells among the target cells. 'target cells only' and 'target cells + mock T cells' were used as controls. As a readout, the number of CD19<sup>+</sup> Thy1.1<sup>-</sup> cells was obtained. C. Numbers of effector Thy1.1<sup>+</sup> T cells and EGFRt<sup>+</sup> cells among effector cells are shown after a 16-hour incubation in cDMEM as a negative control (-), coincubation with target cells (co) and stimulation with PMA/Ionomycin as a positive control (+). All samples were analyzed in triplicates. Means +/- SD are shown in the graphs. Statistical significance was calculated by one-tailed Mann-Whitney test. (\*) for p-values ≤ 0.05.

#### 4.5.2 *In vivo* depletion of functional m1928E<sup>+</sup> T cells

After demonstrating anti-B cell function of m1928E-transduced mouse T cells, they were tested in an *in vivo* study that followed a very similar protocol as the depletion study in the OT-I mouse model (Fig. 4-39A). In this 'first-look' experiment, Thy1.1<sup>+</sup> mouse splenocytes were transduced with the m1928E construct with a transduction efficiency of approximately 25%. Cells were not sorted before transfer into sublethally

irradiated wildtype C57BL/6 mice. Thus, the infusion of  $8 \times 10^6$  m1928E-transduced cells equalled  $2 \times 10^6$  functional CAR<sup>+</sup> cells and therefore,  $2 \times 10^6$  mock T cells were transferred into control mice. Cetuximab or Rituximab were infused at a dose of 1mg/mouse on day 16 and 20 for (partial) depletion of m19-CAR/EGFR<sup>t</sup> T cells. The effect of the m19-specific T cells on endogenous B cell populations was monitored in the blood (Fig. 4-39B). Initially, endogenous B cells were drastically reduced by irradiation on day -1. The B cell population reconstituted within 3-4 weeks after irradiation in mice that were transfused with mock T cells. In contrast, B cell recovery was prevented in mice that had received m1928E-transduced cells. CD19<sup>+</sup> B cells could not be detected for more than 80 days, indicating that functional m1928E<sup>+</sup> T cells persist long-term in this mouse model.

A



B

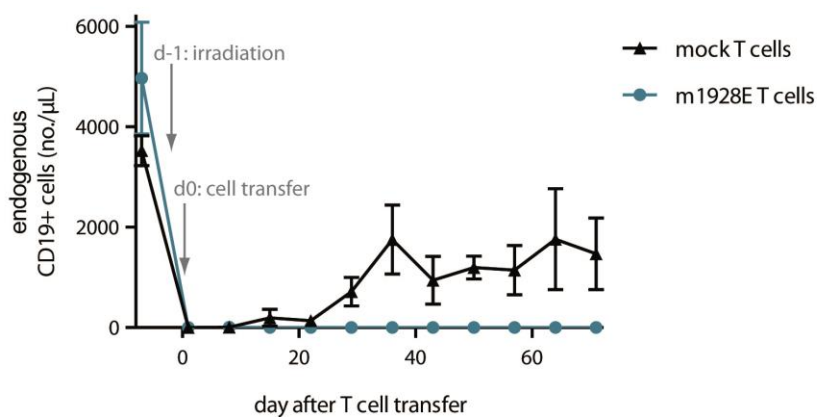


Fig. 4-39: m1928E-transduced T cells prevent B cell recovery after irradiation. A. Experimental layout of depletion study that is based on the transfer of B-cell specific m1928E-transduced cells. B. Numbers of endogenous CD19<sup>+</sup> cells are monitored in the blood. Either mock- or m1928E-transduced T cells were infused into mice to study the T cell function on B cells *in vivo*. Means  $\pm$  SD are plotted.  $n=2$  for both groups.

In this experimental setting, we now could address the question whether EGFRt-targeting depletion of functional T cells would reverse the T cell-mediated toxicity against B cells. To assess the depletion efficiency, frequencies of Thy1.1<sup>+</sup> and EGFRt<sup>+</sup> cells were monitored in the blood (Fig. 4-40A, B). Representative examples of Thy1.1 and EGFR stainings before mAb infusion show good T cell engraftment with approximately 20% EGFRt<sup>+</sup> cells among transferred Thy1.1<sup>+</sup>. Unfortunately, distinct EGFRt-negative and positive cell populations could not be detected in neither of the group at later time points. In addition, the m1928E construct did not contain GFP as a more reliable marker for tracking cells that are potentially masked by Cetuximab for EGFR staining at this time point. As the frequency of CAR<sup>+</sup> cells could not be monitored, only the number of Thy1.1<sup>+</sup> cells was plotted over time (Fig. 4-40B). We did not detect a difference between the mouse group that had been infused with m1928E<sup>+</sup> cells and Cetuximab or the control groups that either had received m1928E<sup>+</sup> cells and Rituximab or mock-transduced cells and no mAb. In this study, CAR/EGFRt<sup>+</sup> cells were not sorted prior to transfer, so depletion of a fraction of EGFRt-high cells might not lead to a detectable decrease in Thy1.1<sup>+</sup> cell numbers. Further, two mice per group could not compensate for the differences in cell engraftment.

Even though it was not possible to directly monitor the depletion of EGFRt<sup>+</sup> cells, B cell recovery in response to T cell depletion could be assessed and was the most important readout of this study. Frequencies of endogenous CD19<sup>+</sup> B cells are shown in blood samples that were obtained from representative mice for each group before mAb infusion and at week 2, 4 and 8 after mAb infusion (Fig. 4-40C). The irradiation effect had already been overcome at the time point of mAb infusion and B cell frequencies were stable in the mock group over this time period (lower row). CD19<sup>+</sup> B cells were not detected in the Rituximab group until week 8 post mAb (middle row). Similarly, B cells were not detected before mAb infusion in the Cetuximab group, but B cells slowly recovered within 6 weeks after administration of Cetuximab (upper row). The number of endogenous CD19<sup>+</sup> cells per  $\mu$ L blood is plotted over time on a log scale (Fig. 4-40D). While B cells recovered within 3-4 weeks after irradiation in the mock group, B cells were not detected in the other groups before mAb application. Only if Cetuximab was injected, B cell numbers started to increase with a 1-2 week delay and reached the level of the mock group after 4-6 weeks. As proof-of-concept, these results demonstrate that Cetuximab-mediated depletion of m1928E<sup>+</sup> T cells could reverse the B cell aplasia, which was maintained in the presence of m1928E<sup>+</sup> T cells, as shown for the control mice treated with Rituximab.

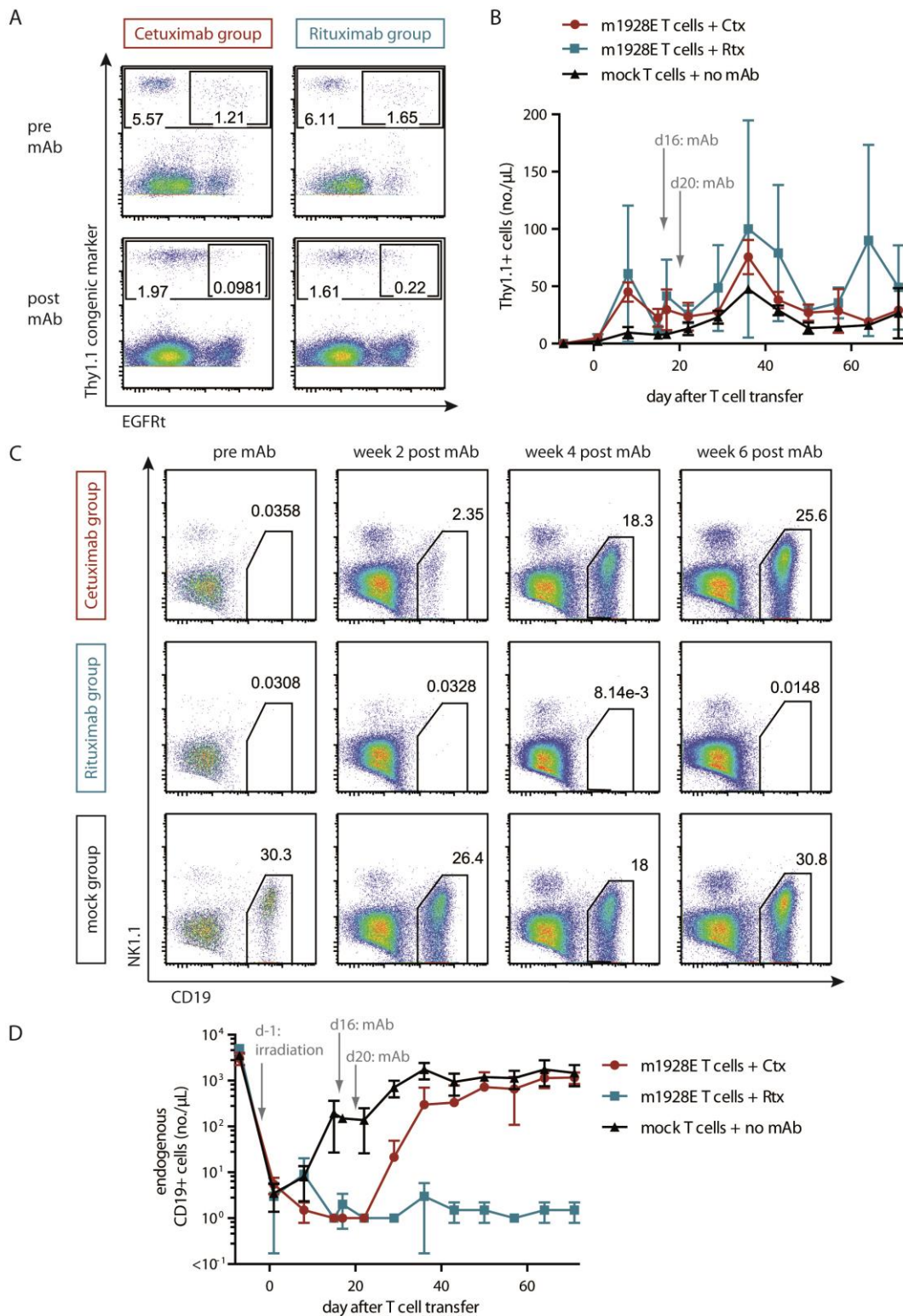


Fig. 4-40: Cetuximab-mediated depletion of m1928E<sup>+</sup> T cells allows for B cell recovery. A. Frequencies of Thy1.1<sup>+</sup> and EGFRt<sup>+</sup> cells before (pre mAb) or after mAb infusion (post mAb). B. Time course of Thy1.1<sup>+</sup> cell numbers for all mouse groups. C. Staining of endogenous CD19<sup>+</sup> B cells before (pre mAb) and 2, 4 and 6 weeks after mAb infusion for one mouse per group that either received m1928E<sup>+</sup> T cells + Cetuximab/Rituximab, or mock T cells + no mAb. D. Number of endogenous CD19<sup>+</sup> B cells per μL blood is plotted over time on a log scale. Means +/- SD are plotted in both graphs. n=2 per group.

## 4.6 In vivo depletion of S-CAR/EGFR<sup>t</sup> T cells in the HBV mouse model

The hepatitis B virus-transgenic (HBV-tg) mouse model is another clinical relevant model, which allows for studying the effect of Cetuximab-mediated depletion of T cells that can induce toxicities. HBV antigens are constitutively expressed on hepatocytes in the liver of HBV-tg mice, which can be therefore used to study HBV-specific therapies. T cell-based immunotherapies are currently investigated, for example a CAR that is specific to the hepatitis B-derived surface antigen (HBsAg), termed S-CAR, has been developed by Ulla Protzer and coworkers. T cells genetically engineered with this S-CAR were transferred into HBV-tg mice and resulted in destruction of hepatocytes upon CAR recognition of HBsAg on the surface of liver cells [221]. T cell-mediated liver pathology can be evaluated by assessing serum levels of the alanine aminotransferase (ALT), which is typically released by injured hepatocytes. Thus, an increase in ALT levels in the serum correlates with infiltration of functional HBV-specific T cells into the liver and massive destruction of hepatocytes. In the HBV-tg mouse model, maximal elevation of ALT serum levels is typically observed 6-8 days after adoptive transfer of S-CAR T cells and prevails only short term as ALT levels return to normal levels by day 12.

The HBV-tg mouse model gave us the opportunity to examine whether liver toxicity could be prevented if S-CAR T cells were depleted before peak levels of ALT were reached. In collaboration with Karin Wisskirchen and Nina Böttinger from the Protzer lab in Munich, CD45.1 CD8<sup>+</sup> mouse cells were retrovirally transduced with an S-CAR/EGFR<sup>t</sup> construct, expanded *in vitro* and transferred into non-irradiated CD45.2 HBV-tg C57BL/6 mice at a dose of  $4 \times 10^6$  cells per mouse without prior enrichment of EGFR<sup>t</sup> cells (Fig. 4-41A). Cetuximab or Rituximab as a control was infused at 1mg per mouse to mediate T cell depletion on day 4. Persistence of transferred cells and ALT levels were monitored in the blood. Before mAb infusion, transferred cells could be detected in the blood of the Cetuximab and Rituximab group (pre mAb, Fig. 4-41B). Approximately 30% of all transferred CD45.1<sup>+</sup> cells stained positive for EGFR. After Cetuximab administration, a distinct EGFR<sup>t</sup> cell population could not be detected (post mAb), but the EGFR staining was also not as bright as in the 'pre mAb' sample in the Rituximab group. For better distinction of CAR/EGFR<sup>t</sup> and untransduced cells, blood samples were stained with an anti-human IgG reagent, which binds to the spacer of the

CAR in addition to the EGFR staining (post mAb, lower row). Indeed, the CAR/EGFR<sup>t+</sup> population could be identified now and made up 27% of all transferred cells in the Rituximab group and possibly slightly less in the Cetuximab group. As observed in prior *in vivo* experiments, the EGFR staining was inhibited in the Cetuximab group. Additionally, the CAR-specific IgG staining seems to be decreased if T cells are stimulated through the CAR (personal communication). This also affected the CAR staining in this experiment and was observed in the Rituximab group to a higher extent than in the Cetuximab group. As S-CAR/EGFR<sup>t+</sup> T cells could not be reliably detected and more importantly, transferred T cells are expected to migrate into the target organ, the efficacy of Cetuximab-mediated T cell depletion could not be directly monitored in the blood in this study. Frequencies of CD45.1<sup>+</sup> T cells in the blood could still be obtained, but did not reveal any differences between the Cetuximab and Rituximab group (Fig. 4-41C).

As a functional readout, ALT levels in the serum were assessed on day 4, 6, 8 and 12 (Fig. 4-41D). In the Rituximab group, ALT levels were elevated on day 8 in 5 out of 8 animals. In contrast, no increase in ALT levels could be detected in any of the Cetuximab-treated mice. This observation is in line with the interpretation that T cell-mediated liver toxicity can be prevented by infusing Cetuximab. To provide further evidence, the number of HBV copies in relation to the reference gene *Nid2* were quantified by qPCR in the DNA, isolated from liver on day 12, by Nina Böttinger (Fig. 4-41E). Control mice that did not receive any adoptively transferred cells or antibodies were included in the analysis to measure the normal level of HBV copies in the liver of untreated HBV-tg mice. If HBV-tg hepatocytes are destroyed by S-CAR T cells, viral copies usually decrease in the liver DNA samples, which indeed was observed in the Cetuximab and Rituximab group on day 12. No differences were detected between both groups. However, the fact that ALT levels were elevated in only 3 out of 4 Rituximab-treated mice that were analyzed on day 12 should be taken into account. The subgroup of Rituximab mice with increased ALT levels on day 8 indeed had a tendency of lower numbers of viral copies as compared to the Cetuximab group, indicating that less HBV<sup>+</sup> hepatocytes were destroyed if T cells got depleted. Viral copies were also quantified on day 20 using liver DNA obtained from 4 additional mice from the Rituximab group (Fig. 4-41E). Consistent with earlier observations in the Protzer lab, the anti-viral effect was only transient and viral copy numbers were already higher on day 20 compared to day 12.

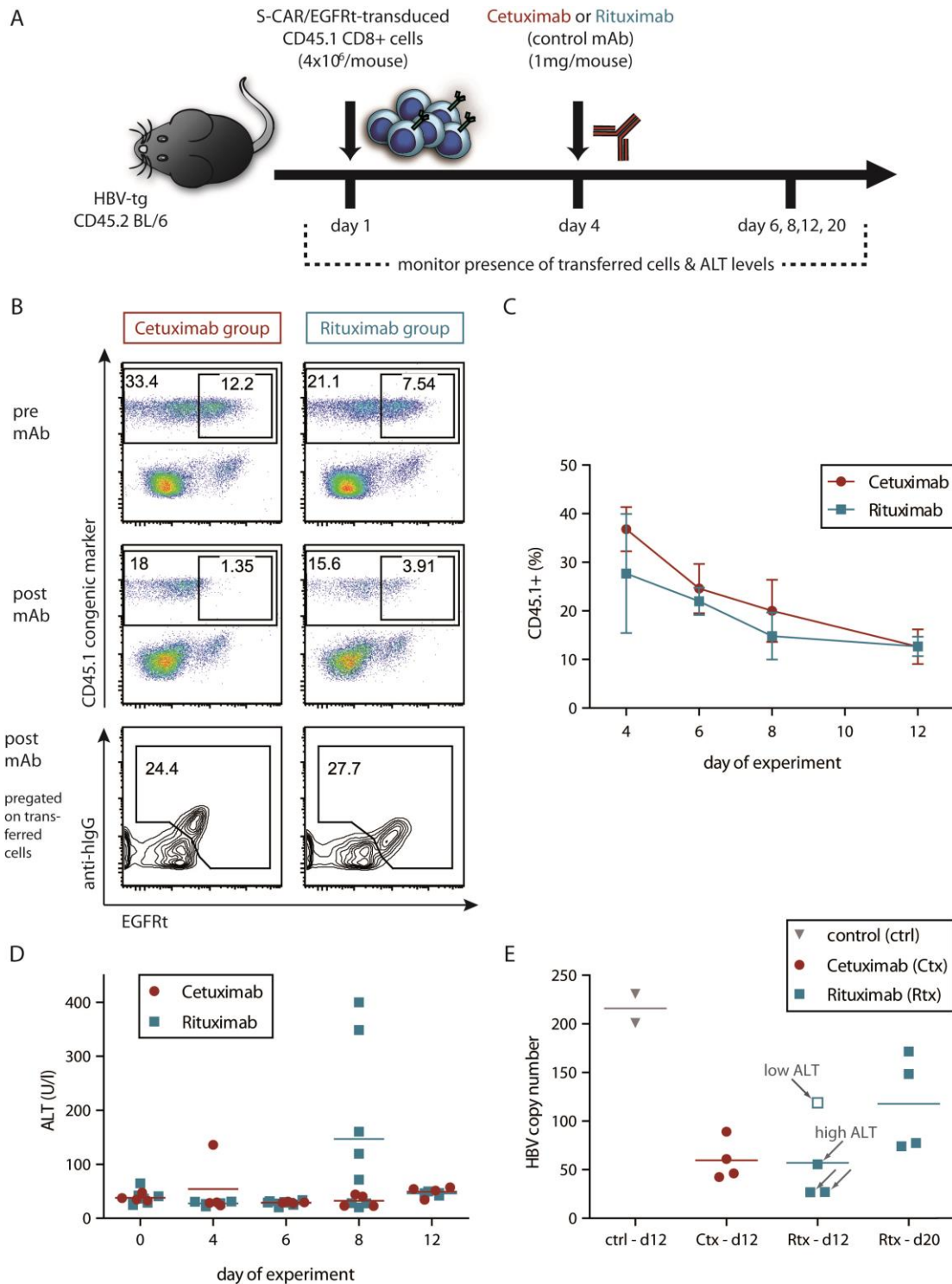


Fig. 4-41: Cetuximab-mediated depletion of S-CAR/EGFRt T cells prevents liver toxicity. A. Layout of the depletion study in HBV-tg mice. B. Representative blood samples were obtained before (pre mAb) or after mAb infusion (post mAb) from the Cetuximab and Rituximab group and stained for EGFRt. The 'post mAb' sample was also stained for the S-CAR with an anti-IgG reagent. C. Frequencies of CD45.1<sup>+</sup> transferred cells are plotted over time as means  $\pm$  SD. D. Alanine aminotransferase (ALT) levels were assessed in blood serum at different time points. E. HBV copy numbers, relative to the reference gene Nid2, were quantified by qPCR. Subgroups of Rituximab-treated mice 'low ALT' and 'high ALT' on day 12 are indicated by arrows. Means and individual data points are plotted in D and E. Cetuximab group: n=4, Rituximab group: n=8.

In this depletion study, endogenous lymphoid and myeloid cells were monitored in an extensive blood screening by flow cytometry. The lymphoid cell screening included CD4<sup>+</sup> and CD8<sup>+</sup> T cells, CD19<sup>+</sup> B cells and natural killer cells, whereas the myeloid cell-specific staining panel covered neutrophils, inflammatory macrophages and monocytes, tissue-resident macrophages and dendritic cells. Interestingly, some cell types were elevated in correlation with observed liver toxicity (Fig. 4-42). The Rituximab group was subdivided into mice with detectable liver toxicity (high ALT) and mice with no signs of liver toxicity based on ALT measurements (low ALT). Coinciding with the ALT peak on day 8, higher frequencies of inflammatory macrophages and neutrophils were detected on day 8 in the blood of the Rituximab (high ALT) group, while frequencies for these myeloid cell types stayed at almost constant levels with some variations for the Cetuximab and Rituximab (low ALT) groups (Fig. 4-42A and B). The analysis of lymphoid cell numbers among liver-associated lymphocytes on day 12 showed no difference between all groups for CD45.1<sup>+</sup> transferred cells and endogenous CD4<sup>+</sup> T cells (Fig. 4-42C). Conversely, higher numbers of endogenous CD8<sup>+</sup> T cell infiltrated the liver in Rituximab-treated mice with high ALT levels (probably in response to the inflammation) than in mice with low ALT levels. B cell numbers increased in livers with elevated ALT only to a low extent in the Rituximab (high ALT) group.

In summary, T cell-mediated liver toxicity could be prevented in mice that were treated with Cetuximab to mediate depletion of transferred S-CAR/EGFR<sup>t</sup> T cells. The depletion efficiency in this study could not be evaluated, as both the EGFR and the CAR-specific staining is constrained by the presence of Cetuximab or downregulation of the CAR after *in vivo* activation, respectively.

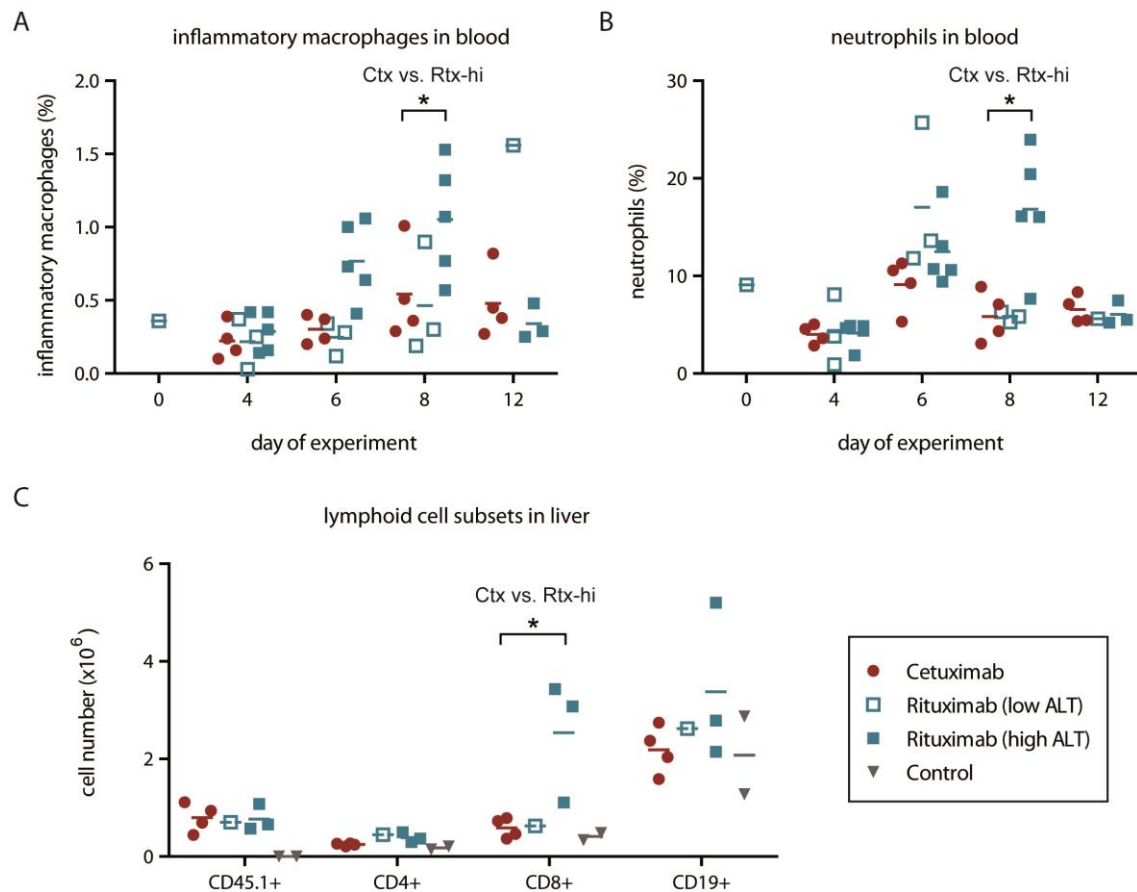


Fig. 4-42: Some immune cell types are elevated in correlation with liver toxicity. A. Frequencies of inflammatory macrophages were assessed in the blood of Cetuximab and Rituximab-treated mice during the course of the experiment. The Rituximab group was subdivided into mice with increased ALT levels (high ALT) and mice with normal ALT levels (low ALT). B. Frequencies of neutrophils in the blood are shown over time. C. Numbers of lymphoid cell subsets in liver-associated lymphocytes are obtained for all groups on day 12. Only 4 out of 8 Rituximab-treated mice were analyzed on day 12. Control mice that were not infused with cells or antibodies were included for comparison. Means and individual data points are shown in each graph. Significance level was assessed by one-tailed Mann-Whitney test. Significant differences with  $p \leq 0.05$  are indicated (\*).  $n=4$  for the Cetuximab and the entire Rituximab group,  $n=2$  for the control group.

## 4.7 Evaluation of the EGFRt marker in the non-human primate

The safety and efficacy of the cell-specific depletion strategy based on introducing the EGFRt into T cells requires detailed evaluation in a large animal model before it can be transferred into clinical application. A non-human primate (NHP) model was established by Carolina Berger and colleagues and allowed for analysis of the safety and persistence of adoptively transferred T cells [188, 222]. The NHP model provided an optimal setting to study the EGFRt-based depletion mechanism in a pilot experiment in collaboration with Carolina Berger and the Washington National Primate Research Center (WaNPRC) in Seattle, USA (Fig. 4-43A). Experiments were conducted by Carolina Berger, except for the magnetic selection of EGFRt<sup>+</sup> T cells, which was performed by myself.

Macaque CD8<sup>+</sup> T cells were selected from peripheral blood of one *M.nemestrina*, subsequently genetically engineered with a lentiviral construct that encodes the EGFRt and no other surface-expressed protein and expanded *in vitro* according to the rapid expansion protocol (REP) [223]. EGFRt<sup>+</sup> macaque T cells were magnetically enriched with the reversible EGFR Fab *Streptamer* and *Strep*-Tactin nanobeads following the experimental protocol that had been optimized before as described in section 4.3.1. In parallel, CD20<sup>+</sup> T cells were generated by lentiviral transduction with a CD20 construct that allows for tracking of these control cells in the animal. The EGFRt could be detected on EGFRt-transduced T cells, whereas the CD20<sup>+</sup> control T cell product stained positive for CD20 and negative for the EGFRt (Fig. 4-43B).

Expanded EGFRt<sup>+</sup> and CD20<sup>+</sup> were co-infused into the macaque at a cell dose of  $3 \times 10^8$ /kg each. Cetuximab (Erbix<sup>TM</sup>) was applied as a 2-hour intravenous infusion to the anaesthetized animal on day 3 and 10 after T cell transfer. Due to high background of the EGFR staining by flow cytometry (data not shown), persistence of EGFRt<sup>+</sup> and CD20<sup>+</sup> T cells was monitored in the blood by quantitative polymerase chain reaction (qPCR) using primers that specifically bind to unique sequences within each of the lentiviral vectors. EGFRt<sup>+</sup> T cells could not be detected in the blood (Fig. 4-43C) or lymph nodes and bone marrow (data not shown) after two infusions of Cetuximab on day 14 and later time points. The control CD20<sup>+</sup> cells were found at stable levels of 1.5-2% of all CD8<sup>+</sup> T cells in the blood, and they were also present in lymph nodes and bone marrow. Importantly, the capacity of transferred T cells to survive in the monkey

is demonstrated by the persistence of CD20<sup>+</sup> T cells in the macaque during the course of the experiment.

In this experimental setting, we could also address the question whether the human EGFRt marker could elicit a cytotoxic T cell response in the macaque due to few differences between the human and macaque EGFR gene sequence. Therefore, PBMCs were obtained on day 7 and 16 and stimulated *ex vivo* with autologous,  $\gamma$ -irradiated, mock- or EGFRt-transduced T cells. Expanded PBMCs were then tested for specific lysis of mock or EGFRt<sup>+</sup> T cells at different effector-to-target ratios in a standard chromium release assay (Fig. 4-43D). No specific recognition of EGFRt<sup>+</sup> T cells was detected for PBMCs obtained on day 7. Conversely, EGFRt<sup>+</sup> T cells were specifically killed by PBMCs from day 14, indicating that a cytolytic T cell response was induced in the monkey at that time point.

Additionally, the macaque was monitored for any signs of toxicities that were associated with the adoptive T cell transfer or Cetuximab infusions. This included assessing the weight, blood cell counts and the blood level of metabolites and liver-associated enzymes. All parameters were within a normal range (data not shown).

Based on this pilot study of the EGFRt-based depletion approach in a large animal, we conclude that transfer of EGFRt-modified T cells and administration of Cetuximab in macaques is safe. Transferred T cells could be detected in the blood and CD20<sup>+</sup> T cells persisted for at least 3 weeks. The number of EGFRt<sup>+</sup> T cells decreased after Cetuximab infusion, but simultaneously, cytolytic T cell responses against EGFRt<sup>+</sup> T cells were developed in the monkey. Further data on the efficacy of the Cetuximab-mediated EGFRt depletion strategy could therefore not be obtained from this study. Nevertheless, the experiments provide valuable insight into how to improve the model, e.g. by switching to another macaque species, the rhesus macaque (*M.mulatta*), where less EGFR background is expected compared to *M.nemestrina*, or by generating the EGFRt from the EGFR gene sequence of the rhesus macaque instead of the human to prevent immune recognition of EGFRt<sup>+</sup> T cells.

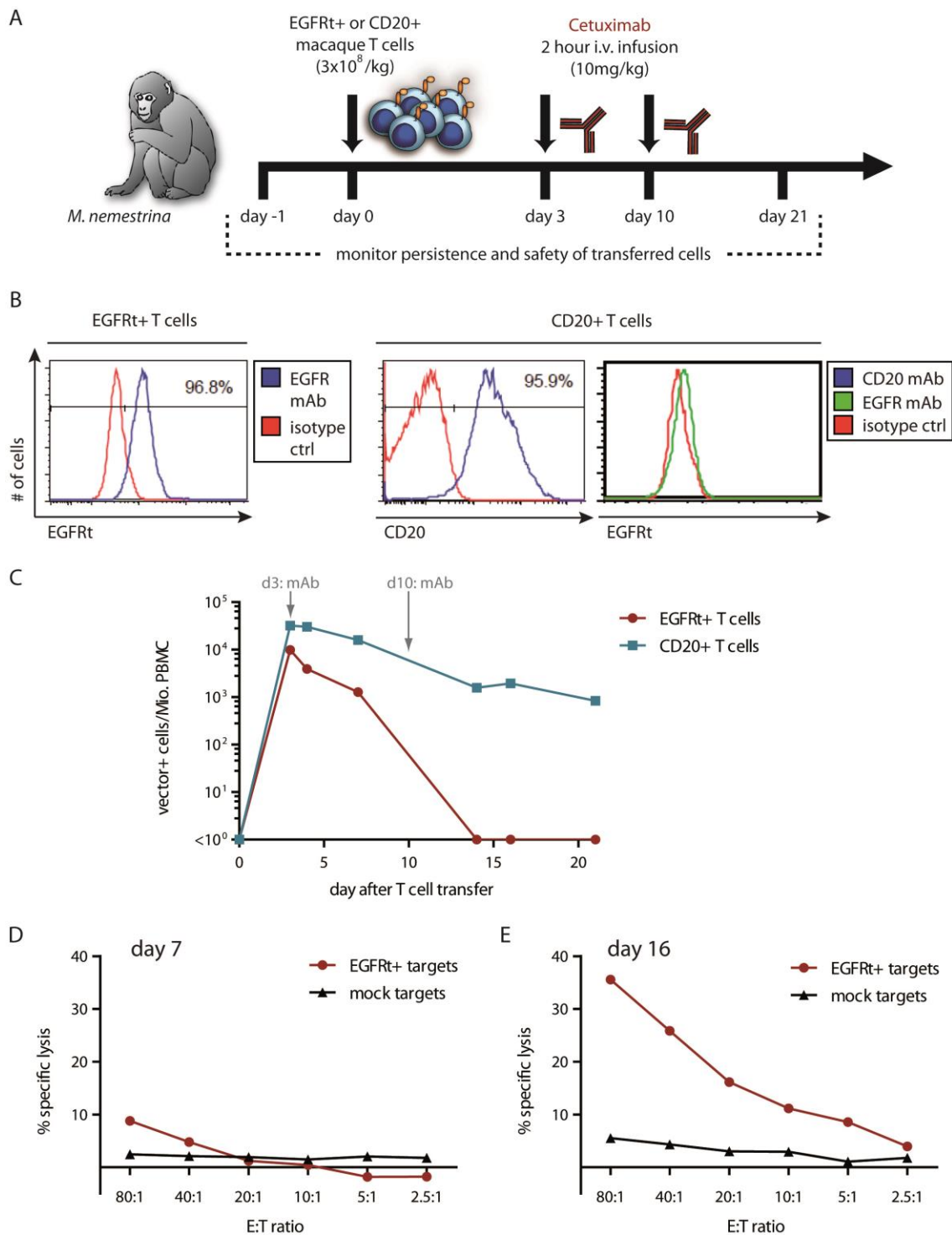


Fig. 4-43: EGFRt<sup>+</sup> T cells could not be detected after Cetuximab-mediated depletion, but might have been rejected due to immunogenicity. A. Experimental layout of the pilot study in *M.nemestrina*. B. Phenotype of the EGFRt<sup>+</sup> and CD20<sup>+</sup> T cells was assessed by staining with anti-EGFR and anti-CD20 mAbs. C. Number of EGFRt<sup>+</sup> or CD20<sup>+</sup> cells per million PBMCs was acquired by qPCR using primers that were specific to each vector. D. A chromium release assay was performed to measure specific lysis of mock- vs. EGFRt-modified T cells due to transgene-specific T cells among PBMCs that were obtained on day 7 and 16 and stimulated with autologous,  $\gamma$ -irradiated, untransduced or EGFRt<sup>+</sup> T cells *ex vivo*.

## 5 Discussion

In this thesis, the truncated EGFR (EGFRt) was carefully studied regarding its proposed properties of a stable tracking marker, a reliable target for cell selection and a cell-specific depletion approach with immediate clinical applicability. The work focused on two main aspects: 1.) development of a reversible EGFR-specific selection reagent and 2.) in-depth analysis of the depletion of EGFRt<sup>+</sup> T cells in several mouse models, including settings with direct clinical relevance.

### 5.1 The EGFRt is a reliable cell-surface tracking marker

The first important step to proceed with evaluating the efficacy of EGFRt-directed cell selection and depletion was to demonstrate that the gene construct provided stable cell surface expression. The use of a T2A linker allows for concordant expression of both the EGFRt and another transgene, which can be a TCR, a CAR or another reporter protein (Fig. 4-2). We could show that implementing the EGFRt in lentiviral or retroviral constructs can allow for robust and simple detection of gene-modified cells. The stability of EGFRt expression was studied under resting as well as stimulatory conditions *in vitro* and *in vivo*. For example, CAR/EGFRt-transduced T cells were activated through their CD19-CAR *in vitro* by cocubation with CD19<sup>+</sup> target cells or their S-CAR *in vivo* by recognition of HBV<sup>+</sup> hepatocytes. Importantly, the expression level of the EGFRt was not affected by the activation status of the monitored cell population, as illustrated by unchanged mean fluorescence intensities of the EGFR staining *in vitro* and *in vivo* (Fig. 4-4).

Stable expression of a marker is also affected by internalization and downregulation processes. In the absence of ligands, the wildtype (wt) EGFR is constitutively internalized and usually transported back to the cell membrane [206]. In epithelial cells, the half-life of EGFR is estimated to be 10-14 hours due to metabolic turnover [224]. Upon ligand binding, the wt EGFR is relocated to clathrin-coated pits for endocytosis [225]. The motifs for receptor internalization were allocated to the cytoplasmic tail [226]. As the truncated EGFR lacks both the intracellular domains and the ligand-binding extracellular domains, it is unlikely that the EGFRt can be downregulated by receptor-mediated endocytosis. Although the EGFRt should still be subject to

constitutive trafficking, overall we expect the EGFRt to be rather stably expressed on the cell surface.

It would be valuable to directly detect recombinantly expressed CARs in a reliable and specific manner. Although it was feasible in some cases to target the CAR with staining reagents that bound the Fc-derived spacer in mice, such anti-Fc antibodies were found to be highly unspecific for human cells. In general, CAR-detecting reagents are not readily available for all CARs, e.g. CARs with very short spacers. In these situations, the CAR can currently only be detected with rather unspecific reagents, such as protein L [227], scFv-specific antibodies [181] or reagents that are based on the extracellular domain of the target molecule. As an example for the latter, we successfully generated the ROR1-*Streptag* fusion protein to detect ROR1-CARs. Unfortunately, the expression of a soluble version of the target protein is not always successful and results in a reagent that can only be used to stain CARs with one specificity (Fig. 4-3). Further, staining with the ROR1 protein can be hampered if the CAR is in close proximity to the cell membrane due to a short spacer, for example. These issues were encountered throughout the project and are prevalent in the field, highlighting the need for a universal marker such as the EGFRt that can be used in combination with any transgene.

The versatility of the EGFRt makes it an attractive marker that cannot only be used for cell tracking, but also as a target molecule for cell ablation. EGFRt<sup>+</sup> cells can be recognized by Cetuximab that is available as a clinical grade reagent and capable of inducing antibody-dependent cellular cytotoxicity (ADCC) against EGFR<sup>+</sup> target cells, e.g. to treat metastatic colorectal and head/neck cancer [206]. However, in the presence of Cetuximab, we encountered issues that limited the use of anti-EGFR reagents for tracking EGFRt<sup>+</sup> cells. After infusing Cetuximab in the *in vivo* depletion studies, the cell-bound antibodies inhibited the *ex vivo* staining with the EGFR mAb (Fig. 4-32). *In vitro* titrations of the amount of Cetuximab showed that a concentration of 30µg/mL already reduced the EGFR staining to a similar extent as a high concentration of 1mg/mL. It would be interesting to analyze whether lower concentrations of Cetuximab still inhibit the EGFR staining, but do not trigger *in vitro* ADCC, as previously reported for Cetuximab concentrations below 0.1µg/mL [202, 228]. It is likely that low numbers of Cetuximab molecules per cell are sufficient to inhibit the EGFR staining, but might not mediate ADCC. Thus, an EGFRt<sup>+</sup> cell population that was spared from Cetuximab-mediated ADCC *in vivo* might still be

covered with a number of Cetuximab molecules to be missed during the monitoring of the presence of EGFRt<sup>+</sup> cells. Although it is appealing to develop a marker that can be targeted for both purposes, tracking and depletion, the EGFRt was not a suitable marker to evaluate the efficiency of depletion in Cetuximab-treated mice in the performed experiments. This problem could be overcome by using an EGFR-specific staining reagent that recognizes a different epitope from Cetuximab, e.g. the anti-EGFR IgG1 Matuzumab that was shown to efficiently bind to the EGFR in the presence of Cetuximab [229]. Alternatively, including a second reporter gene, e.g. a fluorescent protein, allows at least experimentally for rapid detection and selection of cells via flow cytometry [230], so we decided to link GFP to the EGFRt for preclinical evaluation of the depletion approach in mice. For clinical settings, truncated versions of the CD34 or CD19 have already been used as tracking markers in combination with suicide mechanisms, such as the HSV-TK [231, 232] or the iCasp9 [233], respectively.

Due to its preferential expression on epithelial tissues, the EGFRt has been considered as a suitable tracking marker for assessing the persistence of transferred cells in the blood [212]. Occasionally, expression of the EGFR was reported for some human leukocyte populations, e.g. monocytes [234], plasma cells [235] and Tregs under inflammatory conditions [236]. We also observed low levels of EGFR on a CD14<sup>+</sup> monocyte population among human PBMCs, but pre-gating on the lymphocyte population and/or including additional T cell markers could achieve specificity of the EGFR staining on transferred T cells. As no EGFR expression has been reported for mouse hematopoietic cells so far, monitoring the transferred EGFRt<sup>+</sup> cells in mouse models should not be disturbed. Having identified the limitations of using EGFRt for cell tracking, we could modify the procedures and confirm in numerous experimental settings that the EGFRt is a suitable and highly valuable tool for detecting gene-engineered cells during selections and depletion studies.

## 5.2 The quest for a reversible EGFR-specific selection reagent

In addition to EGFR-specific stainings, selections of EGFR<sup>t+</sup> cells can also be performed using the biotinylated anti-EGFR mAb Cetuximab and streptavidin (SA) coupled to a fluorophore or a magnetic bead, respectively [195]. Based on the co-expression of the EGFR<sup>t</sup> and the CAR, magnetic enrichment of EGFR<sup>t+</sup> cells results in a more homogenous and highly functional cell population. While magnetic selections with biotinylated mAbs and SA-coated beads are working well (Fig. 4-22), the selection reagent remains bound on the cell surface, which poses potential problems, especially for clinical applications. Generally, it is still difficult to get approval for cell products that contain magnetic particles; furthermore, residual reagents might affect persistence and functionality of the transferred cells. More specifically, Cetuximab bound to EGFR<sup>t+</sup> cells might potentially interfere with survival of transferred cells due to antibody responses raised against the chimeric IgG1 Cetuximab [195] or because Cetuximab labels the infused cells for immediate *in vivo* depletion. Initial experiments, where Cetuximab-coated or uncoated T cells were transferred into mice, did not reveal profound effects of cell-bound Cetuximab on the frequency of engrafted T cells (data not shown). However, these experiments were performed in an early phase of the project and for a definitive conclusion to this point, experiments would need to be repeated with sorted GFP/EGFR<sup>t+</sup> T cells to allow reliable detection and quantitation of absolute cell numbers that account for changes in the hematopoietic cell compartment after irradiation.

Despite these considerations, Wang *et al.* suggested to enrich EGFR<sup>t+</sup> cells by using 'irreversible' selection reagents and then expand them *in vitro* to increase the number of cells for adoptive transfer into patients [195]. At the same time, cell-bound reagents are diluted out, so any potential negative impact on cell function is minimized. Nevertheless, it is still desirable to develop a reversible EGFR-specific selection reagent because purified label-free cells can be directly transferred into patients after the selection step without prior expansion. This will become an important advantage if clinical experience will confirm that low numbers of gene-modified T cells are indeed sufficient to induce efficient clinical responses [237]. As reversible reagents are not cotransferred with the cell product, they do not need to be validated in extensive pre-clinical tests for clinical approval. Therefore, magnetic selections based on reversible reagents can easily and rapidly be included in clinical protocols [178].

The development of an EGFR-specific selection reagent was based on the *Streptamer* technology. This required the generation of an anti-EGFR Fab-*Streptag* fusion protein of low affinity. The parental anti-EGFR mAb had to meet at least two criteria: 1) the genetic sequence had to be available and 2) its epitope had to be present in the truncated version of the EGFR. The anti-EGFR mAb A13 is a good candidate for being the parental mAb of a reversible EGFR Fab, as the gene sequence of the variable regions of the heavy and light chain has been published and its epitope has been mapped to the region of aa 302-50 that is largely included in the truncated EGFR (aa 310-644) [195]. The affinity of the EGFR mAb A13 was analyzed by surface plasmon resonance (SPR) and resulted in a dissociation constant ( $K_D$ ) of ~5.8 nM, which is comparable to the  $K_D$  value of 5.0 nM of Cetuximab [214]. Thus, the EGFR mAb A13 should be equally suited to generate a low-affinity Fab as Cetuximab itself. Based on the EGFR mAb A13, we generated the wildtype EGFR Fab, fused it to *Streptag* and multimerized it on a *Strep*-Tactin backbone to test its staining capacity. Indeed, the wt EGFR Fab *Streptamer* detected the EGFRt on the T cell lymphoma H9 cell line that was transduced with a EGFRt construct (Fig. 4-8).

As the wildtype EGFR Fab was not reversible, single point mutations were introduced into the framework region of the Fab. As Bès *et al.* showed, substituting single amino acids with alanine can affect the binding capacity of a Fab via changes in the Fab structure [216]. However, these effects can vary between Fab fragments of different specificities, so identification of a low-affinity Fab is still based on screening several candidate mutants. Indeed, many single mutations did not affect the affinity of the EGFR Fab as shown by comparable staining intensities, and no effect on reversibility was observed (Fig. 4-11). Increasing the temperature from 4°C to room temperature accelerated the dissociation kinetics and uncovered differences in reversibility among the EGFR Fab single mutants (Fig. 4-12). Under these conditions, EGFR Fab mut72 was found to be fully reversible on T cells (Fig. 4-15). Although releasing the Fab *Streptamer* is usually performed at 4°C, increasing the temperature to room temperature for 1-2 hours might lead to some increase in staining intensities, but should not have a negative impact on cell viability and functionality [238]. In the case of targeting the functionally inert EGFRt, it is very unlikely that the higher temperature induces signaling by Fab *Streptamer* binding to the cell or results in the selection reagent being internalized.

Nevertheless, we introduced additional mutations to potentially further decrease the affinity of the EGFR Fab to achieve reversibility at 4°C. EGFR staining was completely abolished for all tested double mutants that were based on alanine exchanges that entirely abrogated the structural and binding properties of the original amino acid (Table 2). This led to the strategy to exchange the amino acids at these important positions with a functionally similar amino acid instead of alanine. Remarkably, we could identify new double mutants that preserved the staining capacity of the Fab, albeit staining intensities were relatively low, and reduced the affinity such that Fab monomers could dissociate from the cell surface at room temperature (Fig. 4-16). It would be interesting to apply this strategy of conservative aa exchange to the single Fab mutL2, which abolished the EGFR staining completely (Fig. 4-11).

Since great difficulties were encountered to identify a Fab of sufficiently low affinity for reversible staining at 4°C, it would also be reasonable to try to develop a Fab from a different parental antibody. As an alternative, we generated another EGFR Fab-*Streptag* fusion protein based on the Cetuximab sequence, deposited in DrugBank under DB00002. In contrast to the A13-based EGFR Fab, the wildtype Cetuximab Fab was already reversible to some extent at room temperature (data not shown). This observation is in line with biochemical studies of Cetuximab that reported reduced inhibition of EGF-induced cell proliferation when adding monovalent Fab fragments as compared to the intact bivalent antibody. Moreover, the dissociation rate of the intact murine version of Cetuximab (m225) was five times higher than for its Fab fragment as shown by Fan *et al.* [239]. Nevertheless, further mutagenesis of the Cetuximab-based Fab would have been required to generate a fully reversible Fab without any obvious advantages over the EGFR Fab mut72, which unfortunately was out of the scope of this thesis work. Therefore, the reversible EGFR Fab mut72 was further tested in magnetic selections.

### 5.3 Selection of EGFR<sup>+</sup> T cells works with small magnetic beads

Enrichment of gene-modified cells can be accomplished in multiple ways: antibiotic resistance genes, e.g. *neo*, can be introduced into cells that are then selected in cell cultures, containing high doses of antibiotics that are toxic to unmodified cells [240]. Alternatively, CAR-modified T cells can be enriched by stimulating them with target cells to promote selective expansion [125]. Both methods are time-consuming and therefore not compliant with the aim to accelerate clinical cell processing, minimize culture-dependent effects on the cell product and reduce the costs of cell therapies [178]. Therefore, cell surface markers are frequently integrated into viral vectors for transducing cells to efficiently purify them by straight-forward magnetic selection protocols. Magnetic enrichment of EGFR<sup>+</sup> T cells was successfully established using the EGFR Fab and *Strep*-Tactin nanobeads (Fig. 4-21). Increased amounts of magnetic nanobeads resulted in higher yields of the magnetic selections because EGFR<sup>+</sup> cells were loaded with more magnetic particles, which permitted more efficient retention of labeled cells in the magnetic field. As the reversible EGFR Fab could stably bind to EGFR<sup>+</sup> cells at 4°C, staining the cells with Fab monomers first and adding the magnetic beads in a second incubation step potentially enhanced the number of beads per cell. This strategy of magnetic labeling of EGFR<sup>+</sup> cells resulted in slightly higher yields of magnetic selections as compared to using a pre-formed multimeric complex of Fab monomers and nanobeads (data not shown). Importantly, magnetic selections of EGFR<sup>+</sup> T cells based on the new reversible EGFR Fab and nanobeads were at least as efficient as selections based on the biotinylated EGFR mAb and streptavidin-nanobeads that have been described before (Fig. 4-22) [195]. The experimental protocol of magnetic selection can be transferred to the clinically approved Miltenyi platform that allows for clinical-grade cell purification on the CliniMACS®.

Reversible reagents could also be used in combination with larger beads, as complete removal of the beads can be guaranteed before adoptive transfer of purified cells. Although microbead-based selections have been successfully established for multiple phenotypic markers [178], EGFR<sup>+</sup> T cells could not be efficiently enriched using microbeads or AK12 beads under all tested conditions (Fig. 4-24). While purities above 90% could be reached, yields of microbead-based EGFR<sup>+</sup> cell enrichments have never exceeded 0.5% and most of the EGFR<sup>+</sup> T cells were lost during the washing on the magnet (Fig. 4-26). This led to the hypothesis that magnetically labeled EGFR<sup>+</sup> T cells

could not be effectively retained by the magnetic field of the permanent magnet during washing. We could not recover any magnetically labeled EGFRt<sup>+</sup> cells from the wash fraction. Therefore, it was highly probable that cells had lost their 'label', because pre-formed complexes of EGFR Fab and magnetic microbeads had not stably bound to the cells.

### 5.3.1 Magnetic selections might depend on the number of target molecules

The efficiency of selecting EGFRt<sup>+</sup> T cells with the EGFR Fab and microbeads was very low. As EGFRt<sup>+</sup> cells were also CD4<sup>+</sup> in our experimental setting, we could show that the same target cell population could be enriched using a CD4 Fab with much higher yields of around 10% (Fig. 4-26). We do not expect any major differences in complex formation that involve microbeads and EGFR Fab monomers instead of CD4 Fab monomers. Stable binding of complexes to the cell surface might depend on the affinity of selection reagents. We tested a panel of EGFR-specific Fab monomers in microbead-based selections and preliminary data showed that yields could not be improved with reagents of higher affinity (e.g. A13 Fab wt or Cetuximab Fab) as compared to the reversible A13 Fab mut72 of lower affinity (data not shown). Robust binding of larger beads to the cell requires multiple binding events per bead that can only be established if a minimum number of target molecules are located in close proximity on the cell membrane. In a quantification assay, the number of EGFRt molecules per T cells was found to be relatively low as compared to the number of wildtype EGFR-overexpressing BT-20 cell line (mean of approximately 19,000 vs. approximately 170,000 molecules / cell, Fig. 4-28). According to several reports, the number of CD4 antibody binding sites ranges between 40,000 and 65,000 for lymphocytes which might correspond to double numbers of CD4 molecules as the CD4 clone used for staining was shown to bind bivalently [218, 241]. These estimate numbers of CD4 molecules would indeed be substantially higher than the number of EGFRt molecules per cell. Remarkably, setting gates on T cells with high or low expression level of the EGFRt showed that EGFR-high cells were preferentially selected with microbeads with a 6-27 times higher yield as compared to the EGFR-low cells in three independent experiments (Fig. 4-27). Thus, we observed a correlation between the density of EGFRt molecules and the outcome of magnetic selections with

larger beads. Studies of the CD20 marker have also reported that an appropriate expression level is important for the utility of a selection marker [242].

Therefore, magnetic selections might be improved if more EGFRt molecules per cell were expressed after introducing the EGFRt gene construct into T cells by viral transduction. One strategy might be to increase the multiplicity of infection (MOI) to integrate more viral copies per cell. However, higher MOIs were not correlated neither with better transduction efficiencies nor with higher MFIs of the CAR staining as a readout for transgene expression [217]. In fact, clinically used cell products should contain less than five viral copies/cell to limit the risk of insertional mutagenesis, so it is not recommended to use the virus at higher MOIs [217].

Another approach is based on improving the protein translation by optimizing the genetic sequence such that it only contains codons that are most frequently used in human cells [94]. Codon optimization of the CD20 gene sequence resulted in higher expression of the CD20 marker on the T cell surface [243]. Moreover, Vogler *et al.* showed that an optimized CD20 gene construct also led to higher purities ( $94.2 \pm 2.5\%$ ,  $n=3$ ) and yields ( $11.3 \pm 6.2\%$ ) in magnetic selections of CD20op<sup>+</sup> T cells using nanobeads [193]. In comparison, we achieved similar purities ( $92.9 \pm 3.0$ ,  $n=2$ ) and higher yields ( $17.7 \pm 7.6$ ) when selecting T cells that had been modified with a non-optimized EGFRt<sup>+</sup> using 75 $\mu$ L nanobeads per  $1 \times 10^7$  cells as recommended in the manual that was also followed by Vogler *et al.* Nevertheless, further studies are ongoing to examine the effects of codon-optimization on the EGFRt expression level, which could potentially improve the outcome of magnetic purification, especially when using microbeads.

## 5.4 The EGFRt can be targeted by Cetuximab

Another very important feature of the EGFRt is to allow cell-specific elimination of transferred T cells in case of adverse effects of T cell therapy. Based on *in vitro* and *in vivo* data, potential limitations of the EGFRt-based depletion approach are discussed and thoughts on how to improve the EGFRt and/or the depleting reagent are presented.

### 5.4.1 Cetuximab is a suitable reagent for T cell depletion

Among EGFR-targeting drugs, therapeutic antibodies are the only agents that can engage and re-direct immune effector mechanisms, such as ADCC and complement-dependent cytotoxicity (CDC), towards EGFRt-expressing T cells [190]. The therapeutic efficacy of EGFR-specific antibodies indeed has been attributed to ADCC and also inhibition of EGFR signaling and receptor downregulation [244]. Cetuximab and Panitumumab are the most widely used anti-EGFR mAbs in the clinic [206]. As an IgG2, Panitumumab is probably not interacting with immune effector cells leading to ADCC due to the low affinity of IgG2 isotypes for Fc receptors [212]. In contrast, IgG1 such as Cetuximab has the highest affinity for activating Fc receptors and is the most efficient antibody isotype to trigger ADCC. Therefore, Cetuximab has been suggested to be the most suitable reagent for eliminating EGFRt<sup>+</sup> T cells [195].

Tumor cell killing via Cetuximab has been vigorously studied *in vitro* and in mouse models [202, 203]. Cetuximab binds to an epitope within domain III and directly interferes with binding of the endogenous ligands EGF and TGF- $\beta$  to the wildtype EGFR [200]. In addition, Cetuximab prevents EGFR signaling as was demonstrated by detailed analysis of the crystal structure of the EGFR alone and in a complex with its ligand EGF in comparison to EGFR with bound Cetuximab molecules [245]. This study showed that Cetuximab not only binds to domain III, but also clashes with domain I and thereby prevents the EGFR from adopting its active conformation, also named the untethered conformation, which is required for receptor dimerization. Yet, dimerization of the EGFR precedes the phosphorylation of the intracellular tyrosine kinases of the EGFR, which then induces the signaling pathway [206]. Thus, impaired dimerization via Cetuximab results in inhibited signaling that promotes proliferation of the tumor cells.

Growth of target cells can also be constrained by EGFR internalization, which can also be triggered by Cetuximab [206].

Additionally, Cetuximab can exert Fc-related mechanisms, e.g. by interacting with Fc receptors on immune effector cells that are capable of inducing ADCC [190]. Many studies demonstrated ADCC activity of Cetuximab, e.g. against human lung cancer cell lines [202]. A contribution of ADCC to the anti-tumor activity of Cetuximab was also shown in mice, where inhibition of tumor growth was diminished in the absence of NK effector cells [203]. CDC is another effective killing mechanism that can be initiated by IgG1, but could not be confirmed as a mechanism of Cetuximab [202, 246].

#### 5.4.2 *In vitro* ADCC of EGFR<sup>t</sup> T cells

We wanted to examine whether the ADCC activity of Cetuximab can be re-directed towards EGFR<sup>t</sup> T cells *in vitro*. First, we confirmed that Cetuximab recognizes the truncated form of the EGFR by staining cells expressing EGFR<sup>t</sup> with the biotinylated Cetuximab (e.g. Fig. 4-2).

Based on the correlation between tumor-infiltrating CD56<sup>+</sup> cells and the favorable outcome of Cetuximab treatment, CD56<sup>+</sup> NK cells were proposed to be the major effector cell population of Cetuximab-related ADCC [219]. ADCC-mediating effector cells can be recruited by the interaction of their activating Fc-specific receptors, e.g. FcγRIII (= CD16) on NK cells, with the Fc part of cell-bound IgGs such as Cetuximab [247]. Kurai *et al.* demonstrated ADCC activity of NK cells against EGFR<sup>+</sup> lung cancer cell lines via Cetuximab *in vitro* [248].

Therefore, we performed our *in vitro* cytotoxicity assays with CD16<sup>+</sup> CD56<sup>+</sup> NK cells (Fig. 4-29). NK cells were capable of mediating specific lysis of the NK cell-sensitive K562 or EGFR<sup>+</sup> BT-20 cell lines. EGFR<sup>t</sup>-transduced LCLs were also lysed by NK cells in the presence of Cetuximab, indicating that the EGFR<sup>t</sup> can be targeted for ADCC. Surprisingly, no specific lysis could be demonstrated for EGFR<sup>t</sup> T cells. This observation raised the question whether T cells are generally susceptible to NK cell-mediated lysis. Although much has been learned about the regulatory mechanisms of NK cell function in general, little is known about NK cell killing of T cells as rather unusual target cells [249].

However, antibody-dependent T cell lysis was successfully achieved by targeting other depletion markers, e.g. the CD20 marker or the myc-tag [193, 194]. In more detail, CTL were transduced with a tCD34-2A-CD20 construct and subjected to an *in vitro* ADCC assay, which showed that the CD20-specific IgG1 Rituximab mediated specific lysis of CD20<sup>+</sup> T cells via CD56<sup>+</sup> NK cells [193]. In the other example, *in vitro* lysis of myc-tagged human T cells was achieved by using a murine anti-myc IgG1 and a secondary Fc-specific rabbit anti-mouse IgG1 that induced ADCC via human NK cells [194]. This raised the question whether the anti-myc IgG1 alone did not yield efficient T cell lysis, so that an amplification step via the secondary mAb was required, indicating that it might be difficult to find conditions to show *in vitro* ADCC of T cells. Yet, *in vivo* depletion of myc-tagged T cells did not require the application of a secondary mAb in that study, underlining that the settings for efficient T cell elimination *in vitro* and *in vivo* might differ substantially. Thus, it seemed reasonable to work on an *in vivo* model for T cell depletion despite not yet having shown *in vitro* ADCC of EGFRt<sup>+</sup> T cells.

### 5.4.3 Depletion studies in the OT-I mouse model

To study the use of Cetuximab for *in vivo* depletion of EGFRt<sup>+</sup> T cells in a mouse model, we had to define conditions that allow for efficient transfer of EGFRt<sup>+</sup> T cells, reliable *in vivo* tracking and sensitive analysis of the extent of depletion. To allow for quick engraftment, cells are commonly transferred into lymphopenic Rag1<sup>-/-</sup> mice or sublethally irradiated mice [194]. We decided to irradiate wt C57BL/6 mice before T cell transfer, as it more closely resembles clinical protocols that include pre-conditioning treatments to induce depletion of endogenous lymphocytes that compete with transferred T cells for homeostatic cytokines [80]. However, irradiation globally reduces the number of hematopoietic cells, including NK cells that are the putative main effector cell type for inducing ADCC via Cetuximab [219, 248]. Thus, NK cell frequencies were monitored to show that NK cells are detectable at the time point of Cetuximab infusion, which was usually around two weeks after irradiation (Fig. 4-30).

To further develop the experimental model, we introduced the GFP as a second reporter in the EGFRt retroviral construct, and transduced mouse splenocytes to enable tracking of the EGFRt<sup>+</sup> cells by GFP. This helped to overcome the issue of EGFRt<sup>+</sup> cells being masked by cell-bound Cetuximab and therefore no longer accessible to *ex vivo* EGFR staining reagents (Fig. 4-32). In addition to monitoring the

GFP<sup>+</sup> cells, T cell depletion could also be evaluated by alternative tracking methods (such as qPCR) or other *in vivo* readouts (such as T cell-mediated effects on target organs) [194].

Using OT-I cells for genetic engineering with the GFP/EGFRt construct enabled us to visualize even very small numbers of cells that survived the Cetuximab-mediated depletion by expanding residual OT-I cells *in vivo* upon challenge with MVA-OVA [25]. Both EGFRt<sup>+</sup> and untransduced OT-I cell populations responded to the MVA-OVA challenge. Thus, it might be possible that the untransduced cells – being the larger population after depletion of EGFRt<sup>+</sup> cells – outcompeted the few remaining EGFRt<sup>+</sup> cells during the *in vivo* expansion in response to MVA-OVA (Fig. 4-31). To overcome this issue, GFP/EGFRt<sup>+</sup> cells were sorted before transfer and expanded *in vivo* before administration of Cetuximab. Under these optimized conditions, we could demonstrate that Cetuximab-mediated depletion of GFP/EGFRt<sup>+</sup> OT-I cells was not complete and might depend on the expression level of the EGFRt (Fig. 4-34, Fig. 4-36).

This interpretation was supported by depletion studies, where GFP/EGFRt<sup>+</sup> OT-I cells were sorted for high or low expression of the transgene and transferred into separate mouse groups. EGFRt-high cells were completely eliminated, whereas EGFRt-low cells were only depleted to some extent after two infusions of Cetuximab (Fig. 4-37). Interestingly, we observed a continuous decrease in the numbers of EGFRt-low cells over several weeks after Cetuximab infusions. As Cetuximab persisted in the circulation of mice for at least seven weeks after infusion (data not shown), an on-going depletion of residual EGFRt<sup>+</sup> cells is possible. However, the numbers of mock-transduced OT-I cells also dropped during that time period in control mice that had not received Cetuximab (Fig. 4-37C). Thus, it is difficult to draw conclusions on the long-term kinetics of T cell depletion from these experiments.

Preclinical evaluation of therapeutic mAbs in mouse models need to be interpreted carefully, as chimeric or humanized mAbs are less adapted to interact with the mouse immune system [250]. Cetuximab is a chimeric IgG1 but there are still many studies on Cetuximab-mediated ADCC in mouse models [203, 251]. This already allows the conclusion that generally murine NK cells can mount ADCC in response to Cetuximab to a relevant extent [203]. Moreover, it was shown *in vitro* that human IgG1 – exemplified by an anti-EGFR and an anti-CD20 mAb – can be recognized by all murine Fcγ receptors [252].

The *in vivo* depletion studies in the OT-I mouse model conclusively demonstrate a correlation between EGFRt expression level and efficiency of the elimination via Cetuximab. Derer *et al.* found a similar correlation *in vitro*; Cetuximab-mediated cytotoxicity depended on the level of wildtype EGFR expression in a systematic study on wt EGFR-transfected BHK-21 cells [228]. Neither NK cell nor monocyte-mediated ADCC was observed when targeting BHK-21 cells that expressed only 30,000 EGFR molecules/cell. In line with this finding, we might not have been able to sensitize EGFRt<sup>+</sup> T cells for *in vitro* ADCC (Fig. 4-29), because only around 20,000 EGFRt molecules were detected on T cells using the same quantification method (Fig. 4-28). The antigen density plays an important role in ADCC, because it is known that the Fc receptors on NK cells have to be crosslinked by the cell-bound IgGs to induce FcR signaling and activation of NK cells [253]. Intuitively, the number of IgG molecules that can be deposited on the cell surface, has to correlate with the number of target molecules and their capacity to oligomerize.

Ways of increasing EGFRt expression (e.g. by codon optimization) have already been discussed in section 5.3.1. In the following, the focus is laid on dissecting the characteristics of the EGFRt and Cetuximab with regard to limited ADCC and on exploring ideas how to modulate these components to enhance the efficacy of the EGFRt-based depletion mechanism.

#### 5.4.4 Opportunities to enhance the EGFRt-based depletion strategy

The correlation between ADCC and the number of EGFR molecules does not usually restrict the application of Cetuximab to EGFR-overexpressing tumor types. The main mechanism of action of Cetuximab is actually inhibition of ligand binding, which is even more effective if tumor cells express low amounts of EGFR, as fewer mAb molecules are needed to occupy all EGFR molecules [228, 239].

Similarly to the EGFRt-based approach, CD20 was also examined regarding its properties as a cell-specific depletion marker and the CD20-specific mAb Rituximab mediated effective lysis of CD20<sup>+</sup> T cells *in vitro* and *in vivo* [192, 193]. Thus, identifying the major differences between the two depletion markers might direct the strategy how to further enhance the functionality of the EGFRt as a cell depletion approach. In line with the notion that Fc receptors need to be oligomerized, CD20 molecules were found to associate with lipid rafts upon binding to antibodies [254, 255]. Lipid rafts are

cholesterol and sphingolipid-rich patches in the cell membrane that mediate local accumulation of specific membrane-associated proteins and thereby play an important role for a number of receptor complexes, including Fc-specific receptors [256].

So, what can be assumed with respect to the capability of the EGFRt to cluster? First, the behavior of the EGFRt might be affected by its truncations, especially of domain II, as it contributes to the formation of EGFR dimers through its dimerization arm [245]. Therefore, the EGFRt presumably cannot establish interlinked dimers. The structurally highly constrained EGFRt might still be capable of associating with lipid rafts as the targeting information was allocated to a juxtamembrane region in the extracellular domain of the wildtype EGFR (aa 581-641) [257], which is preserved in the EGFRt (aa 310-644). Assumptions about the allocation of the EGFRt to lipid rafts are hypothetical, but might trigger potentially interesting approaches to improve the EGFRt-based cell depletion mechanism, for example by exchanging its transmembrane domain for a Glycophosphatidylinositol (GPI)-anchor, as GPI-linked proteins are described to be concentrated in lipid rafts [258].

Second, dimerization of the EGFRt could also be impaired by Cetuximab, as shown for the wildtype EGFR [245]. However, this does not necessarily exclude the possibility that target molecules can assemble in higher-ordered clusters. As an example, binding of an EGFR-targeting mAb can induce clustering of EGFR molecules in form of tetramers or oligomers, while reducing the presence of EGFR dimers [259].

Beside ADCC, complement-dependent cytotoxicity (CDC) is another potent effector mechanism that might be adopted for depletion of T cells. In fact, Rituximab is capable of inducing CDC of CD20<sup>+</sup> T cells [193, 260]. As CDC could not be shown for Cetuximab alone [202], it would be interesting to explore strategies that allow for CDC of EGFRt<sup>+</sup> cells. For example, enhanced CDC of human tumor cell lines was achieved by using a combination of two EGFR-specific mAbs with non-overlapping epitopes, Cetuximab and Matuzumab [261]. Matuzumab is a humanized IgG1 that binds an epitope in domain III. Its binding capacity is not affected in the presence of Cetuximab molecules, indicating that these two antibodies recognize distinct epitopes [229, 262]. It is currently tested in Phase II clinical trials [262]. Incubation of EGFR-expressing target cells with both Cetuximab and Matuzumab should allow for loading more antibodies onto the target cell surface, resulting in increased deposition of C1q, C3 and C4 complement factors, which then overcomes complement regulatory proteins CD46, CD55 and CD59 [261]. Based on this potential mechanism, increased CDC could be

achieved by combining two anti-EGFR mAbs, and ultimately, the depletion of target cells should be more efficient. Following this line of thought, we are currently investigating if depletion of EGFRt<sup>+</sup> T cells can be enhanced by infusing Matuzumab into mice, also after the transferred EGFRt<sup>+</sup> T cells have been partially depleted by Cetuximab infusions.

As another strategy, Cetuximab itself could be modified, e.g. by protein- and/or glyco-engineering to enhance ADCC. To improve the interaction between the effector cells and the mAb, the affinity of its Fc domain to the FcγRIII could be increased by substituting amino acids in the hinge or CH<sub>2</sub>-domain or by reducing the amount of fucose in the carbohydrates attached to the Fc portion of the mAb [251, 263].

There are many strategies that might potentially improve the EGFRt-based depletion mechanism, but nevertheless, it is important to test the efficiency of T cell depletion via Cetuximab only. As Cetuximab is already clinically approved, it would be feasible to immediately implement this depletion strategy in clinical protocols. Therefore, the most important goal of this project was to show whether Cetuximab-mediated depletion of EGFRt<sup>+</sup> T cells is sufficient to abrogate T cell-induced toxicities in clinically relevant mouse models.

## 5.5 T cell depletion in clinically relevant mouse models

### 5.5.1 T cell depletion prevents liver toxicity in HBV-tg mice

Suitable mouse models had to be found in which the adoptive transfer of functional T cells induces toxicity. For example, the HBV-tg mouse model offers the opportunity to study how HBV-specific T cells recognize and destroy hepatocytes that continuously express HBV antigens on their cell surface [264]. Destruction of hepatocytes results in release of liver enzymes e.g. alanine aminotransferase (ALT) into the blood, and measuring the serum levels of ALT can easily monitor the course of the experiment. In collaboration with the Protzer group at the Institute of Virology in Munich, we could take advantage that the HBV-tg mouse model has been established to study HBV-specific, S-CAR<sup>+</sup> T cells with regard to their capacity to eliminate the HBV<sup>+</sup> hepatocytes [221].

After implementing the EGFRt into the S-CAR retroviral vector, transduced T cells could be targeted by Cetuximab for depletion after transfer into HBV-tg mice. As the elevation of ALT in serum occurs only in a short time window between day 6 and 8 after cell transfer, we decided to infuse Cetuximab or Rituximab as a control mAb on day 4. While an ALT increase to 100-400 U/L was observed in 5 out of 8 mice that had received the control mAb, ALT levels did not increase in the Cetuximab group (Fig. 4-41). CAR-mediated T cell activity was confirmed by a transient 3-4 fold decrease of HBV copy numbers in the liver on day 12. These data demonstrate that Cetuximab treatment prevented liver toxicity, which was due to S-CAR<sup>+</sup> T cell function. Monitoring the depletion effect on the persistence of T cells in the blood was hampered by the lack of a reliable tracking marker. EGFR staining was inhibited by cell-bound Cetuximab as described in the OT-I model, and the CAR-specific staining with an anti-human IgG reagent was limited by downregulation of the CAR (Fig. 4-41B). Further, functional S-CAR<sup>+</sup> T cells are expected to migrate to the target organ [221]. The successful prevention of liver toxicity by Cetuximab-mediated T cell depletion supports our hypothesis that the depletion mechanism is efficient for T cells with high expression of the S-CAR/EGFRt, which is likely to correlate with high functionality [81].

It would be very interesting to follow up these experiments with some modifications: 1) Sorting of S-CAR/EGFRt<sup>+</sup> T cells before transfer would allow for tracking the infused cells in the blood by using the congenic marker. Additionally, cell sorting ensures that a more uniform and functional CAR/EGFRt-high cell population is infused, which is

expected to result in even more robust liver toxicities in HBV-tg mice. If Cetuximab treatment completely averts an increase in ALT levels here, this would provide further evidence that the EGFRt-based depletion is very efficient. 2) Cetuximab could be infused at a later time point (e.g. day 6) to assess whether on-going liver toxicity can be reversed. It is still in question whether the time frame of just a few days, during which liver toxicity can be detected, allows for testing the EGFRt-based system in a 'treatment setting'. The sensitivity of this model is limited, because massive destruction of hepatocytes is probably required to measure differences in ALT levels in the blood. Therefore, it is not clear if ALT levels really reflect the kinetics of T cell-mediated effects.

Despite the pros and cons of the rigid readout in HBV-tg mice, especially the short time of analysis is a limitation of this model. The ALT levels are only transiently elevated in response to S-CAR<sup>+</sup> T cell attack, possibly because the effector T cell population is contracted by immune regulatory mechanisms [265]. Thus, this model does not allow for long-term studies, which might be of high interest, as we observed in the OT-I model that the depletion of EGFRt<sup>+</sup> T cells might be on-going for longer time periods.

### 5.5.2 B cell aplasia can be reversed by eliminating mCD19-CAR T cells

Based on the encouraging results in the HBV-tg mice, we set out to find a mouse model that reflects the potential long-term side effects of transferred T cells. The application of CD19-CAR T cells for treating B cell leukemias has been correlated with long-term B cell aplasia in some patients in several clinical trials [139, 143]. To establish a physiological pre-clinical model, Sadelain and colleagues developed a syngeneic model of B cell leukemia in immunocompetent mice [220]. Upon transfer of anti-mouse CD19 CAR T cells, not only the tumor cell line E $\mu$ -ALL01, derived from a E $\mu$ -myc transgenic mouse [266], but also the endogenous B cells were eradicated in blood, spleen and bone marrow for at least two months [220].

To adopt this mouse model for the purpose of analyzing T cell depletion after Cetuximab infusion, the mouse CD19 CAR was modified to contain a CD28 costimulatory domain and the EGFRt separated from the CAR with a 2A linker (= m1928E). Mouse splenocytes were transduced with the m1928E construct and functionality of the CAR was confirmed in an *in vitro* killing assay (Fig. 4-38). In a small preliminary study, we transferred  $8 \times 10^6$  unsorted T cells that contained about  $2 \times 10^6$

CAR/EGFR<sup>t+</sup> cells into irradiated mice. In control mice that received mock-transduced cells the endogenous CD19<sup>+</sup> B cells decreased in response to irradiation, but recovered within 3-5 weeks (Fig. 4-39). In contrast, recovery of endogenous B cells was prevented in mice that were infused with m1928E<sup>+</sup> T cells for more than three months, indicating that CAR-T cells are functional *in vivo* over a long period of time. Interestingly, infusion of Cetuximab was followed by a slow recovery of B cells to normal levels of 1000-2000 cells/ $\mu$ L blood within six weeks (Fig. 4-40). These data demonstrate that Cetuximab mediated effective depletion of the functional mCD19-specific T cells.

Unfortunately, the CAR/EGFR<sup>t+</sup> T cell population could not be reliably detected in Cetuximab-treated mice due to inhibition of the EGFR staining (Fig. 4-40A). A suitable reagent was not available to stain this CAR construct that is composed of a rat scFv and lacks an IgG-derived spacer. Instead, the extracellular domain of murine CD8 has been used to link the scFv to the transmembrane domain. This linker might be targeted with an anti-murine CD8 mAb. Alternatively, an antibody against rat scFv or the extracellular domain of the murine CD19 protein could be used as a detection reagent.

Further studies will be required to examine the kinetics of depleting T cells that are constantly stimulated *in vivo* by CD19<sup>+</sup> target cells. In our first pilot experiment, B cell recovery was observed to start at very different time points after Cetuximab treatment in the individual mice (week 2 or 5). Results might become more comparable if m1928E<sup>+</sup> T cells will be sorted before transfer, to enhance uniformity of the T cell product and increase the efficiency of T cell depletion. Further, it might be favorable to infuse Cetuximab at a time point when the B cell compartment has been fully reconstituted, e.g. week 5 after irradiation, to segregate the unspecific effect of irradiation on the hematopoietic cells (including B cells) from the B cell-specific activity of CAR T cells. Potentially, the efficiency of depletion might be enhanced at such a later time point, as the NK cell compartment should have fully recovered within 5 weeks after irradiation (Fig. 4-30). Finally, an in-depth analysis of the recovered B cells in Cetuximab-treated mice is planned. B cell function can be assessed by analyzing the *in vivo* B cell response upon antigenic challenge, overall immunoglobulin levels in the blood plasma and the diversity of the B cell receptor repertoire.

Out of curiosity, we also transferred m1928E-transduced cells into non-irradiated mice, but we did not observe an effect on the endogenous B cell population (data not shown). In this setting, the *in vivo* expansion of CD19-specific T cells might not be

sufficient to eliminate the B cells that usually make up a large fraction of approximately 30-50% among all peripheral leukocytes. If mice are irradiated, B cells are drastically reduced to about 1% of peripheral leukocytes, so it might be easier for the m1928E<sup>+</sup> T cells to suppress the B cell recovery. To tip proportions in favor of transferred T cells, we intend to use OT-I cells for transductions with the mCD19-CAR construct in order to expand the cells *in vivo* by vaccination, e.g. using MVA-OVA.

Altogether, we could demonstrate in this small proof-of-concept study that a long-lasting and clinically relevant side effect of CD19-CAR T cell therapy, e.g. B cell aplasia, can be reversed by depleting the CAR/EGFRt<sup>+</sup> cells via Cetuximab. B cell recovery is on-going for several weeks without the application of further Cetuximab doses. In line with our observations in the OT-I model, this indicates that EGFRt-high T cells can be completely eliminated by Cetuximab. However, as Cetuximab can persist in mice for at least 50 days, absence of EGFRt<sup>+</sup> cells has to be confirmed by long-term monitoring of stable B cell counts.

## 5.6 Clinical scenarios for the application of the EGFRt as a depletion marker

Cell-based immunotherapies have gained a lot of interest after several clinical trials demonstrated the clinical benefit of T cells that were genetically engineered to express a tumor-specific receptor, reviewed in Cieri *et al.* [88]. Enhanced efficacy of T cell therapies was mainly attributed to the longevity and multi-potency of the T cell product as well as to enhanced affinity and/or signaling capacity of the transgenic receptor [117]. Enhanced functionality of the T cells is inevitably correlated with a higher risk of therapy-related adverse effects, which reveals the urgent need for effective safety mechanisms. Observed toxicities include on-target and off-target toxicities that can occur unexpectedly in some cases, and side effects can be transient or long-term. Ideally, safety mechanisms should account for the different circumstances of the adverse effects.

### 5.6.1 Long-term toxicities

The showcase for effective cell immunotherapy is the application of CD19-CAR-engineered T cells in B cell malignancies and promising therapeutic outcomes have recently been reported from several research centers [138, 140, 141]. Eradication of the malignant B cells is usually correlated with B cell aplasia [267]. If a fraction of transferred therapeutic T cells persists as memory T cells, both the beneficial and the adverse effects can prevail for a long time [143]. The loss of B cells can be compensated by infusion of immunoglobulins [140]. However, if the cancer patients go into complete remission, it might be favorable to terminate the T cell therapy and allow for reconstitution of the endogenous B cell compartment.

Preliminary results in the mouse model indicate that Cetuximab-mediated depletion of anti-mouse CD19 CAR/EGFRt<sup>+</sup> T cells correlates with recovery of endogenous B cells (Fig. 4-40). Thus, it seems likely that long-term B cell aplasia can be counteracted by introducing the EGFRt depletion marker into therapeutic T cells and eliminating these cells *in vivo* by administering Cetuximab after tumor eradication. The issues whether EGFRt-high T cells are preferentially eliminated in humans, and whether this is sufficient to abrogate T cell-mediated toxicities awaits validation in a clinical setting. The EGFRt has already been integrated as a selection and tracking marker in the CAR

constructs that are currently used in the clinical trial at the FHCRC in patients with B cell malignancies. Administration of Cetuximab is allowed for patients in remission, so the utility of the EGFRt as a cell-specific depletion marker might be tested in humans soon [117]. A remaining concern is that patients could relapse after complete elimination of the CAR T cells, so benefits and risks need to be compared.

In the clinical setting of B cell malignancies, the EGFRt is the better candidate for a depletion marker than CD20, because for the latter T cell depletion is induced by the CD20-specific Rituximab, which would itself mediate B cell aplasia [268]. Using the HSV-TK as a suicide mechanism is also not favorable over the EGFRt, as T cell persistence is limited due to immune responses raised against the immunogenic HSV-TK [159, 188]. Obviously, the suicide and cell-specific depletion markers should not affect the general persistence of gene-modified T cells, but rather allow for elimination of T cells at the time point of choice and in a controlled manner.

### 5.6.2 Acute toxicities

Acute, sometimes serious adverse effects were reported for both transgenic TCR and CAR-modified T cell products. Such toxicities frequently affect solid organs, e.g. the lung or heart. For instance, lung toxicities were caused by HER2-CAR T cells, presumably because low levels of the target antigen HER2 can be found in the lung tissue [147]. In contrast, unexpected toxicities due to cardiac damage were reported for melanoma patients after transfer of T cells that were engineered with an affinity-enhanced MAGE-A3 TCR [157]. In a retrospective analysis, the MAGE-A3 TCR was found to cross-react with the MAGE-unrelated protein titin that is expressed on cardiac myocytes [158]. This unexpected off-target effect led to lethal toxicities within few days, which highlights the need for a rapid and highly efficient cell depletion mechanism. Consequently, it is highly important to address the question, which *in vivo* cell depletion strategy is most suitable to serve as an 'emergency stop' [268].

We demonstrated in the HBV-tg mouse model that liver toxicity can be prevented if Cetuximab is applied to the mice four days before the ALT peak (Fig. 4-41). We can conclude from these data that EGFRt<sup>+</sup> T cells can be lysed via Cetuximab not only in the blood, but also in solid organs, such as the liver. This is important, because T cell-mediated toxicity can have a severe impact on the function of vital organs. In line with this finding, Cetuximab also reduced the persistence of T cells in other organs in the

OT-I model, as shown for spleen, lymph nodes and the lung (Fig. 4-35). In addition, depletion of T cells via the EGFRt marker is relatively fast, i.e. less than four days in the HBV-tg mice. The depletion kinetics was studied in more detail in the OT-I model. One day after the first mAb infusion, the number of GFP<sup>+</sup> cells had already dropped below 20 cells/ $\mu$ L blood in mice that were infused with GFP/EGFRt-high cells, while the CD45.1<sup>+</sup> mock-transduced cells stayed at a number of approximately 300 cells/ $\mu$ L blood in control mice (Fig. 4-37C). If the number of gene-engineered cells was also significantly reduced within one day in humans, unexpected acute toxic effects during clinical trials might be efficiently countervailed by the EGFRt depletion approach.

However, even faster kinetics were reported for the suicide gene iCasp9 that induces apoptosis of the target T cell after it has been bound by a dimerizing agent AP1903 [269]. In a small study with five patients, this safety marker was introduced into allo-depleted donor T cells that were infused into HSCT recipients to enhance anti-viral immunity, but bearing the risk of GVHD [189]. The truncated CD19 molecule was co-expressed with the iCasp9 to assess the depletion efficiency. Tracking of the tCD19<sup>+</sup> T cells in the blood showed that 90% of gene-modified T cells were eliminated within the first 30 minutes after application of the dimerizer. Simultaneously, signs of GVHD in the skin and liver were significantly reduced [189]. Interestingly, Di Stasi *et al.* have also observed a correlation between depletion efficiency and expression level of the transgene that had been shown to be upregulated on activated cells in an earlier study of this group [233]. In this clinical setting, reducing the number of allogeneic T cells by depleting CD19-high cells is sufficient to curtail the signs of GVHD. At the same time, it is favorable to provide long-lasting anti-virus immunity due to the virus-specific cells that were spared during the depletion because of low or no expression of the iCasp9. Implementation of the iCasp9 into clinical protocols is mainly hampered by the limited availability of the dimerizing agent that is not yet clinically approved [117].

Nevertheless, the iCasp9 suicide approach is appealing due to its fast kinetics. Hence, it might be an interesting approach to link the intracellular caspase 9 domain to another receptor-like molecule that contains an extracellular region that can be bound with a chemical or antibody for dimerization. For example, it might be possible to fuse the caspase 9 domain to the C terminus of the EGFRt, because the EGFRt does not contain an intracellular region on its own. Although binding of Cetuximab to the wildtype EGFR prevents dimerization [200], it might still be feasible to induce activation

of the intracellular caspases by bringing two chimeric EGFRt-Casp9 molecules in close proximity via Cetuximab.

### 5.6.3 Systemic adverse effects of T cell therapies

Anti-tumor activity depends on target-induced activation and subsequent excessive expansion of adoptively transferred T cells, which is often accompanied with systemic adverse effects, such as the tumor lysis syndrome and the cytokine release syndrome [267]. The vast, up to 1000-fold *in vivo* expansion of transferred cells can induce an 'overshooting' immune reaction in the patient, associated with the release of high levels of proinflammatory cytokines, such as IL-6 and TNF- $\alpha$  [143]. These side effects can be controlled by broadly inhibiting the immune system with steroids or infusing antibodies, e.g. the IL-6 receptor antibody (tocilizumab), that antagonize the elevated cytokines [140, 143]. The EGFRt-based depletion approach might offer an alternative 'treatment'. By infusing single doses of Cetuximab, T cell numbers could be potentially adjusted to levels that are not harmful to the patient.

Along this line, initial dose finding studies might benefit from the implementation of this depletion marker as well. According to the long-standing opinion in the field, large numbers of gene-modified T cells have to be infused to achieve relevant clinical responses [73]. Yet, potent anti-tumor responses can be elicited by doses of CAR T cells as low as  $1.5 \times 10^5$ /kg that can expand >1000-fold *in vivo* [143]. Strong T cell expansion was also observed after adoptive transfer of lowest doses of CMV-specific T cells [237]. Especially if highly potent cell types are evaluated, it might be helpful to use the EGFRt depletion system to control the actual number of transferred cells, depending on the *in vivo* expansion. On the one hand, cell numbers could be reduced by Cetuximab infusions, whereat it might be interesting to investigate whether there is a correlation between the dose of Cetuximab and the degree of T cell depletion, similarly to the dose-response correlation found in patients with colorectal cancer [207]. On the other hand, T cells could be expanded by vaccination if CMV or EBV-specific T cells had been used to generate CAR-modified T cells with a known endogenous TCR that can then be targeted [145, 151]. As this strategy of *in vivo* expansion is already tested in clinical studies, including the EGFRt might extend the idea of modulating the size of CAR T cell populations after transfer into the patient.

#### 5.6.4 Clinical use of the EGFRt

The safety of the EGFRt-based cell-specific depletion marker needs to be examined in suitable pre-clinical systems before clinical application. In a pilot study in the non-human primate model [270], we did not observe any signs of toxicity during 3 weeks, neither in response to the transfer of EGFRt<sup>+</sup> macaque T cells nor due to Cetuximab infusions (Fig. 4-43). We could not decipher whether absence of EGFRt<sup>+</sup> cells after Cetuximab infusions was caused by Cetuximab-mediated depletion or by an immune response that might have been elicited to the human EGFRt, as indicated by the *in vitro* killing of EGFRt<sup>+</sup> T cells via PBMCs obtained from the macaque on day 16. The EGFRt-specific immune response might have been boosted by Cetuximab binding to EGFRt<sup>+</sup> cells if macrophages had phagocytosed the mAb-labeled EGFRt<sup>+</sup> T cells and then presented the digested protein content of the T cells (including the EGFRt) to effector cells. The issue of immunogenicity could be overcome by generating a rhesus macaque EGFRt and transferring the engineered T cells into the same macaque species. Repeating the study of EGFRt safety and efficacy in the other macaque model would contribute to our understanding of the depletion mechanism and would enable us to confirm the safety of this approach in a large animal over longer time periods.

Yet, the EGFRt is already included in the CD19-CAR construct evaluated in the ongoing clinical study at the FHCRC and no EGFRt-specific issues have been observed so far (personal communication). Similarly, Cetuximab treatment appears to be associated with only minor side effects, such as skin rash, based on the broad clinical experience with Cetuximab in tumor therapies [209, 212]. As soon as the outstanding clinical success with CAR T cells consolidates in further clinical studies, the application of CAR T cells in a larger group of patients in a clinical phase II study is within reach. Due to the increased CAR functionality and the focus on using highly potent cell subsets, it is evident that a cell-intrinsic safety mechanism is required to keep such effective cellular therapies under control.

In this thesis, the EGFRt cell-specific depletion marker was evaluated in different mouse models that proved efficacy of Cetuximab-mediated T cell depletion in clinically relevant settings. Beyond its use as a depletion marker, the EGFRt can also serve as a tracking and selection molecule, and applicability of the EGFRt for these purposes was also validated *in vitro* and *in vivo* during this PhD project. Taken together, the data

strongly indicate that the EGFRt is a valuable tool to enhance safety of gene-engineered T cells for immunotherapy.

## 6 Bibliography

1. Robins HS, Campregher PV, Srivastava SK, Wacher A, Turtle CJ, Kabsai O, et al. Comprehensive assessment of T-cell receptor beta-chain diversity in alphabeta T cells. *Blood*. 2009;114(19):4099-107.
2. Rudolph MG, Stanfield RL, Wilson IA. How TCRs bind MHCs, peptides, and coreceptors. *Annual review of immunology*. 2006;24:419-66.
3. Palmer E. Negative selection--clearing out the bad apples from the T-cell repertoire. *Nature reviews Immunology*. 2003;3(5):383-91.
4. Bromley SK, Thomas SY, Luster AD. Chemokine receptor CCR7 guides T cell exit from peripheral tissues and entry into afferent lymphatics. *Nature immunology*. 2005;6(9):895-901.
5. Fooksman DR, Vardhana S, Vasiliver-Shamis G, Liese J, Blair DA, Waite J, et al. Functional anatomy of T cell activation and synapse formation. *Annual review of immunology*. 2010;28:79-105.
6. Schwartz RH. T cell anergy. *Annual review of immunology*. 2003;21:305-34.
7. Steinman RM, Hawiger D, Nussenzweig MC. Tolerogenic dendritic cells. *Annual review of immunology*. 2003;21:685-711.
8. Lanzavecchia A, Sallusto F. Dynamics of T lymphocyte responses: intermediates, effectors, and memory cells. *Science*. 2000;290(5489):92-7.
9. Schoenberger SP, Toes RE, van der Voort EI, Offringa R, Melief CJ. T-cell help for cytotoxic T lymphocytes is mediated by CD40-CD40L interactions. *Nature*. 1998;393(6684):480-3.
10. Salmond RJ, Filby A, Qureshi I, Caserta S, Zamoyska R. T-cell receptor proximal signaling via the Src-family kinases, Lck and Fyn, influences T-cell activation, differentiation, and tolerance. *Immunological reviews*. 2009;228(1):9-22.
11. Greenwald RJ, Freeman GJ, Sharpe AH. The B7 family revisited. *Annual review of immunology*. 2005;23:515-48.
12. Watts TH. TNF/TNFR family members in costimulation of T cell responses. *Annual review of immunology*. 2005;23:23-68.
13. Curtsinger JM, Schmidt CS, Mondino A, Lins DC, Kedl RM, Jenkins MK, et al. Inflammatory cytokines provide a third signal for activation of naive CD4+ and CD8+ T cells. *Journal of immunology*. 1999;162(6):3256-62.
14. Harty JT, Tvinnereim AR, White DW. CD8+ T cell effector mechanisms in resistance to infection. *Annual review of immunology*. 2000;18:275-308.
15. Mosmann TR, Cherwinski H, Bond MW, Giedlin MA, Coffman RL. Two types of murine helper T cell clone. I. Definition according to profiles of lymphokine activities and secreted proteins. *Journal of immunology*. 1986;136(7):2348-57.
16. Zhu J, Yamane H, Paul WE. Differentiation of effector CD4 T cell populations (\*). *Annual review of immunology*. 2010;28:445-89.
17. Sallusto F, Lanzavecchia A, Mackay CR. Chemokines and chemokine receptors in T-cell priming and Th1/Th2-mediated responses. *Immunology today*. 1998;19(12):568-74.
18. Park H, Li Z, Yang XO, Chang SH, Nurieva R, Wang YH, et al. A distinct lineage of CD4 T cells regulates tissue inflammation by producing interleukin 17. *Nature immunology*. 2005;6(11):1133-41.
19. Sakaguchi S. Naturally arising CD4+ regulatory t cells for immunologic self-tolerance and negative control of immune responses. *Annual review of immunology*. 2004;22:531-62.
20. Arens R, Schoenberger SP. Plasticity in programming of effector and memory CD8 T-cell formation. *Immunological reviews*. 2010;235(1):190-205.
21. Wong P, Pamer EG. CD8 T cell responses to infectious pathogens. *Annual review of immunology*. 2003;21:29-70.
22. Butz E, Bevan MJ. Dynamics of the CD8+ T cell response during acute LCMV infection. *Advances in experimental medicine and biology*. 1998;452:111-22.

23. Sallusto F, Lenig D, Forster R, Lipp M, Lanzavecchia A. Two subsets of memory T lymphocytes with distinct homing potentials and effector functions. *Nature*. 1999;401(6754):708-12.
24. Mueller SN, Gebhardt T, Carbone FR, Heath WR. Memory T cell subsets, migration patterns, and tissue residence. *Annual review of immunology*. 2013;31:137-61.
25. Buchholz VR, Flossdorf M, Hensel I, Kretschmer L, Weissbrich B, Graf P, et al. Disparate individual fates compose robust CD8+ T cell immunity. *Science*. 2013;340(6132):630-5.
26. Gerlach C, Rohr JC, Perie L, van Rooij N, van Heijst JW, Velds A, et al. Heterogeneous differentiation patterns of individual CD8+ T cells. *Science*. 2013;340(6132):635-9.
27. Wherry EJ. T cell exhaustion. *Nature immunology*. 2011;12(6):492-9.
28. Barber DL, Wherry EJ, Masopust D, Zhu B, Allison JP, Sharpe AH, et al. Restoring function in exhausted CD8 T cells during chronic viral infection. *Nature*. 2006;439(7077):682-7.
29. Hanahan D, Weinberg RA. The hallmarks of cancer. *Cell*. 2000;100(1):57-70.
30. Smyth MJ, Thia KY, Street SE, MacGregor D, Godfrey DI, Trapani JA. Perforin-mediated cytotoxicity is critical for surveillance of spontaneous lymphoma. *The Journal of experimental medicine*. 2000;192(5):755-60.
31. Galon J, Costes A, Sanchez-Cabo F, Kirilovsky A, Mlecnik B, Lagorce-Pages C, et al. Type, density, and location of immune cells within human colorectal tumors predict clinical outcome. *Science*. 2006;313(5795):1960-4.
32. Willimsky G, Blankenstein T. The adaptive immune response to sporadic cancer. *Immunological reviews*. 2007;220:102-12.
33. Dunn GP, Bruce AT, Ikeda H, Old LJ, Schreiber RD. Cancer immunoediting: from immunosurveillance to tumor escape. *Nature immunology*. 2002;3(11):991-8.
34. Vesely MD, Kershaw MH, Schreiber RD, Smyth MJ. Natural innate and adaptive immunity to cancer. *Annual review of immunology*. 2011;29:235-71.
35. Coussens LM, Werb Z. Inflammation and cancer. *Nature*. 2002;420(6917):860-7.
36. Shankaran V, Ikeda H, Bruce AT, White JM, Swanson PE, Old LJ, et al. IFN $\gamma$  and lymphocytes prevent primary tumour development and shape tumour immunogenicity. *Nature*. 2001;410(6832):1107-11.
37. Boshoff C, Weiss R. AIDS-related malignancies. *Nature reviews Cancer*. 2002;2(5):373-82.
38. Chaturvedi AK, Pfeiffer RM, Chang L, Goedert JJ, Biggar RJ, Engels EA. Elevated risk of lung cancer among people with AIDS. *Aids*. 2007;21(2):207-13.
39. Ferradini L, Mackensen A, Genevee C, Bosq J, Duvillard P, Avril MF, et al. Analysis of T cell receptor variability in tumor-infiltrating lymphocytes from a human regressive melanoma. Evidence for in situ T cell clonal expansion. *The Journal of clinical investigation*. 1993;91(3):1183-90.
40. Aguirre-Ghiso JA. Models, mechanisms and clinical evidence for cancer dormancy. *Nature reviews Cancer*. 2007;7(11):834-46.
41. Koebel CM, Vermi W, Swann JB, Zerafa N, Rodig SJ, Old LJ, et al. Adaptive immunity maintains occult cancer in an equilibrium state. *Nature*. 2007;450(7171):903-7.
42. Dunn GP, Old LJ, Schreiber RD. The three Es of cancer immunoediting. *Annual review of immunology*. 2004;22:329-60.
43. Khong HT, Restifo NP. Natural selection of tumor variants in the generation of "tumor escape" phenotypes. *Nature immunology*. 2002;3(11):999-1005.
44. Gajewski TF, Meng Y, Blank C, Brown I, Kacha A, Kline J, et al. Immune resistance orchestrated by the tumor microenvironment. *Immunological reviews*. 2006;213:131-45.
45. Zamarron BF, Chen W. Dual roles of immune cells and their factors in cancer development and progression. *International journal of biological sciences*. 2011;7(5):651-8.
46. Crespo J, Sun H, Welling TH, Tian Z, Zou W. T cell anergy, exhaustion, senescence, and stemness in the tumor microenvironment. *Current opinion in immunology*. 2013;25(2):214-21.
47. van Houdt IS, Sluijter BJ, Moesbergen LM, Vos WM, de Gruijl TD, Molenkamp BG, et al. Favorable outcome in clinically stage II melanoma patients is associated with the presence of

- activated tumor infiltrating T-lymphocytes and preserved MHC class I antigen expression. *International journal of cancer Journal international du cancer*. 2008;123(3):609-15.
48. Sato E, Olson SH, Ahn J, Bundy B, Nishikawa H, Qian F, et al. Intraepithelial CD8+ tumor-infiltrating lymphocytes and a high CD8+/regulatory T cell ratio are associated with favorable prognosis in ovarian cancer. *Proceedings of the National Academy of Sciences of the United States of America*. 2005;102(51):18538-43.
49. Whelan M, Whelan J, Russell N, Dalglish A. Cancer immunotherapy: an embarrassment of riches? *Drug discovery today*. 2003;8(6):253-8.
50. Brahmer JR, Tykodi SS, Chow LQ, Hwu WJ, Topalian SL, Hwu P, et al. Safety and activity of anti-PD-L1 antibody in patients with advanced cancer. *The New England journal of medicine*. 2012;366(26):2455-65.
51. Hodi FS, O'Day SJ, McDermott DF, Weber RW, Sosman JA, Haanen JB, et al. Improved survival with ipilimumab in patients with metastatic melanoma. *The New England journal of medicine*. 2010;363(8):711-23.
52. Bollard CM, Rossig C, Calonge MJ, Huls MH, Wagner HJ, Massague J, et al. Adapting a transforming growth factor beta-related tumor protection strategy to enhance antitumor immunity. *Blood*. 2002;99(9):3179-87.
53. Kershaw MH, Teng MW, Smyth MJ, Darcy PK. Supernatural T cells: genetic modification of T cells for cancer therapy. *Nature reviews Immunology*. 2005;5(12):928-40.
54. Horowitz MM, Gale RP, Sondel PM, Goldman JM, Kersey J, Kolb HJ, et al. Graft-versus-leukemia reactions after bone marrow transplantation. *Blood*. 1990;75(3):555-62.
55. Goldman JM, Gale RP, Horowitz MM, Biggs JC, Champlin RE, Gluckman E, et al. Bone marrow transplantation for chronic myelogenous leukemia in chronic phase. Increased risk for relapse associated with T-cell depletion. *Annals of internal medicine*. 1988;108(6):806-14.
56. Kolb HJ, Schattenberg A, Goldman JM, Hertenstein B, Jacobsen N, Arcese W, et al. Graft-versus-leukemia effect of donor lymphocyte transfusions in marrow grafted patients. *Blood*. 1995;86(5):2041-50.
57. Bleakley M, Riddell SR. Molecules and mechanisms of the graft-versus-leukaemia effect. *Nature reviews Cancer*. 2004;4(5):371-80.
58. Warren EH, Fujii N, Akatsuka Y, Chaney CN, Mito JK, Loeb KR, et al. Therapy of relapsed leukemia after allogeneic hematopoietic cell transplantation with T cells specific for minor histocompatibility antigens. *Blood*. 2010;115(19):3869-78.
59. Walter EA, Greenberg PD, Gilbert MJ, Finch RJ, Watanabe KS, Thomas ED, et al. Reconstitution of cellular immunity against cytomegalovirus in recipients of allogeneic bone marrow by transfer of T-cell clones from the donor. *The New England journal of medicine*. 1995;333(16):1038-44.
60. Einsele H, Roosnek E, Rufer N, Sinzger C, Riegler S, Loffler J, et al. Infusion of cytomegalovirus (CMV)-specific T cells for the treatment of CMV infection not responding to antiviral chemotherapy. *Blood*. 2002;99(11):3916-22.
61. Ho M. Epidemiology of cytomegalovirus infections. *Reviews of infectious diseases*. 1990;12 Suppl 7:S701-10.
62. Becker C, Pohla H, Frankenberger B, Schuler T, Assenmacher M, Schendel DJ, et al. Adoptive tumor therapy with T lymphocytes enriched through an IFN-gamma capture assay. *Nature medicine*. 2001;7(10):1159-62.
63. Knabel M, Franz TJ, Schiemann M, Wulf A, Villmow B, Schmidt B, et al. Reversible MHC multimer staining for functional isolation of T-cell populations and effective adoptive transfer. *Nature medicine*. 2002;8(6):631-7.
64. Riddell SR, Watanabe KS, Goodrich JM, Li CR, Agha ME, Greenberg PD. Restoration of viral immunity in immunodeficient humans by the adoptive transfer of T cell clones. *Science*. 1992;257(5067):238-41.
65. Cobbold M, Khan N, Pourgheysari B, Tauro S, McDonald D, Osman H, et al. Adoptive transfer of cytomegalovirus-specific CTL to stem cell transplant patients after selection by HLA-peptide tetramers. *The Journal of experimental medicine*. 2005;202(3):379-86.
66. Gerdemann U, Keirnan JM, Katari UL, Yanagisawa R, Christin AS, Huye LE, et al. Rapidly generated multivirus-specific cytotoxic T lymphocytes for the prophylaxis and treatment

- of viral infections. *Molecular therapy : the journal of the American Society of Gene Therapy*. 2012;20(8):1622-32.
67. Uttenthal BJ, Chua I, Morris EC, Stauss HJ. Challenges in T cell receptor gene therapy. *The journal of gene medicine*. 2012;14(6):386-99.
68. Cobbold M, De La Pena H, Norris A, Polefrone JM, Qian J, English AM, et al. MHC class I-associated phosphopeptides are the targets of memory-like immunity in leukemia. *Science translational medicine*. 2013;5(203):203ra125.
69. Dudley ME, Wunderlich J, Nishimura MI, Yu D, Yang JC, Topalian SL, et al. Adoptive transfer of cloned melanoma-reactive T lymphocytes for the treatment of patients with metastatic melanoma. *Journal of immunotherapy*. 2001;24(4):363-73.
70. Rosenberg SA, Aebbersold P, Cornetta K, Kasid A, Morgan RA, Moen R, et al. Gene transfer into humans--immunotherapy of patients with advanced melanoma, using tumor-infiltrating lymphocytes modified by retroviral gene transduction. *The New England journal of medicine*. 1990;323(9):570-8.
71. Yee C, Thompson JA, Byrd D, Riddell SR, Roche P, Celis E, et al. Adoptive T cell therapy using antigen-specific CD8+ T cell clones for the treatment of patients with metastatic melanoma: in vivo persistence, migration, and antitumor effect of transferred T cells. *Proceedings of the National Academy of Sciences of the United States of America*. 2002;99(25):16168-73.
72. Goff SL, Smith FO, Klapper JA, Sherry R, Wunderlich JR, Steinberg SM, et al. Tumor infiltrating lymphocyte therapy for metastatic melanoma: analysis of tumors resected for TIL. *Journal of immunotherapy*. 2010;33(8):840-7.
73. Robbins PF, Dudley ME, Wunderlich J, El-Gamil M, Li YF, Zhou J, et al. Cutting edge: persistence of transferred lymphocyte clonotypes correlates with cancer regression in patients receiving cell transfer therapy. *Journal of immunology*. 2004;173(12):7125-30.
74. Perro M, Tsang J, Xue SA, Escors D, Cesco-Gaspere M, Pospori C, et al. Generation of multi-functional antigen-specific human T-cells by lentiviral TCR gene transfer. *Gene therapy*. 2010;17(6):721-32.
75. Klebanoff CA, Gattinoni L, Palmer DC, Muranski P, Ji Y, Hinrichs CS, et al. Determinants of successful CD8+ T-cell adoptive immunotherapy for large established tumors in mice. *Clinical cancer research : an official journal of the American Association for Cancer Research*. 2011;17(16):5343-52.
76. Hinrichs CS, Spolski R, Paulos CM, Gattinoni L, Kerstann KW, Palmer DC, et al. IL-2 and IL-21 confer opposing differentiation programs to CD8+ T cells for adoptive immunotherapy. *Blood*. 2008;111(11):5326-33.
77. Dudley ME, Wunderlich JR, Robbins PF, Yang JC, Hwu P, Schwartzentruber DJ, et al. Cancer regression and autoimmunity in patients after clonal repopulation with antitumor lymphocytes. *Science*. 2002;298(5594):850-4.
78. Dudley ME, Yang JC, Sherry R, Hughes MS, Royal R, Kammula U, et al. Adoptive cell therapy for patients with metastatic melanoma: evaluation of intensive myeloablative chemoradiation preparative regimens. *Journal of clinical oncology : official journal of the American Society of Clinical Oncology*. 2008;26(32):5233-9.
79. Gattinoni L, Finkelstein SE, Klebanoff CA, Antony PA, Palmer DC, Spiess PJ, et al. Removal of homeostatic cytokine sinks by lymphodepletion enhances the efficacy of adoptively transferred tumor-specific CD8+ T cells. *The Journal of experimental medicine*. 2005;202(7):907-12.
80. Rosenberg SA, Dudley ME. Cancer regression in patients with metastatic melanoma after the transfer of autologous antitumor lymphocytes. *Proceedings of the National Academy of Sciences of the United States of America*. 2004;101 Suppl 2:14639-45.
81. Schmitt TM, Ragnarsson GB, Greenberg PD. T cell receptor gene therapy for cancer. *Human gene therapy*. 2009;20(11):1240-8.
82. Chapuis AG, Ragnarsson GB, Nguyen HN, Chaney CN, Pufnock JS, Schmitt TM, et al. Transferred WT1-reactive CD8+ T cells can mediate antileukemic activity and persist in post-transplant patients. *Science translational medicine*. 2013;5(174):174ra27.

83. Dudley ME, Wunderlich JR, Shelton TE, Even J, Rosenberg SA. Generation of tumor-infiltrating lymphocyte cultures for use in adoptive transfer therapy for melanoma patients. *Journal of immunotherapy*. 2003;26(4):332-42.
84. June CH. Adoptive T cell therapy for cancer in the clinic. *The Journal of clinical investigation*. 2007;117(6):1466-76.
85. Dembic Z, Haas W, Weiss S, McCubrey J, Kiefer H, von Boehmer H, et al. Transfer of specificity by murine alpha and beta T-cell receptor genes. *Nature*. 1986;320(6059):232-8.
86. Clay TM, Custer MC, Sachs J, Hwu P, Rosenberg SA, Nishimura MI. Efficient transfer of a tumor antigen-reactive TCR to human peripheral blood lymphocytes confers anti-tumor reactivity. *Journal of immunology*. 1999;163(1):507-13.
87. Dossinger G, Bunse M, Bet J, Albrecht J, Paszkiewicz PJ, Weissbrich B, et al. MHC multimer-guided and cell culture-independent isolation of functional T cell receptors from single cells facilitates TCR identification for immunotherapy. *PloS one*. 2013;8(4):e61384.
88. Cieri N, Mastaglio S, Oliveira G, Casucci M, Bondanza A, Bonini C. Adoptive immunotherapy with genetically modified lymphocytes in allogeneic stem cell transplantation. *Immunological reviews*. 2014;257(1):165-80.
89. Cheever MA, Allison JP, Ferris AS, Finn OJ, Hastings BM, Hecht TT, et al. The prioritization of cancer antigens: a national cancer institute pilot project for the acceleration of translational research. *Clinical cancer research : an official journal of the American Association for Cancer Research*. 2009;15(17):5323-37.
90. Minami Y, Weissman AM, Samelson LE, Klausner RD. Building a multichain receptor: synthesis, degradation, and assembly of the T-cell antigen receptor. *Proceedings of the National Academy of Sciences of the United States of America*. 1987;84(9):2688-92.
91. Cooper LJ, Topp MS, Pinzon C, Plavec I, Jensen MC, Riddell SR, et al. Enhanced transgene expression in quiescent and activated human CD8+ T cells. *Human gene therapy*. 2004;15(7):648-58.
92. Jones S, Peng PD, Yang S, Hsu C, Cohen CJ, Zhao Y, et al. Lentiviral vector design for optimal T cell receptor gene expression in the transduction of peripheral blood lymphocytes and tumor-infiltrating lymphocytes. *Human gene therapy*. 2009;20(6):630-40.
93. Zufferey R, Donello JE, Trono D, Hope TJ. Woodchuck hepatitis virus posttranscriptional regulatory element enhances expression of transgenes delivered by retroviral vectors. *Journal of virology*. 1999;73(4):2886-92.
94. Gustafsson C, Govindarajan S, Minshull J. Codon bias and heterologous protein expression. *Trends in biotechnology*. 2004;22(7):346-53.
95. Szymczak AL, Workman CJ, Wang Y, Vignali KM, Dilioglou S, Vanin EF, et al. Correction of multi-gene deficiency in vivo using a single 'self-cleaving' 2A peptide-based retroviral vector. *Nature biotechnology*. 2004;22(5):589-94.
96. Bendle GM, Linnemann C, Hooijkaas AI, Bies L, de Witte MA, Jorritsma A, et al. Lethal graft-versus-host disease in mouse models of T cell receptor gene therapy. *Nature medicine*. 2010;16(5):565-70, 1p following 70.
97. Cohen CJ, Zhao Y, Zheng Z, Rosenberg SA, Morgan RA. Enhanced antitumor activity of murine-human hybrid T-cell receptor (TCR) in human lymphocytes is associated with improved pairing and TCR/CD3 stability. *Cancer research*. 2006;66(17):8878-86.
98. Davis JL, Theoret MR, Zheng Z, Lamers CH, Rosenberg SA, Morgan RA. Development of human anti-murine T-cell receptor antibodies in both responding and nonresponding patients enrolled in TCR gene therapy trials. *Clinical cancer research : an official journal of the American Association for Cancer Research*. 2010;16(23):5852-61.
99. Sommermeyer D, Uckert W. Minimal amino acid exchange in human TCR constant regions fosters improved function of TCR gene-modified T cells. *Journal of immunology*. 2010;184(11):6223-31.
100. van Loenen MM, de Boer R, Amir AL, Hagedoorn RS, Volbeda GL, Willemze R, et al. Mixed T cell receptor dimers harbor potentially harmful neoreactivity. *Proceedings of the National Academy of Sciences of the United States of America*. 2010;107(24):10972-7.
101. Cohen CJ, Li YF, El-Gamil M, Robbins PF, Rosenberg SA, Morgan RA. Enhanced antitumor activity of T cells engineered to express T-cell receptors with a second disulfide bond. *Cancer research*. 2007;67(8):3898-903.

102. Okamoto S, Mineno J, Ikeda H, Fujiwara H, Yasukawa M, Shiku H, et al. Improved expression and reactivity of transduced tumor-specific TCRs in human lymphocytes by specific silencing of endogenous TCR. *Cancer research*. 2009;69(23):9003-11.
103. Urnov FD, Miller JC, Lee YL, Beausejour CM, Rock JM, Augustus S, et al. Highly efficient endogenous human gene correction using designed zinc-finger nucleases. *Nature*. 2005;435(7042):646-51.
104. Provasi E, Genovese P, Lombardo A, Magnani Z, Liu PQ, Reik A, et al. Editing T cell specificity towards leukemia by zinc finger nucleases and lentiviral gene transfer. *Nature medicine*. 2012;18(5):807-15.
105. Nauerth M, Weissbrich B, Knall R, Franz T, Dossinger G, Bet J, et al. TCR-ligand koff rate correlates with the protective capacity of antigen-specific CD8+ T cells for adoptive transfer. *Science translational medicine*. 2013;5(192):192ra87.
106. Engels B, Engelhard VH, Sidney J, Sette A, Binder DC, Liu RB, et al. Relapse or eradication of cancer is predicted by peptide-major histocompatibility complex affinity. *Cancer cell*. 2013;23(4):516-26.
107. Richman SA, Kranz DM. Display, engineering, and applications of antigen-specific T cell receptors. *Biomolecular engineering*. 2007;24(4):361-73.
108. Holler PD, Holman PO, Shusta EV, O'Herrin S, Wittrup KD, Kranz DM. In vitro evolution of a T cell receptor with high affinity for peptide/MHC. *Proceedings of the National Academy of Sciences of the United States of America*. 2000;97(10):5387-92.
109. Thomas S, Xue SA, Bangham CR, Jakobsen BK, Morris EC, Stauss HJ. Human T cells expressing affinity-matured TCR display accelerated responses but fail to recognize low density of MHC-peptide antigen. *Blood*. 2011;118(2):319-29.
110. Zhong S, Malecek K, Johnson LA, Yu Z, Vega-Saenz de Miera E, Darvishian F, et al. T-cell receptor affinity and avidity defines antitumor response and autoimmunity in T-cell immunotherapy. *Proceedings of the National Academy of Sciences of the United States of America*. 2013;110(17):6973-8.
111. Holler PD, Chlewicki LK, Kranz DM. TCRs with high affinity for foreign pMHC show self-reactivity. *Nature immunology*. 2003;4(1):55-62.
112. Eshhar Z, Waks T, Gross G, Schindler DG. Specific activation and targeting of cytotoxic lymphocytes through chimeric single chains consisting of antibody-binding domains and the gamma or zeta subunits of the immunoglobulin and T-cell receptors. *Proceedings of the National Academy of Sciences of the United States of America*. 1993;90(2):720-4.
113. Gilham DE, Debets R, Pule M, Hawkins RE, Abken H. CAR-T cells and solid tumors: tuning T cells to challenge an inveterate foe. *Trends in molecular medicine*. 2012;18(7):377-84.
114. Dotti G, Gottschalk S, Savoldo B, Brenner MK. Design and development of therapies using chimeric antigen receptor-expressing T cells. *Immunological reviews*. 2014;257(1):107-26.
115. Chmielewski M, Hombach A, Heuser C, Adams GP, Abken H. T cell activation by antibody-like immunoreceptors: increase in affinity of the single-chain fragment domain above threshold does not increase T cell activation against antigen-positive target cells but decreases selectivity. *Journal of immunology*. 2004;173(12):7647-53.
116. Hudecek M, Lupo-Stanghellini MT, Kosasih PL, Sommermeyer D, Jensen MC, Rader C, et al. Receptor affinity and extracellular domain modifications affect tumor recognition by ROR1-specific chimeric antigen receptor T cells. *Clinical cancer research : an official journal of the American Association for Cancer Research*. 2013;19(12):3153-64.
117. Jensen MC, Riddell SR. Design and implementation of adoptive therapy with chimeric antigen receptor-modified T cells. *Immunological reviews*. 2014;257(1):127-44.
118. Hombach AA, Schildgen V, Heuser C, Finfern R, Gilham DE, Abken H. T cell activation by antibody-like immunoreceptors: the position of the binding epitope within the target molecule determines the efficiency of activation of redirected T cells. *Journal of immunology*. 2007;178(7):4650-7.
119. Chmielewski M, Hombach AA, Abken H. CD28 cosignalling does not affect the activation threshold in a chimeric antigen receptor-redirectioned T-cell attack. *Gene therapy*. 2011;18(1):62-72.
120. Hombach A, Sent D, Schneider C, Heuser C, Koch D, Pohl C, et al. T-cell activation by recombinant receptors: CD28 costimulation is required for interleukin 2 secretion and receptor-

mediated T-cell proliferation but does not affect receptor-mediated target cell lysis. *Cancer research*. 2001;61(5):1976-82.

121. Imai C, Mihara K, Andreansky M, Nicholson IC, Pui CH, Geiger TL, et al. Chimeric receptors with 4-1BB signaling capacity provoke potent cytotoxicity against acute lymphoblastic leukemia. *Leukemia*. 2004;18(4):676-84.

122. Torikai H, Reik A, Liu PQ, Zhou Y, Zhang L, Maiti S, et al. A foundation for universal T-cell based immunotherapy: T cells engineered to express a CD19-specific chimeric-antigen-receptor and eliminate expression of endogenous TCR. *Blood*. 2012;119(24):5697-705.

123. Bridgeman JS, Hawkins RE, Bagley S, Blaylock M, Holland M, Gilham DE. The optimal antigen response of chimeric antigen receptors harboring the CD3zeta transmembrane domain is dependent upon incorporation of the receptor into the endogenous TCR/CD3 complex. *Journal of immunology*. 2010;184(12):6938-49.

124. Savoldo B, Ramos CA, Liu E, Mims MP, Keating MJ, Carrum G, et al. CD28 costimulation improves expansion and persistence of chimeric antigen receptor-modified T cells in lymphoma patients. *The Journal of clinical investigation*. 2011;121(5):1822-6.

125. Terakura S, Yamamoto TN, Gardner RA, Turtle CJ, Jensen MC, Riddell SR. Generation of CD19-chimeric antigen receptor modified CD8+ T cells derived from virus-specific central memory T cells. *Blood*. 2012;119(1):72-82.

126. Rappl G, Riet T, Awerkiew S, Schmidt A, Hombach AA, Pfister H, et al. The CD3-zeta chimeric antigen receptor overcomes TCR Hypo-responsiveness of human terminal late-stage T cells. *PloS one*. 2012;7(1):e30713.

127. Dao T, Yan S, Veomett N, Pankov D, Zhou L, Korontsvit T, et al. Targeting the intracellular WT1 oncogene product with a therapeutic human antibody. *Science translational medicine*. 2013;5(176):176ra33.

128. Grada Z, Hegde M, Byrd T, Shaffer DR, Ghazi A, Brawley VS, et al. TanCAR: A Novel Bispecific Chimeric Antigen Receptor for Cancer Immunotherapy. *Molecular therapy Nucleic acids*. 2013;2:e105.

129. Fedorov VD, Themeli M, Sadelain M. PD-1- and CTLA-4-based inhibitory chimeric antigen receptors (iCARs) divert off-target immunotherapy responses. *Science translational medicine*. 2013;5(215):215ra172.

130. Tamada K, Geng D, Sakoda Y, Bansal N, Srivastava R, Li Z, et al. Redirecting gene-modified T cells toward various cancer types using tagged antibodies. *Clinical cancer research : an official journal of the American Association for Cancer Research*. 2012;18(23):6436-45.

131. Urbanska K, Lanitis E, Poussin M, Lynn RC, Gavin BP, Kelderman S, et al. A universal strategy for adoptive immunotherapy of cancer through use of a novel T-cell antigen receptor. *Cancer research*. 2012;72(7):1844-52.

132. Morgan RA, Dudley ME, Wunderlich JR, Hughes MS, Yang JC, Sherry RM, et al. Cancer regression in patients after transfer of genetically engineered lymphocytes. *Science*. 2006;314(5796):126-9.

133. Dudley ME, Wunderlich JR, Yang JC, Sherry RM, Topalian SL, Restifo NP, et al. Adoptive cell transfer therapy following non-myeloablative but lymphodepleting chemotherapy for the treatment of patients with refractory metastatic melanoma. *Journal of clinical oncology : official journal of the American Society of Clinical Oncology*. 2005;23(10):2346-57.

134. Robbins PF, Morgan RA, Feldman SA, Yang JC, Sherry RM, Dudley ME, et al. Tumor regression in patients with metastatic synovial cell sarcoma and melanoma using genetically engineered lymphocytes reactive with NY-ESO-1. *Journal of clinical oncology : official journal of the American Society of Clinical Oncology*. 2011;29(7):917-24.

135. Kershaw MH, Westwood JA, Parker LL, Wang G, Eshhar Z, Mavroukakis SA, et al. A phase I study on adoptive immunotherapy using gene-modified T cells for ovarian cancer. *Clinical cancer research : an official journal of the American Association for Cancer Research*. 2006;12(20 Pt 1):6106-15.

136. Park JR, Digiusto DL, Slovak M, Wright C, Naranjo A, Wagner J, et al. Adoptive transfer of chimeric antigen receptor re-directed cytolytic T lymphocyte clones in patients with neuroblastoma. *Molecular therapy : the journal of the American Society of Gene Therapy*. 2007;15(4):825-33.

137. Kowolik CM, Topp MS, Gonzalez S, Pfeiffer T, Olivares S, Gonzalez N, et al. CD28 costimulation provided through a CD19-specific chimeric antigen receptor enhances in vivo persistence and antitumor efficacy of adoptively transferred T cells. *Cancer research*. 2006;66(22):10995-1004.
138. Kochenderfer JN, Dudley ME, Feldman SA, Wilson WH, Spaner DE, Maric I, et al. B-cell depletion and remissions of malignancy along with cytokine-associated toxicity in a clinical trial of anti-CD19 chimeric-antigen-receptor-transduced T cells. *Blood*. 2012;119(12):2709-20.
139. Kochenderfer JN, Wilson WH, Janik JE, Dudley ME, Stetler-Stevenson M, Feldman SA, et al. Eradication of B-lineage cells and regression of lymphoma in a patient treated with autologous T cells genetically engineered to recognize CD19. *Blood*. 2010;116(20):4099-102.
140. Grupp SA, Kalos M, Barrett D, Aplenc R, Porter DL, Rheingold SR, et al. Chimeric antigen receptor-modified T cells for acute lymphoid leukemia. *The New England journal of medicine*. 2013;368(16):1509-18.
141. Brentjens RJ, Davila ML, Riviere I, Park J, Wang X, Cowell LG, et al. CD19-targeted T cells rapidly induce molecular remissions in adults with chemotherapy-refractory acute lymphoblastic leukemia. *Science translational medicine*. 2013;5(177):177ra38.
142. Porter DL, Levine BL, Kalos M, Bagg A, June CH. Chimeric antigen receptor-modified T cells in chronic lymphoid leukemia. *The New England journal of medicine*. 2011;365(8):725-33.
143. Kalos M, Levine BL, Porter DL, Katz S, Grupp SA, Bagg A, et al. T cells with chimeric antigen receptors have potent antitumor effects and can establish memory in patients with advanced leukemia. *Science translational medicine*. 2011;3(95):95ra73.
144. Davila ML, Riviere I, Wang X, Bartido S, Park J, Curran K, et al. Efficacy and Toxicity Management of 19-28z CAR T Cell Therapy in B Cell Acute Lymphoblastic Leukemia. *Science translational medicine*. 2014;6(224):224ra25.
145. Louis CU, Savoldo B, Dotti G, Pule M, Yvon E, Myers GD, et al. Antitumor activity and long-term fate of chimeric antigen receptor-positive T cells in patients with neuroblastoma. *Blood*. 2011;118(23):6050-6.
146. Lamers CH, Sleijfer S, Vulto AG, Kruit WH, Kliffen M, Debets R, et al. Treatment of metastatic renal cell carcinoma with autologous T-lymphocytes genetically retargeted against carbonic anhydrase IX: first clinical experience. *Journal of clinical oncology : official journal of the American Society of Clinical Oncology*. 2006;24(13):e20-2.
147. Morgan RA, Yang JC, Kitano M, Dudley ME, Laurencot CM, Rosenberg SA. Case report of a serious adverse event following the administration of T cells transduced with a chimeric antigen receptor recognizing ERBB2. *Molecular therapy : the journal of the American Society of Gene Therapy*. 2010;18(4):843-51.
148. Morgan RA, Johnson LA, Davis JL, Zheng Z, Woolard KD, Reap EA, et al. Recognition of glioma stem cells by genetically modified T cells targeting EGFRvIII and development of adoptive cell therapy for glioma. *Human gene therapy*. 2012;23(10):1043-53.
149. Tran E, Chinnasamy D, Yu Z, Morgan RA, Lee CC, Restifo NP, et al. Immune targeting of fibroblast activation protein triggers recognition of multipotent bone marrow stromal cells and cachexia. *The Journal of experimental medicine*. 2013;210(6):1125-35.
150. Chinnasamy D, Yu Z, Theoret MR, Zhao Y, Shrimali RK, Morgan RA, et al. Gene therapy using genetically modified lymphocytes targeting VEGFR-2 inhibits the growth of vascularized syngenic tumors in mice. *The Journal of clinical investigation*. 2010;120(11):3953-68.
151. Pule MA, Savoldo B, Myers GD, Rossig C, Russell HV, Dotti G, et al. Virus-specific T cells engineered to coexpress tumor-specific receptors: persistence and antitumor activity in individuals with neuroblastoma. *Nature medicine*. 2008;14(11):1264-70.
152. Abate-Daga D, Hanada K, Davis JL, Yang JC, Rosenberg SA, Morgan RA. Expression profiling of TCR-engineered T cells demonstrates overexpression of multiple inhibitory receptors in persisting lymphocytes. *Blood*. 2013;122(8):1399-410.
153. Johnson LA, Morgan RA, Dudley ME, Cassard L, Yang JC, Hughes MS, et al. Gene therapy with human and mouse T-cell receptors mediates cancer regression and targets normal tissues expressing cognate antigen. *Blood*. 2009;114(3):535-46.
154. Parkhurst MR, Yang JC, Langan RC, Dudley ME, Nathan DA, Feldman SA, et al. T cells targeting carcinoembryonic antigen can mediate regression of metastatic colorectal cancer but

- induce severe transient colitis. *Molecular therapy : the journal of the American Society of Gene Therapy*. 2011;19(3):620-6.
155. Morgan RA, Chinnasamy N, Abate-Daga D, Gros A, Robbins PF, Zheng Z, et al. Cancer regression and neurological toxicity following anti-MAGE-A3 TCR gene therapy. *Journal of immunotherapy*. 2013;36(2):133-51.
156. Chinnasamy N, Wargo JA, Yu Z, Rao M, Frankel TL, Riley JP, et al. A TCR targeting the HLA-A\*0201-restricted epitope of MAGE-A3 recognizes multiple epitopes of the MAGE-A antigen superfamily in several types of cancer. *Journal of immunology*. 2011;186(2):685-96.
157. Linette GP, Stadtmauer EA, Maus MV, Rapoport AP, Levine BL, Emery L, et al. Cardiovascular toxicity and titin cross-reactivity of affinity-enhanced T cells in myeloma and melanoma. *Blood*. 2013;122(6):863-71.
158. Cameron BJ, Gerry AB, Dukes J, Harper JV, Kannan V, Bianchi FC, et al. Identification of a Titin-derived HLA-A1-presented peptide as a cross-reactive target for engineered MAGE A3-directed T cells. *Science translational medicine*. 2013;5(197):197ra03.
159. Jensen MC, Popplewell L, Cooper LJ, DiGiusto D, Kalos M, Ostberg JR, et al. Antitransgene rejection responses contribute to attenuated persistence of adoptively transferred CD20/CD19-specific chimeric antigen receptor redirected T cells in humans. *Biology of blood and marrow transplantation : journal of the American Society for Blood and Marrow Transplantation*. 2010;16(9):1245-56.
160. Lamers CH, Willemsen R, van Elzaker P, van Steenberghe-Langeveld S, Broertjes M, Oosterwijk-Wakka J, et al. Immune responses to transgene and retroviral vector in patients treated with ex vivo-engineered T cells. *Blood*. 2011;117(1):72-82.
161. Arber C, Abhyankar H, Heslop HE, Brenner MK, Liu H, Dotti G, et al. The immunogenicity of virus-derived 2A sequences in immunocompetent individuals. *Gene therapy*. 2013;20(9):958-62.
162. Wu X, Li Y, Crise B, Burgess SM. Transcription start regions in the human genome are favored targets for MLV integration. *Science*. 2003;300(5626):1749-51.
163. Hacein-Bey-Abina S, Von Kalle C, Schmidt M, McCormack MP, Wulffraat N, Leboulch P, et al. LMO2-associated clonal T cell proliferation in two patients after gene therapy for SCID-X1. *Science*. 2003;302(5644):415-9.
164. Scholler J, Brady TL, Binder-Scholl G, Hwang WT, Plesa G, Hege KM, et al. Decade-long safety and function of retroviral-modified chimeric antigen receptor T cells. *Science translational medicine*. 2012;4(132):132ra53.
165. Recchia A, Bonini C, Magnani Z, Urbinati F, Sartori D, Muraro S, et al. Retroviral vector integration deregulates gene expression but has no consequence on the biology and function of transplanted T cells. *Proceedings of the National Academy of Sciences of the United States of America*. 2006;103(5):1457-62.
166. Sakuma T, Barry MA, Ikeda Y. Lentiviral vectors: basic to translational. *The Biochemical journal*. 2012;443(3):603-18.
167. Hackett PB, Largaespada DA, Switzer KC, Cooper LJ. Evaluating risks of insertional mutagenesis by DNA transposons in gene therapy. *Translational research : the journal of laboratory and clinical medicine*. 2013;161(4):265-83.
168. Ertl HC, Zaia J, Rosenberg SA, June CH, Dotti G, Kahn J, et al. Considerations for the clinical application of chimeric antigen receptor T cells: observations from a recombinant DNA Advisory Committee Symposium held June 15, 2010. *Cancer research*. 2011;71(9):3175-81.
169. Huang J, Khong HT, Dudley ME, El-Gamil M, Li YF, Rosenberg SA, et al. Survival, persistence, and progressive differentiation of adoptively transferred tumor-reactive T cells associated with tumor regression. *Journal of immunotherapy*. 2005;28(3):258-67.
170. Berger C, Jensen MC, Lansdorp PM, Gough M, Elliott C, Riddell SR. Adoptive transfer of effector CD8+ T cells derived from central memory cells establishes persistent T cell memory in primates. *The Journal of clinical investigation*. 2008;118(1):294-305.
171. Kaneko S, Mastaglio S, Bondanza A, Ponzoni M, Sanvito F, Aldrighetti L, et al. IL-7 and IL-15 allow the generation of suicide gene-modified alloreactive self-renewing central memory human T lymphocytes. *Blood*. 2009;113(5):1006-15.

172. Stemberger C, Huster KM, Koffler M, Anderl F, Schiemann M, Wagner H, et al. A single naive CD8+ T cell precursor can develop into diverse effector and memory subsets. *Immunity*. 2007;27(6):985-97.
173. Hinrichs CS, Borman ZA, Cassard L, Gattinoni L, Spolski R, Yu Z, et al. Adoptively transferred effector cells derived from naive rather than central memory CD8+ T cells mediate superior antitumor immunity. *Proceedings of the National Academy of Sciences of the United States of America*. 2009;106(41):17469-74.
174. Gattinoni L, Lugli E, Ji Y, Pos Z, Paulos CM, Quigley MF, et al. A human memory T cell subset with stem cell-like properties. *Nature medicine*. 2011;17(10):1290-7.
175. Zhang Y, Joe G, Hexner E, Zhu J, Emerson SG. Host-reactive CD8+ memory stem cells in graft-versus-host disease. *Nature medicine*. 2005;11(12):1299-305.
176. Graef P, Buchholz VR, Stemberger C, Flossdorf M, Henkel L, Schiemann M, et al. Serial transfer of single-derived immunocompetence reveals stemness of CD8+ central memory T cells. *Immunity*. 2014;accepted.
177. Sathaliyawala T, Kubota M, Yudanin N, Turner D, Camp P, Thome JJ, et al. Distribution and compartmentalization of human circulating and tissue-resident memory T cell subsets. *Immunity*. 2013;38(1):187-97.
178. Stemberger C, Dreher S, Tschulik C, Piossek C, Bet J, Yamamoto TN, et al. Novel serial positive enrichment technology enables clinical multiparameter cell sorting. *PLoS one*. 2012;7(4):e35798.
179. Tey SK, Brenner MK. The continuing contribution of gene marking to cell and gene therapy. *Molecular therapy : the journal of the American Society of Gene Therapy*. 2007;15(4):666-76.
180. Barese CN, Dunbar CE. Contributions of gene marking to cell and gene therapies. *Human gene therapy*. 2011;22(6):659-68.
181. Lacey SF, Kalos M. Biomarkers in T-cell therapy clinical trials. *Cytherapy*. 2013;15(6):632-40.
182. Bonini C, Bondanza A, Perna SK, Kaneko S, Traversari C, Ciceri F, et al. The suicide gene therapy challenge: how to improve a successful gene therapy approach. *Molecular therapy : the journal of the American Society of Gene Therapy*. 2007;15(7):1248-52.
183. Bonini C, Ferrari G, Verzeletti S, Servida P, Zappone E, Ruggieri L, et al. HSV-TK gene transfer into donor lymphocytes for control of allogeneic graft-versus-leukemia. *Science*. 1997;276(5319):1719-24.
184. Bonini C, Grez M, Traversari C, Ciceri F, Marktel S, Ferrari G, et al. Safety of retroviral gene marking with a truncated NGF receptor. *Nature medicine*. 2003;9(4):367-9.
185. Yaghoubi SS, Jensen MC, Satyamurthy N, Budhiraja S, Paik D, Czernin J, et al. Noninvasive detection of therapeutic cytolytic T cells with 18F-FHBG PET in a patient with glioma. *Nature clinical practice Oncology*. 2009;6(1):53-8.
186. Chen YY, Jensen MC, Smolke CD. Genetic control of mammalian T-cell proliferation with synthetic RNA regulatory systems. *Proceedings of the National Academy of Sciences of the United States of America*. 2010;107(19):8531-6.
187. Traversari C, Marktel S, Magnani Z, Mangia P, Russo V, Ciceri F, et al. The potential immunogenicity of the TK suicide gene does not prevent full clinical benefit associated with the use of TK-transduced donor lymphocytes in HSCT for hematologic malignancies. *Blood*. 2007;109(11):4708-15.
188. Berger C, Flowers ME, Warren EH, Riddell SR. Analysis of transgene-specific immune responses that limit the in vivo persistence of adoptively transferred HSV-TK-modified donor T cells after allogeneic hematopoietic cell transplantation. *Blood*. 2006;107(6):2294-302.
189. Di Stasi A, Tey SK, Dotti G, Fujita Y, Kennedy-Nasser A, Martinez C, et al. Inducible apoptosis as a safety switch for adoptive cell therapy. *The New England journal of medicine*. 2011;365(18):1673-83.
190. Adams GP, Weiner LM. Monoclonal antibody therapy of cancer. *Nature biotechnology*. 2005;23(9):1147-57.
191. Introna M, Barbui AM, Bambacioni F, Casati C, Gaipa G, Borleri G, et al. Genetic modification of human T cells with CD20: a strategy to purify and lyse transduced cells with anti-CD20 antibodies. *Human gene therapy*. 2000;11(4):611-20.

192. van Meerten T, Claessen MJ, Hagenbeek A, Ebeling SB. The CD20/alphaCD20 'suicide' system: novel vectors with improved safety and expression profiles and efficient elimination of CD20-transgenic T cells. *Gene therapy*. 2006;13(9):789-97.
193. Vogler I, Newrzela S, Hartmann S, Schneider N, von Laer D, Koehl U, et al. An improved bicistronic CD20/tCD34 vector for efficient purification and in vivo depletion of gene-modified T cells for adoptive immunotherapy. *Molecular therapy : the journal of the American Society of Gene Therapy*. 2010;18(7):1330-8.
194. Kieback E, Charo J, Sommermeyer D, Blankenstein T, Uckert W. A safeguard eliminates T cell receptor gene-modified autoreactive T cells after adoptive transfer. *Proceedings of the National Academy of Sciences of the United States of America*. 2008;105(2):623-8.
195. Wang X, Chang WC, Wong CW, Colcher D, Sherman M, Ostberg JR, et al. A transgene-encoded cell surface polypeptide for selection, in vivo tracking, and ablation of engineered cells. *Blood*. 2011;118(5):1255-63.
196. Burgess AW, Cho HS, Eigenbrot C, Ferguson KM, Garrett TP, Leahy DJ, et al. An open-and-shut case? Recent insights into the activation of EGF/ErbB receptors. *Molecular cell*. 2003;12(3):541-52.
197. Klein P, Mattoon D, Lemmon MA, Schlessinger J. A structure-based model for ligand binding and dimerization of EGF receptors. *Proceedings of the National Academy of Sciences of the United States of America*. 2004;101(4):929-34.
198. Yarden Y, Sliwkowski MX. Untangling the ErbB signalling network. *Nature reviews Molecular cell biology*. 2001;2(2):127-37.
199. Kawamoto T, Sato JD, Le A, Polikoff J, Sato GH, Mendelsohn J. Growth stimulation of A431 cells by epidermal growth factor: identification of high-affinity receptors for epidermal growth factor by an anti-receptor monoclonal antibody. *Proceedings of the National Academy of Sciences of the United States of America*. 1983;80(5):1337-41.
200. Li S, Schmitz KR, Jeffrey PD, Wiltzius JJ, Kussie P, Ferguson KM. Structural basis for inhibition of the epidermal growth factor receptor by cetuximab. *Cancer cell*. 2005;7(4):301-11.
201. Fan Z, Lu Y, Wu X, Mendelsohn J. Antibody-induced epidermal growth factor receptor dimerization mediates inhibition of autocrine proliferation of A431 squamous carcinoma cells. *The Journal of biological chemistry*. 1994;269(44):27595-602.
202. Kimura H, Sakai K, Arao T, Shimoyama T, Tamura T, Nishio K. Antibody-dependent cellular cytotoxicity of cetuximab against tumor cells with wild-type or mutant epidermal growth factor receptor. *Cancer science*. 2007;98(8):1275-80.
203. Hara M, Nakanishi H, Tsujimura K, Matsui M, Yatabe Y, Manabe T, et al. Interleukin-2 potentiation of cetuximab antitumor activity for epidermal growth factor receptor-overexpressing gastric cancer xenografts through antibody-dependent cellular cytotoxicity. *Cancer science*. 2008;99(7):1471-8.
204. Clynes RA, Towers TL, Presta LG, Ravetch JV. Inhibitory Fc receptors modulate in vivo cytotoxicity against tumor targets. *Nature medicine*. 2000;6(4):443-6.
205. Mellor JD, Brown MP, Irving HR, Zalberg JR, Dobrovic A. A critical review of the role of Fc gamma receptor polymorphisms in the response to monoclonal antibodies in cancer. *Journal of hematology & oncology*. 2013;6:1.
206. Yewale C, Baradia D, Vhora I, Patil S, Misra A. Epidermal growth factor receptor targeting in cancer: a review of trends and strategies. *Biomaterials*. 2013;34(34):8690-707.
207. Rivera F, Vega-Villegas ME, Lopez-Brea MF. Cetuximab, its clinical use and future perspectives. *Anti-cancer drugs*. 2008;19(2):99-113.
208. Baselga J, Pfister D, Cooper MR, Cohen R, Burtness B, Bos M, et al. Phase I studies of anti-epidermal growth factor receptor chimeric antibody C225 alone and in combination with cisplatin. *Journal of clinical oncology : official journal of the American Society of Clinical Oncology*. 2000;18(4):904-14.
209. Perez-Soler R, Saltz L. Cutaneous adverse effects with HER1/EGFR-targeted agents: is there a silver lining? *Journal of clinical oncology : official journal of the American Society of Clinical Oncology*. 2005;23(22):5235-46.
210. Mendelsohn J, Baselga J. Epidermal growth factor receptor targeting in cancer. *Seminars in oncology*. 2006;33(4):369-85.

211. King LE, Jr., Gates RE, Stoscheck CM, Nanney LB. The EGF/TGF alpha receptor in skin. *The Journal of investigative dermatology*. 1990;94(6 Suppl):164S-70S.
212. Hansel TT, Kropshofer H, Singer T, Mitchell JA, George AJ. The safety and side effects of monoclonal antibodies. *Nature reviews Drug discovery*. 2010;9(4):325-38.
213. Riddell SR, Greenberg PD. The use of anti-CD3 and anti-CD28 monoclonal antibodies to clone and expand human antigen-specific T cells. *Journal of immunological methods*. 1990;128(2):189-201.
214. Hong KW, Kim CG, Lee SH, Chang KH, Shin YW, Ryoo KH, et al. A novel anti-EGFR monoclonal antibody inhibiting tumor cell growth by recognizing different epitopes from cetuximab. *Journal of biotechnology*. 2010;145(1):84-91.
215. Orlandi R, Gussow DH, Jones PT, Winter G. Cloning immunoglobulin variable domains for expression by the polymerase chain reaction. *Proceedings of the National Academy of Sciences of the United States of America*. 1989;86(10):3833-7.
216. Bes C, Briant-Longuet L, Cerutti M, Heitz F, Troadec S, Pugniere M, et al. Mapping the paratope of anti-CD4 recombinant Fab 13B8.2 by combining parallel peptide synthesis and site-directed mutagenesis. *The Journal of biological chemistry*. 2003;278(16):14265-73.
217. Wang X, Naranjo A, Brown CE, Bautista C, Wong CW, Chang WC, et al. Phenotypic and functional attributes of lentivirus-modified CD19-specific human CD8+ central memory T cells manufactured at clinical scale. *Journal of immunotherapy*. 2012;35(9):689-701.
218. Hultin LE, Matud JL, Giorgi JV. Quantitation of CD38 activation antigen expression on CD8+ T cells in HIV-1 infection using CD4 expression on CD4+ T lymphocytes as a biological calibrator. *Cytometry*. 1998;33(2):123-32.
219. Marechal R, De Schutter J, Nagy N, Demetter P, Lemmers A, Deviere J, et al. Putative contribution of CD56 positive cells in cetuximab treatment efficacy in first-line metastatic colorectal cancer patients. *BMC cancer*. 2010;10:340.
220. Davila ML, Kloss CC, Gunset G, Sadelain M. CD19 CAR-targeted T cells induce long-term remission and B Cell Aplasia in an immunocompetent mouse model of B cell acute lymphoblastic leukemia. *PloS one*. 2013;8(4):e61338.
221. Krebs K, Bottinger N, Huang LR, Chmielewski M, Arzberger S, Gasteiger G, et al. T cells expressing a chimeric antigen receptor that binds hepatitis B virus envelope proteins control virus replication in mice. *Gastroenterology*. 2013;145(2):456-65.
222. Berger C, Huang ML, Gough M, Greenberg PD, Riddell SR, Kiem HP. Nonmyeloablative immunosuppressive regimen prolongs In vivo persistence of gene-modified autologous T cells in a nonhuman primate model. *Journal of virology*. 2001;75(2):799-808.
223. Riddell SR, Elliott M, Lewinsohn DA, Gilbert MJ, Wilson L, Manley SA, et al. T-cell mediated rejection of gene-modified HIV-specific cytotoxic T lymphocytes in HIV-infected patients. *Nature medicine*. 1996;2(2):216-23.
224. Wiley HS. Trafficking of the ErbB receptors and its influence on signaling. *Experimental cell research*. 2003;284(1):78-88.
225. Sorkin A, Waters CM. Endocytosis of growth factor receptors. *BioEssays : news and reviews in molecular, cellular and developmental biology*. 1993;15(6):375-82.
226. Chen WS, Lazar CS, Lund KA, Welsh JB, Chang CP, Walton GM, et al. Functional independence of the epidermal growth factor receptor from a domain required for ligand-induced internalization and calcium regulation. *Cell*. 1989;59(1):33-43.
227. Zheng Z, Chinnasamy N, Morgan RA. Protein L: a novel reagent for the detection of chimeric antigen receptor (CAR) expression by flow cytometry. *Journal of translational medicine*. 2012;10:29.
228. Derer S, Bauer P, Lohse S, Scheel AH, Berger S, Kellner C, et al. Impact of epidermal growth factor receptor (EGFR) cell surface expression levels on effector mechanisms of EGFR antibodies. *Journal of immunology*. 2012;189(11):5230-9.
229. Schmiedel J, Blaukat A, Li S, Knochel T, Ferguson KM. Matuzumab binding to EGFR prevents the conformational rearrangement required for dimerization. *Cancer cell*. 2008;13(4):365-73.
230. Persons DA, Allay JA, Allay ER, Smeyne RJ, Ashmun RA, Sorrentino BP, et al. Retroviral-mediated transfer of the green fluorescent protein gene into murine hematopoietic

- cells facilitates scoring and selection of transduced progenitors in vitro and identification of genetically modified cells in vivo. *Blood*. 1997;90(5):1777-86.
231. Fehse B, Kustikova OS, Li Z, Wahlers A, Bohn W, Beyer WR, et al. A novel 'sort-suicide' fusion gene vector for T cell manipulation. *Gene therapy*. 2002;9(23):1633-8.
232. Rettig MP, Ritchey JK, Meyerrose TE, Haug JS, DiPersio JF. Transduction and selection of human T cells with novel CD34/thymidine kinase chimeric suicide genes for the treatment of graft-versus-host disease. *Molecular therapy : the journal of the American Society of Gene Therapy*. 2003;8(1):29-41.
233. Tey SK, Dotti G, Rooney CM, Heslop HE, Brenner MK. Inducible caspase 9 suicide gene to improve the safety of allodepleted T cells after haploidentical stem cell transplantation. *Biology of blood and marrow transplantation : journal of the American Society for Blood and Marrow Transplantation*. 2007;13(8):913-24.
234. Chan G, Nogalski MT, Yurochko AD. Activation of EGFR on monocytes is required for human cytomegalovirus entry and mediates cellular motility. *Proceedings of the National Academy of Sciences of the United States of America*. 2009;106(52):22369-74.
235. Mahtouk K, Hose D, Reme T, De Vos J, Jourdan M, Moreaux J, et al. Expression of EGF-family receptors and amphiregulin in multiple myeloma. Amphiregulin is a growth factor for myeloma cells. *Oncogene*. 2005;24(21):3512-24.
236. Zaiss DM, van Loosdregt J, Gorlani A, Bekker CP, Grone A, Sibilica M, et al. Amphiregulin enhances regulatory T cell-suppressive function via the epidermal growth factor receptor. *Immunity*. 2013;38(2):275-84.
237. Stemberger C, Graef P, Odendahl M, Albrecht J, Dossinger G, Anderl F, et al. Lowest numbers of primary CD8+ T cells can reconstitute protective immunity upon adoptive immunotherapy. *Blood*. 2014.
238. Jamsa J, Huotari V, Savolainen ER, Syrjala H, Ala-Kokko T. Analysis of the temperature affects on leukocyte surface antigen expression. *Journal of clinical laboratory analysis*. 2011;25(2):118-25.
239. Fan Z, Masui H, Altas I, Mendelsohn J. Blockade of epidermal growth factor receptor function by bivalent and monovalent fragments of 225 anti-epidermal growth factor receptor monoclonal antibodies. *Cancer research*. 1993;53(18):4322-8.
240. Dick JE, Magli MC, Huszar D, Phillips RA, Bernstein A. Introduction of a selectable gene into primitive stem cells capable of long-term reconstitution of the hemopoietic system of W/W<sup>v</sup> mice. *Cell*. 1985;42(1):71-9.
241. Lee B, Sharron M, Montaner LJ, Weissman D, Doms RW. Quantification of CD4, CCR5, and CXCR4 levels on lymphocyte subsets, dendritic cells, and differentially conditioned monocyte-derived macrophages. *Proceedings of the National Academy of Sciences of the United States of America*. 1999;96(9):5215-20.
242. Griffioen M, van Egmond EH, Kester MG, Willemze R, Falkenburg JH, Heemskerk MH. Retroviral transfer of human CD20 as a suicide gene for adoptive T-cell therapy. *Haematologica*. 2009;94(9):1316-20.
243. van Loenen MM, de Boer R, Hagedoorn RS, Jankipersadsing V, Amir AL, Falkenburg JH, et al. Multi-cistronic vector encoding optimized safety switch for adoptive therapy with T-cell receptor-modified T cells. *Gene therapy*. 2013;20(8):861-7.
244. Mendelsohn J. Targeting the epidermal growth factor receptor for cancer therapy. *Journal of clinical oncology : official journal of the American Society of Clinical Oncology*. 2002;20(18 Suppl):1S-13S.
245. Talavera A, Friemann R, Gomez-Puerta S, Martinez-Fleites C, Garrido G, Rabasa A, et al. Nimotuzumab, an antitumor antibody that targets the epidermal growth factor receptor, blocks ligand binding while permitting the active receptor conformation. *Cancer research*. 2009;69(14):5851-9.
246. Naramura M, Gillies SD, Mendelsohn J, Reisfeld RA, Mueller BM. Therapeutic potential of chimeric and murine anti-(epidermal growth factor receptor) antibodies in a metastasis model for human melanoma. *Cancer immunology, immunotherapy : CII*. 1993;37(5):343-9.
247. Graziano RF, Fanger MW. Fc gamma RI and Fc gamma RII on monocytes and granulocytes are cytotoxic trigger molecules for tumor cells. *Journal of immunology*. 1987;139(10):3536-41.

248. Kurai J, Chikumi H, Hashimoto K, Yamaguchi K, Yamasaki A, Sako T, et al. Antibody-dependent cellular cytotoxicity mediated by cetuximab against lung cancer cell lines. *Clinical cancer research : an official journal of the American Association for Cancer Research*. 2007;13(5):1552-61.
249. Smyth MJ, Cretney E, Kelly JM, Westwood JA, Street SE, Yagita H, et al. Activation of NK cell cytotoxicity. *Molecular immunology*. 2005;42(4):501-10.
250. Loisel S, Ohresser M, Pallardy M, Dayde D, Berthou C, Cartron G, et al. Relevance, advantages and limitations of animal models used in the development of monoclonal antibodies for cancer treatment. *Critical reviews in oncology/hematology*. 2007;62(1):34-42.
251. Gerdes CA, Nicolini VG, Herter S, van Puijenbroek E, Lang S, Roemmele M, et al. GA201 (RG7160): a novel, humanized, glycoengineered anti-EGFR antibody with enhanced ADCC and superior in vivo efficacy compared with cetuximab. *Clinical cancer research : an official journal of the American Association for Cancer Research*. 2013;19(5):1126-38.
252. Overdijk MB, Verploegen S, Ortiz Buijsse A, Vink T, Leusen JH, Bleeker WK, et al. Crosstalk between human IgG isotypes and murine effector cells. *Journal of immunology*. 2012;189(7):3430-8.
253. Sanchez-Mejorada G, Rosales C. Signal transduction by immunoglobulin Fc receptors. *Journal of leukocyte biology*. 1998;63(5):521-33.
254. van Meerten T, van Rijn RS, Hol S, Hagenbeek A, Ebeling SB. Complement-induced cell death by rituximab depends on CD20 expression level and acts complementary to antibody-dependent cellular cytotoxicity. *Clinical cancer research : an official journal of the American Association for Cancer Research*. 2006;12(13):4027-35.
255. Li H, Ayer LM, Polyak MJ, Mutch CM, Petrie RJ, Gauthier L, et al. The CD20 calcium channel is localized to microvilli and constitutively associated with membrane rafts: antibody binding increases the affinity of the association through an epitope-dependent cross-linking-independent mechanism. *The Journal of biological chemistry*. 2004;279(19):19893-901.
256. Cherukuri A, Dykstra M, Pierce SK. Floating the raft hypothesis: lipid rafts play a role in immune cell activation. *Immunity*. 2001;14(6):657-60.
257. Yamabhai M, Anderson RG. Second cysteine-rich region of epidermal growth factor receptor contains targeting information for caveolae/rafts. *The Journal of biological chemistry*. 2002;277(28):24843-6.
258. Brown DA, London E. Functions of lipid rafts in biological membranes. *Annual review of cell and developmental biology*. 1998;14:111-36.
259. Furuuchi K, Berezov A, Kumagai T, Greene MI. Targeted antireceptor therapy with monoclonal antibodies leads to the formation of inactivated tetrameric forms of ErbB receptors. *Journal of immunology*. 2007;178(2):1021-9.
260. Serafini M, Manganini M, Borleri G, Bonamino M, Imberti L, Biondi A, et al. Characterization of CD20-transduced T lymphocytes as an alternative suicide gene therapy approach for the treatment of graft-versus-host disease. *Human gene therapy*. 2004;15(1):63-76.
261. Dechant M, Weisner W, Berger S, Peipp M, Beyer T, Schneider-Merck T, et al. Complement-dependent tumor cell lysis triggered by combinations of epidermal growth factor receptor antibodies. *Cancer research*. 2008;68(13):4998-5003.
262. Kamat V, Donaldson JM, Kari C, Quadros MR, Lelkes PI, Chaiken I, et al. Enhanced EGFR inhibition and distinct epitope recognition by EGFR antagonistic mAbs C225 and 425. *Cancer biology & therapy*. 2008;7(5):726-33.
263. Schlaeth M, Berger S, Derer S, Klausz K, Lohse S, Dechant M, et al. Fc-engineered EGF-R antibodies mediate improved antibody-dependent cellular cytotoxicity (ADCC) against KRAS-mutated tumor cells. *Cancer science*. 2010;101(5):1080-8.
264. Guidotti LG, Matzke B, Schaller H, Chisari FV. High-level hepatitis B virus replication in transgenic mice. *Journal of virology*. 1995;69(10):6158-69.
265. Isogawa M, Furuichi Y, Chisari FV. Oscillating CD8(+) T cell effector functions after antigen recognition in the liver. *Immunity*. 2005;23(1):53-63.
266. Corcoran LM, Tawfilis S, Barlow LJ. Generation of B lymphoma cell lines from knockout mice by transformation in vivo with an Emu-myc transgene. *Journal of immunological methods*. 1999;228(1-2):131-8.

267. Brentjens RJ, Riviere I, Park JH, Davila ML, Wang X, Stefanski J, et al. Safety and persistence of adoptively transferred autologous CD19-targeted T cells in patients with relapsed or chemotherapy refractory B-cell leukemias. *Blood*. 2011;118(18):4817-28.
268. Marin V, Cribioli E, Philip B, Tettamanti S, Pizzitola I, Biondi A, et al. Comparison of different suicide-gene strategies for the safety improvement of genetically manipulated T cells. *Human gene therapy methods*. 2012;23(6):376-86.
269. Straathof KC, Pule MA, Yotnda P, Dotti G, Vanin EF, Brenner MK, et al. An inducible caspase 9 safety switch for T-cell therapy. *Blood*. 2005;105(11):4247-54.
270. Berger C, Blau CA, Huang ML, Iliucci JD, Dalgarno DC, Gaschet J, et al. Pharmacologically regulated Fas-mediated death of adoptively transferred T cells in a nonhuman primate model. *Blood*. 2004;103(4):1261-9.

## 7 Publication list

Dossinger, G., Bunse, M., Bet, J., Albrecht, J., Paszkiewicz, P. J., Weissbrich, B., Schiedewitz, I., Henkel, L., Schiemann, M., Neuenhahn, M., Uckert, W., & Busch, D. H. (2013). MHC multimer-guided and cell culture-independent isolation of functional T cell receptors from single cells facilitates TCR identification for immunotherapy. *PLoS One*, 8(4), e61384. doi: 10.1371/journal.pone.0061384

Nauerth, M., Weissbrich, B., Knall, R., Franz, T., Dossinger, G., Bet, J., Paszkiewicz, P. J., Pfeifer, L., Bunse, M., Uckert, W., Holtappels, R., Gillert-Marien, D., Neuenhahn, M., Krackhardt, A., Reddehase, M. J., Riddell, S. R., & Busch, D. H. (2013). TCR-ligand koff rate correlates with the protective capacity of antigen-specific CD8<sup>+</sup> T cells for adoptive transfer. *Sci Transl Med*, 5(192), 192ra187. doi: 10.1126/scitranslmed.3005958

## 8 Acknowledgements

First of all, I want to sincerely thank Prof. Dirk Busch and Prof. Stan Riddell for their dedicated supervision of my PhD thesis and their invaluable advice that advanced my work. I am very grateful that my project offered the opportunity to both immerse into basic research and to participate in developments of clinical relevance. Working in close collaboration with Prof. Busch and Prof. Riddell was extremely motivating and the constant support through countless skype conferences showed their exceptional commitment to the project. Further, I am especially thankful that I have had the opportunity to join Stan Riddell's group at the FHCRC in Seattle for six months. It was a great learning experience both scientifically and personally. The scientific exchange between Munich and Seattle, including research visits both ways, was also supported by the Institute for Advanced Studies at the TUM. Finally, I highly appreciate the great effort applied to the revision of the manuscript.

I would also like to thank Prof. Busch for encouraging me to participate in the PhD program 'Medical Life Science and Technology' and to visit several inspiring conferences. As part of my PhD committee, Prof. Angela Krackhardt contributed to my work through helpful discussions and I want to thank her for being a great mentor.

During my research visit in Seattle and beyond, I received a lot of support from Dr. Michael Hudecek who also set an excellent example how to work in a structured way. Furthermore, it was exciting to work together with Dr. Carolina Berger during the NHP study and I am thankful for her commitment and help. Big thanks go to Dr. Steven Liu and Dr. Daniel Sommermeyer who provided gene constructs that were vital for my *in vivo* experiments.

I would like to express my gratitude to Prof. Ulla Protzer, Dr. Karin Wisskirchen and Nina Böttinger from the Institute of Virology in Munich for the wonderful collaboration. Performing experiments together was a lot of fun and I highly appreciate all technical and personal advice.

Special thanks are given to Dr. Stefan Dreher and Dr. Christian Stemberger for their crucial assistance regarding the development of the EGFR Fab, helpful input at any occasion and for sharing their patience about working in research.

Thanks also go to Dr. Matthias Schiemann and Lynette Henkel for performing the FACS sorts. The OT-I transgenic mice were kindly provided by Katherine Molter and Inge Hensel who I also want to thank for their warmth and happiness, they have shared every day. I want to acknowledge Simon Fräßle's help with some of the cloning. I also want to thank Veit Buchholz, Bianca Weißbrich, Fabian Mohr, Patricia Gräf and all other members of the Busch lab for sharing protocols and technical know-how and creating a great working atmosphere. I am very happy to be part of the group that enjoys being together even after working hours, whenever that may be. I would like to

extend this appreciation to all colleagues on the second floor, who made me looking forward to coming to the lab every day.

During writing the thesis, I received vital support from Dr. Karin Wisskirchen, Dr. Stefan Dreher, Dr. Helge Frebel, Dr. Ronny Milde, Dr. Magdalena Nauerth and Shwetha Lakshmipathi who I would like to thank for critically reading the manuscript and/or other extremely helpful suggestions.

Very special thanks go to Jeannette Bet with who I have shared all ups and downs, at work and beyond, in Munich and Seattle, as a co-worker and friend. These 4 years really bonded us together and I value all the shared experiences.

Of course, I could not have coped with all the challenges along the way without my family and friends. In first place, I want to thank my parents who accompanied me at all times, were always willing to listen and share their views, who gave me strength and belief, when I needed it the most. Thanks to my sister Viola that brings sunshine into my life with her energetic nature.

I would like to thank Dr. Achim Doerner for being a supportive friend for many years and for exploring ideas, views and visions together. Achim, Stefan, Johannes, Steffen, Helge, Tina and Evy, I am very happy that we stay together, just like family... Anna and Verena have been very special friends to me for a long time; we will meet on July, 6th in 2015 and many, many more times in the future!

Most special thanks are due to Nico Wintergerst for his indispensable advice, remarkable patience and endless support that helped me to stay a little calmer during tough times. Thank you for sharing wonderful times with each other!